

The effect of fluorine substituents on
intramolecular C-H bond activation reactions
at transition metals

Jessica Milani

Ph.D.

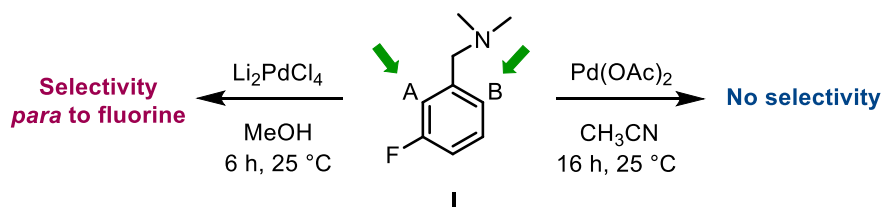
University of York

Chemistry

March 2016

Abstract

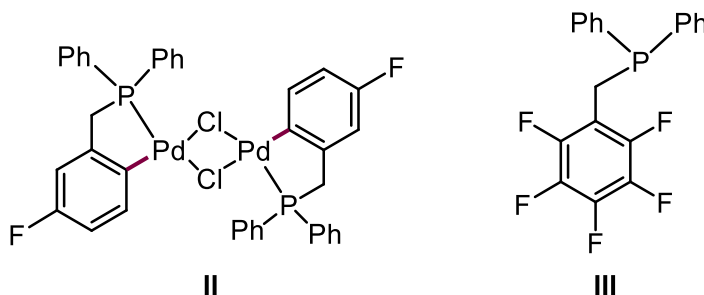
This thesis describes an investigation into the effects of fluorine substituents on the regioselectivity of intramolecular C–H activation reactions at different transition metals, including Pd, Ir, Rh and Ru. A range of mono- and di-fluorinated *N,N*-dimethylbenzylamines (*e.g.* **I**) were synthesised initially and their behaviour towards cyclometallation at Pd was studied (Chapter 2), revealing an unprecedented difference in the regioselectivity of the C–H activation between the formation of acetate- and chloro-bridged palladacycles. The spectroscopic and crystallographic properties of all of these palladacycles are described and analysed in detail. Acetate-bridged palladacycles present a “clam-shell” structure, which shows a dramatic variation with the number and the position of the fluorine atoms on the aromatic ring of the ligand. Conversely the planar chloride-bridged palladacycles do not show any structural variation.



Biological assays have been performed on two of the fluorinated amino-derived palladacycles against ovarian cancer cells, revealing promising activity.

A series of fluorinated diphenylbenzylphosphines and their corresponding chloride-bridged phosphapalladacycles (*e.g.* **II**) have also been synthesised (Chapter 3), and a similar regioselectivity observed to that seen for the corresponding amino-derived palladacycles.

Various successful attempts at cyclometallation reactions using the fluorinated amines as substrates at Rh, Ir and Ru demonstrate a preference for C–H activation *ortho* to fluorine (Chapter 4). Finally the synthesis of the novel pentafluorobenzyl phosphine **III**, and some preliminary work towards C–F activation reactions using this substrate at Pt is described (Chapter 5).



List of Contents

Abstract.....	2
List of Contents.....	3
List of Figures.....	10
List of Schemes.....	15
List of Tables.....	20
Acknowledgements.....	21
Author's Declaration.....	24
Chapter 1: Introduction.....	26
1.1 C–H activation and functionalisation reactions.....	26
1.2 Regioselectivity in the C–H activation of fluorinated aromatics.....	30
1.3 Fluoroaromatics: applications and synthesis.....	35
1.4 C–H activation mechanisms.....	36
1.5 C–H activation in cyclometallation reactions.....	39
1.5.1 Cyclopalladation reactions.....	40
1.6 Project aims and objectives.....	45
1.6.1 Aims.....	45
1.6.2 Objectives.....	45
Chapter 2: Fluorinated aminopalladacycles.....	47
2.1 Introduction.....	47
2.1.1 Model reaction.....	48
2.1.2 Fluorinated <i>N,N</i> -dimethylbenzylamines.....	52
2.1.3 Acetate-bridged and chloride-bridged palladacycles.....	52
2.2 Results.....	53
2.2.1 Fluorinated <i>N,N</i> -dimethylbenzylamines.....	53
2.2.2 Reaction of fluorinated <i>N,N</i> -dimethylbenzylamines with Pd(OAc) ₂	56
2.2.3 Reaction of fluorinated <i>N,N</i> -dimethylbenzylamines with Li ₂ PdCl ₄	66
2.2.4 Bridging halide conversion at Pd(II).....	74

2.2.5 Chlorinated amino palladacycles	76
2.3 Discussion.....	80
2.4 Crystallographic analysis.....	84
2.4.1 Molecular structure of acetate-bridged palladacycles.....	84
2.4.2 Molecular structure of chloride-bridged palladacycles.....	88
2.5 Biological evaluation of novel palladacycles.....	90
2.5.1 Results and discussion	91
2.6 Conclusions.....	93
Chapter 3. Fluorinated benzylphosphines and relevant palladacycles.....	95
3.1 Introduction.....	95
3.1.1 Synthesis of fluorinated phosphapalladacycles.....	96
3.1.1.1 Direct reactions	97
3.1.1.2 Transmetallation reactions	100
3.1.2 Fluorinated benzylphosphines.....	101
3.2 Results.....	102
3.2.1 Syntheses of fluorinated benzylphosphines	102
3.2.2 Synthesis of fluorinated palladacycles.....	108
3.2.2.1 Fluorinated chloride-bridged phosphapalladacycles.....	118
3.2.2.2 Fluorinated acetate-bridged phosphapalladacycles.....	128
3.3 Discussion.....	130
3.4. Crystallographic analysis of chloride-bridged phosphapalladacycles	132
3.5 Summary.....	134
Chapter 4: C–H activation reactions of benzylamines at Ir, Rh and Ru	135
4.1 Introduction.....	135
4.2 Results and discussion	137
4.2.1 Reactions at Ir	137
4.2.2 Reactions at Ru	144
4.2.3 Reactions at Rh	147
4.3 Summary.....	149

Chapter 5: C–F activation experiments at Ni(0), Pd(0) and Pt(0).....	150
5.1 Catalytic C–F functionalisation at Pd(0).....	150
5.1.1 Introduction.....	150
5.1.2 Results and discussion	154
5.2 Stoichiometric C–F activation attempts of fluorinated benzylamines and benzylphosphines at Ni(0) and Pt(0).....	159
5.2.1 Introduction.....	159
5.2.2 Results and discussion	160
5.2.2.1 Reaction of fluorinated <i>N,N</i> -dimethylbenzylamines at Ni(0)	160
5.2.2.2 Reactions of fluorinated benzylphosphines at Pt(0).....	162
5.2.2.3 Reaction of phosphine 5.48 at Pt(0).....	169
5.3 Conclusions.....	172
Chapter 6: Conclusions and Future Work.....	174
6.1 Conclusions.....	174
6.2 Future work.....	179
6.2.1 Biological tests on fluorinated palladacycles	179
6.2.2 Investigation of catalytic activity of fluorinated phospho- and amino-palladacycles	179
6.2.3 Electrochemistry and UV-studies of acetate-bridged palladacycles.....	180
6.2.4 Cyclometallation reactions at Ir, Ru and Rh of fluorinated benzylphosphines...	180
6.2.5 Synthesis of hydroxyl-bridged and bromine-bridged palladacycles.....	181
6.2.6 Cyclometallation of fluorinated benzylamines at Mn	182
Chapter 7: Experimental Section	183
7.1 General experimental techniques	183
7.1.1 Solvent and Reagents.....	183
7.1.2 Melting Points.....	183
7.1.3 Nuclear Magnetic Resonance Spectroscopy	183
7.1.4 X-ray Crystallography.....	184
7.1.5 Infrared Spectroscopy	184
7.1.6 Mass Spectrometry.....	184

7.1.7 Elemental Analysis	184
7.1.8 Chromatographic methods	185
7.1.9 Waste and disposal.....	185
7.2 General Procedures	185
7.2.1 General procedure A: Synthesis of fluorinated benzylamines	185
7.2.2 General procedure B: Synthesis of fluorinated amino-derived acetate-bridged palladacycles from Pd(OAc) ₂	185
7.2.3 General procedure C: Synthesis of fluorinated amino-derived chloride-bridged palladacycles from Li ₂ PdCl ₄	186
7.2.4 General procedure D: Synthesis of fluorinated amino-derived acetate-bridged palladacycles from chloride-bridged palladacycles	186
7.2.5 General procedure E: Synthesis of fluorinated amino-derived chloride-bridged palladacycles from acetate-bridged palladacycles	186
7.2.6 General procedure F: Synthesis of fluorinated diphenylbenzylphosphines	187
7.2.7 General procedure G: Synthesis of fluorinated phosphino-derived chloride-bridged palladacycles.....	187
7.2.8 General procedure H: Synthesis of fluorinated amino-iridacycles	188
7.2.9 General procedure I: Synthesis of fluorinated amino metallacycles (L = CH ₃ CN)	188
7.2.10 General procedure J: Synthesis of fluorinated amino metallacycles (L = Cl) ..	188
7.2.11 General procedure K: Cross-coupling reactions with Pd(0)	188
7.3 Synthetic procedures and Compound Data.....	190
7.3.1 Compounds in Chapter 2.....	190
<i>N,N</i> -Dimethyl-2-fluorobenzylamine (2.7b)	190
<i>N,N</i> -Dimethyl-3-fluorobenzylamine (2.7c).....	190
<i>N,N</i> -Dimethyl-2,5-difluorobenzylamine (2.7d)	191
<i>N,N</i> -Dimethyl-3,5-difluorobenzylamine (2.7f)	192
<i>N,N</i> -Dimethyl-3-chlorobenzylamine (2.7g)	192
Representative compound numbering for acetate-bridged palladacycles	193
Di- μ -acetato-bis-[<i>o</i> -dimethylaminomethylphenyl- <i>C,N</i>] dipalladium(II) (2.8a).....	193

Di- μ -acetato-bis-[<i>o</i> -dimethylaminomethyl-2-fluorophenyl- <i>C,N</i>] dipalladium(II)(2.8b)	193
Di- μ -acetato-bis-[<i>o</i> -dimethylaminomethyl-3- <i>p</i> -fluorophenyl- <i>C,N</i>] dipalladium(II) (2.8c ₆).....	194
Acetato- <i>O</i> -[<i>o</i> -dimethylaminomethyl-3-fluorophenyl- <i>C,N</i>](pyridine- <i>d</i> ₅)palladium(II) (2.8c _{pyr2} and 2.8c _{pyr6}).....	195
Di- μ -acetato-bis-[<i>o</i> -dimethylaminomethyl-2,5- <i>o,m</i> -difluorophenyl- <i>C,N</i>] dipalladium(II) (2.8d).....	195
Di- μ -acetato-bis-[<i>o</i> -dimethylaminomethyl-3,4- <i>p,m</i> -difluorophenyl- <i>C,N</i>] dipalladium(II) (2.8e ₆)	196
Di- μ -acetato-bis-[<i>o</i> -dimethylaminomethyl-3,5-difluorophenyl- <i>C,N</i>] dipalladium(II) (2.8f).....	196
Di- μ -chloro-bis-[<i>o</i> -dimethylaminomethyl-phenyl- <i>C,N</i>] dipalladium(II) (2.9a)	197
Di- μ -chloro-bis-[<i>o</i> -dimethylaminomethyl-2- <i>m</i> -fluorophenyl- <i>C,N</i>] dipalladium(II) (2.9b).....	197
Di- μ -chloro-bis-[<i>o</i> -dimethylaminomethyl-3- <i>p</i> -fluorophenyl- <i>C,N</i>] dipalladium(II) (2.9c ₆).....	198
Chloro- κ O-[<i>o</i> -dimethylaminomethyl-3- <i>p</i> -fluorophenyl- <i>C,N</i>](pyridine- <i>d</i> ₅) palladium(II) (2.9c _{6pyr}).....	199
Di- μ -chloro-bis-[<i>o</i> -dimethylaminomethyl-2,5- <i>o,m</i> -difluorophenyl- <i>C,N</i>] dipalladium(II) (2.9d).....	199
Di- μ -chloro-bis-[<i>o</i> -dimethylaminomethyl-3,4- <i>p,m</i> -difluorophenyl- <i>C,N</i>] dipalladium(II) (2.9e ₆)	200
Chloro- κ -[<i>o</i> -dimethylaminomethyl-3,4-difluorophenyl- <i>C,N</i>](pyridine- <i>d</i> ₅) palladium(II) (2.9e _{pyr6}).....	200
Dichloropalladium-bis-2,4-difluoro- <i>N,N</i> -dimethylbenzylamine (2.28d).....	201
Di- μ -chloro-bis-[<i>o</i> -dimethylaminomethyl-3- <i>p</i> -chlorophenyl- <i>C,N</i>] dipalladium(II) (2.8g ₆).....	201
Di- μ -acetato-bis-[<i>o</i> -dimethylaminomethyl-3- <i>p</i> -chlorophenyl- <i>C,N</i>] dipalladium(II) (2.9g ₆).....	202
Biological tests.....	202
7.3.2 Compounds in Chapter 3.....	204

2-Fluoro-diphenylbenzylphosphine (3.2).....	204
3-Fluoro-diphenylbenzylphosphine (3.3).....	204
3,4-Difluoro-diphenylbenzylphosphine (3.4).....	205
3,5-Difluoro-diphenylbenzylphosphine (3.5).....	205
Di- μ -chloro-bis-[<i>o</i> -diphenylphosphinomethyl-2-difluorophenyl- <i>C,P</i>] dipalladium(II) (3.23).....	206
Di- μ -chloro-bis-[<i>o</i> -diphenylphosphinomethyl-3- <i>p</i> -difluorophenyl- <i>C,P</i>] dipalladium(II) (3.28 <i>p</i>).....	207
Di- μ -chloro-bis-[<i>o</i> -diphenylphosphinomethyl-3,5- <i>p,o</i> -difluorophenyl- <i>C,P</i>] dipalladium(II) (3.30 <i>p</i>).....	207
Di- μ -acetato-bis-[<i>o</i> -diphenylphosphinomethyl-2-difluorophenyl- <i>C,P</i>] dipalladium(II) (3.31).....	208
7.3.3 Compounds in Chapter 4.....	209
[(η^6 -C ₁₀ H ₁₅)Ir(2F-C ₆ H ₃ -6-CH ₂ NMe ₂)Cl] (4.7)	209
Mixture of isomers of [(η^6 -C ₁₀ H ₁₅)Ir(3F-C ₆ H ₃ -6-CH ₂ NMe ₂)Cl] (4.8)	209
[(η^6 -C ₆ H ₆)Ru(2-F-C ₆ H ₃ -6-CH ₂ NMe ₂)(CH ₃ CN)]PF ₆ (4.11).....	210
[(η^6 -C ₆ H ₆)Ru(2-F-C ₆ H ₃ -6-CH ₂ NMe ₂)Cl] (4.12).....	210
Mixture of isomers of [(η^6 -C ₆ H ₆)Ru(3-F-C ₆ H ₃ -6-CH ₂ NMe ₂)(CH ₃ CN)]PF ₆ (4.13).211	
Mixture of isomers of [(η^6 -C ₆ H ₆)Ru(3-F-C ₆ H ₃ -6-CH ₂ NMe ₂)Cl] (4.14).....	211
[(η^6 -C ₁₀ H ₁₅)Rh(2-F-C ₆ H ₃ -6-CH ₂ NMe ₂)Cl] (4.15)	212
7.3.4 Compounds in Chapter 5.....	212
2,3,4,5,6-Pentafluoro- <i>N,N</i> -dimethylbenzylamine (5.26)	212
<i>N,N</i> -Dimethyl-2,6-difluorobenzylamine (5.25)	213
<i>N,N</i> -Dimethyl-2,3,4,5,6-pentafluoropyridine-4-phenylbenzylamine (5.30).....	213
2,3,4,5,6-Pentafluoro-diphenylbenzylphosphine (Jess-Phos, 5.48)	214
Appendix I: Published paper.....	215
Appendix II: X-Ray diffraction data.....	226
Crystallographic data for compound 2.8a	226
Crystallographic data for compound 2.8b.....	227
Crystallographic data for compound 2.8c ₆	228

Crystallographic data for compound 2.8d.....	229
Crystallographic data for compound 2.8e ₆	230
Crystallographic data for compound 2.8f	231
Crystallographic data for compound 2.9b.....	232
Crystallographic data for compound 2.9c ₆	233
Crystallographic data for compound 2.9d.....	234
Crystallographic data for compound 2.9e ₆	235
Crystallographic data for compound 2.28d.....	236
Crystallographic data for compound 2.9g.....	237
Crystallographic data for compound 2.30.....	238
Crystallographic data for compound 3.3.....	239
Crystallographic data for compound 3.5 oxide.....	240
Crystallographic data for compound 3.24.....	241
Crystallographic data for compound 3.26.....	242
Crystallographic data for compound 3.27	243
Crystallographic data for compound 3.23.....	244
Crystallographic data for compound 3.28 <i>p</i>	245
Crystallographic data for compound 3.29.....	246
Crystallographic data for compound 3.30.....	247
Crystallographic data for compound 3.31	248
Crystallographic data for compound 5.30.....	249
Crystallographic data for compound 5.44.....	250
Crystallographic data for compound 5.48 oxide.....	251
Crystallographic data for compound 6.6.....	252
Abbreviations.....	253
References.....	253

List of Figures

Figure 1: Substrates able to undergo C–H arylation reactions.....	27
Figure 2: Correlation between Rh–C bond dissociation energies and C–H bond dissociation energies of fluoroaromatics. (Image taken with permission from ref. 37. Copyright 2009, ACS.)	32
Figure 3: Electrophilic fluorinating agent Selectfluor.	36
Figure 4: First examples of cyclometallation products reported separately by Cope and Kleiman.....	39
Figure 5: Four- (CY) or six- electron (YCY) donor palladacycles.....	40
Figure 6: <i>syn</i> and <i>anti</i> isomeric forms of palladacycles.....	40
Figure 7: An example of a six-membered ring palladacycle.	41
Figure 8: Example of the Wheland intermediate in a S_EAr mechanism. ¹²⁴	44
Figure 9: Resonance forms of Wheland intermediate.....	50
Figure 10: General structure of fluorinated acetate- and chloride-bridged palladacycles.	53
Figure 11: Fluorinated <i>N,N</i> -dimethylbenzylamines.....	54
Figure 12: 1H -NMR of 2.7b at 294.35 K in $CDCl_3$ (400 MHz).....	54
Figure 13: ^{19}F -NMR of 2.7b at 294.35 K in $CDCl_3$ (376 MHz).	55
Figure 14: 1H -NMR of palladacycle 2.8b at 294.15 K in $CDCl_3$ (400 MHz).....	59
Figure 15: $^{13}C\{^1H\}$ -NMR of palladacycle 2.8b at 298 K in $CDCl_3$ (126 MHz).....	59
Figure 16: ^{19}F -NMR of palladacycle 2.8b at 300 K in $CDCl_3$ (471 MHz).	60
Figure 17: Molecular structure of palladacycle 2.8b. Hydrogen atoms were omitted for clarity; thermal ellipsoids shown with probability of 50%.	60
Figure 18: Synthesis of palladacycle 2.8c (mixture of isomeric forms).	61
Figure 19: ^{19}F -NMR spectrum of mixture of isomers of palladacycle 2.8c in $CDCl_3$ (471 MHz).....	62
Figure 20: ^{19}F -NMR spectrum of palladacycle 2.8c _{pyr2} and 2.8c _{pyr6} at 293.45 K in $pyr-d_5$ (376 MHz).....	63
Figure 21: 1H -NMR spectrum of palladacycle 2.8c _{pyr2,6} and 2.8c _{pyr6} at 293.45 K in $pyr-d_5$ (400 MHz).....	64
Figure 22: Molecular structure of palladacycle 2.8d. Hydrogen atoms were omitted for clarity; thermal ellipsoids shown with probability of 50%.	66
Figure 23: Molecular structure of palladacycle 2.9b. Hydrogen atoms were omitted for clarity; thermal ellipsoids shown with probability of 50%.	68
Figure 24: Substrate 2.7c offers two sites (C-2 or C-6) for the C–H activation reaction.....	69

Figure 25: Molecular structure of palladacycle 2.9c ₆ . Hydrogen atoms were omitted for clarity; thermal ellipsoids shown with probability of 50%.	69
Figure 26: ¹ H-NMR of palladacycle 2.9c ₆ at 298 K in CDCl ₃ (500 MHz) (<i>syn</i> and <i>anti</i> isomeric forms).	70
Figure 27: ¹⁹ F-NMR of palladacycle 2.9c ₆ at 298 K in CDCl ₃ (471 MHz) (<i>syn</i> and <i>anti</i> isomeric forms).	71
Figure 28: Molecular structure of palladacycle 2.9e ₆ . Hydrogen atoms were omitted for clarity; thermal ellipsoids shown with probability of 50%.	71
Figure 29: Molecular structure of complex 2.28d. Hydrogen atoms were omitted for clarity; thermal ellipsoids shown with probability of 50%.	73
Figure 30: Molecular structure of palladacycle 2.8c ₆ . Hydrogen atoms were omitted for clarity; thermal ellipsoids shown with probability of 50%.	76
Figure 31: Molecular structure of palladacycle 2.8e ₆ . Hydrogen atoms were omitted for clarity; thermal ellipsoids shown with probability of 50%.	76
Figure 32: Molecular structure of palladacycle 2.8g ₆ . Hydrogen atoms were omitted for clarity; thermal ellipsoids shown with probability of 50%.	78
Figure 33: ¹ H-NMR spectrum of palladacycle 2.9g ₆ at 293.45 K in CDCl ₃ (400 MHz). ..	79
Figure 34: Comparison of ¹ H-NMR of palladacycle 2.9g ₆ obtained <i>via</i> two different routes.	80
Figure 35: Representation of the electronic repulsion in palladacycle 2.8c ₂	80
Figure 36: Representation of the electronic repulsion in palladacycle 2.9c ₂	81
Figure 37: Molecular structure of palladacycle 2.8c ₆	81
Figure 38: Molecular structure of palladacycle 2.9c ₆	82
Figure 39: Molecular structure of palladacycle 2.30. Hydrogen atoms were omitted for clarity; thermal ellipsoids shown with probability of 50%.	82
Figure 40: Molecular structure of palladacycle 2.8a. Hydrogen atoms were omitted for clarity; thermal ellipsoids shown with probability of 50%.	84
Figure 41: Interplane angle in palladacycle 2.8b.	86
Figure 42: Angle between benzene planes (γ) in palladacycle 2.8b.	87
Figure 43: Structural comparison between molecular structures showing the different level of twisting (clockwise from top left 2.8a, 2.8b, 2.8c, 2.8d, 2.8e, 2.8f).	87
Figure 44: Molecular structure of palladacycle 2.9b. Hydrogen atoms were omitted for clarity; thermal ellipsoids shown with probability of 50%.	89
Figure 45: Molecular structure of palladacycle 2.9d. Hydrogen atoms were omitted for clarity; thermal ellipsoids shown with probability of 50%.	89
Figure 46: Mono and di-fluorinated palladacycles tested against ovarian cancer cells A2780.	91

Figure 47: Plate containing 96 wells: each column contains a different concentration of compound from 0 μM to 260 μM	92
Figure 48: IC_{50} calculation for compound 2.9c ₆ on ovarian cancer cells A2780.	92
Figure 49: IC_{50} calculation for compound 2.9e ₆ on ovarian cancer cells A2780.	93
Figure 50: Herrmann's catalyst.....	95
Figure 51: Mixing of P–R σ^* (phosphine) and P 3d orbitals resulting in the π -acceptor LUMOs on phosphorus.....	96
Figure 52: Fluorinated acetate-bridged and chloride-bridged palladacycles.	96
Figure 53: Fluorinated benzylphosphines synthesised and used in this study.	102
Figure 54: ^1H -NMR spectrum of 3.2 in C_6D_6 at 294 K (400 MHz).....	103
Figure 55: ^{31}P -NMR spectrum of 3.2 in C_6D_6 at 294 K (162 MHz).	104
Figure 56: ^{19}F -NMR spectrum of 3.2 in C_6D_6 at 294 K (376MHz).	104
Figure 57: ^{13}C -NMR spectrum of 3.2 in CDCl_3 at 298 K (126 MHz).	105
Figure 58: Molecular structure of compound 3.3. Hydrogen atoms were omitted for clarity; thermal ellipsoids shown with probability of 50%.	107
Figure 59: Molecular structure of compound 3.5 in the oxide form. Hydrogen atoms were omitted for clarity; thermal ellipsoids shown with probability of 50%.	108
Figure 60: Molecular structure of complex 3.24. Hydrogen atoms were omitted for clarity; thermal ellipsoids shown with probability of 50%.	110
Figure 61: Palladacycle 3.12 synthesised by Shaw <i>et al.</i>	111
Figure 62: Molecular structure of complex 3.26. Hydrogen atoms were omitted for clarity; thermal ellipsoids shown with probability of 50%.	114
Figure 63: Molecular structure of complex 3.27. Hydrogen atoms were omitted for clarity; thermal ellipsoids shown with probability of 50%.	115
Figure 64: ^1H -NMR spectrum of palladacycle 3.23 in CDCl_3 at 298 K (500 MHz).	120
Figure 65: ^{31}P -NMR spectrum of palladacycle 3.23 in CDCl_3 at 298 K (202 MHz).....	120
Figure 66: ^{19}F -NMR spectrum of palladacycle 3.23 in CDCl_3 at 298 K (471 MHz).....	121
Figure 67: Molecular structure of palladacycle 3.23 Hydrogen atoms were omitted for clarity; thermal ellipsoids shown with probability of 50%.	121
Figure 68: Possible isomers of palladacycle 3.28 (Scheme 70).	122
Figure 69: Expansion of aromatic region in ^1H - ^1H -COSY NMR spectrum of palladacycle 3.28 at 298 K (500 MHz) in CDCl_3	124
Figure 70: <i>para</i> isomer (palladacycle 3.28 <i>p</i>).	124
Figure 71: $^1\text{H}\{^1\text{H}\}$ -NMR (700 MHz) spectrum (above) and ^1H -NMR spectrum (below) of palladacycle 3.28 <i>p</i> at 298 K (700 MHz) in CDCl_3	125
Figure 72: Molecular structure of palladacycle 3.28 <i>p</i> . Hydrogen atoms were omitted for clarity; thermal ellipsoids shown with probability of 50%.	125

Figure 73: Palladacycles 3.29 and 3.30 <i>p</i>	127
Figure 74: Molecular structure of palladacycle 3.29 along with a molecule of toluene in the unit cell. Hydrogen atoms were omitted for clarity; thermal ellipsoids shown with probability of 50%.	127
Figure 75: Molecular structure of palladacycle 3.30 <i>p</i> along with disordered molecule of chloroform. Hydrogen atoms were omitted for clarity; thermal ellipsoids shown with probability of 50%.	128
Figure 76: Molecular structure of palladacycle 3.31. Hydrogen atoms were omitted for clarity; thermal ellipsoids shown with probability of 50%.	129
Figure 77: ³¹ P-NMR spectrum of palladacycle 3.31 in CDCl ₃ at 294K (162 MHz).....	130
Figure 78: ¹⁹ F-NMR spectrum of palladacycle 3.31 in CDCl ₃ at 294K (471 MHz).....	130
Figure 79: Representation of the electronic repulsion in palladacycle 3.30 <i>o</i>	131
Figure 80: Fluorinated tertiary phosphines 3.32 and 3.33 used by Vrieze <i>et al.</i> to assess the regioselectivity of C–H activation at different transition metals.	131
Figure 81: ¹ H-NMR of 4.7 in CDCl ₃ at 298 K (400 MHz).	138
Figure 82: ¹⁹ F-NMR of 4.7 in CDCl ₃ at 298 K (376 MHz).	139
Figure 83: ¹ H-NMR spectrum of mixture of isomers 4.8 in CDCl ₃ at 298 K (400 MHz). ..	140
Figure 84: ¹⁹ F-NMR spectrum of mixture of isomers 4.8 in CDCl ₃ at 298 K (376 MHz)...	141
Figure 85: Comparison ¹⁹ F-NMR spectra of metallacycle 4.8 obtained via different syntheses.	143
Figure 86: ¹ H-NMR spectrum of 4.11 in CD ₃ CN at 298 K (500 MHz).....	145
Figure 87: ¹ H-NMR spectrum of 4.14 in CD ₃ CN at 298 K (500 MHz).....	146
Figure 88: ¹⁹ F-NMR spectrum of 4.14 in CD ₃ CN at 298 K (471 MHz).	147
Figure 89: ¹ H-NMR spectrum of 4.15 in CDCl ₃ at 298 K (400 MHz).	148
Figure 90: Fluorinated substrates considered for the catalytic C–F activation at Pd(0).	154
Figure 91: Molecular structure of palladacycle 5.30. Hydrogen atoms were omitted for clarity; thermal ellipsoids shown with probability of 50%. Selected bond lengths(Å): C(5)–F(1): 1.350(3), C(6)–F(2): 1.353(3), C(8)–F(3): 1.346(3), C(9)–F(4): 1.346(3), C(7)–C(10): 1.482(4); selected bond angles (°): C(15)–C(10)–C(7): 119.6(2), C(11)–C(10)–C(7): 121.1(2), F(4)–C(9)–C(4): 119.8(2), F(1)–C(5)–C(4): 119.7(2).	156
Figure 92: ¹⁹ F-NMR spectrum of reaction in Scheme 100. Blue stars indicate signals arising from compound 5.35 while green stars indicate the starting material 5.34.	158
Figure 93: Substrates 5.25 and 5.26 used in the attempted C–F activation reactions at Ni(0).	161
Figure 94: X Molecular structure of palladacycle 5.44. Hydrogen atoms were omitted for clarity; thermal ellipsoids shown with probability of 50%. Selected bond lengths (Å): Ni(1)–P(1): 2.1717(7), Ni(1)–P(2): 2.1786(7), Ni(1)–C(1): 2.095(2), Ni(1)–C(2): 2.092(2),	

Ni(1)–C(5), Ni(1)–C(6): 2.096(2); selected bond angles (°): Ni(1)–P(1)–P(2): 103.26(3), C(2)–N(1)–P(2): 95.43(7), C(6)–N(1)–P(1): 95.62(6), N(1)–P(2)–C(17): 114.18(8), N(1)–P(1)–C(9): 116.84(8).	161
Figure 95: Byproduct 5.60 of reaction in Scheme 114.	165
Figure 96: ³¹ P{ ¹ H}-NMR spectrum of 5.48 in C ₆ D ₆ at 298 K (202 MHz).	167
Figure 97: ¹⁹ F-NMR spectrum of 5.48 in C ₆ D ₆ at 298 K (471 MHz).	168
Figure 98: ¹ H-NMR spectrum of 5.48 in C ₆ D ₆ at 298 K (500 MHz).	168
Figure 99: Molecular structure of phosphine 5.48 in the oxide form. Hydrogen atoms were omitted for clarity; thermal ellipsoids shown with probability of 50%. Selected bond lengths (Å): C(3)–F(1): 1.3346(15), C(4)–F(2): 1.3361(15), C(5)–F(3): 1.3393(15), C(6)–F(4): 1.3388(16), C(7)–F(5): 1.3399(15), C(1)–P(1): 1.8263(13), O(1)–P(1): 1.4836(9); selected bond angles (°): C(2)–C(1)–P(1): 108.63(9), F(1)–C(3)–C(2): 120.23(11), F(5)–C(7)–C(2): 119.95 (11).	169
Figure 100: Presumed structure of the minor complex (5.65) obtained from the reaction in Scheme 116.	170
Figure 101: ¹⁹⁵ Pt- ¹ H- HSQC-NMR spectrum of reaction in Scheme 116 at 298 K in C ₆ D ₆ (107/500 MHz). ¹ H decoupled in ¹⁹⁵ Pt dimension (y-axis).	170
Figure 102: ³¹ P{ ¹ H}-NMR spectrum of the products resulting from the reaction in Scheme 116 at 298 K in C ₆ D ₆ (202 MHz).	171
Figure 103: Comparison between the molecular geometries of the molecular structures of clam shell palladacycle 2.8e ₆ and planar 2.9e ₆	175
Figure 104: Molecular structure of palladacycle 3.28p (planar structure).	177
Figure 105: Molecular structure of dinuclear hydroxyl-bridged palladacycle 6.5 reported by Fairlamb <i>et al.</i> ¹³¹ (Image taken with permission from ref. 131. Copyright 2014, RSC.)	181
Figure 106: Molecular structure of Mn complex 6.6. Hydrogen atoms were omitted for clarity; thermal ellipsoids shown with probability of 50%.	182

List of Schemes

Scheme 1: Representation of C–H activation and C–H functionalisation processes.	26
Scheme 2: Biaryl C–H functionalisations and cross-coupling reactions.	27
Scheme 3: Regioselective olefination catalysed by transition metals.	28
Scheme 4: Regioselective C–H functionalisation and allylation reaction (Glorius <i>et al.</i>)....	28
Scheme 5: Monoselective C–H functionalisation of α -phenylglycine and mandelic acid (Yu <i>et al.</i>).	29
Scheme 6: Activation of inert benzylic sp^3 C–H bonds with Pd(II) (Yu <i>et al.</i>).....	29
Scheme 7: Copper(II) catalysed <i>meta</i> -selective C–H arylation (Gaunt <i>et al.</i>).....	29
Scheme 8: Palladium(II) catalysed <i>meta</i> -selective C–H arylation (Dong <i>et al.</i>).	30
Scheme 9: C–H activation of fluoroaromatic at Rh(I) (Perutz <i>et al.</i>).	31
Scheme 10: C–H activation reaction of fluorinated substrates at Re (Perutz <i>et al.</i>).	32
Scheme 11: C–H activation reactions at W of alkylidene complexes (Legzdins <i>et al.</i>).	33
Scheme 12: Regioselective intermolecular C–H functionalisation reaction at Pd of fluorinated aromatics (Fagnou <i>et al.</i>).	34
Scheme 13: Regioselective C–H functionalisation of monofluoroarenes at Pd (Doucet <i>et al.</i>).	34
Scheme 14: Direct arylation of <i>para</i> -substituted fluorobenzenes (Doucet <i>et al.</i>).....	35
Scheme 15: σ -CAM mechanism.	37
Scheme 16: Oxidative addition (general scheme).....	37
Scheme 17: C–H bond functionalisation of perfluoroarenes at Pd <i>via</i> CMD (Fagnou <i>et al.</i>).	38
Scheme 18: Cyclopalladation reaction of dmbs with PdCl ₂	40
Scheme 19: Reaction of tetrachloropalladate salts with amines of type Ph(CH ₂) _{<i>n</i>} NMe ₂ , with <i>n</i> = 0–3.	41
Scheme 20: Cyclopalladation reactions with substituted alkylquinolines.	42
Scheme 21: Difference in reactivity of benzylideneazines with Pd(OAc) ₂ and PdX ₂	43
Scheme 22: Example of transcyclometallation reaction (Pfeffer <i>et al.</i>).	43
Scheme 23: CMD mechanism suggested by Macgregor <i>et al.</i> ⁹⁴	45
Scheme 24: C–H activation reactions at Ir and Rh of substituted phenylimines (Jones <i>et al.</i>).	47
Scheme 25: Intermolecular C–H functionalisation reaction at Pd of fluorinated aromatics (Fagnou <i>et al.</i>).....	48
Scheme 26: Synthesis of palladacycle 2.8a taken as model reaction.....	49
Scheme 27: Synthesis of palladacycle 2.9a taken as model reaction.....	49

Scheme 28: Electrophilic aromatic substitution mechanism suggested by Ryabov <i>et al.</i>	50
Scheme 29: Computational reaction profile (kcal/mol) and bond lengths (Å) for the cyclometallation of Pd(OAc) ₂ (DMBA-H) proceeding <i>via</i> an AMLA-6 mechanism (Macgregor <i>et al.</i>).	51
Scheme 30: Proposed electrophilic aromatic substitution mechanism for 2.17a.	52
Scheme 31: Synthesis of 2.7c (originally reported by Liu <i>et al.</i>).	52
Scheme 32: Cyclopalladation reactions of fluorinated tertiary amines with Pd(OAc) ₂	56
Scheme 33: Synthesis of palladacycle 2.8b.	58
Scheme 34: Formation of monomers 2.8c _{pyr₂} and 2.8c _{pyr₆} from 2.8c isomers.	62
Scheme 35: Synthesis of palladacycle 2.8e (mixture of isomeric forms).	65
Scheme 36: Cyclopalladation reactions of fluorinated tertiary amines with Li ₂ PdCl ₄	66
Scheme 37: Synthesis of palladacycle 2.9b.	68
Scheme 38: Synthesis of palladacycle 2.9c ₆ (geometrical isomers <i>syn</i> and <i>anti</i>).	69
Scheme 39: Formation of palladium complex 2.28d instead of palladacycle 2.9d.	73
Scheme 40: Synthesis of palladacycle 2.9d (geometrical isomers <i>syn</i> and <i>anti</i>).	74
Scheme 41: Bridging halide conversion from chloride-bridged to acetate-bridged palladacycles.	74
Scheme 42: Synthesis of chlorinated tertiary amine 2.7g.	77
Scheme 43: Regioselective synthesis of palladacycle 2.8g ₆	77
Scheme 44: Synthesis of chlorinated acetate-bridged palladacycle 2.9g ₆	78
Scheme 45: Bridge-conversion reaction of 2.8g ₆ to 2.9g ₆	79
Scheme 46: Exchange reaction between palladacycle 2.8a in the presence of 2.7cH ⁺	84
Scheme 47: Synthesis of palladacycles 3.9 and 3.10 (Hiraki <i>et al.</i>).	97
Scheme 48: Synthesis of palladacycle 3.8 (Shaw <i>et al.</i>).	98
Scheme 49: Synthesis of palladacycle 3.15 (Leung <i>et al.</i>).	99
Scheme 50: Synthesis of fluorinated palladacycle 3.17.	99
Scheme 51: Synthesis of palladacycle 3.10 by ligand-exchange reaction.	100
Scheme 52: Improved synthesis of palladacycle 3.10 by ligand-exchange reaction.	100
Scheme 53: Synthesis of palladacycle 3.10 in a solvent-free system.	101
Scheme 54: Synthesis of fluorinated diphenylbenzylphosphines.	102
Scheme 55: S _N 2 mechanism for the synthesis of fluorinated tertiary phosphines.	103
Scheme 56: Synthesis of palladacycles 3.6 and 3.7 (based on Hiraki <i>et al.</i> method).	109
Scheme 57: Failed synthesis of palladacycle 3.23 along with the unexpected product 3.24.	110
Scheme 58: Attempted at cyclometallation reaction from monomer 3.24.	111
Scheme 59: Attempted synthesis of palladacycle 3.23 using the procedure of Shaw <i>et al.</i>	112

Scheme 60: Attempted synthesis of palladacycle 3.23 using the method of Smoliakova <i>et al.</i>	112
Scheme 61: Failed synthesis of palladacycle 3.10 (Smoliakova <i>et al.</i>).	112
Scheme 62: Synthesis of palladacycle 3.10 reported by Ryabov <i>et al.</i>	113
Scheme 63: Transmetallation reaction following the procedure of Ryabov <i>et al.</i>	113
Scheme 64: Synthesis of palladacycle 3.10 by Pfeffer <i>et al.</i>	116
Scheme 65: Formation of monomer 3.26 instead of palladacycle 3.10.	116
Scheme 66: Synthesis of palladacycle 3.10 from monomer 3.26	116
Scheme 67: Synthesis of palladacycle 3.10	117
Scheme 68: Synthesis of fluorinated palladacycles (general scheme).....	119
Scheme 69: Synthesis of palladacycle 3.23.	119
Scheme 70: Synthesis of palladacycle 3.28 (regioselectivity <i>para</i> to F).....	122
Scheme 71: Bridge halide conversion reaction from 3.28 to 3.31.	128
Scheme 72: General cyclometallation reaction of amines at Ir and Rh (Pfeffer <i>et al.</i>).....	135
Scheme 73: General cyclometallation reaction of amines at Ru (Pfeffer <i>et al.</i>).....	135
Scheme 74: Cyclometallation reaction at Ir of amine 2.17a (Davies <i>et al.</i>).	136
Scheme 75: Cyclometallation reaction of phenylimines at Ir and Rh (Jones <i>et al.</i>).	137
Scheme 76: Cyclometallation reaction at Ir of 2.7b following Davies' method.....	138
Scheme 77: Cyclometallation reaction at Ir of 2.7c following Davies' method.	139
Scheme 78: Cyclometallation reaction at Ir of 2.7b following the Pfeffer method.	141
Scheme 79: Conversion of metallacycle 4.9 to metallacycle 4.7 with KCl.	142
Scheme 80: Cyclometallation reaction at Ir of 2.7c following Pfeffer method.	142
Scheme 81: Conversion of metallacycle 4.10 to metallacycle 4.8 with KCl.	142
Scheme 82: Synthesis of metallacycle 4.11 by the Pfeffer's method.	144
Scheme 83: Conversion of metallacycle 4.11 to metallacycle 4.12 with KCl.	144
Scheme 84: Synthesis of metallacycle 4.13 by Pfeffer <i>et al.</i> method.	145
Scheme 85: Conversion of metallacycle 4.13 to metallacycle 4.14 with KCl.	146
Scheme 86: Synthesis of metallacycle 4.15 by Pfeffer <i>et al.</i> method.	148
Scheme 87: First example of catalytic C–C bond formation using Ni(II) complex (Kumada <i>et al.</i>).....	150
Scheme 88: First catalytic C–C bond formation with a polyfluoroarene (Jones <i>et al.</i>).	151
Scheme 89: Functionalisation of monofluoroarene with Ni(II) and <i>N</i> -heterocyclic carbene ligand (Herrmann <i>et al.</i>).....	151
Scheme 90: Functionalisation of monofluoroarene with Ni(II) with phosphine oxide ligand (Ackermann <i>et al.</i>).	151
Scheme 91: Stoichiometric C–F activation reactions at Ni(0) of perfluoropyridine (Perutz <i>et al.</i>).....	152

Scheme 92: Selective C–F functionalisation in the presence of a weaker chlorine–carbon bond (Braun <i>et al.</i>)	152
Scheme 93: First example of a Ni(0) Suzuki cross-coupling reaction (Radius <i>et al.</i>)	153
Scheme 94: Pd(0)-catalysed functionalisation of hexafluorobenzene (Ogoshi <i>et al.</i>)	153
Scheme 95: Ogoshi's proposed mechanism for catalytic C–F activation of hexafluorobenzene	154
Scheme 96: Formation of expected product 5.26 along with byproduct 5.28	155
Scheme 97: Cross coupling reaction of 5.26 using Ogoshi's conditions	155
Scheme 98: Attempted C–F functionalisation reaction of 2.7e following the Ogoshi method	157
Scheme 99: Attempted C–H functionalisation reaction of 5.25 following the Ogoshi method	157
Scheme 100: C–F functionalisation reaction of 5.34 following Ogoshi method	157
Scheme 101: First example of a stoichiometric C–F activation reaction at Ni(0) of hexafluorobenzene (Fahey and Mahan)	159
Scheme 102: C–F activation reactions at Ni(0) of fluorinated heterocycles (Perutz and Braun)	159
Scheme 103: C–F activation reactions at Pd(0) of fluorinated pyridine (Perutz <i>et al.</i>)	160
Scheme 104: C–F activation reactions at Pt(0) of fluorinated pyridine (Perutz <i>et al.</i>)	160
Scheme 105: General scheme of C–F activation reactions of fluorinated substrates M(0)	160
Scheme 106: Reaction of Ni(0) with fluorinated benzylamine 5.26	162
Scheme 107: Reaction of Ni(0) with fluorinated benzylamine 5.25	162
Scheme 108: Desired reaction of Ni(0) with fluorinated benzylphosphine 5.48	163
Scheme 109: Attempted synthesis of 5.48 <i>via</i> nucleophilic substitution using ⁿ BuLi as a base	163
Scheme 110: Attempted synthesis of 5.48 <i>via</i> nucleophilic substitution using CsOH as a base	163
Scheme 111: Attempted synthesis of 5.48 using Grignard reagent	164
Scheme 112: Attempted synthesis of 5.48 using Ni-catalysed cross coupling reaction	164
Scheme 113: Synthesis of pyridyl phosphine 5.56	165
Scheme 114: Attempted synthesis of 5.59 following Drury <i>et al.</i> method	165
Scheme 115: Successful synthesis of 5.47, also called Jess-phos	166
Scheme 116: Synthesis of complex 5.64	169
Scheme 117: Proposed synthesis of Pt complex 5.67	172
Scheme 118: Reactivity of substrate 2.7c towards C–H bond activation at Pd(OAc) ₂ and Li ₂ PdCl ₄	174

Scheme 119: Bridge conversion reaction to acetate-bridged palladacycle with retention of regioselectivity.....	175
Scheme 120: Transcyclometallation reaction example of substrate 3.3 gives regioselectively <i>para</i> isomer 3.28 <i>p</i>	176
Scheme 121: Comparison between the two methods to obtain Ir metallacycle 4.4.....	177
Scheme 122: Cross-coupling reaction <i>via</i> catalytic C–F activation reaction at Pd(0).	178
Scheme 123: Attempted stoichiometric C–F activation reaction of 5.26 at Ni(0).	178
Scheme 124: Stoichiometric attempted C–F activation reaction of 5.48 at Pt(0).	179
Scheme 125: Proposed stoichiometric C–H functionalisation reaction of 2.7 <i>c</i> with iodotoluene to assess regioselectivity in cross-coupling reactions.	180
Scheme 126: Cyclometallation reaction of substrate 2.7 <i>c</i> forming <i>in situ</i> OH-bridged palladacycles 6.4 and 6.5.	181
Scheme 127: Cyclometallation reaction of 2.7 at Mn leading to the formation of 6.6 (95%).	182

List of Tables

Table 1: ^1H -NMR and ^{19}F -NMR spectroscopic signals of <i>N,N</i> -dimethyl-fluorobenzylamines 2.7b–f.	56
Table 2: Products from intramolecular C–H activation of fluorinated benzylamines with $\text{Pd}(\text{OAc})_2$	57
Table 3: ^1H -NMR and ^{19}F -NMR signals of monomers 2.8c _{pyr2} and 2.8c _{pyr6} in pyr- <i>d</i> ₅ at 293.45 K (400 MHz).	64
Table 4: ^1H - and ^{19}F -NMR signals of palladacycles 2.8a, 2.8b and 2.8d.	65
Table 5: Intramolecular C–H activation of fluorinated benzylamines with Li_2PdCl_4	67
Table 6: ^1H -NMR and ^{19}F -NMR signals of palladacycles 2.9a–e at 293.45 K (400 and 500 MHz).	72
Table 7: Acetate-bridged palladacycle obtained by bridging halide conversion.	75
Table 8: ^1H -NMR (500 MHz) and ^{19}F -NMR (471 MHz) signals of monomers 2.8c ₆ and 2.8e ₆ in CDCl_3 at 298 K.	75
Table 9: Selected distances and angles of acetate-bridged palladacycles 2.8a–f.	85
Table 10: Selected bond lengths of palladacycles 2.8a–f.	88
Table 11: Selected bond angles of palladacycles 2.8a–f.	88
Table 12: Selected bond lengths of palladacycles 2.9a–f.	90
Table 13: Selected bond angles of palladacycles 2.9a–f.	90
Table 14: NMR Data (δ (J/Hz)) for tertiary diphenylbenzylphosphines 3.8 and 3.3–3.5.	106
Table 15: ^{13}C -NMR Data (δ (J/Hz)) in CDCl_3 for the tertiary diphenylbenzylphosphines 3.2–3.5.	107
Table 16: Selected distances (Å) and angles (°) in fluorinated phosphines 3.3 and 3.5 oxide.	108
Table 17: Selected distances (Å) and angles (°) complexes 3.26 and 3.27.	115
Table 18: ^1H -NMR signals of palladacycle 3.10 (500 MHz in CDCl_3 at 300 K).	118
Table 19: ^{31}P -NMR signals of palladacycle 3.10 (202 MHz in CDCl_3 at 300 K).	118
Table 20: NMR spectroscopic data for complexes 3.10, 3.23 and 3.28–3.30.	126
Table 21: Selected distances (Å) and angles (°) in chloride-bridged palladium dimer structures.	133
Table 22: ^1H -NMR signals of the two isomeric forms <i>ortho</i> and <i>para</i> of 4.8.	140
Table 23: Dilution of compound 2.9c ₆ for biological tests.	203

Acknowledgements

I have thought several times during the past four years about where I would be whilst writing the acknowledgements that form the end of this adventure known as a PhD: no longer in York, I find myself enjoying the milder London winter whilst missing the peace and quiet of wonderful North Yorkshire.

I would like to thank my two supervisors, Ian Fairlamb and Robin Perutz, for giving me the opportunity to grow up as researcher and as a person. I am grateful for their help, their advice and for their different ways of seeing things which has made my journey both challenging and very stimulating. Without them I would not be the independent and strong person I am now.

I would also like to thank my supervisors and Tony Wild (Wild fund scholarship) for financial support.

The PhD path is tough, difficult, and most of the time you are thinking “why am I doing this?”, until you arrive at this point, when you see the last four years written out in front of you. This moment gives you the same emotion as seeing the printed version of your first paper, and it is in these moments that you smile and think that everything is worthwhile. To arrive successfully at the end of this journey I have had an amazing group of people around me who, although they have varied and changed during the four years for different reasons, have all made their contribution to this thesis and I’ll try to find a way to thank all of them.

Thanks to Stefanie for being an incredible Erasmus student, it was a pleasure working together and part of this thesis would not exist without all that TLC! Thanks to Amy and Stefan for the tricky manganese work, it’s amazing you both found an *ortho* fluorine effect in your first experiment while it took me 4 years!

Thanks to all the technical staff in York for their valuable help (Charlotte, Naser, Pedro, Heather, Karl and Graeme), to the fantastic admin team, especially Rachel for always bringing a smile into the room, and to all the academic staff, in particular Paul Walton for the Athena Swan chats.

The Fairlamb and Perutz groups have been two fantastic sources of fun, laughter and unforgettable moments. Past and present members of both groups made a huge contribution to these four years; I will not list names but all of them have brought me unforgettable memories: from different musical tastes in the lab to spectra drawn by hand because

TopSpin was not working, from truffle dinners (*mamma che bona*) to very long Sunday afternoons watching the Six Nations. Thank you to all of you.

Thanks especially to Josh and Lyndsay, for always being ready to go to the pub after the dark days and for staying late at work to mark the undergraduate scripts, which was often a source of hilarity. Thanks also for the Fairchops nights out, which always seemed to end with a surprise, unforgettable!

Thanks to Natalie and Adrian for introducing me to the amazing world of crystallography, I hope you will always have the Jess factor with you!

Thanks to all the people on the E114 floor for making their office a welcoming place where I could share a laugh or a dessert or an amazing Italian coffee! Lucy and Luisa: *grazie per tutte le chiacchierate e gli sfoghi che avete ascoltato, siete state uniche, grazie!*

Thanks to David for the opportunity to spend so many hours in the teaching labs, doing something I love and which gave me a huge amount of satisfaction.

Thanks to all the friendly people in the department from the great “ground floor family” to top floor (Julia I am still thinking about the amazing cakes in Vienna!) with the best beer/wine tasting companions (the Taylors). All of you made at least one day of my PhD life, thank you!

Thanks to Lucía for never allowing me to feel alone, despite the distance, and being present every single day since I moved to London, *gracias guapa!*

Thanks to Madhuri, Na, Laura, Lucia and especially Blanca for making me feel at home in York and spending amazing time together in Escrick Terrace.

Thank you to everyone at Eonic, and especially Anthea, for putting up with all my thesis writing complaints over the past three months. Thanks also to my amazing flatmate Stefano for bringing a small piece of Italy into my London life!

I am not sure how I can say thanks to Tom, my life, my rock, able to be so present despite living in another country, the best proof reader ever, who taught me everything from the hyphen to the en-dash, from chromatography columns to British politics; I could not desire anyone better, *grazie amore mio*.

This journey ends with a big thank you to my best friends in Italy, who are always there *via* a WhatsApp voice mail or a text, *grazie per esserci sempre*, and to my family, especially to

the great woman who is my mum, who taught me that anything is possible if you really want it.

Author's Declaration

The work presented in this thesis is my own except where referenced or acknowledged in the body of the text, and has not previously been presented for an award at this or any other university. The work was carried out at the University of York between April 2012 and December 2015.

Parts of this work have been reproduced in a published paper, a copy of which can be found in Appendix 1:

Milani, J., Pridmore, N. E., Whitwood, A. C., Fairlamb, I. J. S., Perutz, R. N.; The role of fluorine substituents in the regioselectivity of intramolecular C–H bond functionalization of benzylamines at palladium, *Organometallics* **2015**, *34*, 4376–4386.

Jessica Milani

March 2016

*‘Fluorine leaves nobody indifferent;
it inflames emotions, be that affections or aversions.
As a substituent it is rarely boring, always good for a surprise,
but often completely unpredictable.’*

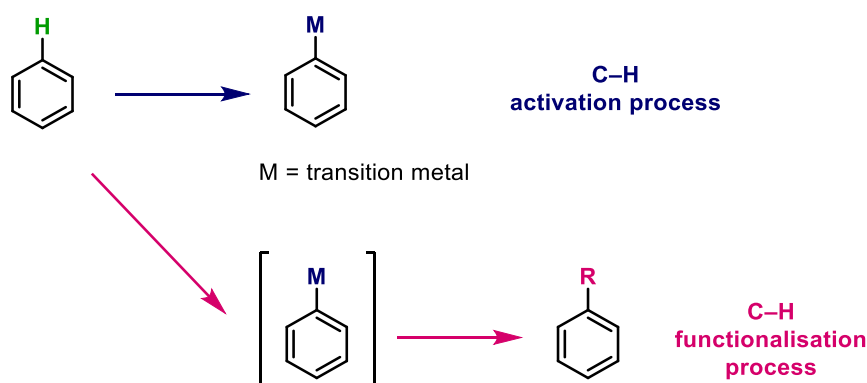
M. Schlosser¹

Chapter 1: Introduction

1.1 C–H activation and functionalisation reactions

The “invisibility of C–H bonds reflects both their ubiquitous nature and their lack of reactivity”.² This quote from Alan Goldman and Karen Goldberg hints at how the ability to activate any C–H bond selectively could represent one of the most useful and powerful tools available for chemical synthesis.

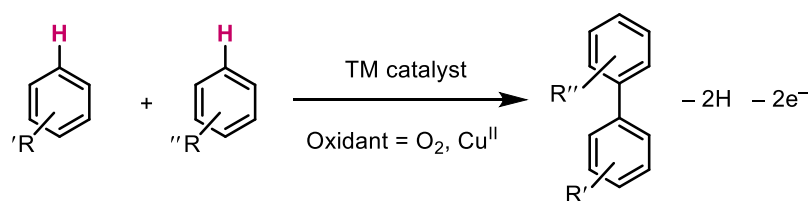
The “Holy Grail” for direct C–H bond activation, as defined by Bergman *et al.*, is the development of new reagents able to make these transformations selectively in complex molecules.³ Transition metal-catalysed C–H bond activation seems to be the solution to address this considerable challenge. C–H activation processes describe the replacement of the unreactive C–H bond with a more reactive C–M bond, which can then be functionalised.⁴ C–H bond functionalisation, instead, describes the process where a C–H bond is transformed into a C–R bond, *via* a C–H activation step (Scheme 1). The two terms are often used to describe the same concept in an erroneous manner.



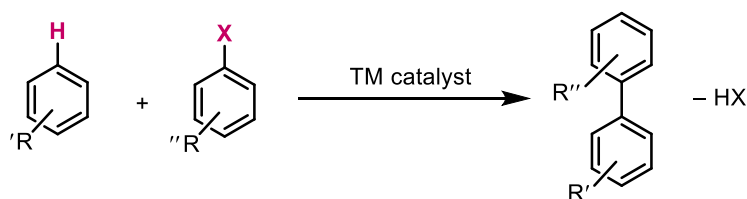
Scheme 1: Representation of C–H activation and C–H functionalisation processes.

The formation of a C–C bond *via* the functionalisation of a C–H bond is an appealing method for the synthesis of synthetic building blocks, due to the atom economy and efficiency of the overall process.⁵ Analogous traditional methods for C–C bond formation often involve cross-coupling reactions,^{6–9} processes that require pre-activation of substrates (c in Scheme 2).^{10–13} By contrast direct arylations or oxidative arene cross-coupling reactions (a and b in Scheme 2) do not require any pre-activation and extensive investigations are currently being dedicated to understanding the mechanisms of these processes.^{8,14}

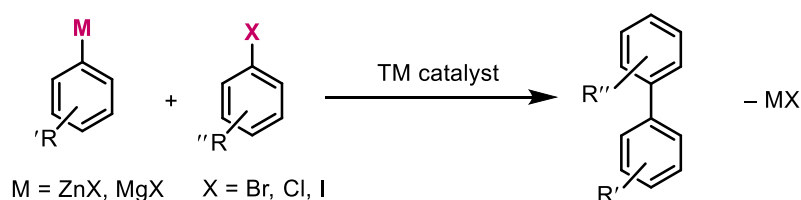
a) Oxidative arene cross-coupling reactions



b) Direct arylation reactions



c) Cross-coupling reactions



Scheme 2: Biaryl C–H functionalisations and cross-coupling reactions.

To make a C–H activation (or functionalisation) process synthetically useful, one of the C–H bonds in the molecule must be selectively activated over the other functional groups; in a traditional cross-coupling, for example, one position in the molecule has a special reactivity as a result of the presence of the electrophilic heteroatom.¹⁵ The problem arises for molecules such as benzene derivatives, which possess multiple unreactive C–H bonds with little difference in reactivity between them. Hence the C–H functionalisation of arenes is normally limited to three categories of substrates: highly electron rich systems (such as thiophene and furan derivatives or indoles),^{16–18} highly electron poor arenes (such as polyfluorinated benzenes), or those bearing directing groups (Figure 1).^{19–21}

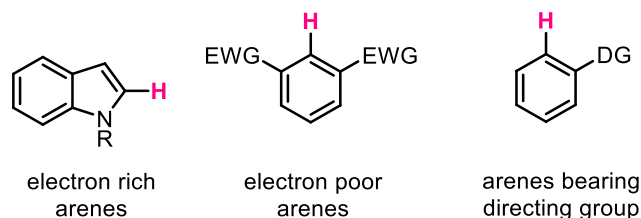
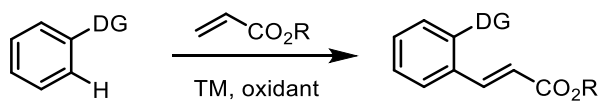


Figure 1: Substrates able to undergo C–H arylation reactions.

Directing groups, such as amides and acetanilidines, have a dual activity that leads to both high reactivity and regioselectivity; they are in fact able to coordinate to the metal centre and

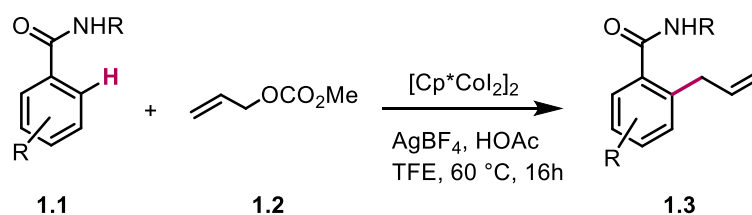
direct it in proximity to the bond to activate.²²⁻²⁴ A general example scheme of selective olefination is illustrated in Scheme 3.



Scheme 3: Regioselective olefination catalysed by transition metals.

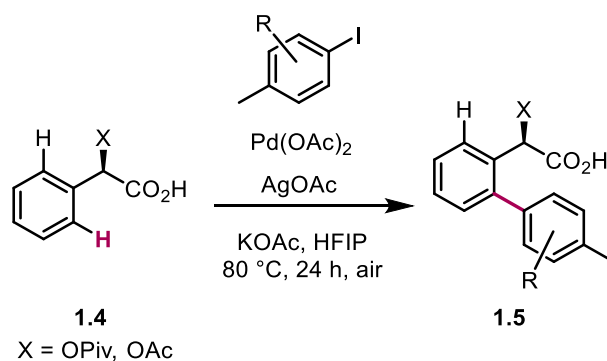
This strategy does however have limitations, as the directing group needs to be pre-installed in the molecule, increasing the synthetic challenge and complexity of the substrate. Another potential limitation is that the activation usually occurs *ortho* to the directing group. The following selected recent examples illustrate the use of directing groups in C–H functionalisation reactions.

Glorius *et al.* reported in 2015 several papers on regioselective C–H functionalisation using directing groups, and in particular the highly challenging activation of sp^3 C–H bonds using Rh(II)²⁵ and the activation and allylation of arenes at Co(III) using an amide as an *ortho* directing group (Scheme 4).²⁶



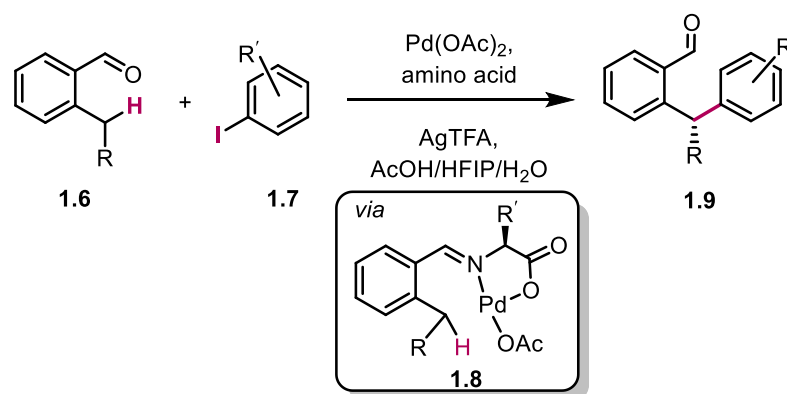
Scheme 4: Regioselective C–H functionalisation and allylation reaction (Glorius *et al.*).

In the same year Yu and co-workers reported the *ortho* monoselective C–H functionalisation of α -phenylglycine and mandelic acid (Scheme 5). They reported several different protocols such as acetoxylation, arylation and iodination of these substrates catalysed by Pd, suggesting that the reactions can proceed *via* two different catalytic cycles at Pd (Pd(II/0) and Pd(II/IV)).²⁷



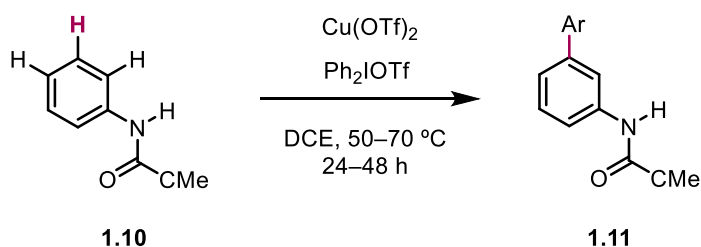
Scheme 5: Monoselective C–H functionalisation of α -phenylglycine and mandelic acid (Yu *et al.*).

In recent years several research groups have investigated approaches to obtain regioselectivity other than that *ortho* to the directing group.²⁸ Yu and co-workers in 2016 reported the use of an amino acid reagent as a transient directing group that can react with ketones and aldehydes in a reversible manner. The resulting imines can facilitate the activation of inert benzylic sp^3 C–H bonds with Pd(II) (Scheme 6).²⁹



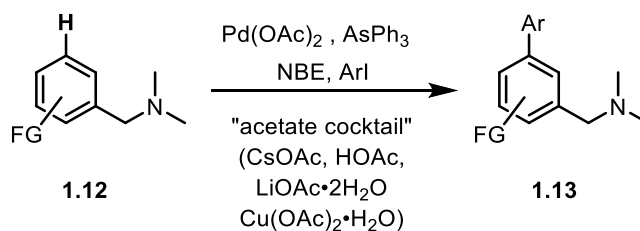
Scheme 6: Activation of inert benzylic sp^3 C–H bonds with Pd(II) (Yu *et al.*).

In 2009 Phipps and Gaunt achieved the *meta*-C–H arylation of arenes containing electron-donating groups, catalysed by copper(II) in the presence of an oxidant (Scheme 7).³⁰



Scheme 7: Copper(II) catalysed *meta*-selective C–H arylation (Gaunt *et al.*).

In 2015, Dong *et al.* also reported the *meta* selective C–H arylation of tertiary amines using the Catellani reaction,³¹ promoted by an “acetate cocktail” and $\text{Pd(OAc)}_2/\text{AsPh}_3$ (Scheme 8).³²



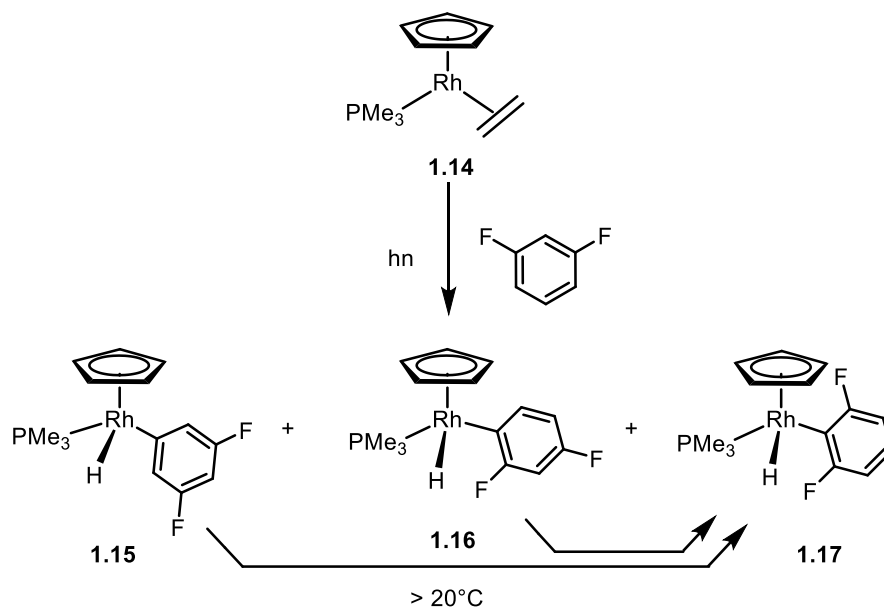
Scheme 8: Palladium(II) catalysed *meta*-selective C–H arylation (Dong *et al.*).

Previously, Yu and co-workers developed a different method to obtain *meta* functionalisation by using a recyclable nitrile-containing template to functionalise distal C–H bonds, which, especially in direct cyclometallation reactions, are geometrically inaccessible. They reported direct acetoxylation and olefination of *meta* C–H bonds of benzylic amines and anilines through conformational control.³³ NMR spectroscopic and X-ray crystallographic studies revealed that by inserting a fluorine substituent into the template, the selectivity could be switched from *meta* to *ortho*.

1.2 Regioselectivity in the C–H activation of fluorinated aromatics

Fluorine substituents in fluoroarenes can also act as directing groups in C–H activation reactions¹⁴ and their behaviour toward these transformations has been studied experimentally and computationally with different transition metals.^{20,34} The following section gives an overview of a number of key studies into the nature and origin of this ‘*ortho* fluorine effect’.

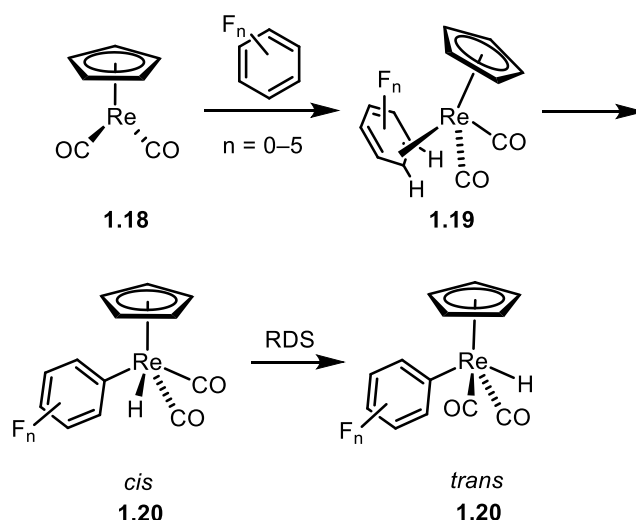
In 1994, Jones and Perutz investigated the thermal and photochemical behaviour of Rh(I) complexes with fluorinated aromatics, and found that the products in which the C–H activation had occurred *ortho* to the fluorine atoms were favoured.



Scheme 9: C–H activation of fluoroaromatic at Rh(I) (Perutz *et al.*).

Complex [(Cp*)Rh(PMe₃)] (generated thermally) and complex [(Cp*)Rh(PMe₃)] (generated photochemically) both react with fluoroaromatics (aryl_F) to give (Cp*)Rh(PMe₃)(aryl_F)H (Scheme 9). In particular, the reaction of 1,3-difluorobenzene, which initially gives the kinetic product with activation *meta* to both fluorine atoms (**1.15**), can be driven to the thermodynamic product **1.17**, where the C–H activation occurs *ortho* to the two fluorine. However, further investigation did not reveal any evidence for an interaction of the fluorine lone pair with a coordination site on the metal, and so the regioselectivity was not explored any further in this context.³⁵

Eisenstein and Perutz later in 2003 investigated the reaction of [CpRe(CO)₂] with fluorinated benzenes revealing that the stronger the C–H bond to activate, the stronger the resulting Re–C bond that was formed (Scheme 10). They also found that this bond strength was in fact heavily influenced by the number of fluorine atoms on the ring, with more fluorine atoms leading to a stronger C–H and C–M bond.³⁶



Scheme 10: C–H activation reaction of fluorinated substrates at Re (Perutz *et al.*).

Depending on the number of fluorines present on the ring there was in fact a difference in the product outcome: in a non-fluorinated ring, simple η^2 -coordination (**1.19** in Scheme 10) was favoured, whilst if at least two fluorines were present, C–H activation was observed (**1.20** in Scheme 10). They also demonstrated that the rate-determining step was the isomerisation between the *cis* and *trans* isomers (Scheme 10) which had an energetic barrier that decreased as the number of fluorine atoms in the *ortho* position to the Re increased.

Later the same authors reported a similar correlation for C–H activation reactions of polyfluoroarenes at different metal fragments. They showed a correlation between the M–C bond dissociation energies and the C–H bond dissociation energies of the polyfluoroarenes. The data points were divided into three main groups of molecules with zero, one and two fluorine atoms, again showing a correlation of the C–H bond strength with the M–aryl bond strength, and higher bond strengths in molecules bearing the most fluorine atoms.³⁷

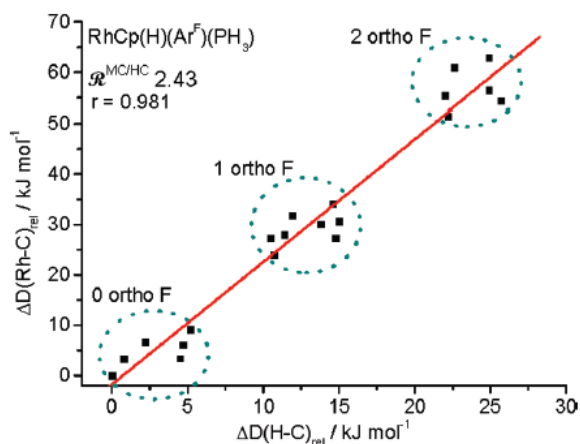
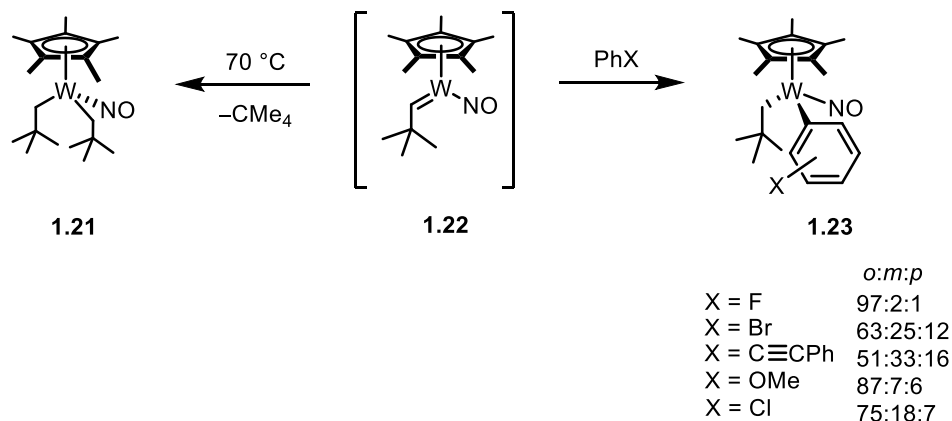


Figure 2: Correlation between Rh–C bond dissociation energies and C–H bond dissociation energies of fluoroaromatics. (Image taken with permission from ref. 37. Copyright 2009, ACS.)

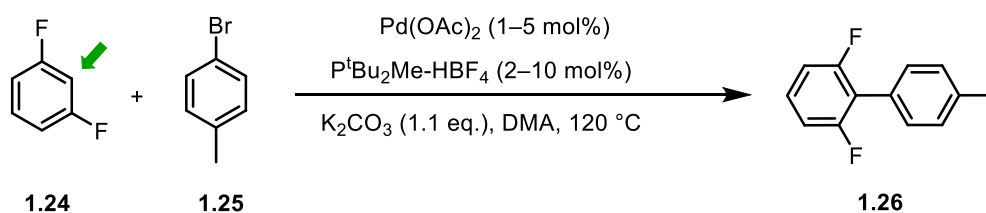
This behaviour has been also observed experimentally by Legzdins and co-workers in intermolecular C–H activation reactions at W of alkylidene complexes where the ability of the substituent to *ortho*-direct the reaction diminished in the order F > OMe > Cl (Scheme 11).³⁸



Scheme 11: C–H activation reactions at W of alkylidene complexes (Legzdins *et al.*).

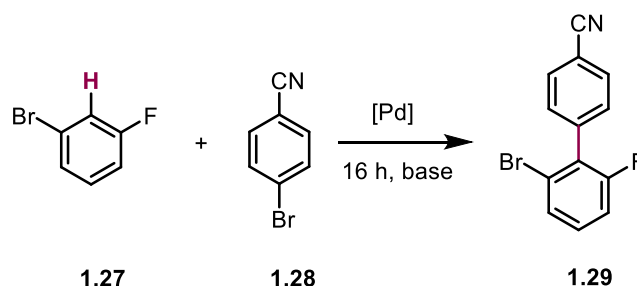
Fagnou and co-workers have pioneered the Pd-catalysed direct arylation of fluoroaromatics using aryl halides.^{20,39-40} In the course of their investigations they have also suggested a new mechanism, called CMD (concerted metallation deprotonation, which will be discussed in more detail in section 1.4) in order to explain the reactivity of electron-deficient substrates towards C–H bond cleavage. These types of substrates were known to be unreactive in reactions proceeding *via* an S_EAr (electrophilic aromatic substitution) mechanism, which usually involves nucleophilic aromatic rings.^{14,41} Direct arylation of electron-deficient arenes has since been extensively investigated, substituting aryl halides with boronic acids,⁴² tosylates,⁴³ diaryliodonium salts⁴⁴ or simple arenes,⁴⁵ as well as using different metals, such as Cu.⁴⁶

In 2006 Fagnou and co-workers performed a number of competition experiments toward different polyfluoroarenes in direct arylation reactions and discovered that C–H functionalisation was favoured for fluorinated aromatics, and moreover that for substrates bearing two or more different C–H bonds, the activation occurred preferentially *ortho* to the fluorine atom, this being the most acidic position (Scheme 12).²⁰ The regioselectivity and reactivity of these functionalisation reactions correlated with the acidity of the functionalised fluoroaromatic.



Scheme 12: Regioselective intermolecular C–H functionalisation reaction at Pd of fluorinated aromatics (Fagnou *et al.*).

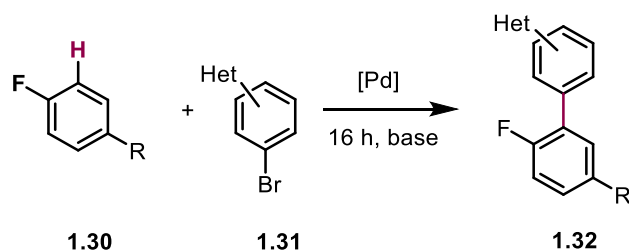
In 2014, Doucet and co-workers investigated the effect of other substituents on the reactivity of monofluorobenzenes towards C–H functionalisation catalysed by Pd, showing that the introduction of another functional group *meta* to fluorine can modify the reactivity of the substrate as well as altering the regioselectivity (Scheme 13). Using electron-withdrawing groups a complete regioselectivity *ortho* to fluorine was observed while in the case of electron-donating groups, such as methoxy group, a mixture of isomers was noted.⁴⁷



Scheme 13: Regioselective C–H functionalisation of monofluoroarenes at Pd (Doucet *et al.*).

Using a Gorelsky rationalisation of the factors influencing the reactivity and regioselectivity of direct arylation reactions catalysed by Pd it is possible to understand the difference in behaviour.¹⁴ The two main factors that play a role are the interaction energies of the substrate with the metal, and the arene distortion energy due to the group on the ring. Despite the C–H bond of fluorobenzene being more acidic than the C–H bond of 1-fluoro-3-methoxybenzene, the latter is more reactive due to its more favourable arene distortion energy, which favours C–H bond functionalisation.⁴⁷

The same authors subsequently reported an investigation into the reactivity of *para*-substituted fluorobenzenes in direct arylation reactions at Pd using aryl bromides (Scheme 14) where the use of electron-donating or electron-withdrawing groups does not influence the regioselectivity, in all cases reaction occurs *ortho* to the fluorine atom.⁴⁸



Scheme 14: Direct arylation of *para*-substituted fluorobenzenes (Doucet *et al.*).

These studies all demonstrate that a fluorine atom can act as a powerful directing group in C–H activation and functionalisation reactions. However, a number of mechanistic investigations show that, in contrast to classical directing groups, a fluorine atom does this not by coordinating to the transition metal atom and bringing it in proximity to a particular position on the ring, but by making the activation of a particular C–H bond more thermodynamically favourable. An *ortho* fluorine atom has three effects on the adjacent position: it makes both the C–H and C–M bonds in that position stronger (higher bond dissociation energy) and it also withdraws electrons inductively, which stabilises the partial negative charge that forms upon deprotonation and thus increases the ‘acidity’ of the C–H bond. A stronger C–M bond makes its formation more thermodynamically favourable but a stronger C–H bond opposes this by creating a higher barrier to C–H activation; this is counteracted by the increased acidity of the position and C–M bond strength, with the result that the overall C–H activation becomes more favourable.

1.3 Fluoroaromatics: applications and synthesis

Whilst, as the previous sections have alluded to, fluorine can play an important role in the regiochemistry of C–H activation reactions, it can also impart many other useful properties on a compound. This raises the possibility of using fluorine as a directing group in synthesis, but also retaining it in the final target molecule. Fluorinated compounds are increasingly playing an important role both in the development of novel pharmaceutical agents and agrochemicals, and in the production of high performance materials. Since the discovery that the presence of fluorine in a system can help the introduction of a molecule into a cell while bringing metabolic stability, changes in chemical properties and enhancing binding interactions,⁴⁹ the production of fluorinated compounds has become very important.⁵⁰

The production of fluoroaromatics is usually carried out using one of two different approaches: nucleophilic fluorination or electrophilic fluorination. The driving force in the fluorination reaction is the formation of thermodynamically favorable C–F bond (107

kcal/mol).⁵¹ Using the electrophilic approach, the substrate, which usually has a high electron-density centre, is treated with a fluorinating agent in which fluorine behaves as an electrophile. Because of its high electronegativity, in order to obtain an electrophilic fluorine it is necessary to withdraw charge through the inductive effect by putting a good leaving group near it, as in N–F compounds, *e.g.* *Selectfluor*TM (F-TEDA-BF₄) (**1.33** in Figure 3); the main disadvantages of using this kind of fluorinating agent are its high cost and low atom economy.⁵¹

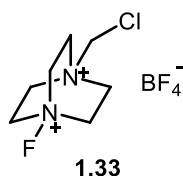


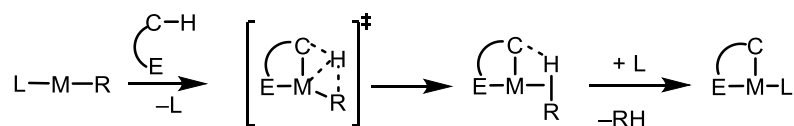
Figure 3: Electrophilic fluorinating agent Selectfluor.

If the fluorine is introduced as an anion, using nucleophilic reagents, problems can arise due to the fact that it can act as a base as well as a nucleophile. In the unsolvated form it has strongly basic behavior but it can also be solvated, decreasing the nucleophilicity necessary to fluorinate a substrate, and leading to side reactions.⁵² One alternative to traditional fluorination methods would be the use of the cross-coupling reactions of fluorinated fragments that proceed *via* C–H activation reactions. Understanding the mechanism of these processes and using fluorine substituents as directing groups (see section 1.2) could lead to new and efficient methodologies to obtain fluoroaromatic motifs.⁵²⁻⁵⁶

1.4 C–H activation mechanisms

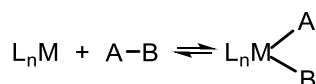
Many reviews are available concerning the mechanisms and the types of C–H activation reactions.^{2,4,22,24,41,57-58} Bercaw and Labinger have attempted to divide these reactions into a number of main categories.⁵⁹

- σ -Bond metathesis: These reactions are typical of electron-poor metal centers,⁶⁰⁻⁶¹ such as high-valent early transition metals and usually include the formation of a four-membered transition state during which the formal oxidation state of the metal does not change.⁵⁸ When the precursors are osmium, iridium, rhenium or ruthenium hydrides, the process is better described as σ -CAM (complex-assisted metathesis)⁶² due to the stabilisation of the σ -complex by the metal.⁶³



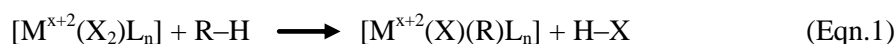
Scheme 15: σ -CAM mechanism.

- Oxidative addition: these reactions usually proceed *via* a highly unstable coordinatively unsaturated intermediate, followed by an increase in the oxidation state of the metal; it is typical of low valent, electron-rich transition metals, such as Pt, Ir, Ru and Rh.



Scheme 16: Oxidative addition (general scheme).

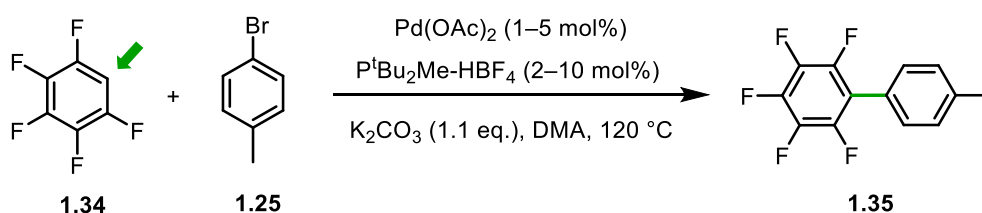
- Electrophilic substitution: these reactions typically involve late transition metals, such as Pd(II) or Pt(II) in strong acids, such as acetic acid, or in polar solvents, *e.g.* methanol. The term electrophilic derives from the origin of the organometallic intermediate $[M^{x+2}(X)(R)L_n]$ where the transition metal attacks an electron rich carbon followed by a deprotonation step.



In particular the electrophilic aromatic substitution mechanism (S_EAr)⁶⁴ is known for C–H activation reactions where the reaction proceeds *via* a Wheland intermediate, in which the aromaticity of the ring is lost, and the bond orders of the C–C bonds of the ring are no longer 1.5.⁶⁵

In addition to these three subtypes, the CMD (concerted metallation deprotonation) mechanism, also called AMLA (ambiphilic metal-ligand assisted C–H activation) is known.^{20,66} This mechanism was first suggested by Fagnou in 2006 for the intermolecular C–H activation of perfluoroarenes at Pd to explain the complete inversion in the reactivity of electron-deficient substrates compared to electron-rich arenes going *via* the S_EAr mechanism as mentioned in section 1.2. The CMD (or AMLA-6) mechanism,^{41,57,67} similar to the one proposed by Echavarren and Maseras for Pd-catalysed arylation reactions,⁶⁶ proceeds *via* an agostic C–H interaction followed by six-membered cyclic transition state, generally involving an acetate or a carbonate, which is believed to have a multiple role by acting as a base, but also enhancing the electrophilicity of the Pd(II) center. Computational study revealed that the regioselectivity in the activation was directly dependent on the C–H bond acidity, meaning that the *ortho* fluorine effect can have a strong effect on the regioselectivity

of reactions proceeding by this mechanism.²⁰ In order to prove the hypothesised mechanism, Fagnou and co-workers started their investigation with the highly electron-deficient pentafluorobenzene due to its inability to undergo reactions *via* an S_EAr mechanism.



Scheme 17: C–H bond functionalisation of perfluoroarenes at Pd *via* CMD (Fagnou *et al.*).

They then performed competition experiments using different fluoroarenes finding that the most electron-deficient arene reacted preferentially, and thus showing the completely opposite trend compared to functionalisation reactions proceeding *via* the S_EAr mechanism. Measurement of the KIE made clear that the CMD was the rate determining step, so they also performed computational calculations demonstrating that the regioselectivity *ortho* to the fluorine atom, in cases where more than one site is available for functionalisation, was the result of the C–H acidity and not of the stabilisation of the Pd by the fluorine atom.²⁰

Perutz and co-workers reported a subsequent computational study on Fagnou’s reactions comparing different fluorinated aromatics. In contrast to Fagnou’s own calculations, not just the CMD step was taken in account, but also the oxidative addition and the reductive elimination steps. They demonstrated that the Pd–C bond energies change the energetic barriers in the CMD, but also in the reductive elimination step, and that the presence of the fluorine atoms lowers the activation energy of the overall reactions making the C–H functionalisation regioselective.⁶⁸

These computational and experimental studies were performed on intermolecular C–H functionalisation reactions at Pd but intramolecular systems, which would form fluorinated metallacycles, have not been studied. Changing the ligand at Pd from a phosphine (as in Fagnou’s and Perutz’s calculations) to a different donor atom could change the electronic environment on the metal centre and lead to a different behaviour in the oxidative addition and in the consequent formation of the M–C bond, possibly also resulting in a change in mechanism. Finally the choice of the base could also affect the system making a possible transmetallation step the rate determining step.

A more detailed discussion of intramolecular C–H activation mechanisms is given in the next section, and specific substrates are considered in more detail in Chapter 2.

1.5 C–H activation in cyclometallation reactions

Directed C–H bond activation frequently results in the generation of a metallacycle, *i.e.* a ring containing a metal–carbon bond. Metallacycle formation is also the first step of many transition metal-catalysed C–H functionalisation processes. This section will give a brief historical overview of metallacycles and their synthesis and relevant mechanisms with an emphasis on Pd.

Cyclometallation reactions *via* C–H activation at various transition metals have been known since the 1960s when the groups of Cope⁶⁹ and Kleiman⁷⁰ discovered the formation of a new C–M σ -bond between a transition metal and a ligand also containing a donor atom, such as N, resulting in a ring containing a metal atom (Figure 4).

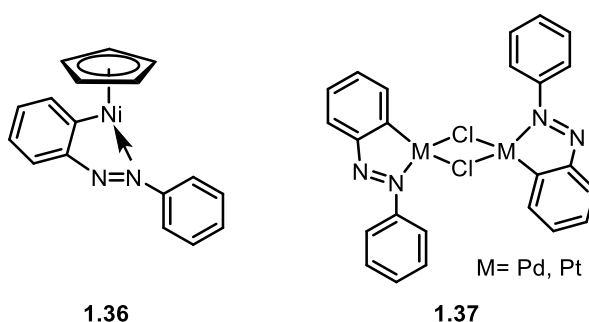


Figure 4: First examples of cyclometallation products reported separately by Cope and Kleiman.

This type of metallacycle formation, also known as a cyclometallation reaction,⁷¹ usually occurs in two steps: firstly the metal coordinates to a soft donor atom such as P, N, O or S, and secondly, an intramolecular C–X (X = H, F) bond activation closes the n -membered-ring (typically $n = 5$ or 6 depending on the nature of M).^{60,72} The activation of a C–F bond to obtain a metallacycle is much rarer than the analogous C–H bond activation and few examples are reported.⁷³⁻⁷⁸

Since their initial discovery, metallacycles⁷⁹ themselves have come to play an important role in organometallic and organic chemistry⁸⁰ being successfully employed as precursors, intermediates or catalysts⁸¹⁻⁸⁴ to obtain organic molecules,⁸⁵⁻⁸⁷ and also used as anticancer agents or for other biological applications in their own right.⁸⁸⁻⁸⁹ They have been extensively studied and several reviews and books cover different aspects such as their synthesis from different transition metals^{72,90-91} and mechanistic investigations.⁹²⁻⁹⁴

1.5.1 Cyclopalladation reactions

Almost all the transition metals can form metallacycles, but the most extensively studied and used are those derived from palladium, known as palladacycles.^{72,82} They contain a Pd–C bond that can be stabilised by one or two neutral donor atoms **Y** (P, N, S, *etc.*) and they can be defined as four- (CY) or six-electron donor (YCY) palladacycles (Figure 5).⁹⁰

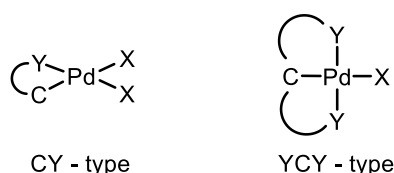


Figure 5: Four- (CY) or six- electron (YCY) donor palladacycles.

The CY type usually exist as acetate- or halogen-bridged dimers, as *syn* and *anti* geometrical isomers depending on the relative positions of the Pd–C bonds (Figure 6).

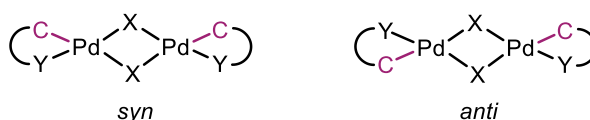
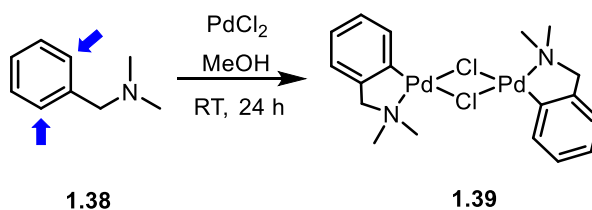


Figure 6: *syn* and *anti* isomeric forms of palladacycles.

They can be monomeric,⁹⁵ cationic,⁹⁶ neutral⁹⁷ or anionic⁹⁸ depending on the X ligand(s) on the metal. The carbon atom, which forms the bond with the metal, can be sp^2 or sp^3 hybridised.⁹⁹

The cyclopalladation reactions are also called *ortho*-palladation reactions, due to the activation of the *ortho* position in the aromatic ligand with respect to the donor atom “arm” (*e.g.* *N,N*-dimethylbenzylamine, **1.38** in Scheme 18).^{69,97,100}



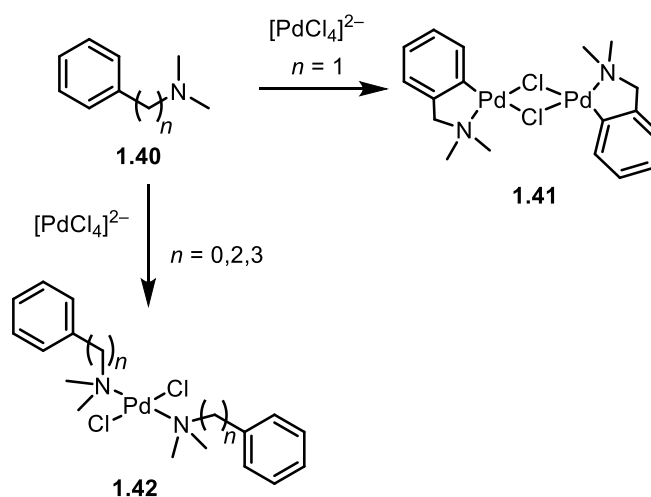
Scheme 18: Cyclopalladation reaction of dmbs with PdCl₂.

A series of factors influences the success of cyclopalladation reactions:^{60,101}

- The nature of the donor atom (Y) and its basicity: palladium coordinates with the donor atom (Y) in the first step of the process, so the exact nature of it affects the

rate and the success of the reaction. Different donor atoms on the same general structure of the substrate give different results: for example in the case of certain dimethylphosphine and arsine derivatives the cyclopalladation does not occur,¹⁰²⁻¹⁰³ while for the equivalent dimethylamines it is successful.¹⁰⁴ The donor atom also stabilises the Pd–C bond, making the chelate effect an important feature: *e.g.* the intramolecular reaction of azobenzene with PdCl₂ is 10⁴ times faster with respect to the same reaction with benzene and this is due to the chelation of the azo-group that can change the process from an intermolecular to an intramolecular one.¹⁰¹

- Ring size of the resulting metallacycle: most known palladacycles contain a five-membered ring. Taking for example the reaction of tetrachloropalladate salts (Na, Li or K) with amines of the type Ph(CH₂)_nNMe₂, with *n* = 0–3, the cyclic product forming is exclusively the one with a five-membered ring (*n* = 1).⁹⁷



Scheme 19: Reaction of tetrachloropalladate salts with amines of type Ph(CH₂)_nNMe₂, with *n* = 0–3.

The same behaviour has also been observed for similar phosphine ligands.^{102,105} Six-membered palladacycles have, however, been obtained from different classes of ligands containing N, P and O, where the structure does not provide any feasible alternative (*e.g.* 1.43, Figure 7);¹⁰⁶

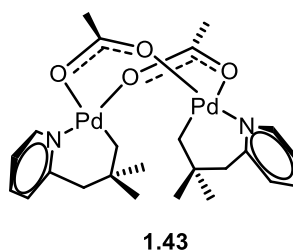
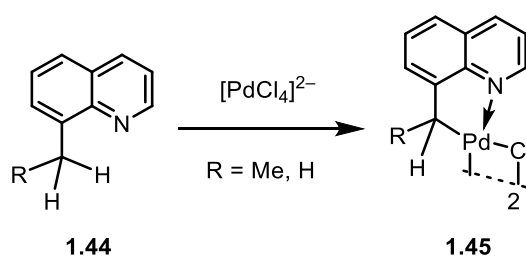


Figure 7: An example of a six-membered ring palladacycle.

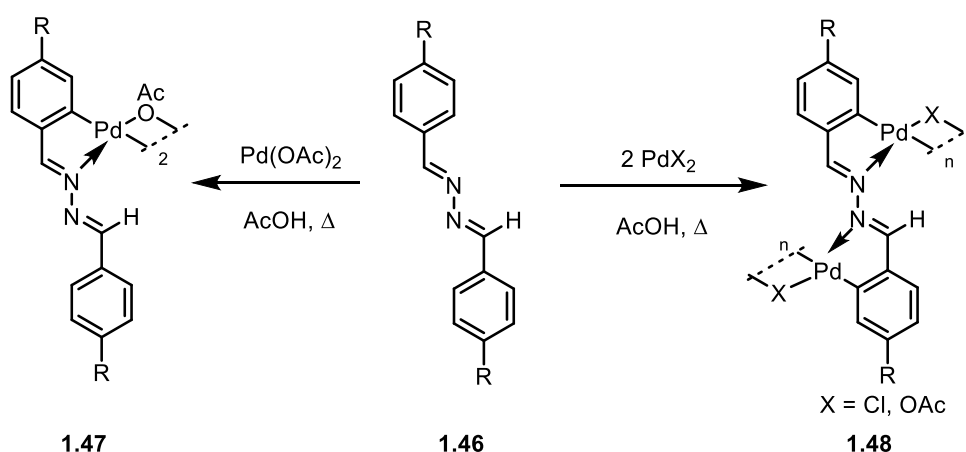
- Steric arrangement around the donor atom and the metal: the ease of cyclometallation reactions for saturated carbon atoms decreases from primary to tertiary, *e.g.* compounds with large *N*-substituents such as 8-alkylquinolines react with palladium(II) much faster if there is methyl group on the 8-position than an ethyl group (Scheme 20), due to the decrease in the steric shielding of the nitrogen atom.¹⁰⁷



Scheme 20: Cyclopalladation reactions with substituted alkylquinolines.

The same trend has been observed in *P*- and *S*-donor ligands; for example tertiary carbons in phosphines cannot be palladated even in the presence of bulky substituents.¹⁰⁸

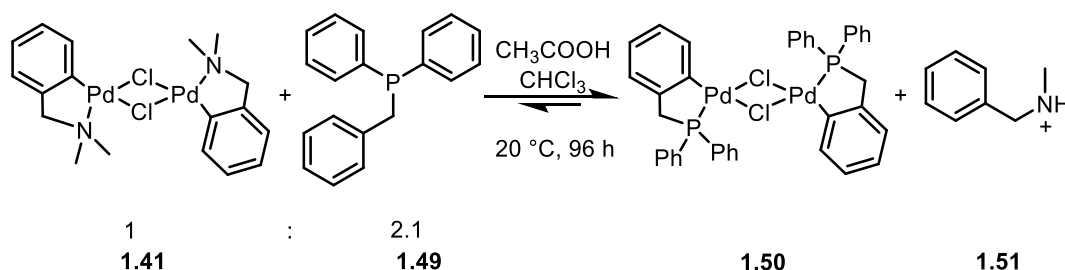
Many external factors beyond the features of the substrate are also important in the formation of palladacycles, including the solvent, metallating agent, specific reaction conditions and presence or absence of an external base. The most commonly used sources of palladium are palladium(II) salts such as $\text{Pd}(\text{OAc})_2$ or $\text{Pd}(\text{acac})_2$, and tetrachloropalladate salts of the form $\text{M}_2[\text{PdCl}_4]$ ($\text{M} = \text{Li, Na, K}$).¹⁰¹ The structural features of palladium acetate and their effects on its reactivity have been extensively studied.¹⁰⁹⁻¹¹⁰ By varying the cyclopalladating agent, it is possible to obtain different degrees of metallation for some ligands, such as in the reaction of benzylideneazines with $\text{Pd}(\text{OAc})_2$ and PdCl_2 (Scheme 21), where the reaction with palladium chloride produces only dicyclopalladated compounds whereas the reaction with palladium acetate gives mono- and di-metallated derivatives depending on the reaction conditions.^{104,111-112}



Scheme 21: Difference in reactivity of benzylideneazines with Pd(OAc)₂ and PdX₂.

Different sources of palladium can also lead to different mechanisms in reactions with the same substrate; this important aspect will be further discussed in Chapter 2.

An alternative source of palladium could also be a pre-formed Pd complex where a cyclometallated ligand is exchanged for a different one in a reaction called transcyclometallation (Scheme 22).^{60,113} It is a particular type of C–H bond activation reaction to form metallacycles where a ligand-exchange process takes place using another pre-made metallacycle and involves M–C bond breaking followed by a M–C' formation.



Scheme 22: Example of transcyclometallation reaction (Pfeffer *et al.*).

This kind of reaction has been extensively studied by different research groups and will be further discussed in Chapter 3.^{99,114-115}

The choice of the solvent in cyclopalladation reactions is very important and is often linked to the palladium source used. The most commonly used solvent is methanol due to its ability to dissolve a wide range of palladium salts and the fact that it favours the formation of vacant sites of coordination on the palladium atom.¹⁰¹ A typical example of this solvent effect is the cyclopalladation reaction of azobenzene which does not take place in non-polar solvents but occurs after the addition of an alcohol or water to the reaction mixture.¹⁰¹ Sometimes the choice of the solvent can also strongly affect the yield of the reaction (see Chapter 2).

Cyclopalladation reactions are often linked with the elimination of a proton from the starting substrate and if this proton forms a strong acid such as HCl a base is necessary to neutralise it. Bases often used for this purpose are sodium acetate,^{102,116-118} NaOH¹¹⁹⁻¹²¹ or aliphatic amines such as trimethylamine or tributylamine.⁹⁷ If the substrate has basic properties (*e.g.* an amine), it can also be used in excess (see Chapter 2).¹²²

The formation of palladacycles, *via* C–H activation, can proceed by a number of different mechanistic pathways: electrophilic substitution, oxidative addition, σ -bond metathesis^{59,93} or concerted metalation deprotonation (CMD or AMLA-6).^{20,66} The cyclopalladation of amino-based substrates has been extensively studied^{94,123-124} and the main two mechanisms proposed for this process are electrophilic aromatic substitution ($S_{E}Ar$)⁶⁴ and concerted metalation deprotonation (AMLA-6 or CMD).^{20,66} In the first, the C–H activation proceeds *via* a Wheland intermediate (Figure 8)⁶⁵ and a covalent bond is consequently formed between the carbon atom of the arene and the Pd. In these mechanisms the palladium acetate is acting as an intramolecular base and is electrophilically activating the arene.

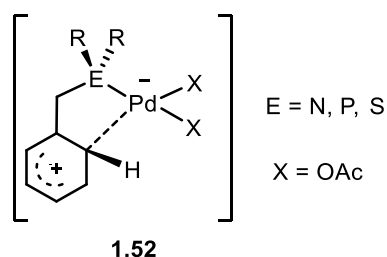
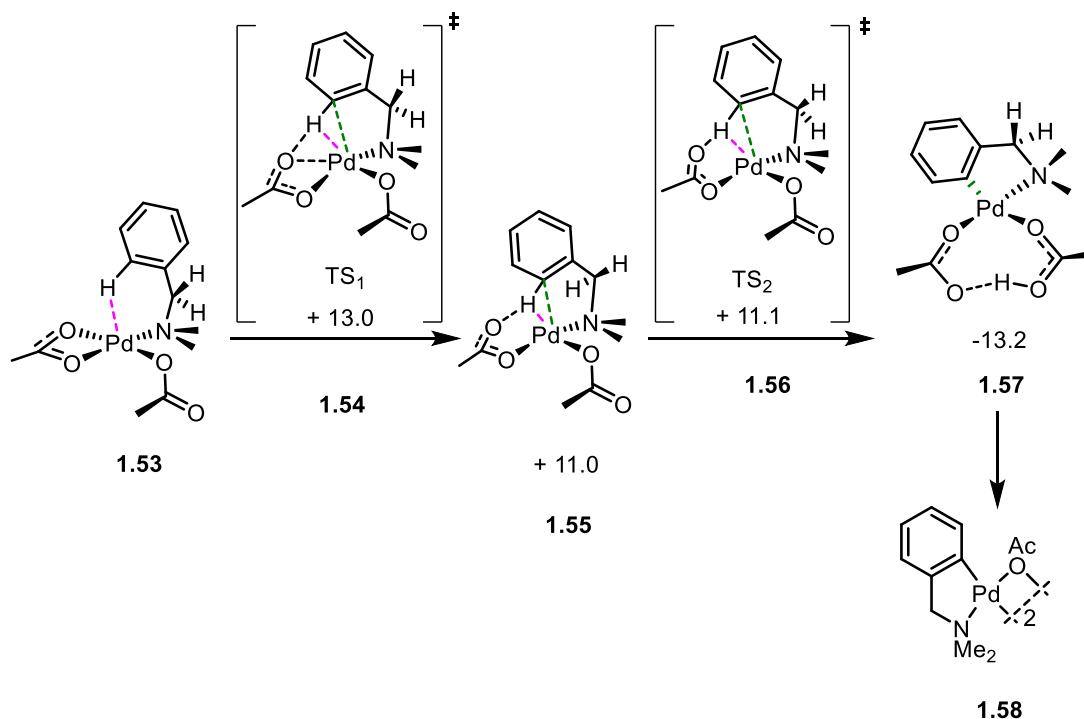


Figure 8: Example of the Wheland intermediate in a $S_{E}Ar$ mechanism.¹²⁴

Macgregor and co-workers suggested an AMLA-6 (or CMD) mechanism^{41,57,67} which, as previously discussed, proceeds *via* an agostic C–H interaction followed by six-membered cyclic transition state (Scheme 23) involving an acetate, which is acting as a base, but also enhancing the electrophilicity of the Pd(II) center. The formation of the agostic species is the rate determining step in their calculation, showing a parallel with Fagnou's intermolecular C–H functionalisation reaction.



Scheme 23: CMD mechanism suggested by Macgregor *et al.*⁹⁴

A further discussion of these two mechanisms will be given in Chapter 2 where the investigation of intramolecular C–H activation of fluorinated benzylamines will be described.

1.6 Project aims and objectives

1.6.1 Aims

The aim of this project was the investigation of the effect of fluorine substituents on the regioselectivity of intramolecular C–H activation reactions of fluoroaromatics at different transition metals. The substrates taken into consideration were a series of partially and totally fluorinated *N,N*-dimethyl-benzylamines and diphenylbenzylphosphines.

1.6.2 Objectives

- I. To investigate intramolecular C–H activation reactions of fluorinated *N,N*-dimethyl-benzylamines at Pd(II) to assess if the presence of fluorine atoms on the aromatic ring can lead to a regioselective C–H activation, in particular if an *ortho* fluorine effect could be observed (Chapter 2);¹²²

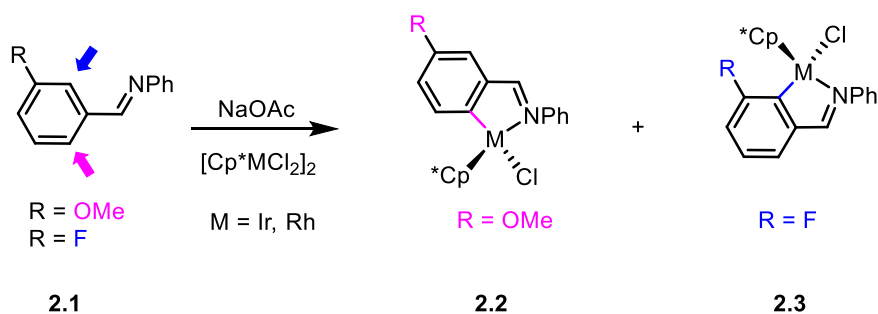
- II. To investigate the regioselectivity of direct and transmetallation C–H activation reactions of fluorinated diphenylbenzylphosphines at Pd(II) (Chapter 3);
- III. To explore the behaviour of fluorinated *N,N*-dimethylbenzylamines on C–H activation reactions at Rh(III), Ir(III) and Ru(III) to assess if regioselective transformations could be obtained (Chapter 4);
- IV. To undertake a preliminary investigation of fluorinated *N,N*-dimethylbenzylamines and diphenylbenzylphosphines towards stoichiometric C–F activation and catalytic C–F functionalisation reactions (Chapter 5).

Chapter 2: Fluorinated aminopalladacycles

2.1 Introduction

In the synthesis of active pharmaceuticals and the construction of building blocks for the total synthesis of natural products, the functionalisation of a C–H bond to form a new C–Het or C–C bond is one of the most useful processes available, thanks to its inherent atom economy and efficiency.⁵ In the past decade the field has expanded to the point where it has become a potential replacement for traditional cross-coupling reactions,^{6–9} processes that require pre-activation of substrates.^{10–13} Control of regioselectivity however remains one of the main challenges for the field, as discussed in Chapter 1, and the use of directing groups *ortho* or *meta* to the target C–H site,^{22,33} offers a starting point to develop regioselective reactions, despite certain limitations, *e.g.* requirement for directing groups which are often difficult to remove.

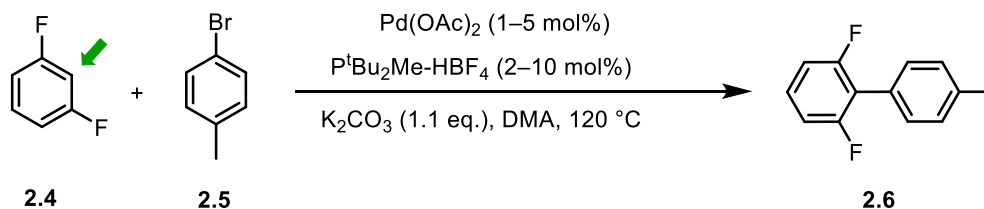
The role of fluorine substituents as directing groups in intramolecular reactions at Ir and Rh has been described by Jones and co-workers for C–H activation reactions of 2-phenylpyridines and phenylimines, and the regioselectivity, mechanism and kinetics of the reactions have been investigated (Scheme 24).¹¹⁶



Scheme 24: C–H activation reactions at Ir and Rh of substituted phenylimines (Jones *et al.*).

Jones and co-workers reported that substrates with electron-withdrawing substituents reacted significantly more slowly than those with electron-donating substituents, which suggests an electrophilic aromatic substitution mechanism (S_EAr).¹²⁵ They also noted that the regioselectivity was extremely sensitive to steric effects, but temperature independent for Ir and Rh. Finally the authors also found that the regioselectivity was solvent dependent in reactions at Ir but solvent independent in reactions at Rh and that an *ortho*-fluorine effect was observed for substrates bearing a *meta*-F substituent, favoring the activation of the C–H bond *ortho* to the C–F bond.¹¹⁶

Fagnou and co-workers, as discussed in Chapter 1, also reported the use of fluorine atoms as directing groups in intermolecular reactions catalyzed by Pd, in reactions proceeding *via* concerted metallation deprotonation mechanism (known as CMD^{20,66} or AMLA-6^{57,94}), promoting C–H functionalisation *ortho* to the fluorine atoms (Scheme 25).^{14,20}



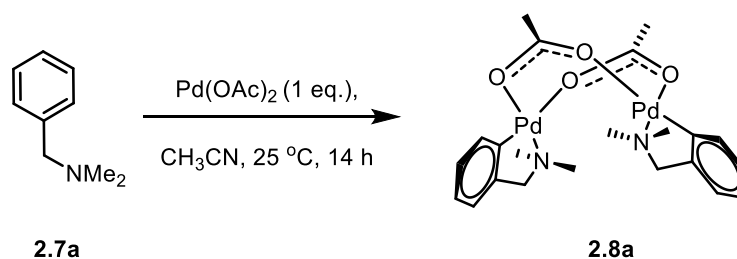
Scheme 25: Intermolecular C–H functionalisation reaction at Pd of fluorinated aromatics (Fagnou *et al.*).

In this chapter the effect of fluorine substituents on the regioselectivity of directed intramolecular reactions⁹⁴ of fluorobenzylamines at Pd^{II} to form fluorinated palladacycles and on the structures of the resulting metallacycles are investigated. The aim was to explore whether an *ortho* fluorine effect could be observed in intramolecular reactions that proceed *via* a concerted metallation deprotonation mechanism^{20,66} (CMD) or an electrophilic aromatic substitution (S_EAr) mechanism to form fluorinated metallacycles. The same mechanisms have been investigated computationally⁶⁸ and experimentally for intermolecular reactions at Pd,²⁰ Rh and Ir,¹¹⁶ where an *ortho* fluorine effect could be observed, due to the acidity increase of the proton *ortho* to fluorine and strengthening of the Pd–C bond as suggested by Perutz and co-workers.⁶⁸

2.1.1 Model reaction

The study concerning the regioselectivity of intramolecular C–H activation started with the selection of two model reactions:

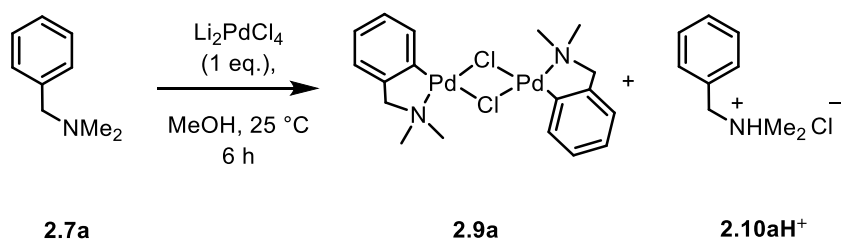
- The cyclometallation of the non-fluorinated *N,N*-dimethylbenzylamine (**2.7a**) with Pd(OAc)₂ forming the known palladacycle **2.8a** (Scheme 26).¹⁰⁴



Scheme 26: Synthesis of palladacycle 2.8a taken as model reaction.

The reaction conditions in Scheme 26 were slightly altered with respect to the original procedure reported by Thompson and Heck,¹⁰⁴ following studies conducted in the Fairlamb group, and acetonitrile was used as the solvent instead of acetone.^{109,122} These improved conditions afforded a 90% yield of palladacycle **2.8a** and single crystals of the complex, suitable for X-ray analysis, were obtained by slow diffusion of hexane into a saturated solution of the compound in chloroform.

- The cyclometallation of the non-fluorinated *N,N*-dimethylbenzylamine with Li_2PdCl_4 forming the known palladacycle **2.9a** (Scheme 27).



Scheme 27: Synthesis of palladacycle 2.9a taken as model reaction.

The reaction conditions in Scheme 27 have again been slightly changed from the original procedure reported by Cope and co-workers for the synthesis of palladacycle **2.9a**:⁹⁷ the reaction time was decreased from 20 to 6 hours.¹²²

The model reactions were chosen on the basis of their known and well-studied reaction mechanisms. The cyclometallation reaction of *N,N*-dimethylbenzylamine (**2.7a**) with $\text{Pd}(\text{OAc})_2$ has been investigated extensively over the last 30 years. Ryabov and co-workers initially proposed that the reaction proceeds *via* an electrophilic aromatic substitution, where the Wheland intermediate (Figure 9) is formed by the intramolecular attack on the C–H bond by the electrophilic palladium followed by the coordination of the nitrogen to the metal centre.⁶⁴

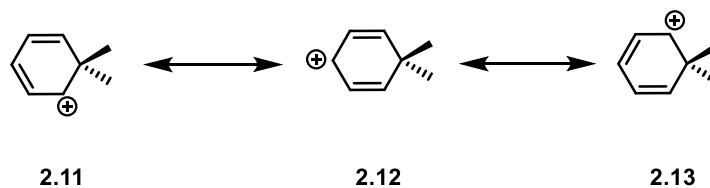
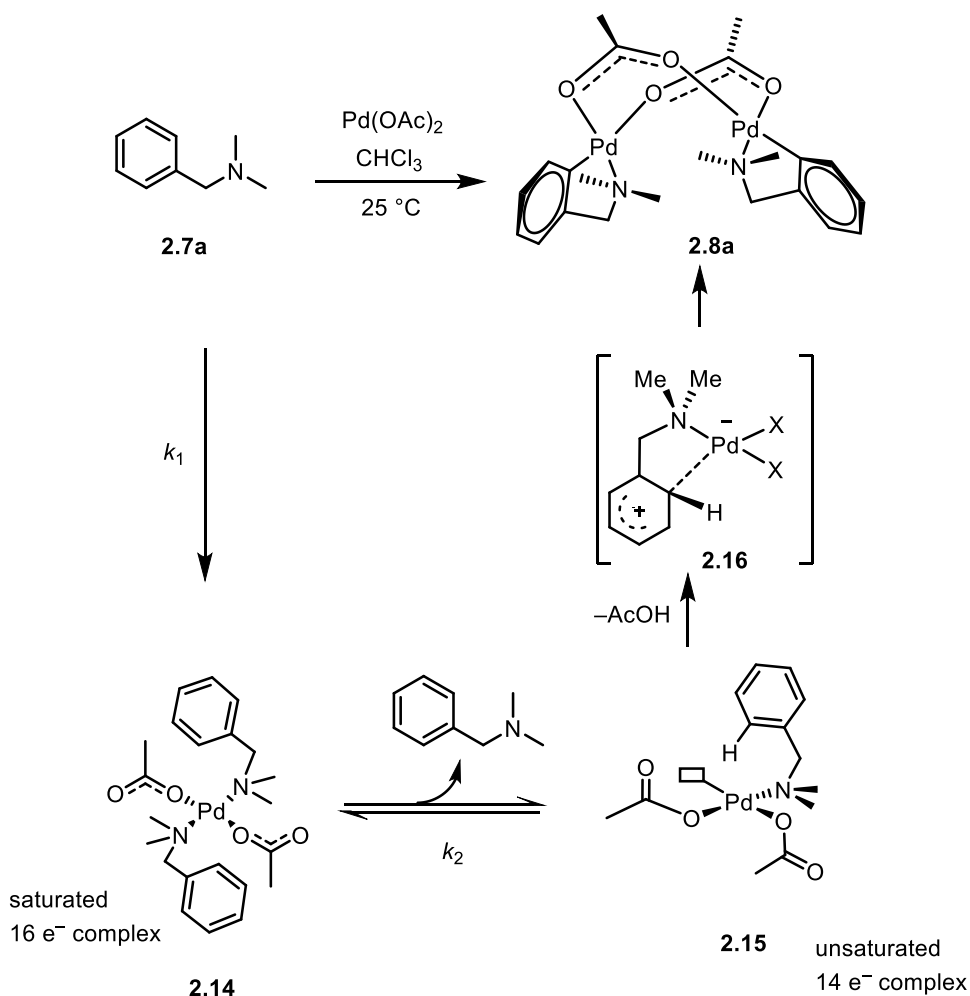


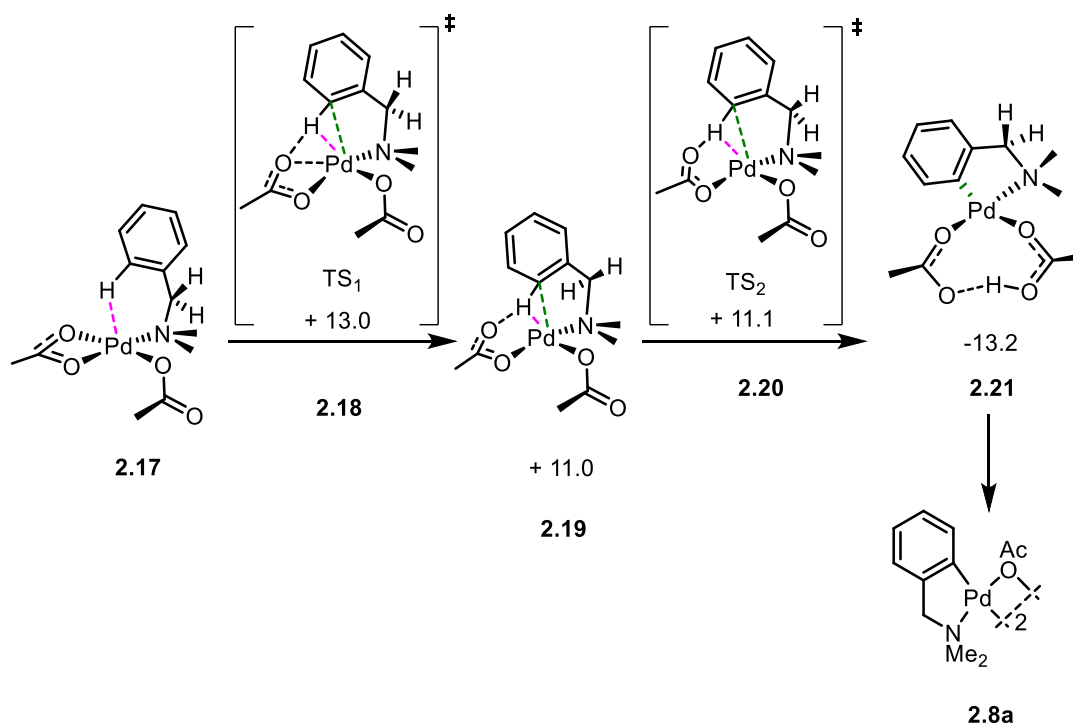
Figure 9: Resonance forms of Wheland intermediate.

Ryabov *et al.* suggested the formation of palladacycle **2.8a** *via* an unsaturated 14 e⁻ complex (**2.14**) formed after the 16 e⁻ complex (**2.15**) due to the rate constant k_1 being smaller than k_2 (Scheme 28).



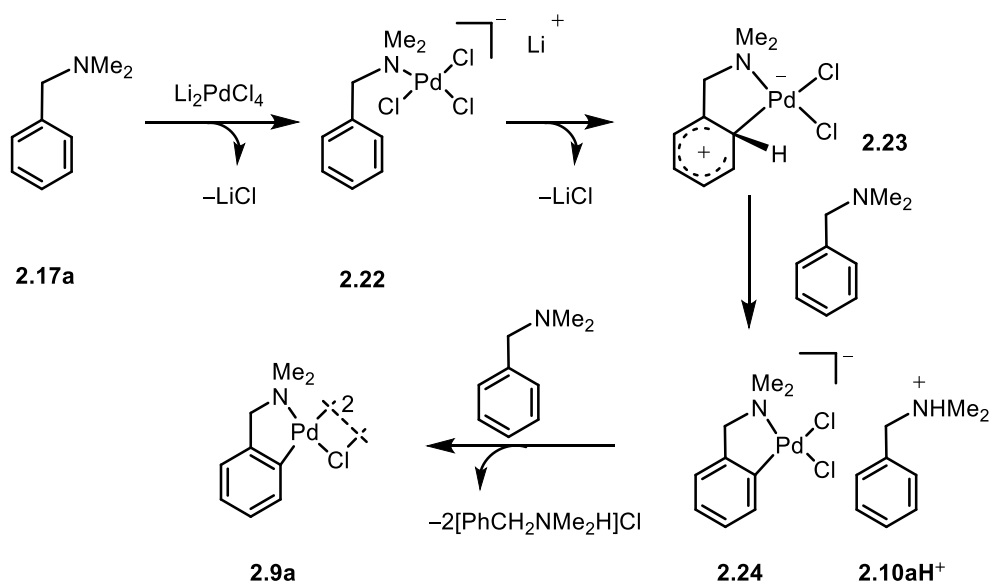
Scheme 28: Electrophilic aromatic substitution mechanism suggested by Ryabov *et al.*

Macgregor and co-workers later studied the mechanism of the same reaction using DFT calculations, suggesting that the reaction proceeds *via* an agostic C–H intermediate and not *via* the arenium intermediate, in an AMLA-6 mechanism,^{20,66} whereby the acetate group coordinated to the metal deprotonates the C–H bond whilst the Pd–C bond is forming (Scheme 29).⁹⁴



Scheme 29: Computational reaction profile (kcal/mol) and bond lengths (Å) for the cyclometallation of Pd(OAc)₂(DMBA-H) proceeding via an AMLA-6 mechanism (Macgregor *et al.*).

The mechanism of the cyclometallation reaction of the non-fluorinated *N,N*-dimethylbenzylamine **2.7a** with Li₂PdCl₄ forming the known palladacycle **2.9a** is instead suggested to be an electrophilic aromatic substitution (S_EAr) mechanism (Scheme 30) as reported by Jones and co-workers in the C–H activation of phenylimines at Rh and Ir discussed previously.¹¹⁶

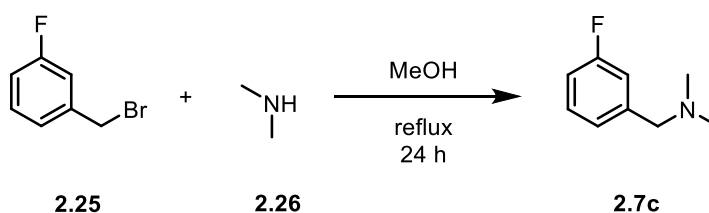


Scheme 30: Proposed electrophilic aromatic substitution mechanism for 2.17a.

Using the optimised conditions (Scheme 26 and Scheme 27), the synthesis of fluorinated palladacycles **2.8a–f** and **2.9a–f** (see X-ray structures in Appendix II) was attempted to assess the regioselectivity of cyclometallation reactions of fluorinated benzylamines **2.7a–f**.

2.1.2 Fluorinated *N,N*-dimethylbenzylamines

The synthesis of 3-fluoro *N,N*-dimethylbenzylamine (**2.7c**) was already reported by Liu and Sayre,¹²⁶ whereby a methanolic solution of dimethylamine reacts with 3-fluorobenzylbromide (**2.25**) in a nucleophilic substitution reaction to form the desired product, which was isolated following an aqueous workup (Scheme 31).



Scheme 31: Synthesis of 2.7c (originally reported by Liu *et al.*).

The reaction was taken as a model and used to synthesise all the required pre-ligands (**2.7b–f**, Figure 11). Their characterisation is discussed in more detail below.

2.1.3 Acetate-bridged and chloride-bridged palladacycles

The metallacycles discussed in this chapter are both acetate-bridged and chloride-bridged palladacycles **2.8a–f** and **2.9a–f**, respectively (Figure 10).

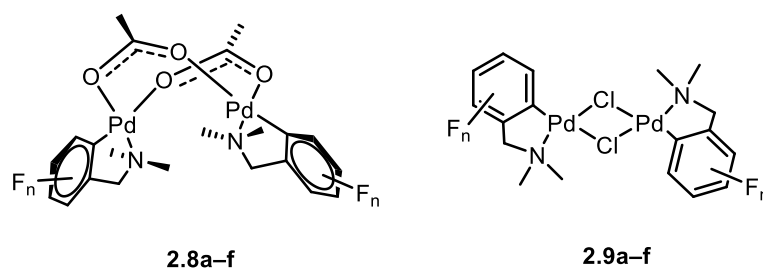


Figure 10: General structure of fluorinated acetate- and chloride-bridged palladacycles.

The acetate-bridged palladacycles (**2.8a–f**) obtained from Pd(OAc)₂ possess a “clamshell” type structure, non-planar at palladium, similar to that reported for [(2-phenylpyridine)Pd(μ-OAc)]₂ by Bercaw and co-workers,¹²⁷ where the coordination plane containing the palladium atom is almost perpendicular to the acetate bridge. Bercaw *et al.* suggested that this geometry is a consequence of the d⁸–d⁸ interaction of the two palladium atoms and a π-stacking interaction between the aromatic rings.¹²⁷⁻¹²⁸ The chloride-bridged palladacycles (**2.9a–f**) show a square-planar geometry with two ligands, bound through an M–N and an M–C(sp²) bond, forming two equal five-membered rings, as reported by Mendes for the equivalent non-fluorinated palladacycle **2.9a**.¹²⁹ The structural analysis of all the palladacycles (**2.8a–f** and **2.9a–f**) is discussed in section 2.4 of this chapter.

Palladacycles in general are widely used as pre-catalysts in Heck, Suzuki¹³⁰⁻¹³¹ and Sonogashira reactions,¹³² Stille cross-couplings^{84,133-134} and carbonylation reactions,¹³⁵ and recently their anti-cancer activities have been assessed and reviewed.⁸⁸ The addition of a fluorine substituent on the benzyl ring of these metallacycles could lead to different catalytic activity in cross coupling reactions and further investigation is ongoing.

2.2 Results

2.2.1 Fluorinated *N,N*-dimethylbenzylamines

The fluorinated substrates chosen for the cyclometallation reactions with Pd(OAc)₂ were mono- and di-fluorinated tertiary benzylamines **2.7b** and **2.7d**, respectively, presenting just one position (C-6 in Figure 11) for the C–H activation reaction, and mono- and di-fluorinated benzylamines **2.7c** and **2.7e** offering two possibilities for the reaction at C-2 and C-6 (indicated with coloured arrows in Figure 11). Compound **2.7f** shows two equivalent positions thus offering no choice.

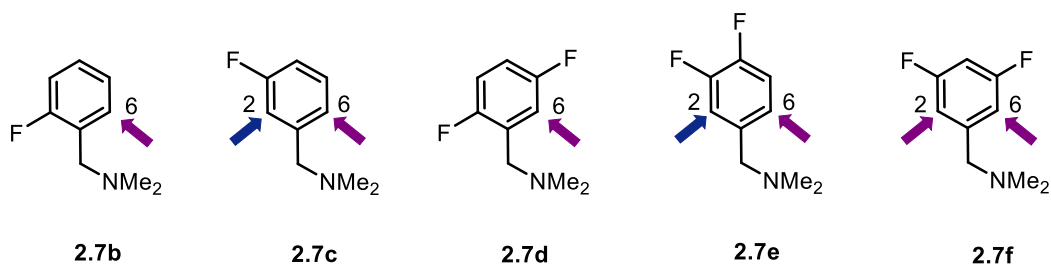


Figure 11: Fluorinated *N,N*-dimethylbenzylamines.

All of the fluorinated benzylamines (**2.7a–f**) were fully characterised by NMR (Table 1) and IR spectroscopies and ESI mass spectrometry. Taking *N,N*-dimethyl-2-fluorobenzylamine (**2.7b**) as an example, the $^1\text{H-NMR}$ spectrum shows two singlets at δ 2.28 and 3.52 for the methyl and methylene protons respectively. It also shows two triplets of doublets at δ 7.36 ($J = 7.5, 1.7$ Hz) and 7.11 ($J = 7.5, 1.2$ Hz), a multiplet at δ 7.25 and a doublet of doublets of doublets at δ 7.04 ($J = 9.6, 8.2, 1.1$ Hz) for the four magnetically inequivalent aromatic protons (Figure 12).

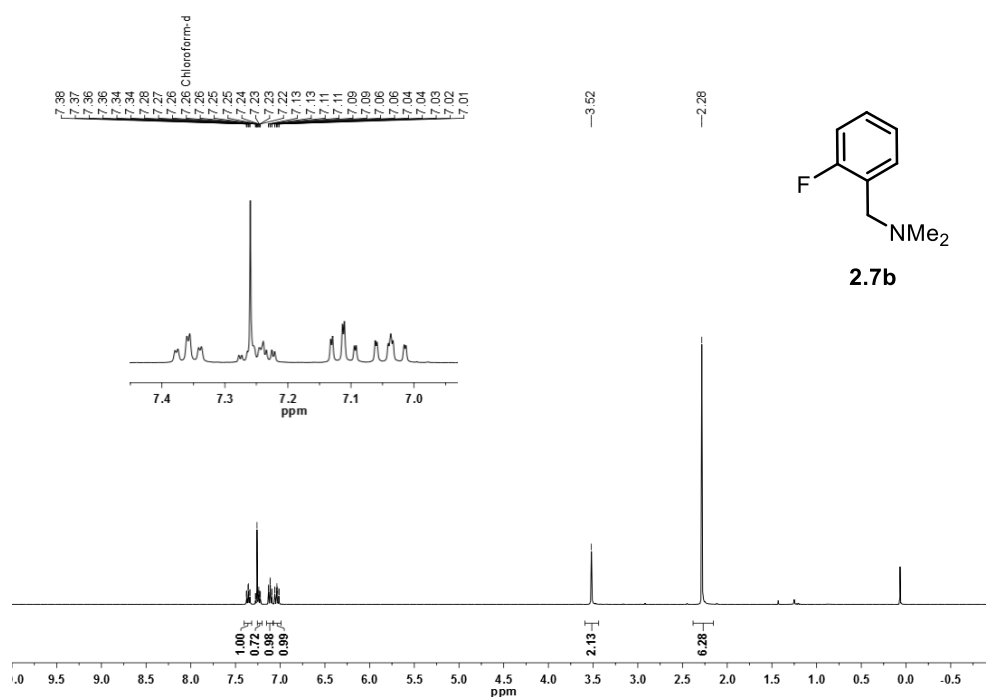


Figure 12: $^1\text{H-NMR}$ of **2.7b at 294.35 K in CDCl_3 (400 MHz).**

The $^{19}\text{F-NMR}$ spectrum shows a multiplet at δ -118.10 (Figure 13) while the $^{13}\text{C-NMR}$ spectrum in CDCl_3 shows six doublets at δ 161.6 ($J = 246.3$ Hz), 131.8 ($J = 4.5$ Hz), 129.1 ($J = 8.1$ Hz), 124.0 ($J = 3.6$ Hz), 115.4 ($J = 22.3$ Hz) and 56.6 ($J = 1.9$ Hz), and a singlet for the methyl carbons at δ 45.3. The first doublet corresponds to the carbon bonded directly to fluorine with a coupling constant typical for a $^1J_{\text{C-F}}$ value.

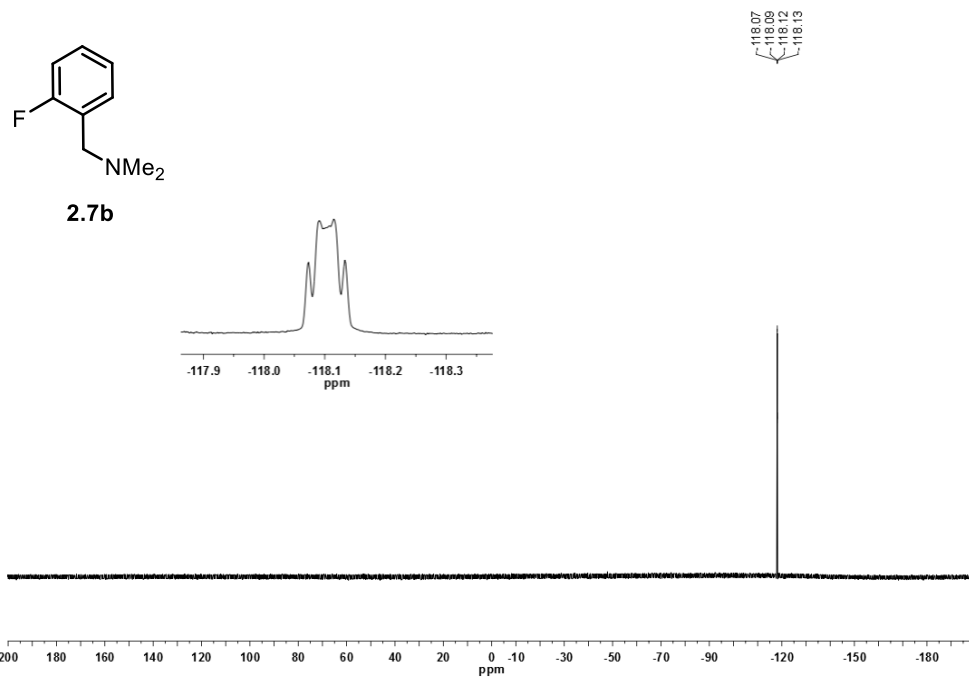


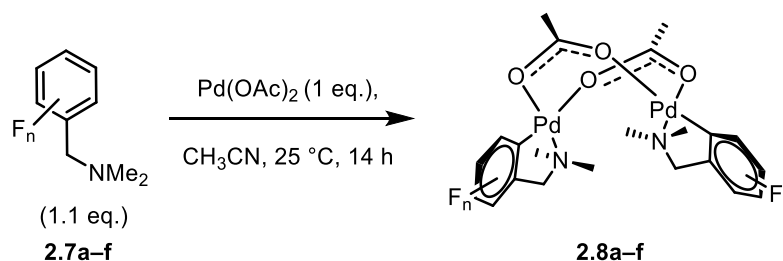
Figure 13: ^{19}F -NMR of 2.7b at 294.35 K in CDCl_3 (376 MHz).

Table 1: $^1\text{H-NMR}$ and $^{19}\text{F-NMR}$ spectroscopic signals of *N,N*-dimethyl-fluorobenzylamines **2.7b–f**.

Compound	δ (^1H) / ppm	δ (^{19}F) / ppm
2.7b	7.36 (td, $J = 7.5, 1.7$ Hz, 1H), 7.25 (m, 1H), 7.11 (td, $J = 7.5, 1.2$ Hz, 1H), 7.04 (ddd, $J = 9.6, 8.2, 1.1$ Hz, 1H), 3.52 (s, 2H), 2.28 (s, 6H);	-118.10 (m)
2.7c	7.27 (m, 1H), 7.08 (d, $J = 7.6$ Hz, 1H), 7.10–7.02 (m, 1H), 6.95 (td, $J = 8.3, 1.8$ Hz, 1H), 3.43 (s, 2H), 2.25 (s, 6H);	-113.70 (m)
2.7d	7.09 (ddd, $J = 8.8, 5.7, 3.2$ Hz, 1H), 6.98 (td, $J = 9.0, 4.5$ Hz, 1H), 6.91 (m, 1H), 3.46 (d, $J = 1.2$ Hz, 2H), 2.27 (s, 6H)	-119.46 (m), -124.33 (dtd, $J = 13.7, 9.1, 4.9$ Hz)
2.7e	7.14 (m, 1H), 7.08 (m, 1H), 7.00 (m, 1H), 3.35 (s, 2H), 2.22 (s, 6H)	-138.4 (m), -140.4 (m)
2.7f	6.91–6.80 (m, 2H), 6.68 (tt, $J = 8.7, 2.2$ Hz, 1H), 3.38 (s, 2H), 2.23 (s, 6H)	-110.55 (m)

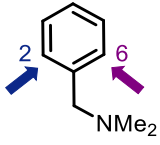
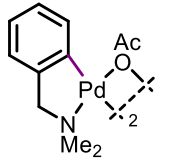
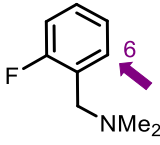
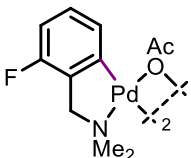
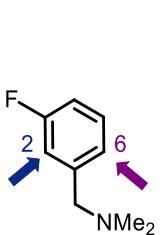
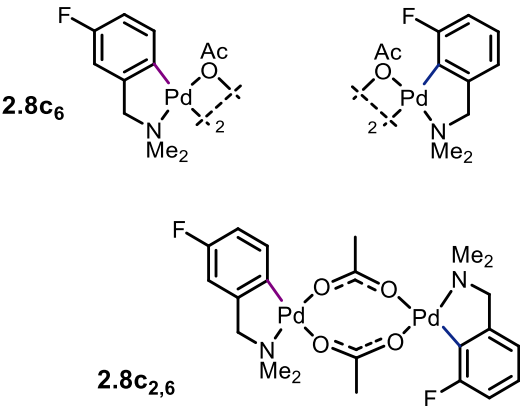
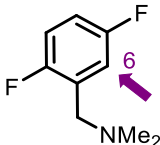
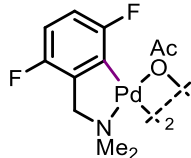
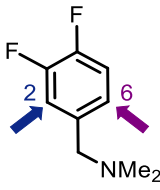
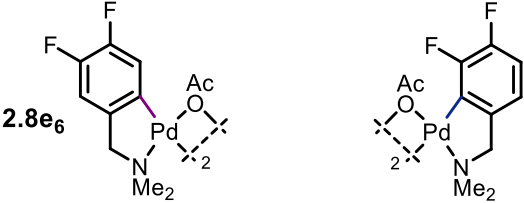
2.2.2 Reaction of fluorinated *N,N*-dimethylbenzylamines with $\text{Pd}(\text{OAc})_2$

Following the identification of the optimised reaction conditions shown in Scheme 32, palladacycles **2.8a–f** were synthesised in good to excellent yields (Table 2).¹²²



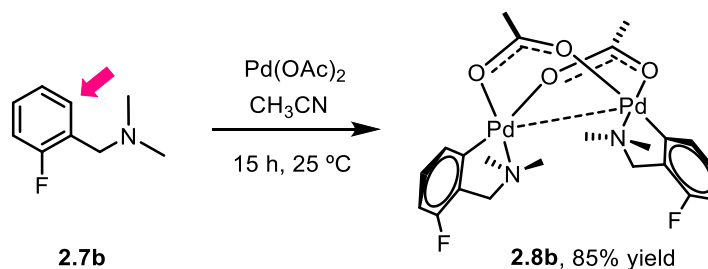
Scheme 32: Cyclopalladation reactions of fluorinated tertiary amines with $\text{Pd}(\text{OAc})_2$.

Table 2: Products from intramolecular C–H activation of fluorinated benzylamines with Pd(OAc)₂.

Substrate	Complex	Combined yield / %
 <p>2.7a</p>	 <p>2.8a</p>	90
 <p>2.7b</p>	 <p>2.8b</p>	85
 <p>2.7c</p>	 <p>2.8c₆ 2.8c₂ 2.8c_{2,6}</p>	76
 <p>2.7d</p>	 <p>2.8d</p>	78
 <p>2.7e</p>	 <p>2.8e₆ 2.8e₂</p>	75

		82

By way of example, a full spectroscopic analysis of complex **2.8b** is described below. Reaction of *N,N*-dimethyl-2-fluorobenzylamine (**2.7b**) with Pd(OAc)₂ for 14 h in acetonitrile afforded palladacycle **2.8b** in 85% yield.



Scheme 33: Synthesis of palladacycle 2.8b.

The ¹H-NMR spectrum of **2.8b** (Figure 14) is consistent with a dinuclear complex showing C₂ symmetry, and with the diastereotopic protons in the CH₂ group appearing as an AB quartet at δ 3.47 (*J*_{H-H} = 14.2 Hz). An additional coupling could be observed in the low frequency component of the AB quartet due to the coupling with the fluorine atom (*J*_{H-F} = 1.4 Hz). The carbons and protons of the *N*-methyls are split into two sets of signals corresponding to the axial and equatorial positions of the five-membered ring. While in the free substrate (**2.7b**) the methyl protons resonate at δ 2.28, in palladacycle **2.8b** they are shifted to high and low frequency into two different signals at δ 2.07 and 2.83. In the ¹³C-NMR spectrum the resonances of the two methyl groups also appear as two separate signals, shifted to high frequency from δ 45.3 (free substrate) at δ 51.6 and δ 52.9 (Figure 15).

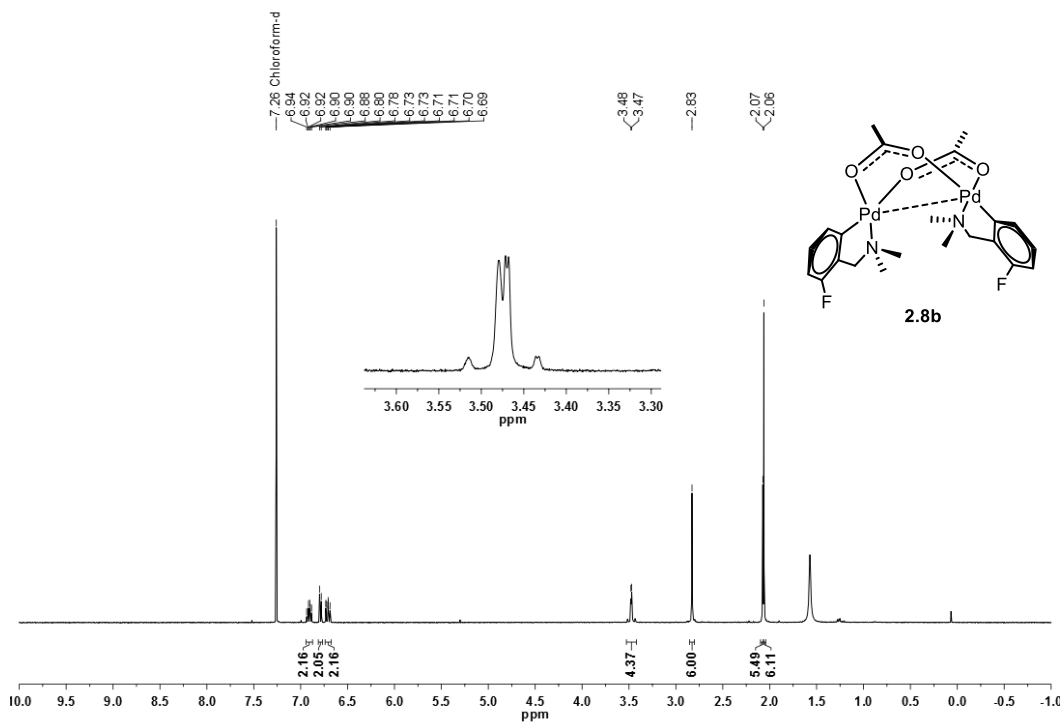


Figure 14: ^1H -NMR of palladacycle **2.8b** at 294.15 K in CDCl_3 (400 MHz).

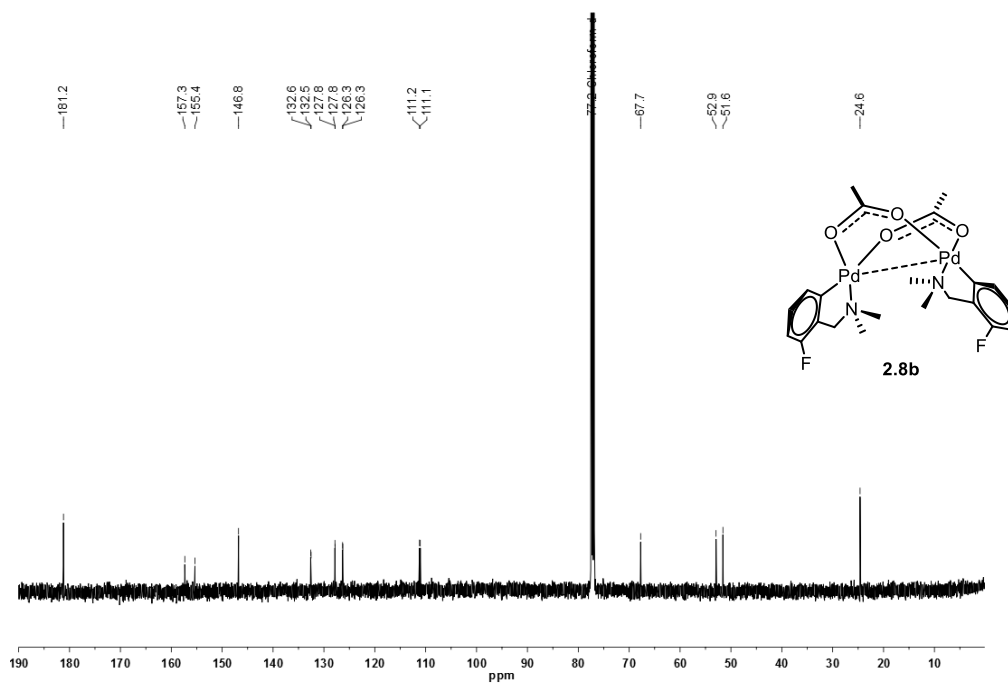


Figure 15: $^{13}\text{C}\{^1\text{H}\}$ -NMR of palladacycle **2.8b** at 298 K in CDCl_3 (126 MHz).

The ^{19}F -NMR spectrum shows a doublet of doublets at $\delta -115.01$ ($J = 9.7, 5.5$ Hz), similar to the free substrate **2.7b**.

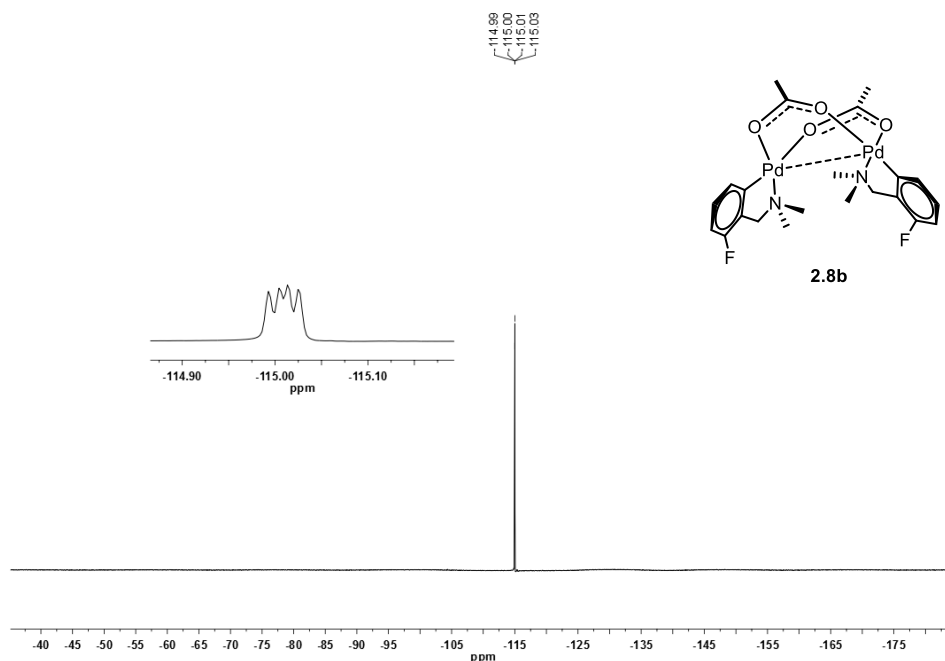


Figure 16: ^{19}F -NMR of palladacycle **2.8b** at 300 K in CDCl_3 (471 MHz).

The LIFDI method¹³⁶ was used to record mass spectra and the molecular ion with the typical isotopic pattern of a dinuclear palladium complex was the only peak observed ($m/z = 636.02$) confirming that the dinuclear Pd_2 species is present in solution. Palladacycle **2.8b** was crystallized by slow diffusion of hexane into a concentrated solution of the compound in chloroform (Figure 17).

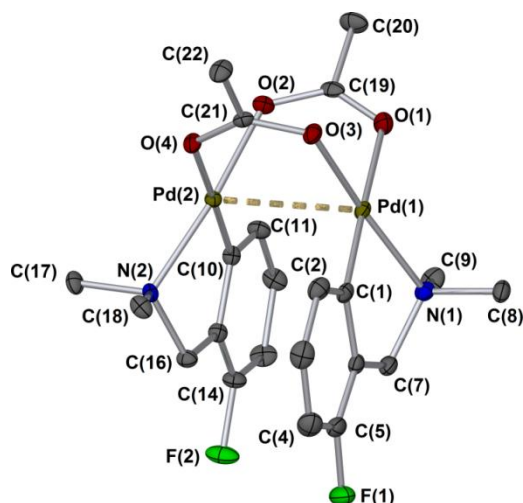


Figure 17: Molecular structure of palladacycle **2.8b**. Hydrogen atoms were omitted for clarity; thermal ellipsoids shown with probability of 50%.

All the other palladacycles **2.8a–f** were synthesised, characterised and crystallised in the same way as **2.8b** (see crystallographic analysis in section 2.4).

The reaction with 3-fluoro-*N,N*-dimethylbenzylamine (**2.7c**) allowed an assessment of the effect of the presence of a fluorine atom on the regioselectivity of C–H activation reactions due to the two possible options for attack, *ortho* or *para* to fluorine (arrows in Figure 18).

A mixture of isomeric forms of palladacycle **2.8c** (**2.8c₂**, **2.8c₆**, and **2.8c_{2,6}** in Figure 18) was obtained in 76% overall yield, and a single crystal analysed by X-ray gave a disordered crystal structure due to the different positions of the fluorine atoms on the ring.[†]

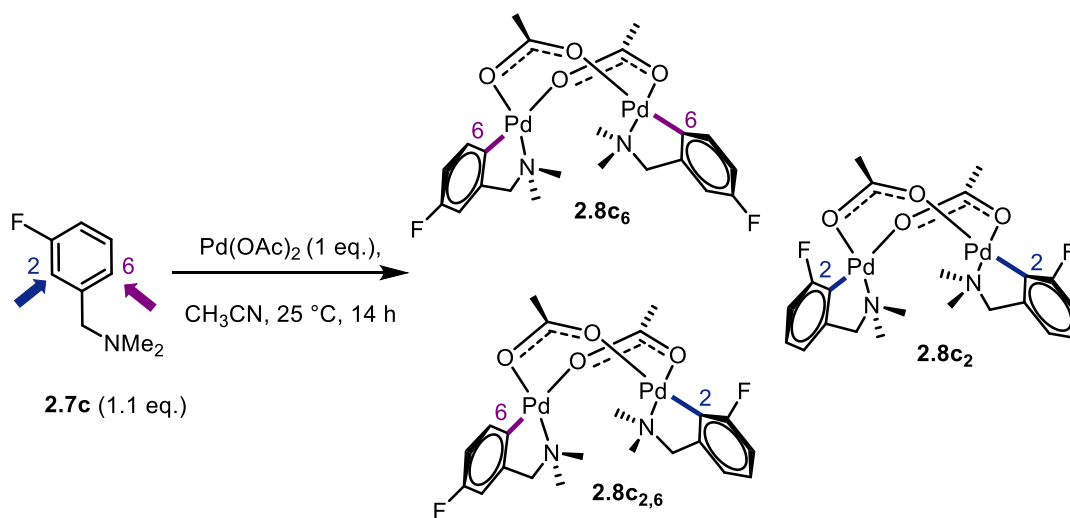


Figure 18: Synthesis of palladacycle **2.8c (mixture of isomeric forms).**

The ¹⁹F-NMR spectrum of the mixture of isomers **2.8c** shows four signals for the four magnetically inequivalent fluorine atoms: two doublets of doublets at $\delta -104.25$ ($J = 8.8, 5.2$ Hz) and $\delta -104.47$ ($J = 8.8, 5.1$ Hz) for the fluorines *ortho* to palladium in **2.8c₂** and **2.8c_{2,6}**, and a multiplet at $\delta -119.46 - -119.51$ corresponding to two overlapping signals for the fluorines *para* to palladium in **2.8c₆** and **2.8c_{2,6}** (observed in a ¹⁹F-COSY-NMR spectrum).

[†] The nomenclature of the complex, *e.g.*, **2.8c₆**, indicates complex **2.8c** formed from substrate **2.7c** by C–H activation in position 6 (numbering from the benzyl arm). Arrows represent the available sites for C–H activation.

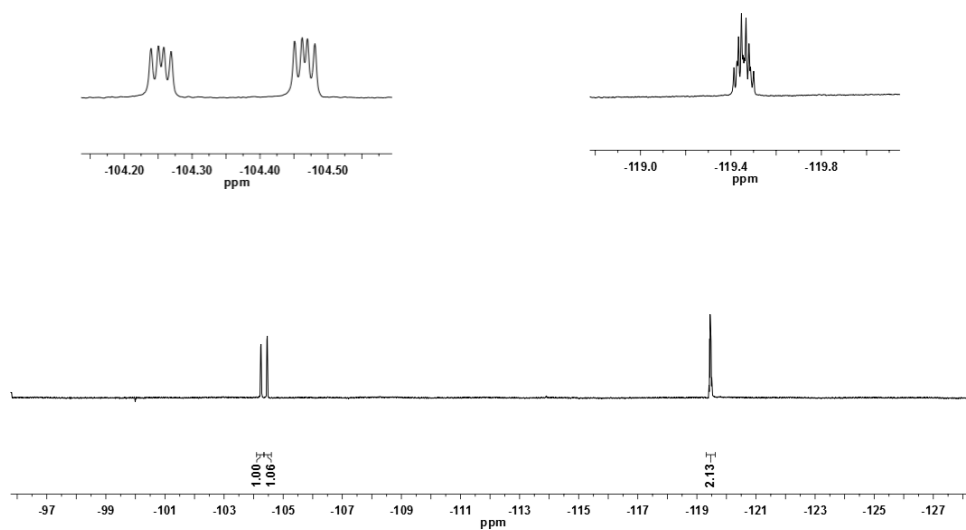
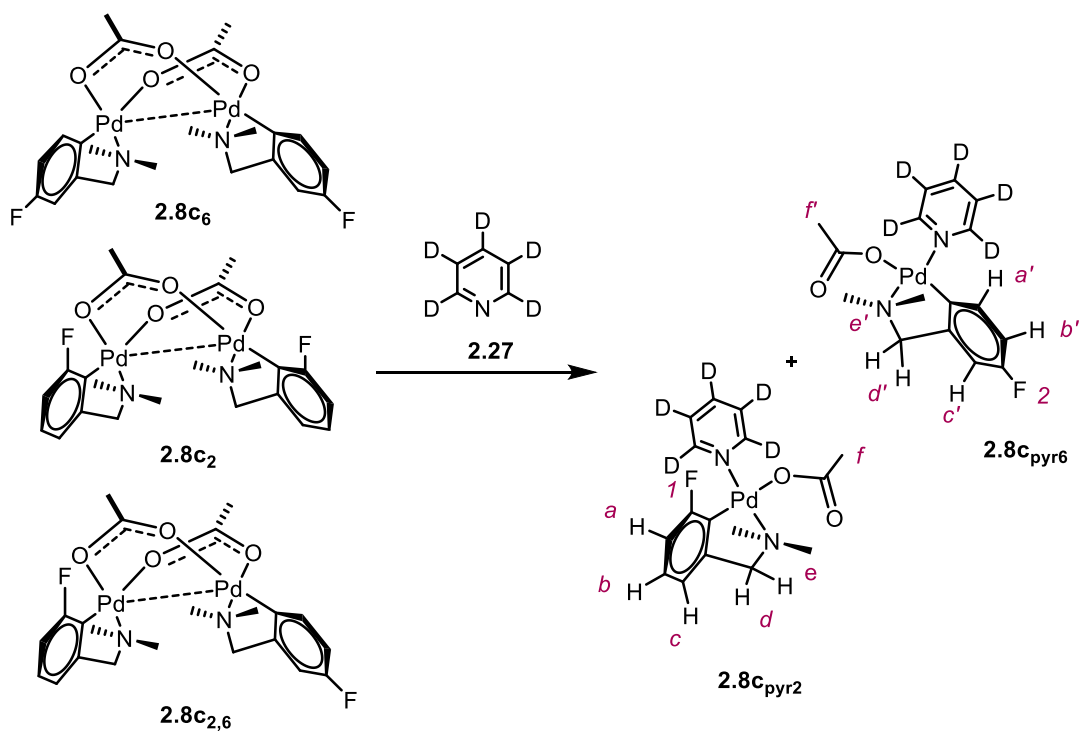


Figure 19: ^{19}F -NMR spectrum of mixture of isomers of palladacycle **2.8c** in CDCl_3 (471 MHz).

To determine the ratio between the regioisomers and assess whether the *para* or the *ortho* isomer was the major species, the mixture of isomers was reacted with pyridine- d_5 in order to split each palladacycle into two monomers by coordination to the palladium.



Scheme 34: Formation of monomers **2.8c_{pyr2}** and **2.8c_{pyr6}** from **2.8c** isomers.

In the ^1H -NMR spectrum of the resulting products, the integration of the methylene protons of each monomer gives a ratio of 1:0.9 (confirmed by integration of the fluorine signals) indicating a lack of any significant regioselectivity in the intramolecular C–H activation

reactions with Pd(OAc)₂. The two monomers obtained, **2.8c_{pyr2}** and **2.8c_{pyr6}**, have two different environments in the ¹⁹F-NMR spectrum (Figure 20): a doublet of doublets at δ -100.98 (*J* = 8.7, 5.4 Hz) for monomer **2.8c_{pyr2}** with the fluorine *ortho* to palladium and a doublet of doublets at δ -119.88 (*J* = 15.9, 9.6 Hz) for monomer **2.8c_{pyr6}** with the fluorine *para* to palladium. The ¹H-NMR spectrum (Figure 21) shows a chemical shift for the proton *a'* (label in Scheme 34) of 6.28 ppm that is upfield due to anisotropic shielding of the pyridine ring suggesting that the two nitrogens are *trans* to each other as reported for similar systems.¹³⁷ Moreover the ¹H-NMR spectrum shows just one doublet for the methylene protons and one singlet for the methyl groups bonded to the nitrogen atom.

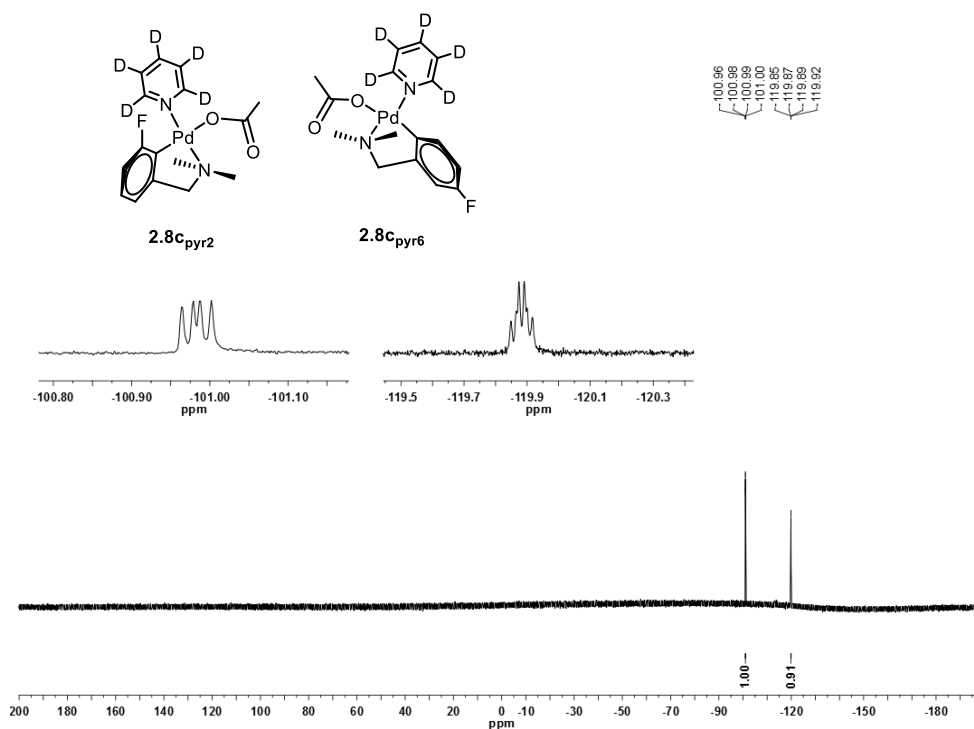


Figure 20: ¹⁹F-NMR spectrum of palladacycle **2.8c_{pyr2}** and **2.8c_{pyr6}** at 293.45 K in pyr-*d*₅ (376 MHz).

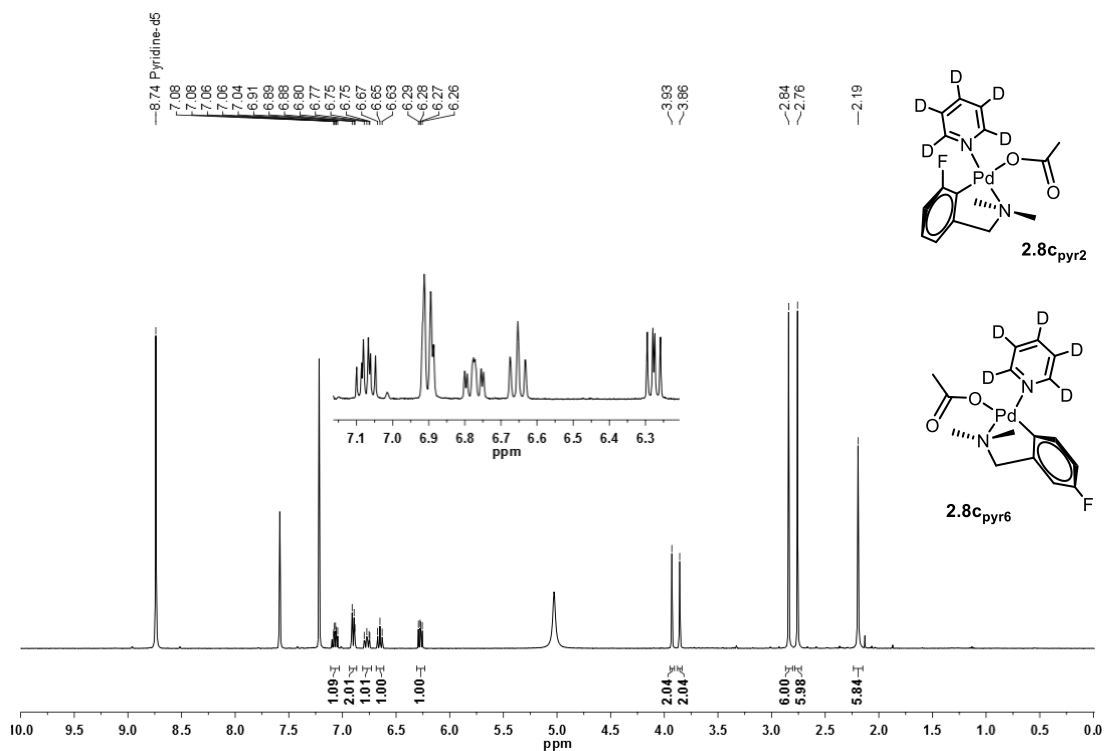
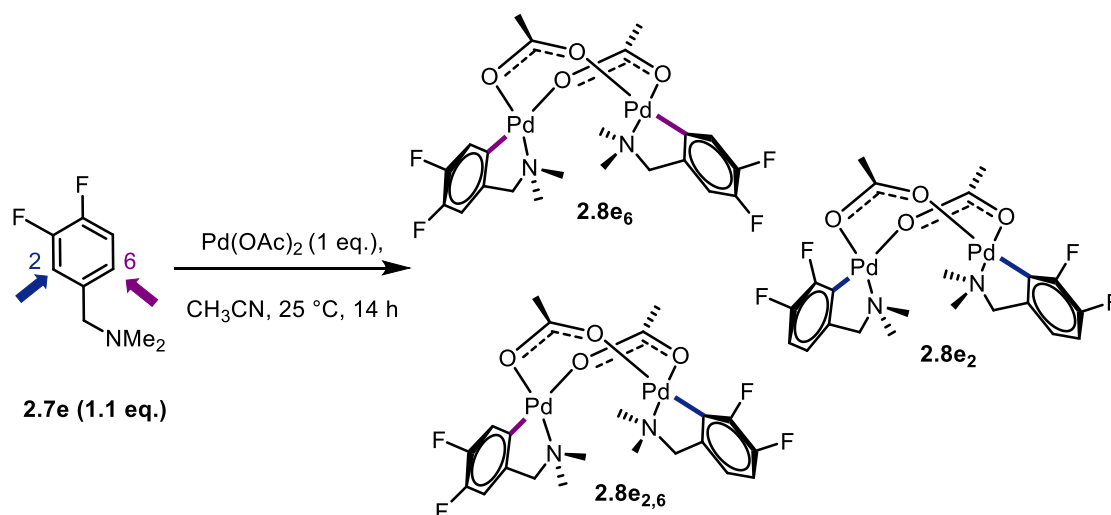


Figure 21: ^1H -NMR spectrum of palladacycle $2.8c_{\text{pyr}2,6}$ and $2.8c_{\text{pyr}6}$ at 293.45 K in $\text{pyr-}d_5$ (400 MHz).

Table 3: ^1H -NMR and ^{19}F -NMR signals of monomers $2.8c_{\text{pyr}2}$ and $2.8c_{\text{pyr}6}$ in $\text{pyr-}d_5$ at 293.45 K (400 MHz).

^1H -NMR signals / ppm			
Assignment (Scheme 34)			
<i>a</i>	6.77 (m, 1H)	<i>a'</i>	6.28 (dd, $J = 8.4, 6.2$ Hz, 1 H)
<i>b</i>	7.07 (td, $J = 7.7, 5.5$ Hz, 1 H)	<i>b'</i>	6.65 (t, $J = 8.4$ Hz, 1 H)
<i>c</i>	6.92–6.88 (m, 1 H)	<i>c'</i>	6.92–6.88 (m, 1 H)
<i>d</i>	3.86 (br s, 2 H)	<i>d'</i>	3.93 (br s, 2 H)
<i>e</i>	2.84 (s, 6H)	<i>e'</i>	2.76 (s, 6H)
<i>f</i>	2.19 (s, 3H)	<i>f'</i>	2.19 (s, 3H)
^{19}F -NMR signals / ppm			
<i>1</i>	-100.98 (dd, $J = 8.7, 5.4$ Hz)	<i>2</i>	-119.88 (dd, $J = 15.9, 9.6$ Hz)

Difluorinated substrate **2.7e** behaved in the same manner as **2.7c** showing a lack of regioselectivity in the cyclometallation reaction with $\text{Pd}(\text{OAc})_2$, and giving a mixture of isomers **2.8e₂**, **2.8e₆**, and **2.8e_{2,6}** (Scheme 35).



Scheme 35: Synthesis of palladacycle 2.8e (mixture of isomeric forms).

NMR characteristics of palladacycles **2.8a**, **2.8b** and **2.8d** synthesised under the same reaction conditions as **2.8c**, are reported in Table 4.

Table 4: ^1H - and ^{19}F -NMR signals of palladacycles 2.8a, 2.8b and 2.8d.

Compound	δ (^1H) / ppm	δ (^{19}F) / ppm
2.8a	7.02 (d, $J = 7.1$ Hz, 2H), 6.97 (t, $J = 7.3$ Hz, 2H), 6.89 (t, $J = 7.2$ Hz, 2H), 6.84 (d, $J = 7.2$ Hz, 2H), 3.58 (d, $J = 13.7$ Hz, 2H, RCH_2N), 3.09 (d, $J = 13.7$ Hz, 2H, CH_2), 2.80 (s, 6H, NCH_3), 2.06 (s, 6H, NCH_3), 2.05 (s, 6H, CH_3CO).	-
2.8b	6.91 (td, $J = 7.8, 5.6$ Hz, 2H, H-4), 6.79 (d, $J = 7.4$ Hz, 2H, H-5), 6.71 (ddd, $J = 9.5, 8.1, 0.9$ Hz, 2H, H-3), 3.50 (d, $J = 14.1$ Hz, 2H, CHH'), 3.45 (dd, $J = 14.3, 1.4$ Hz, 2H, CHH'), 2.83 (s, 6H, NCH_3), 2.07 (s, 6H, NCH_3), 2.06 (s, 6H, CH_3CO).	-115.01 (dd, $J = 9.7, 5.5$ Hz)
2.8d	6.67 (td, $J = 8.7, 3.7$ Hz, 2H, H-3), 6.51 (td, $J = 7.7, 4$ Hz, 2H, H-4), 3.76 (dd, $J = 14.4, 1.8$ Hz, 2H, CHH'), 3.54 (d, $J = 14.4$ Hz, 2H, CHH'), 2.83 (s, 6H, NCH_3), 2.23 (s, 6H, NCH_3), 2.00 (s, 6H, CH_3CO).	-111.12 (ddd, $J = 20.9, 7.6, 3.6$ Hz, 2F), -121.08 (m, 2F).

Palladacycle **2.8d** was also crystallized by slow diffusion of hexane into a concentrated solution of the compound in chloroform (Figure 22).

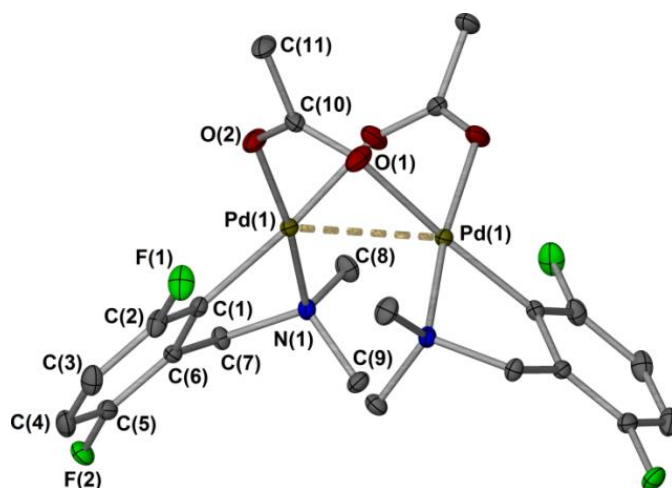
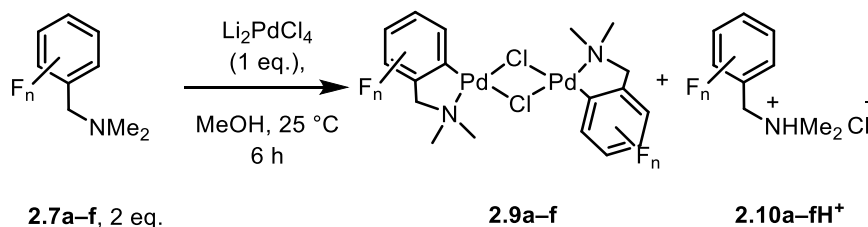


Figure 22: Molecular structure of palladacycle **2.8d**. Hydrogen atoms were omitted for clarity; thermal ellipsoids shown with probability of 50%.

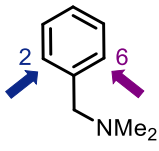
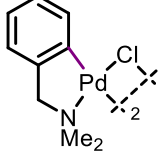
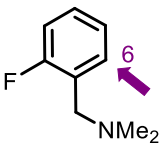
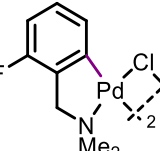
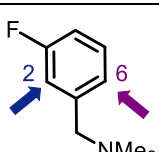
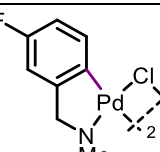
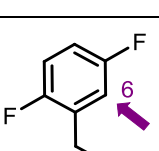
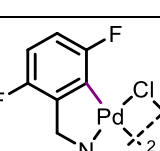
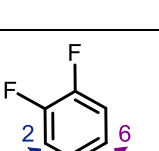
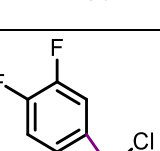
2.2.3 Reaction of fluorinated *N,N*-dimethylbenzylamines with Li_2PdCl_4

The same fluorinated benzylamines **2.7a–f** were reacted with Li_2PdCl_4 in methanol based on the procedure of Cope and co-workers (Scheme 36) to obtain chloride-bridged palladacycles **2.9a–f** (Table 5).⁹⁷



Scheme 36: Cyclopalladation reactions of fluorinated tertiary amines with Li_2PdCl_4 .

Table 5: Intramolecular C–H activation of fluorinated benzylamines with Li₂PdCl₄.

Substrate 2.7a–e	Complex 2.9a–e	Yield / %
 2.7a	 2.9a	70
 2.7b	 2.9b	86
 2.7c	 2.9c	76
 2.7d	 2.9d	67
 2.7e	 2.9e	71

Two equivalents of 2-fluoro-*N,N*-dimethylbenzylamine (**2.7b**) were reacted with Li₂PdCl₄ in methanol for 6 h affording palladacycle **2.9b** in 86% yield along with the protonated substrate **2.10bH⁺** (Scheme 37). In contrast to the acetate-bridged palladacycles (**2.8a–f**) and similar to the reported non-fluorinated example **2.9a**,⁹⁷ the chloride-bridged compounds appear in solution in two geometrical isomeric forms: *syn* and *anti*, depending on the relative

position of the Pd–C bonds (Scheme 37), whilst in the solid state only the *anti* isomer was observed (Figure 23).⁷²

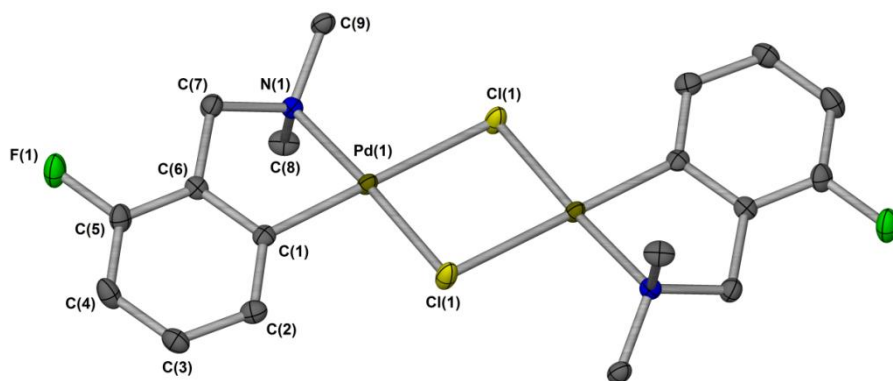
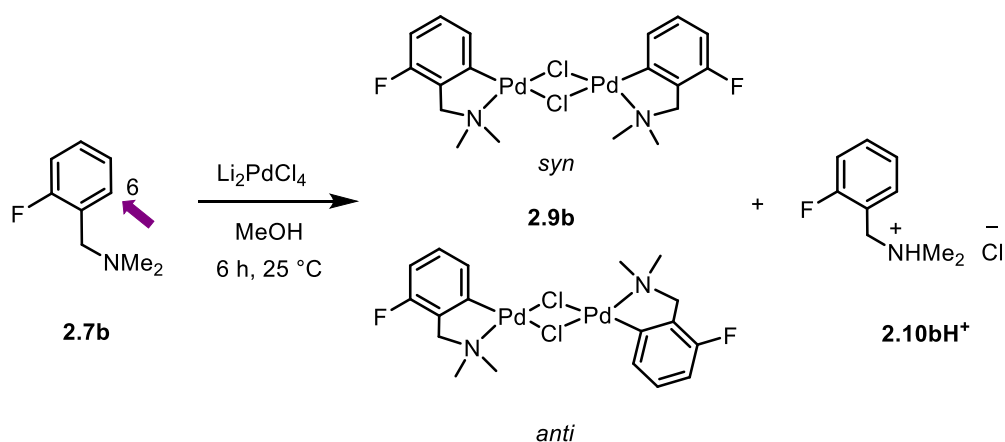


Figure 23: Molecular structure of palladacycle 2.9b. Hydrogen atoms were omitted for clarity; thermal ellipsoids shown with probability of 50%.

In the ¹H-NMR spectrum of palladacycle **2.9b**, the methyl groups resonate as two singlets at δ 2.86 and 2.88 due to the *syn* and *anti* isomeric forms, shifting to high frequency with respect to the free substrate **2.7b**, which shows a single resonance at δ 2.28. The same can be observed for the methylene protons which resonate at δ 4.01 in palladacycle **2.9b** and at 3.52 in the free substrate **2.7b**. The ¹⁹F-NMR spectrum shows a broad multiplet due to the overlap of *syn* and *anti* isomeric signals at δ -113.97 to high frequency compared to the free substrate **2.7b** (δ -118.10).

To investigate the regioselectivity of the cyclopalladation reaction forming chloride-bridged palladacycles, substrate **2.7c** was reacted with Li₂PdCl₄ in the same way as **2.7b** (Scheme 36). Substrate **2.7c** offers two sites (C-2 or C-6) for the C–H activation reaction (arrows in Figure 24).

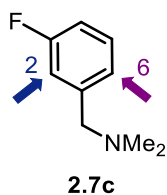
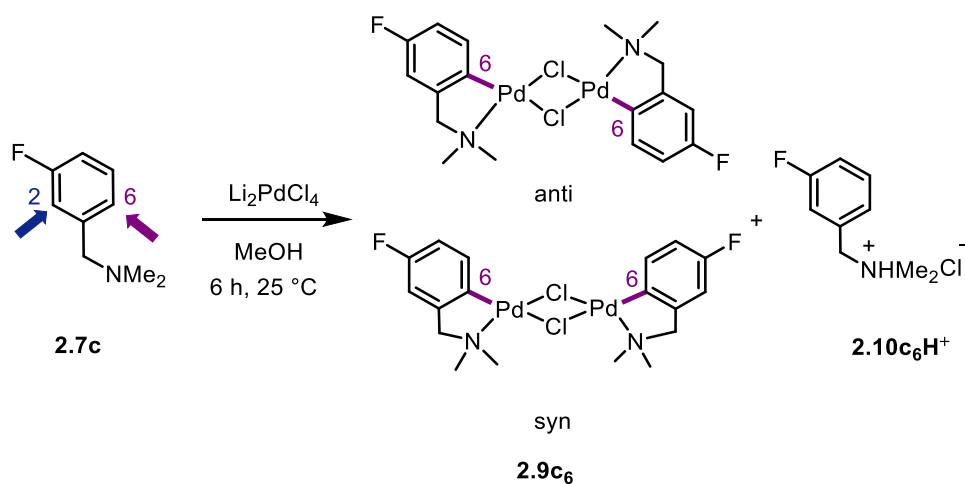


Figure 24: Substrate 2.7c offers two sites (C-2 or C-6) for the C–H activation reaction.

The reaction contrasts with that of palladium acetate, giving exclusively one regioisomer, **2.9c₆**, in 76% yield along with the protonated substrate **2.10cH⁺**. Complex **2.9c₆** was crystallized by slow evaporation of a saturated solution of the complex in chloroform at $-20\text{ }^{\circ}\text{C}$ (Figure 25) confirming that the cyclopalladation had taken place only *para* to the fluorine atom, in position C-6 (Scheme 38).



Scheme 38: Synthesis of palladacycle 2.9c₆ (geometrical isomers *syn* and *anti*).

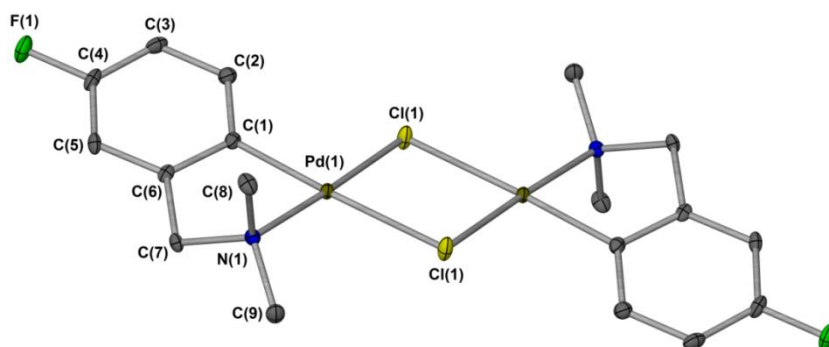


Figure 25: Molecular structure of palladacycle 2.9c₆. Hydrogen atoms were omitted for clarity; thermal ellipsoids shown with probability of 50%.

Interestingly, the regioselectivity obtained differs from that *ortho* to fluorine of intermolecular reactions of fluorinated arenes reported by Fagnou *et al.*²⁰ and from the intramolecular systems reported by Jones and co-workers.¹¹⁶

In the $^1\text{H-NMR}$ spectrum of palladacycle **2.9c₆** (Figure 26) the methylene protons resonate as a broad singlet at δ 3.90, while the two methyl groups bound to nitrogen exhibit two singlets at δ 2.83 and 2.86. The aromatic protons couple to each other and to fluorine and resonate at δ 7.10 (m) and 6.64 (m).

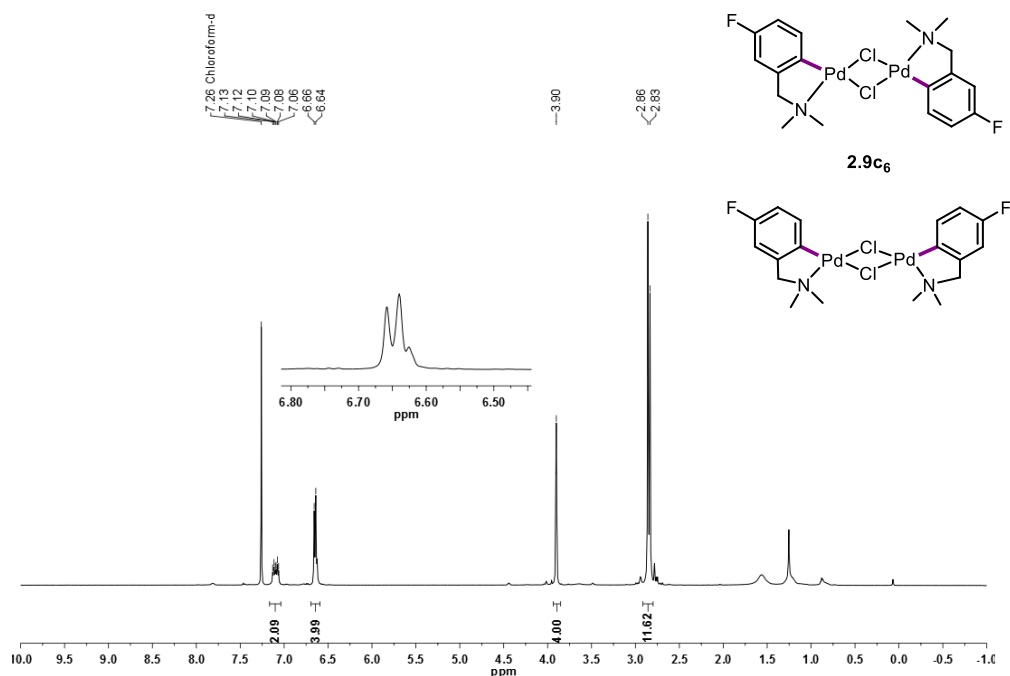


Figure 26: $^1\text{H-NMR}$ of palladacycle **2.9c₆**, at 298 K in CDCl_3 (500 MHz) (*syn* and *anti* isomeric forms).

In the $^{19}\text{F-NMR}$ spectrum (Figure 27) two multiplets appear centered at δ -119.01 and -119.10 , corresponding to the minor and major isomers in the ratio 1:1.2. It is not possible to distinguish which is due to *syn* and which is due to the *anti* isomer.

The $^{13}\text{C-NMR}$ spectrum also shows two sets of signals for the two geometrical isomers *syn* and *anti*. The *N*-methyl groups resonate in each isomer as two singlets at δ 53.1 and 52.8 while the methylene carbons as two doublets at δ 73.2 and 73.0 ($J = 2.6$ and 2.9 Hz respectively), confirmed by a $^{13}\text{C-DEPT-135}$ NMR experiment. Two singlets appear at δ 109.0 and 108.8 for the carbons *ipso* to the benzyl arm of the two geometrical isomers and the aromatic carbons *para* to the C–F bond resonate as two sets of doublets at δ 112.0 ($J = 9.8$ Hz) and 111.9 ($J = 9.8$ Hz). Two sets of doublets appear at δ 147.6 ($J = 6.3$ and 6.5 Hz, respectively) corresponding to the aromatic carbon *ortho* to the C–F bond in both isomers. Finally at δ 161.41 and 161.38 ($J = 241.5$ and 241.6 Hz respectively) two doublets appear corresponding to the carbons bonded to fluorine in the minor and major isomers.

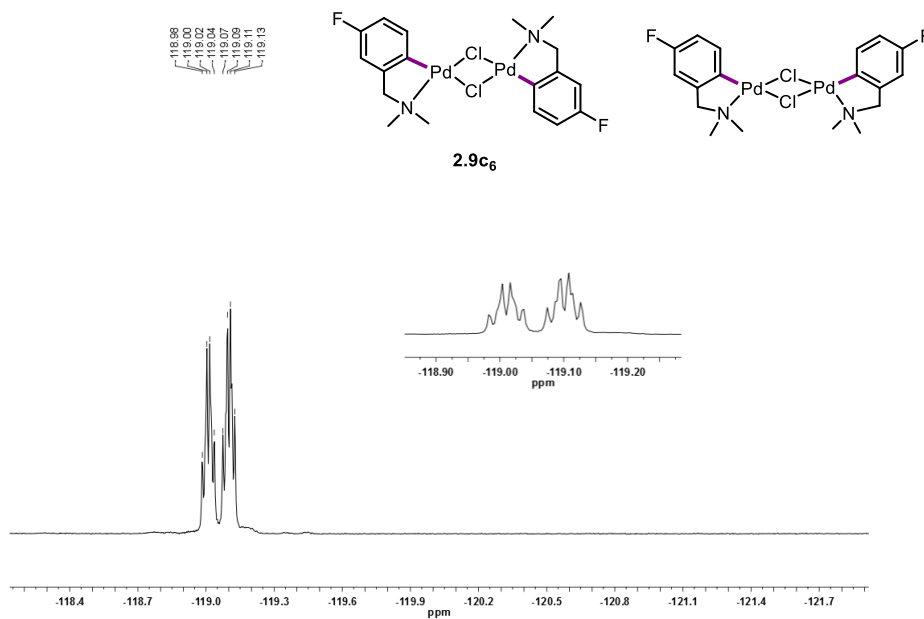


Figure 27: ^{19}F -NMR of palladacycle **2.9c₆** at 298 K in CDCl_3 (471 MHz) (*syn* and *anti* isomeric forms).

Palladacycles **2.9a–e** were synthesised and crystallised following the same procedures used for **2.9c** (Figure 28); their NMR spectroscopic signals are reported in Table 6 and a crystallographic analysis is reported in section 2.4.2 of this chapter.

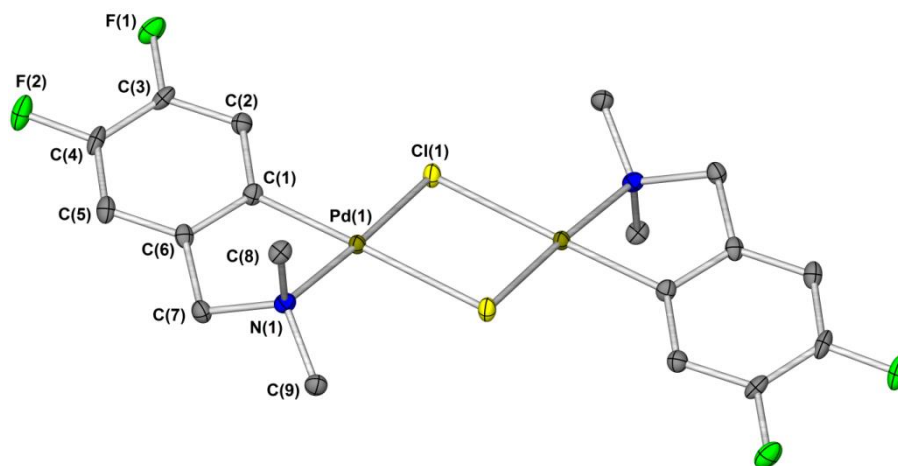
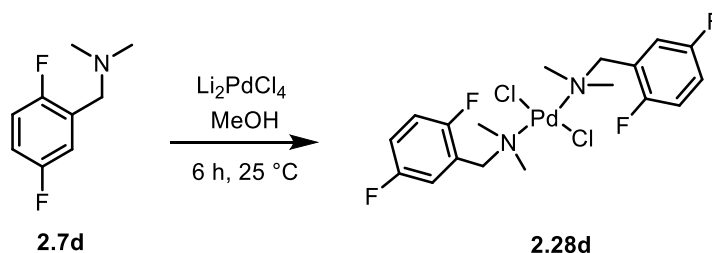


Figure 28: Molecular structure of palladacycle **2.9e₆**. Hydrogen atoms were omitted for clarity; thermal ellipsoids shown with probability of 50%.

Table 6: ^1H -NMR and ^{19}F -NMR signals of palladacycles **2.9a–e at 293.45 K (400 and 500 MHz).**

Compound	δ (^1H) / ppm	δ (^{19}F) / ppm
2.9a ⁹⁷	7.17 (dd, $J = 19.3, 7.6$ Hz, 2H), 6.99–6.94 (m, 2H), 6.87 (t, $J = 6.8$ Hz, 4H), 3.93 (s, 4H), 2.87 (s, 6H), 2.84 (s, 6H)	-
2.9b	6.94 (dd, $J = 20.1, 7.7$ Hz, 2H), 6.70 (dd, $J = 13.6, 4.9$ Hz, 2H), 6.87 (td, $J = 7.9,$ 5,6 Hz, 2H), 4.01 (d, $J = 2.3$ Hz, 4H), 2.88 (s, 6H), 2.86 (s, 6H).	-113.97 (m)
2.9c ₆	7.10 (m, 2H), 6.64 (m, 4H), 3.90 (br s, 4H), 2.86 (s, 6H), 2.83 (s, 6H).	-119.01 (m, minor isomer), -119.10 (m, major isomer).
2.9d	6.66 (qd, $J = 8.5, 3.6$ Hz, 2H), 6.52 (m, 2H), 4.05 (d, $J = 4.1$ Hz, 4H), 2.77 (s, 6H), 2.75 (s, 6H).	δ -102.94 (ddd, $J = 20.0, 7.7,$ 3.6 Hz), -105.75 (ddd, $J = 20.1, 7.9,$ 3.6 Hz), -120.49 (m), -120.90 (m).
2.9e ₆	6.92 (ddd, $J = 19.1, 10.6, 8.6$ Hz, 2H), 6.74 (dd, $J = 10.6, 7.6$ Hz, 2H), 3.88 (s, 4H), 2.85 (s, 6H), 2.82 (s, 6H).	-140.22 (m, major isomer), -140.55 (m, minor isomer), -143.50 (m, major isomer), -143.67 (m, minor isomer).

Substrate **2.7d** reacted with Li_2PdCl_4 under the conditions used for the other fluorinated amines giving the non-cyclometallated palladium complex **2.28d**, instead of the expected chloride-bridged palladacycle **2.9d** (Scheme 39).



Scheme 39: Formation of palladium complex 2.28d instead of palladacycle 2.9d.

The ^{19}F -NMR spectrum of complex **2.28d** shows two multiplets for the two sets of chemically inequivalent fluorine atoms at δ -121.52 and -118.22. The ^1H -NMR shows two singlets for the protons of the methyl groups bound to nitrogen and for the methylene protons at δ 2.60 and 3.90 respectively. The aromatic protons resonate as a doublet of doublets of doublets centered at δ 8.77 ($J = 8.8, 5.5, 3.2$ Hz), a multiplet centered at 7.12 and a triplet of doublets at 7.06 ($J = 9.0, 4.6$ Hz). Complex **2.28d** was crystallised by slow evaporation of a saturated solution of the complex in dichloromethane at 2 $^\circ\text{C}$ (Figure 29).

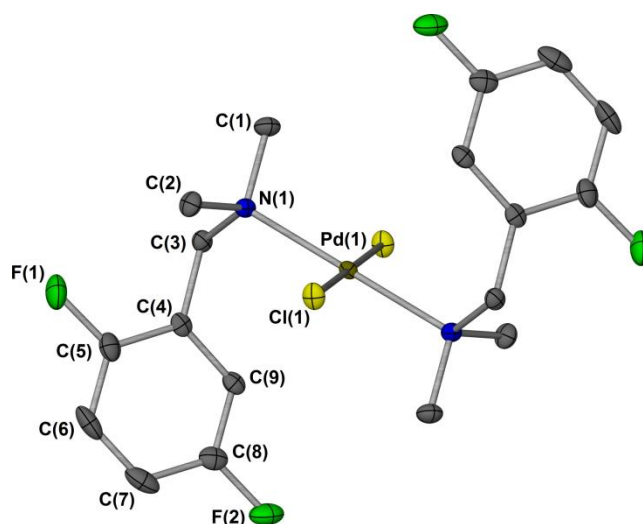
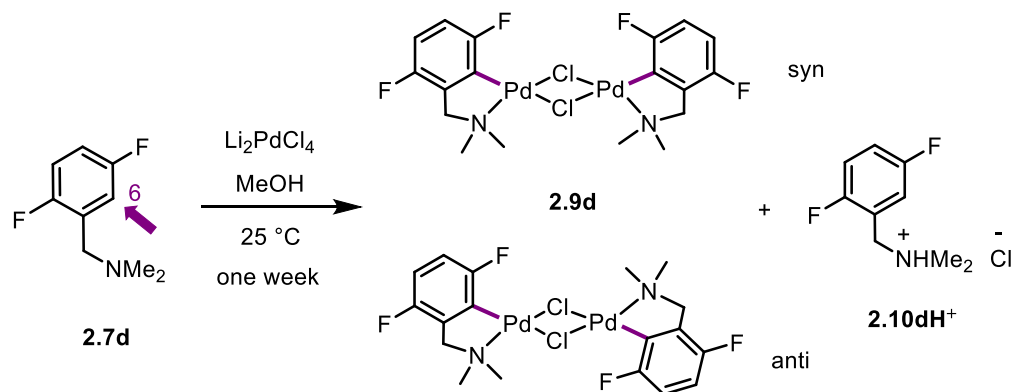


Figure 29: Molecular structure of complex 2.28d. Hydrogen atoms were omitted for clarity; thermal ellipsoids shown with probability of 50%.

Palladacycle **2.9d** was obtained reacting substrate **2.7d** with Li_2PdCl_4 with a reaction time of one week (Scheme 40) suggesting that complex **2.28d** is one of the species at equilibrium in the electrophilic aromatic substitution mechanism described in the introduction to this chapter (Scheme 30).

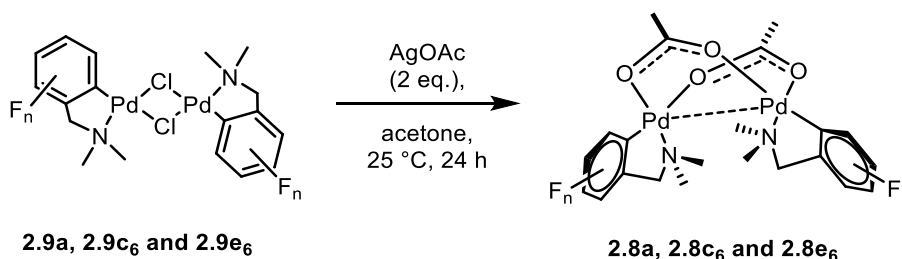


Scheme 40: Synthesis of palladacycle 2.9d (geometrical isomers *syn* and *anti*).

The cyclopalladation reactions with Li_2PdCl_4 were also carried out in acetonitrile on the same reaction scale and with the same reaction conditions to assess the role of the solvent in the regioselectivity obtained for substrate **2.7c** and **2.7e**. The C–H activation reactions also occurred *para* to the fluorine atom suggesting that the regioselectivity is not solvent dependent.

2.2.4 Bridging halide conversion at Pd(II)

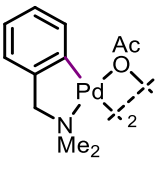
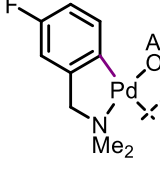
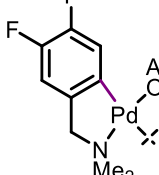
Chloride-bridged palladacycles **2.9a**, **2.9c₆** and **2.9e₆** were reacted in acetone at 25 °C with silver acetate (Scheme 41) to give the corresponding acetate-bridged palladacycles **2.8a**, **2.8c₆** and **2.8e₆** (Table 7).



Scheme 41: Bridging halide conversion from chloride-bridged to acetate-bridged palladacycles.

In the case of the fluorinated palladacycles **2.9c₆** and **2.9e₆**, only the *para* isomers were formed, giving a new route to obtain fluorinated acetate-bridged palladacycles regioselectively.

Table 7: Acetate-bridged palladacycle obtained by bridging halide conversion.

Complex	 2.8a	 2.8c₆	 2.8e₆
Yield / %	91	98	95

Complexes **2.8c₆** and **2.8e₆** were fully characterised and their NMR data are reported in Table 8.

Table 8: ¹H-NMR (500 MHz) and ¹⁹F-NMR (471 MHz) signals of monomers **2.8c₆ and **2.8e₆** in CDCl₃ at 298 K**

Compound	δ (¹H) / ppm	δ (¹⁹F) / ppm
2.8c₆	6.95 (dd, $J = 8.3, 6.2$ Hz, 2H, H-1), 6.71–6.61 (m, 4H, H-2, H-4), 3.52 (d, $J = 13.9$ Hz, 2H, CHH'), 3.09 (d, $J = 13.9$ Hz, 2H, CHH'), 2.79 (s, 6H, NCH ₃), 2.06 (s, 6H, NCH ₃), 2.05 (s, 6H, CH ₃ CO)	-119.31 (td, $J = 9.6, 6.2$ Hz)
2.8e₆	6.78–6.72 (m, 4H, H-2, H-5), 3.58 (d, $J = 13.8$ Hz, 2H, CHH'), 3.13 (d, $J = 13.8$ Hz, 2H, CHH'), 2.79 (s, 6H, NCH ₃), 2.11 (s, 6H, NCH ₃), 2.06 (s, 6H, CH ₃ CO).	-140.92 (m, 2F), -143.94 (ddd, $J = 19.7, 10.7, 8.8$ Hz, 2F).

Palladacycles **2.8c₆** and **2.8e₆** were crystallised by slow diffusion of hexane into a concentrated solution of the compound in chloroform (Figure 30 and Figure 31).

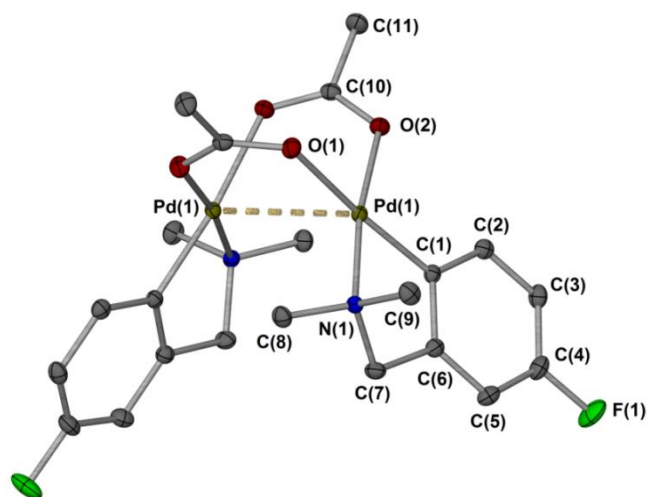


Figure 30: Molecular structure of palladacycle **2.8c₆**. Hydrogen atoms were omitted for clarity; thermal ellipsoids shown with probability of 50%.

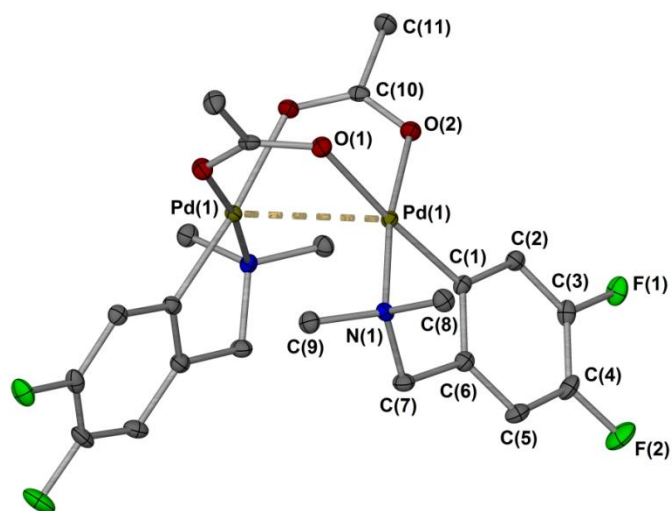
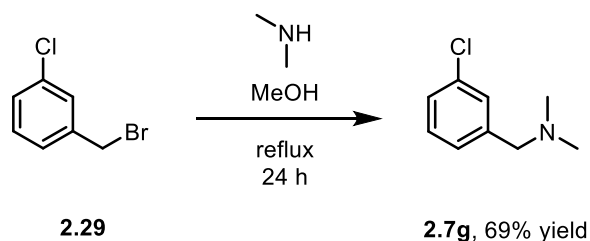


Figure 31: Molecular structure of palladacycle **2.8e₆**. Hydrogen atoms were omitted for clarity; thermal ellipsoids shown with probability of 50%.

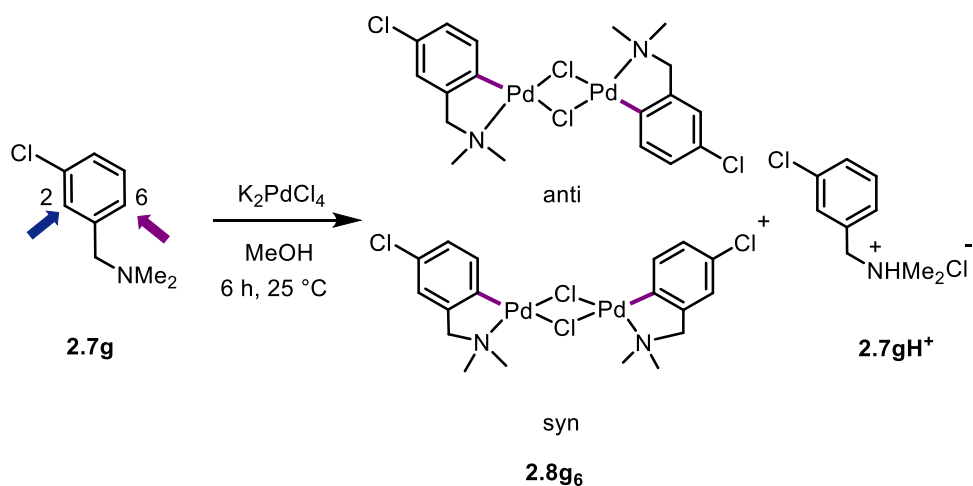
2.2.5 Chlorinated amino palladacycles

The chlorinated substrate 3-chloro-*N,N*-dimethylbenzylamine (**2.7g**) was synthesised following the same procedure used for the synthesis of the fluorinated tertiary amines **2.7b–f** (Scheme 42) and reacted with Pd(OAc)₂ and Li₂PdCl₄ to obtain chlorine substituted chloride- and acetate-bridged palladacycles **2.8g** and **2.9g**.



Scheme 42: Synthesis of chlorinated tertiary amine 2.7g.

Reaction of *N,N*-dimethyl-3-chlorobenzylamine (**2.7g**) with Li_2PdCl_4 allowed an assessment of the effect the chlorine atom on the regioselectivity of C–H activation reaction due to the two possible options for attack, *ortho* or *para* to chlorine. The reaction, as for the fluorinated substrates, gave one regioisomer, **2.8g₆**, where the C–H activation occurs *para* to the chlorine atom (Scheme 43).



Scheme 43: Regioselective synthesis of palladacycle 2.8g₆.

The $^1\text{H-NMR}$ spectrum two multiplets at δ 7.08 and 6.90–6.85 for the aromatic protons while the methylene protons resonate as a singlet at δ 3.89. The two inequivalent methyl groups bound to the nitrogen resonate at δ 2.85 and 2.82. A single crystal, suitable for the X-ray analysis, was grown by slow evaporation of a saturated solution of the compound in chloroform and confirmed the regioselectivity *para* to the chlorine atom (Figure 32).

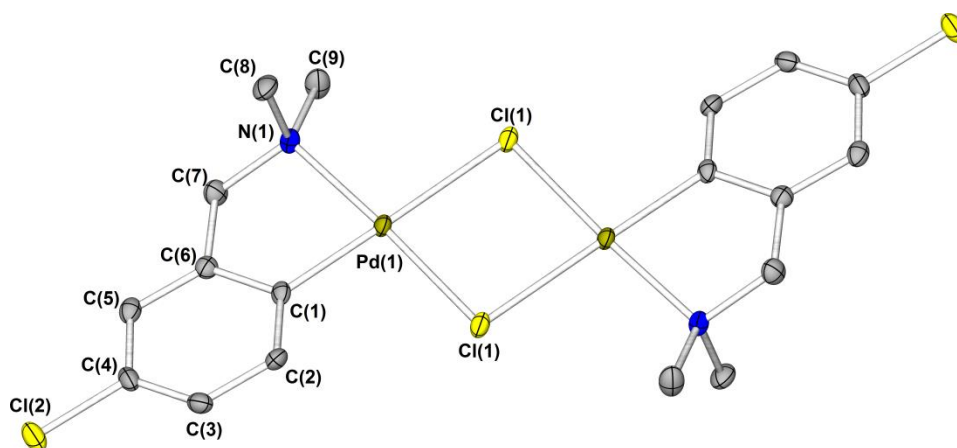
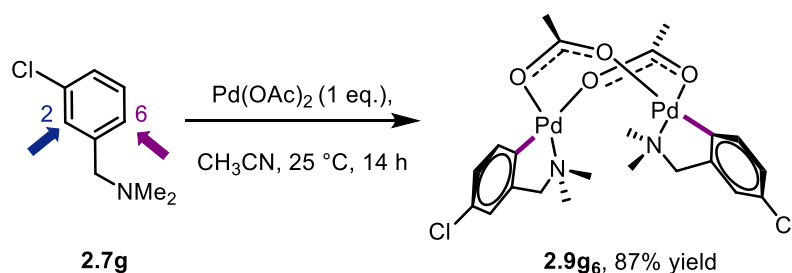


Figure 32: Molecular structure of palladacycle **2.8g₆**. Hydrogen atoms were omitted for clarity; thermal ellipsoids shown with probability of 50%.

The same chlorinated tertiary amine, **2.7g**, was also reacted in acetonitrile for 14 h with Pd(OAc)₂ affording only palladacycle **2.9g₆** in 87% yield (Scheme 44) and showing complete regioselectivity *para* to chlorine.



Scheme 44: Synthesis of chlorinated acetate-bridged palladacycle **2.9g₆**.

The ¹H-NMR spectrum (Figure 33) shows two multiplets at δ 6.97–6.87 and 6.74 for the six aromatic protons and only two doublets at δ 3.55 ($J = 13.9$ Hz) and 3.10 ($J = 13.9$ Hz) for the diastereotopic methylene protons of the palladacycle **2.9g₆** showing the formation of just one isomer. The inequivalent methyl groups bound to the nitrogen and the methyl group of the acetate bridge resonate as three singlets at δ 2.78, 2.08 and 2.05, respectively.

Due to the difficulty in obtaining a single crystal suitable for X-ray analysis of palladacycle **2.9g₆**, the compound was synthesised *via* a different route in order to confirm the position of attack of the C–H activation reaction. As reported in section 2.2.3 the conversion of chloride- to acetate-bridged palladacycles can be carried out straightforwardly whilst maintaining the regioselectivity of the starting materials.

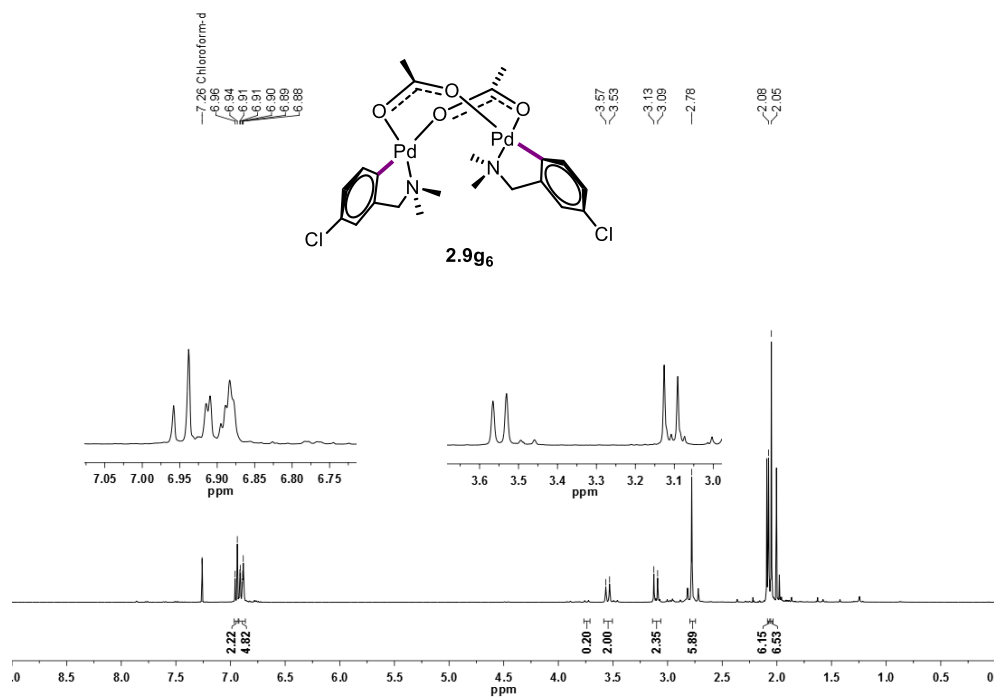
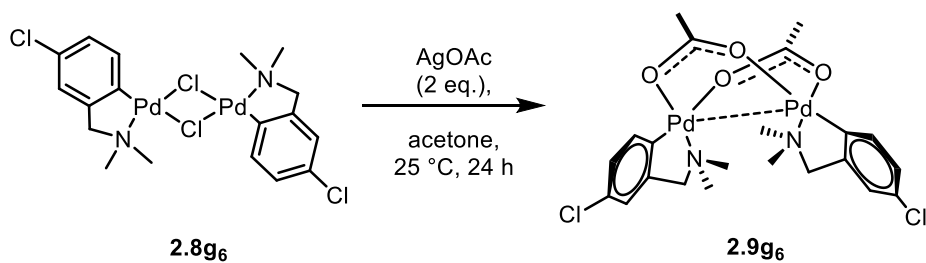


Figure 33: $^1\text{H-NMR}$ spectrum of palladacycle **2.9g₆** at 293.45 K in CDCl_3 (400 MHz).

Palladacycle **2.8g₆** was thus reacted with silver acetate in acetone (Scheme 45) and the $^1\text{H-NMR}$ spectrum of the resulting acetate-bridged palladacycle, **2.9g₆**, was compared with the one of an authentic sample of **2.9g₆**. It was found to be consistent, confirming the hypothesised *para* substitution (Figure 34).



Scheme 45: Bridge-conversion reaction of **2.8g₆** to **2.9g₆**.

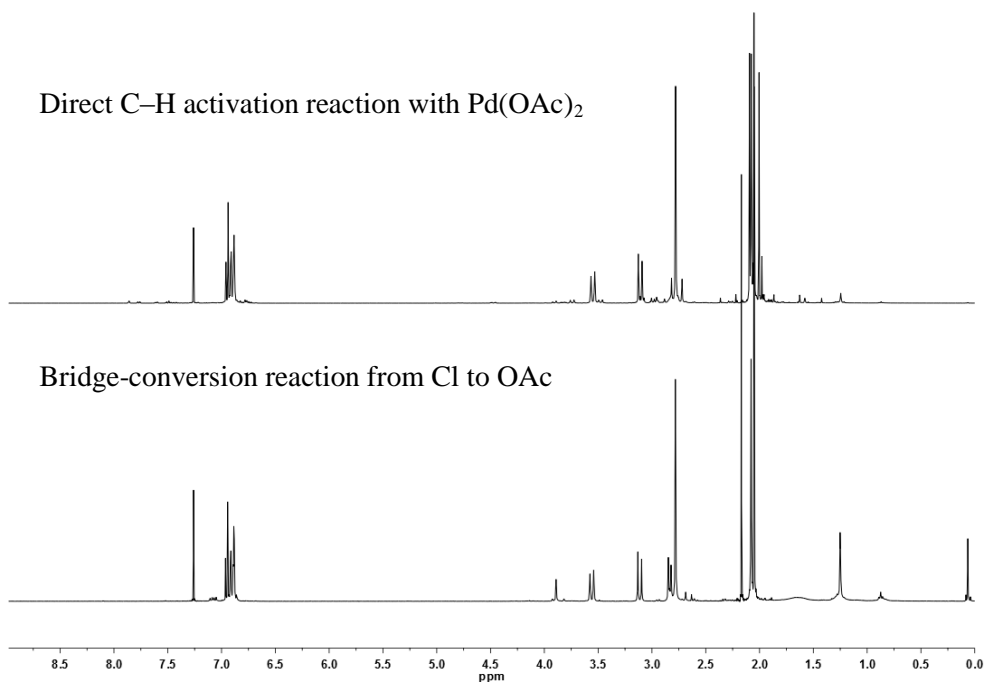


Figure 34: Comparison of $^1\text{H-NMR}$ of palladacycle **2.9g₆** obtained *via* two different routes.

2.3 Discussion

In this study a fluorinated benzylamine **2.7c** that undergoes cyclometallation in a system where a choice is presented in the position of C–H activation (*ortho* or *para* to the fluorine atom) does not show any regioselectivity, forming a mixture of isomers (**2.8c₂**, **2.8c₆**, and **2.8c_{2,6}**). It is feasible that the lack of regioselectivity is the result of two opposing effects: while the activation in the *ortho* position (isomer **2.8c₂** in Figure 35) is favoured due to the *ortho* fluorine effect as for the intermolecular reactions, proceeding *via* a CMD mechanism, of fluorinated substrates,²⁰ the same position is disfavoured by the electronic repulsion between the lone pair of the oxygen in the acetate bridge pointing towards the aromatic ring and the fluorine lone pair (Figure 35).

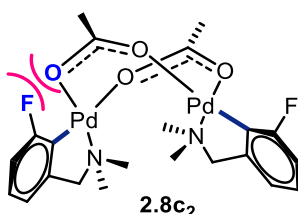


Figure 35: Representation of the electronic repulsion in palladacycle **2.8c₂**.

Such steric and electronic effects could manifest themselves if C–H activation occurred through a dinuclear Pd complex. Future kinetic studies would be necessary to confirm this

proposal. To explore the steric and electronic effect theory the cyclometallation reaction of the same substrate **2.7c**, was investigated using a different source of palladium (Li_2PdCl_4) which is reported to undergo cyclometallation *via* a different mechanism ($\text{S}_{\text{E}}\text{Ar}$).⁹⁷ The resulting cyclometallation reaction gave just isomer **2.9c₆** regioselectively, where the C–H activation occurs *para* to the fluorine atom. It is proposed that the formation of isomer **2.9c₂** is prevented by electronic repulsion between the chlorine and the fluorine lone pairs, which cannot be avoided due to the structural features of the chloride-bridged palladacycle (see below).

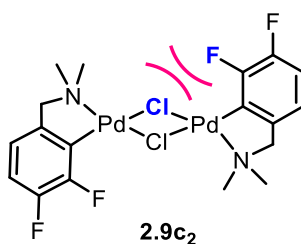


Figure 36: Representation of the electronic repulsion in palladacycle **2.9c₂.**

Comparing the two X-ray crystal structures in Figure 37 and Figure 38, it is possible to observe a key difference between the geometries of the two complexes. While the acetate-bridged palladacycle **2.8c₆** (obtained as a single isomer *via* reaction in Scheme 41) has a clam-shell structure that is able to twist (see crystallographic analysis in section 2.4), the chloride-bridged palladacycle **2.9c₆** has a planar structure where the aromatic ring cannot twist away and the repulsion cannot be avoided.

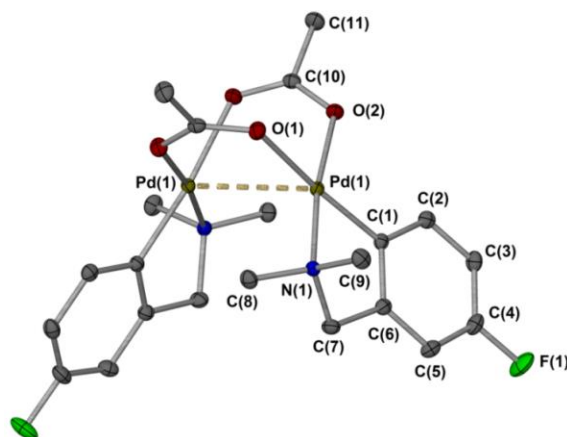


Figure 37: Molecular structure of palladacycle **2.8c₆.**

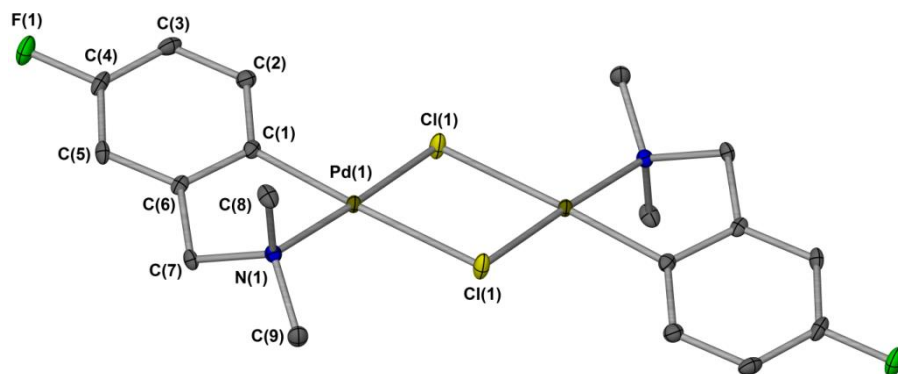


Figure 38: Molecular structure of palladacycle 2.9c₆.

An additional experiment with difluorinated amine **2.7e** was performed to confirm this effect: the amine was reacted with Pd(TFA)₂ to give a trifluoroacetate-bridged palladacycle **2.30**. Although the NMR spectra were complex and the ratio between the *ortho* and *para* isomers could not be determined, an X-ray crystal structure was obtained showing disorder in the position of the fluorine (Figure 39), which is consistent with the explanation given above.

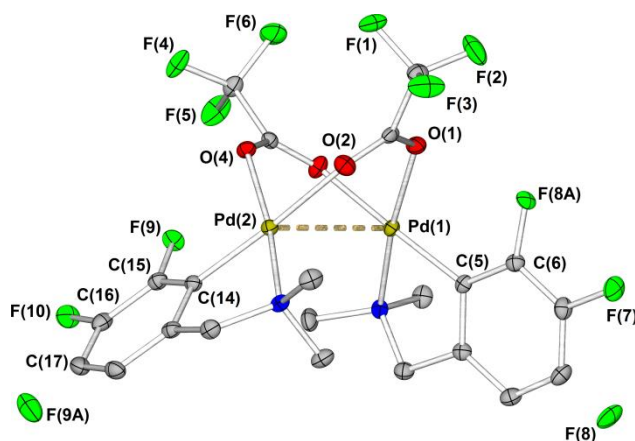


Figure 39: Molecular structure of palladacycle 2.30. Hydrogen atoms were omitted for clarity; thermal ellipsoids shown with probability of 50%.

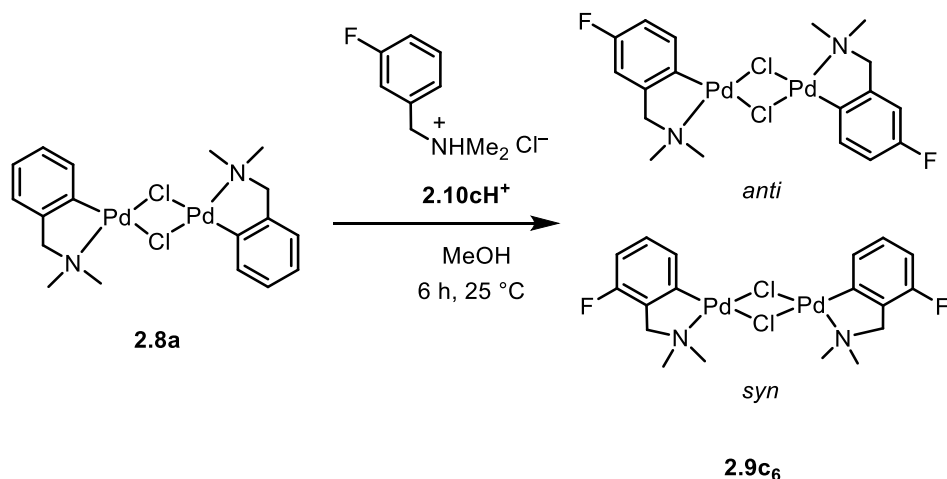
This theory is also supported by the experiment with the chlorinated substrate **2.7g** (Scheme 43) that gives, regioselectively, the *para* chloride-bridged palladacycle **2.8g₆** for the same steric and electronic repulsion mentioned above and also gives regioselectivity in the formation of the acetate-bridged palladacycle **2.9g₆**, where the C–H activation *ortho* to chlorine is disfavoured by repulsions but in contrast to the fluorinated substrates the influence of the *ortho* fluorine effect is missing.

The regioselectivity of these examples of cyclometallation reactions seems to be associated with a particular mechanism (CMD for the acetate-bridged and S_EAr for the

chloride-bridged palladacycles) in addition to important electronic factors and the structural features of the palladacycles themselves. Interestingly Jones and co-workers have found an *ortho* fluorine effect in fluorinated imines, which react with Ir and Rh *via* an electrophilic aromatic substitution reaction as mentioned in section 2.1.¹¹⁶ The difference between the systems reported here and that reported by Jones *et al.* may be associated with a change in the rate determining step and also with differences in ligand conformation and identity. Furthermore as mentioned above, the amino-system is dimeric while the imino-system is monomeric and the regioselectivity could be different due to the C–H activation happening *via* a dinuclear Pd complex.

The observed regioselectivity raises the question of thermodynamic or kinetic control in the step where the Pd–C bond is formed. Looking at the mechanism (Scheme 29) studied by Macgregor *et al.* and at the proposed mechanism for the S_EAr (Scheme 30), in order to have thermodynamic control of the reaction in the acetate-bridged system, the second and third steps need to be reversible (to have the aromatic ring flipped vertically) while in the chloride-bridged system the last three need to be reversible. To assess whether the reactions were reversible, several experiments were performed to test:

- Changes in isomeric distribution at higher temperature than the standard reaction: for the acetate system the isomer **2.8c₆** was reacted with acetic acid at 75 °C and the reaction was monitored over 16 h, but no conversion to the *ortho* isomer **2.8c₂** was observed; for the chloride-system the standard reaction was carried out in methanol at reflux resulting in the formation of the *para* isomer **2.9c₆** only, suggesting that these reactions are under kinetic control.
- Exchange reaction between non-fluorinated palladacycle **2.8a** in the presence of fluorinated substrate **2.7c** and acetic acid: the reaction performed in toluene, at reflux, for 24 h showed formation of a mixture of fluorinated isomers **2.8c₂–2.8c₆** (conversion 33%) showing a lack of regioselectivity; the same reaction for the chloride-bridged palladacycle **2.9a** in the presence of **2.7cH⁺Cl⁻** in deuterated acetonitrile gave selectively just the *para* isomer **2.9c₆**, again suggesting kinetic control (Scheme 46).



Scheme 46: Exchange reaction between palladacycle 2.8a in the presence of 2.7cH⁺.

2.4 Crystallographic analysis

2.4.1 Molecular structure of acetate-bridged palladacycles

As mentioned in Section 2.1.3, all the acetate-bridged palladacycles **2.8a–f** show a typical “clamshell” structure, non-planar at palladium, where the coordination plane containing the palladium atom is almost perpendicular to the acetate bridge, similar to that reported by Bercaw and co-workers.¹²⁷

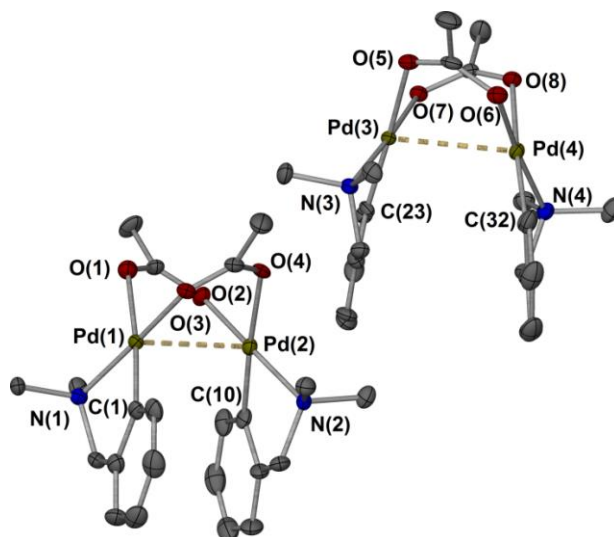


Figure 40: Molecular structure of palladacycle 2.8a. Hydrogen atoms were omitted for clarity; thermal ellipsoids shown with probability of 50%.

Detailed crystallographic data can be found in Appendix II, but the most interesting differences between the structures are described by the following three parameters, listed in Table 9:

- Pd···Pd distance;
- interplane angle: angle between plane C (aromatic metallacycle)–C(*ipso*)–Pd(1) and the corresponding plane at Pd(2);
- torsion angle N'–Pd'–Pd–N.

Table 9: Selected distances and angles of acetate-bridged palladacycles 2.8a–f.

Compound	Pd···Pd distance (Å)	Interplane angle (°)	Torsion angle N'–Pd'–Pd–N (°)
2.8a	2.9324(6)	19.5(3)	–104.3(3)
	2.9279(7)	19.3(3)	–104.4(3)
2.8b	2.9600(2)	9.45(16)	71.94(9)
2.8c	3.0185(7)	37.22(13)	–98.18(12)
2.8d	3.0974(8)	85.66(15)	–84.03(11)
2.8e	3.0369(7)	37.88(13)	–99.83(9)
2.8f	3.0285(5)	86.30(11)	–77.81(13)

Analysing the data, a correlation between the Pd···Pd distance and the number of the fluorine atoms in the aromatic ring can be observed, potentially due to the withdrawal of electron density by the fluorine atoms that decreases the d⁸–d⁸ interactions. C–F bond lengths (Table 10) show that there is almost no variation across the series, and all of them are slightly larger than 1.30 Å, corresponding to the sum of the covalent radii (Csp²: 0.73 Å, F: 0.57 Å).

In Figure 41 is shown a graphical representation of the interplane angle for palladacycle **2.8b** with the C (aromatic metallacycle), C(*ipso*) and Pd(1) highlighted in yellow.

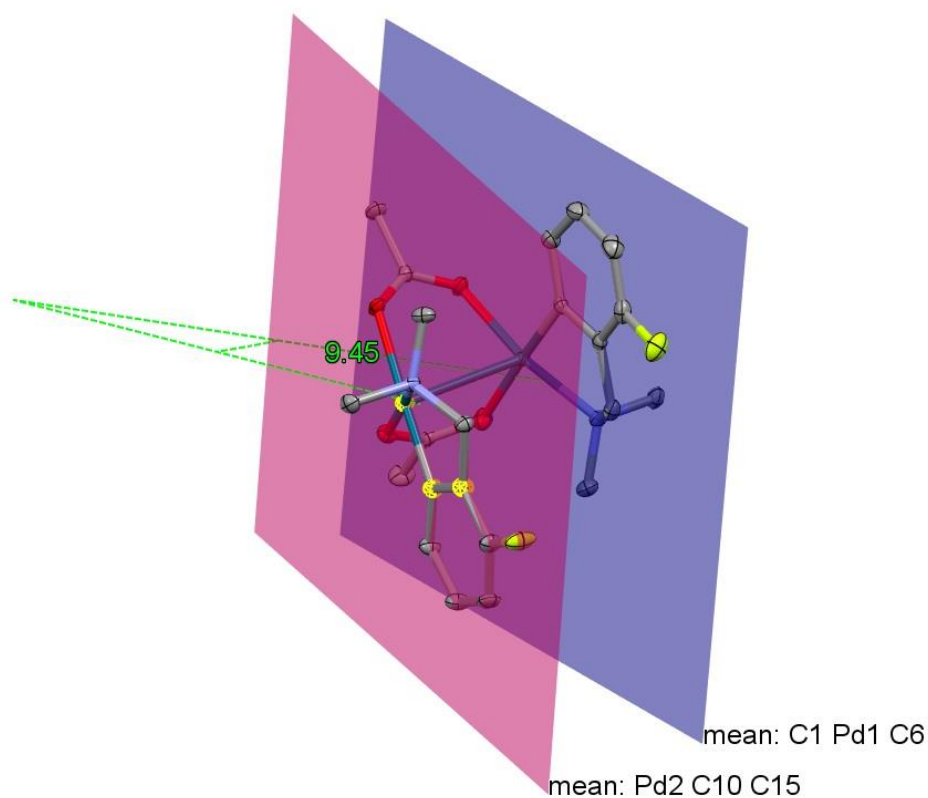


Figure 41: Interplane angle in palladacycle 2.8b.

Across the series the interplane angle values increase from $9.45(16)^\circ$ for the fluorinated palladacycle **2.8b**, $19.5(3)^\circ$ for the non-fluorinated compound **2.8a** to $37.22(13)^\circ$ and $37.88(13)^\circ$ for palladacycles **2.8c** and **2.8e** (mono- and di-fluorinated palladacycles respectively) and to $86.30(11)^\circ$ for the difluorinated palladacycle **2.8d**. It is possible to observe that as well as the number of fluorine atoms, the position of the fluorine has an effect on these values; in fact the highest value is for the palladacycle **2.8d** where the fluorine atom occupies the position *ortho* to the Pd–C bond. It also possible to observe corresponding increases in the angle (hereafter called γ) between the two benzene ring planes, represented in Figure 42.

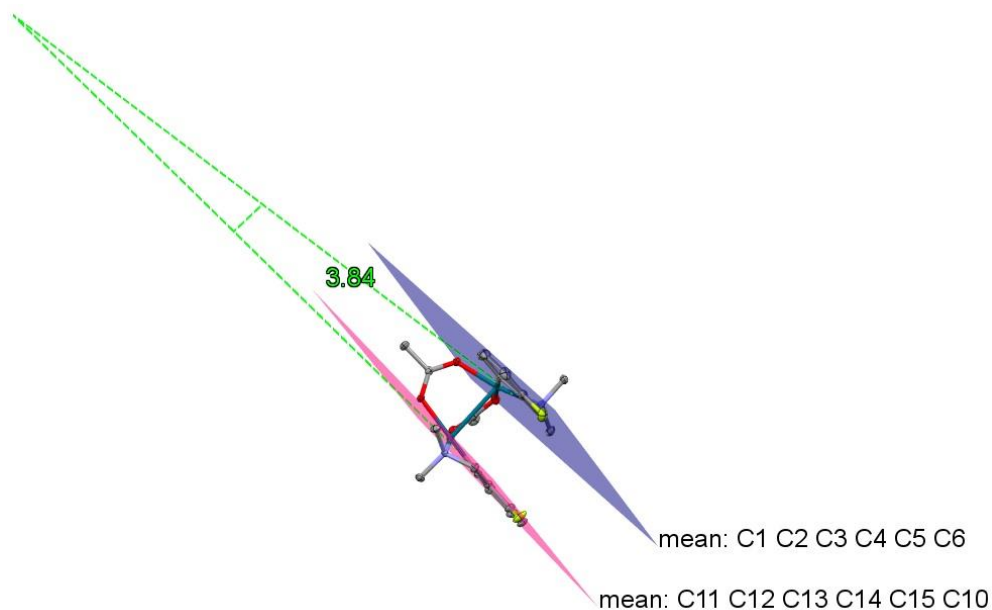


Figure 42: Angle between benzene planes (γ) in palladacycle 2.8b.

The twisting of the benzene ring with respect to the coordination plane at palladium, (especially in structure **2.8d**) is due to the electronic repulsion between the oxygen of the acetate bridge and the fluorine on the aromatic ring (distance (F(1)···O(2) is 2.886(2) Å in **2.8d**, compared to the sum of the van der Waals radii of 2.99 Å, a reduction of only 3%).¹³⁸ The structural comparison in Figure 43 shows the different level of twisting and the opening of the clam shell as the fluorine substituents are introduced.

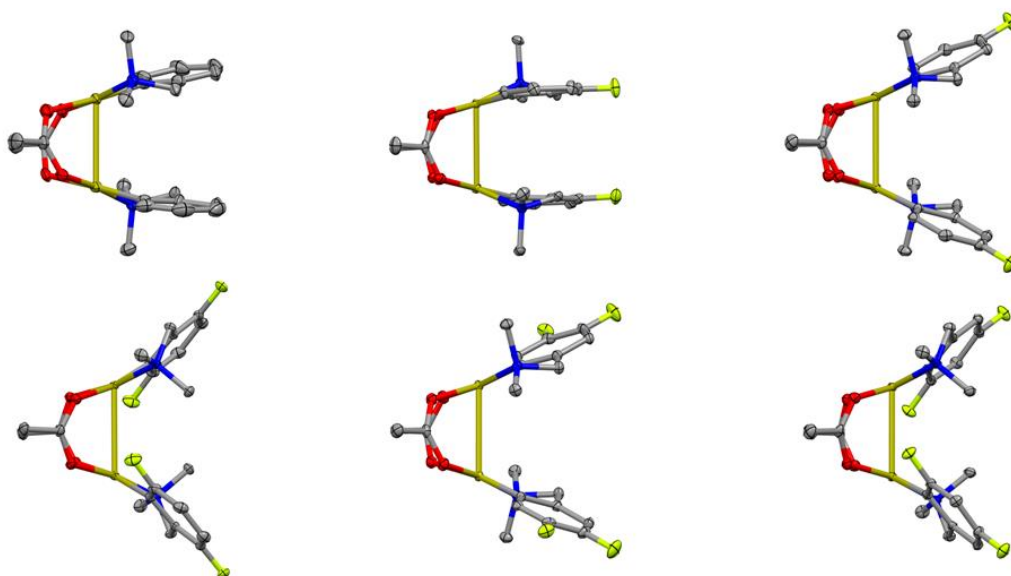


Figure 43: Structural comparison between molecular structures showing the different level of twisting (clockwise from top left 2.8a, 2.8b, 2.8c, 2.8d, 2.8e, 2.8f).

Table 10: Selected bond lengths of palladacycles 2.8a–f.

Bond length (Å)	2.8a	2.8b	2.8c ₆	2.8d	2.8e ₆	2.8f
C(1)–Pd(1)	1.963(7)	1.952(3)	1.958(2)	1.966(2)	1.9525(19)	1.974(2)
O(1)–Pd(1)	2.145(5)	2.135(2)	2.1426(9)	2.0996(17)	2.1383(14)	2.0363(17)
O(n)–Pd(1)	O(3) 2.040(5)	O(3) 2.05010(19)	O(2) 2.0358(16)	O(2) 2.0276(17)	O(2) 2.0328(13)	O(2) 2.1192(17)
C(n)–F(n)	-	C(5)–F(1) 1.368(3)	C(4)–F(1) 1.363(3)	C(2)–F(1) 1.371(3) C(5)–F(2) 1.357(3)	C(3)–F(1) 1.363(2) C(4)–F(2) 1.348(2)	C(2)–F(1) 1.366(3) C(4)–F(2) 1.363(3)
N(1)–Pd(1)	2.064(6)	2.070(2)	2.0608(18)	2.0500(19)	2.0639(16)	2.057(2)

Table 11: Selected bond angles of palladacycles 2.8a–f.

Bond angle (°)	2.8a	2.8b	2.8c ₆	2.8d	2.8e ₆	2.8f
C(1)–Pd(1)–O(n)	O(3) 92.5(3)	O(3) 92.36(10)	O(1) 91.51(8)	O(2) 95.10(8)	O(2) 91.42(7)	O(1) 93.58(8)
C(1)–Pd(1)–N(1)	82.2(3)	82.06(10)	82.58(8)	81.72(8)	82.26(7)	81.25(9)
N(1)–Pd(1)–O(n)	O(1) 93.3(2)	O(1) 95.60(8)	O(1) 93.70(7)	O(1) 94.30(7)	O(1) 94.15(6)	O(2) 93.70(7)
O(n)–Pd(1)–O(1)	O(3) 91.8(2)	O(3) 90.04(8)	O(2) 91.36(7)	O(2) 87.48(8)	O(2) 91.41(5)	O(2) 90.24(7)

2.4.2 Molecular structure of chloride-bridged palladacycles

As mentioned above all the X-ray crystal structures of the chloride-bridged palladacycles (**2.9a–f**) show a square-planar geometry with two ligands, bound through an M–N bond and an M–C(sp²), forming two equal five-membered rings, as reported by Montes for the equivalent non-fluorinated palladacycle (see structure of palladacycle **2.9b** in Figure 44).¹²⁹ Principal bond lengths and angles are given in Table 13 below.

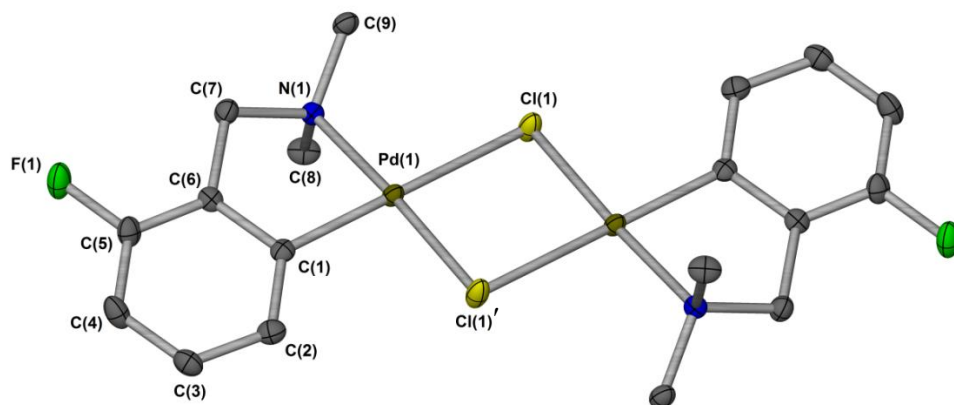


Figure 44: Molecular structure of palladacycle 2.9b. Hydrogen atoms were omitted for clarity; thermal ellipsoids shown with probability of 50%.

In the solid-state all the complexes adopt the *anti* isomeric form while in solution it is possible to observe both isomeric forms. The effective symmetry of these complexes in solution is expected to be C_{2h} for the *anti* isomer and C_{2v} for the *syn* assuming that the five-membered ring inverts rapidly. In contrast to the acetate-bridged structures, there is no folding at the bridging atom. A survey of the Cambridge Structural Database shows that this behaviour is characteristic of similar complexes with the majority having the Pd_2C_2 unit planar or very close to it. The Pd–Cl bonds in each structure are not the same due to the *trans* influence of the nitrogen and the aromatic carbon. Palladacycle **2.9d** (Figure 45) is the only complex with the potential for repulsion between the fluorine and the chlorine atom, and in fact the $Cl\cdots F(1)$ distance is 2.9264(1) Å, smaller (9%) than the sum of the van der Waals radii of 3.22 Å.¹³⁸ The complex shows a twist in the five-membered ring plane with respect to the plane containing both chlorine and palladium atoms.

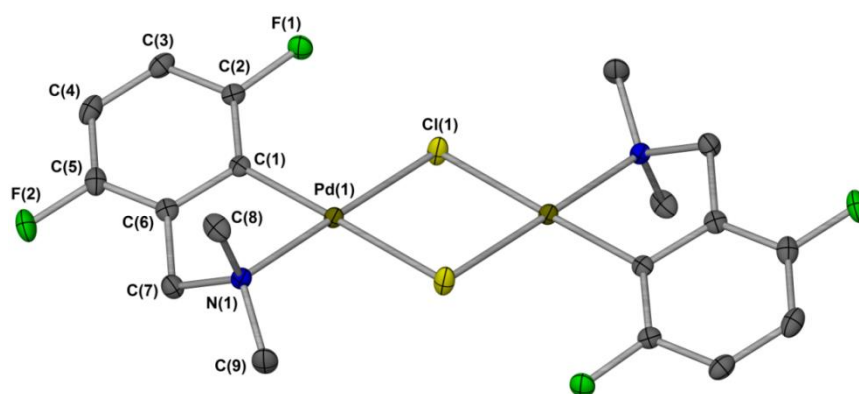


Figure 45: Molecular structure of palladacycle 2.9d. Hydrogen atoms were omitted for clarity; thermal ellipsoids shown with probability of 50%.

A similar twist was observed by Smith and co-workers for the complex methoxy-substituted di- μ -chlorobis(dialkylbenzylamine-2-C,N)-dipalladium(II).¹³⁹

The geometries of the planar structures are also defined by the same angles reported above for the acetate-bridged palladacycles in section 2.4.1. All the crystallographic data are reported in Appendix II, the main bond angles are repeated here in Table 13. There are no significant changes in the geometries of these palladacycles according to substitution.

Table 12: Selected bond lengths of palladacycles 2.9a–f.

Bond length (Å)	2.9b	2.9c ₆	2.9d	2.9e
C(1)–Pd(1)	1.967(4)	1.975(2)	1.997(3)	1.972(4)
Cl(1)–Pd(1)	2.4565(11)	2.4658(6)	2.4379(7)	2.4336(11)
Cl(1')–Pd(1)	2.3264(10)	2.3352(6)	2.3277(7)	2.3415(10)
C(n)–F(n)	C(5)–F(1) 1.363(5)	C(4)–F(1) 1.365(2)	C(2)–F(1) 1.366(3) C(5)–F(2) 1.369(3)	C(3)–F(1) 1.361(5) C(4)–F(2) 1.353(5)
N(1)–Pd(1)	2.073(3)	2.0820(19)	2.079(2)	2.080(3)

Table 13: Selected bond angles of palladacycles 2.9a–f.

Bond angle (°)	2.9b	2.9c ₆	2.9d	2.9e
C(1)–Pd(1)–Cl(1')	94.51(12)	95.16(7)	98.22(8)	94.899(11)
C(1)–Pd(1)–N(1)	82.69(14)	81.96(8)	82.18(10)	81.99(15)
N(1)–Pd(1)–Cl(1)	96.85(9)	97.49(5)	95.25(7)	97.73(10)
Cl(1')–Pd(1)–Cl(1)	85.92(4)	85.42(2)	84.36(3)	85.38(4)

2.5 Biological evaluation of novel palladacycles

Over the past decade it has been demonstrated that palladacycles show potent anticancer activity towards several cancer cell lines, as described by Kapdi and Fairlamb recently.⁸⁸ In particular Karami *et al.*¹⁴⁰⁻¹⁴¹ reported a study on palladacycles similar to those described in this chapter. The palladacycles synthesised here are fluorinated and due to the extensive studies on fluoroaromatics as pharmaceutical drugs^{50,142-143} a number of them (see 2.9c₆ and 2.9e₆ in Figure 46) were tested against ovarian cancer cells (A2780) provided by

the European Collection of Authenticated Cell Cultures (ECACC). All other compounds of interest, shown in Figure 46, could not be examined due to insolubility in the aqueous medium used to grow the cancer cells.

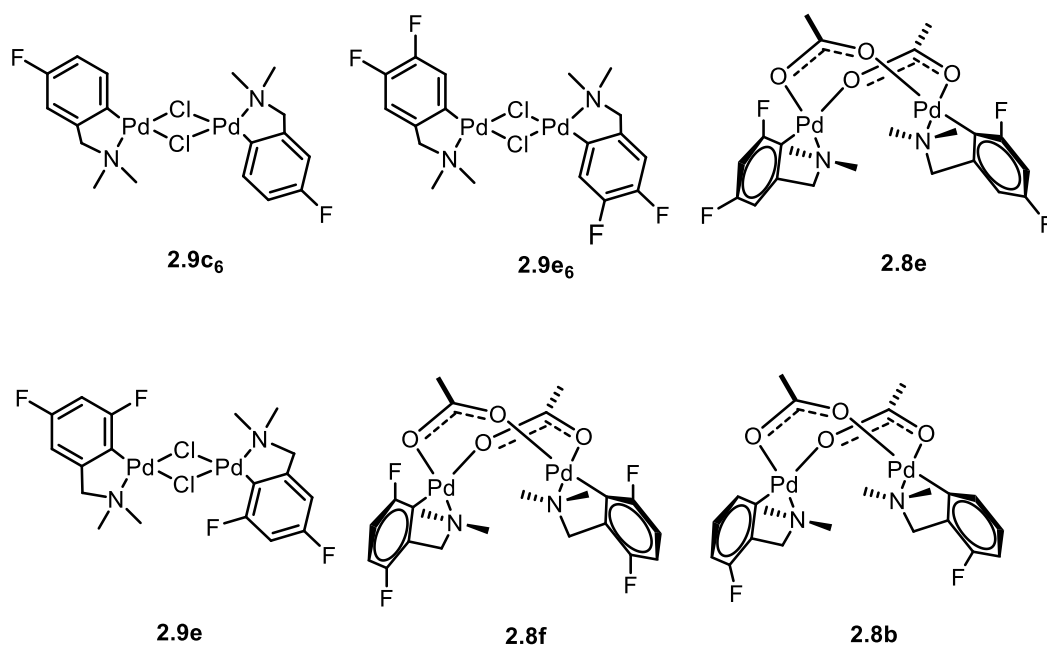


Figure 46: Mono and di-fluorinated palladacycles tested against ovarian cancer cells A2780.

2.5.1 Results and discussion

Palladacycle **2.9c₆** was dissolved in DMSO and the medium used to grow the cancer cells was added. The solution was sterilised through a filter and diluted as reported in the experimental Chapter 7. An aliquot of the prepared solution was added to each well of the plate (Figure 47). On the plate two controls were set up (one positive and one negative) and it was then left incubating for three days. An MTT assay was performed dissolving MTT (3-(4,5-dimethylthiazol-2-yl)-2,5-diphenyltetrazolium bromide) in phosphate-buffered saline, filtered through sterilising filters and the solution was added to each well. The plate was left incubating for 2 hours then it was centrifuged. An aliquot of medium was removed from each well and DMSO was added to dissolve the formazan (precipitate formed after metabolism, see colour of the wells in Figure 47).

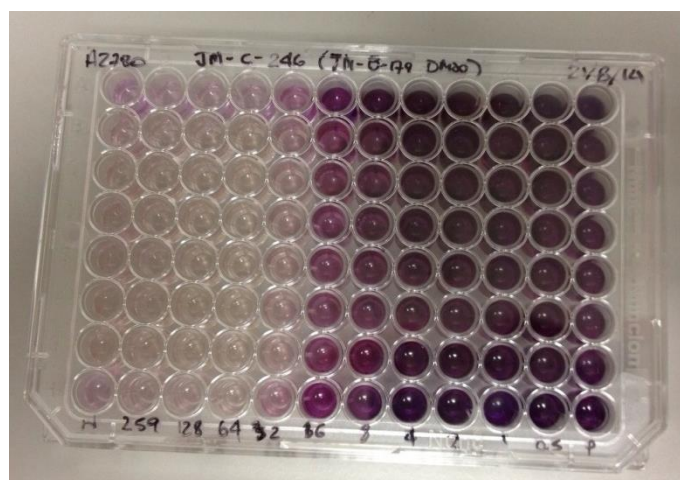


Figure 47: Plate containing 96 wells: each column contains a different concentration of compound from 0 μM to 260 μM .

The wells coloured in purple contain ovarian cancer cells which are still alive and correspond to the wells where the concentration of palladacycle is low. Absorbance was recorded at 540 nm using the plate reader and cell viability plotting as percentage from negative to positive controls. Figure 48 shows the curve used to calculate the IC_{50} value.

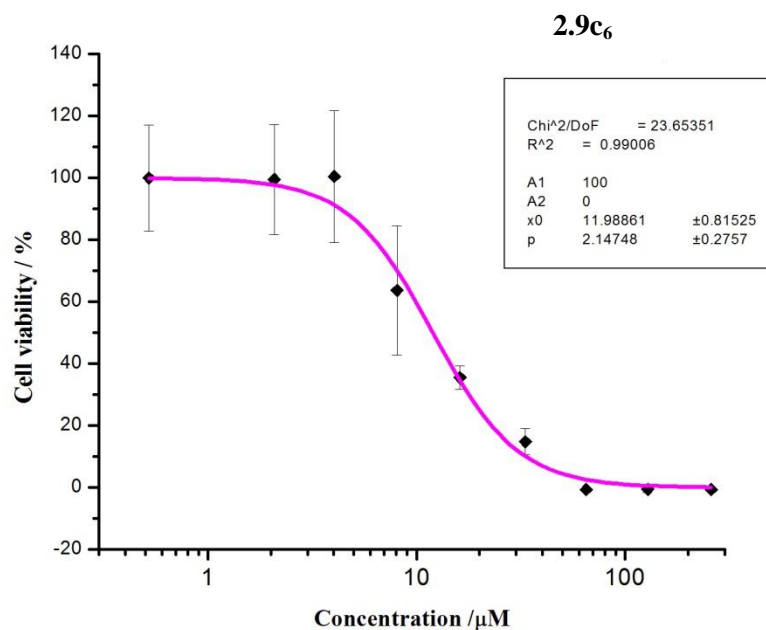


Figure 48: IC_{50} calculation for compound 2.9c₆ on ovarian cancer cells A2780.

The same experiment was performed with palladacycle 2.9e₆ and the curve used to calculate the IC_{50} is shown in Figure 49.

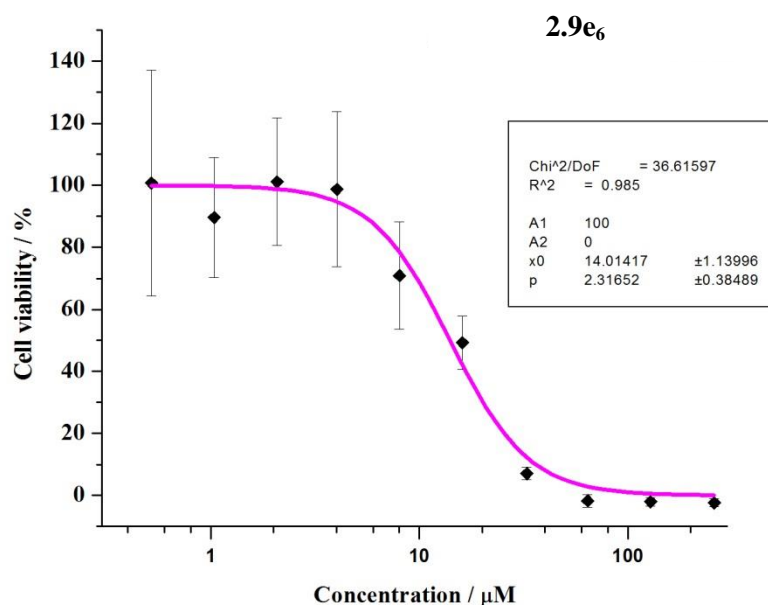


Figure 49: IC₅₀ calculation for compound 2.9e₆ on ovarian cancer cells A2780.

Palladacycles **2.9c₆** and **2.9e₆** show IC₅₀ values of 11.99 and 14.01 μM respectively, similar to those reported by Karami and co-workers (12–14 μM).⁸⁸

The study needs to be expanded to better explore the activity, in particular the palladacycles should be tested for a smaller and more detailed range of concentrations (*e.g.* between 11 and 15 μM) to obtain an exact IC₅₀ value. Moreover the test should be performed on three different batches of the same palladacycle to assess the reproducibility of the results. The error bars on the experimental results are typical for this kind of experiment due to the natural variations in living organisms.

2.6 Conclusions

This chapter has described the synthesis and full characterisation of novel fluorinated acetate- and chloride-bridged palladacycles (**2.8a–f** and **2.9a–f**, respectively) obtained from fluorinated *N,N*-dimethylbenzylamines **2.7a–f**.

The aim of this study was to assess the effect of fluorine substituents on the regioselectivity of intramolecular C–H activation reactions at palladium. The fluorinated *N,N*-dimethylbenzylamines **2.7a–f** were reacted with two different sources of palladium (Pd(OAc)₂ and Li₂PdCl₄) to study the regioselectivity in two different reaction mechanisms (CMD and S_EAr, respectively).

The study showed that when fluorinated benzylamines **2.7c** and **2.7e** react with Pd(OAc)₂ the products do not exhibit any regioselectivity for the C–H activation reaction, while the same substrates react with Li₂PdCl₄ to give selectively palladacycles **2.9c₆** and **2.9e₆** where the C–H activation occurs *para* to fluorine. The same palladacycles can then be converted to the relevant acetate-bridged palladacycles **2.8c₆** and **2.8e₆** by reaction with silver acetate, maintaining the regioselectivity.

The lack of regioselectivity in the acetate-bridged palladacycle system, which proceeds *via* a CMD mechanism, contrasts with the behaviour of fluorinated substrates in intermolecular reactions at palladium that give *ortho* selectivity.²⁰ Also the *para* selectivity obtained in the chloride-bridged palladacycle system, which proceed *via* an S_EAr mechanism, diverges completely from the previously reported intramolecular reaction of fluorinated imines at rhodium proceeding *via* the same mechanism.¹¹⁶

The presence of fluorine substituents has a distinct effect on the clamshell shape of the acetate-bridged palladacycle. Depending on the number and position of the fluorine atoms on the aromatic ring, the shape of the palladacycle changes, *e.g.* the difluorinated palladacycle **2.8d** has a more open clam shell structure than the non-fluorinated palladacycle **2.8a**, consistent with the weaker d⁸–d⁸ interaction between the palladium atoms. Also palladacycle **2.8d** shows a big twisting of the aromatic ring to relieve the repulsion between the oxygen and fluorine lone pairs. By contrast the chloride-bridged palladacycles **2.9a–f** have rigid planar structures that do not allow great structural variation. The impossibility of this important twist of the aromatic ring disfavors the formation of the *ortho* isomer in the C–H activation reaction of substrates, such as **2.7c** and **2.7e**, where there is a choice for the C–H activation, resulting in the formation of the *para* isomer only. In the case of **2.7d** where there is no choice, the fluorine has to occupy the *ortho* position and a slight twist is observed along with a very slow reaction. More general conclusions are given in Chapter 6.

Part of the work described in this chapter has been published and a full copy of the paper can be found in Appendix I.¹²²

Chapter 3. Fluorinated benzylphosphines and relevant palladacycles

3.1 Introduction

Phosphapalladacycles are an important class of compounds in catalytic processes at palladium, due to the important role phosphine ligands play in many reaction mechanisms involving transition metals.^{133,144-145} Their investigation and scope has developed enormously in recent decades following the early synthesis of Herrmann's catalyst (**3.1**, Figure 50) used in the Heck cross-coupling reactions of chloro- and bromoarenes.¹⁴⁶

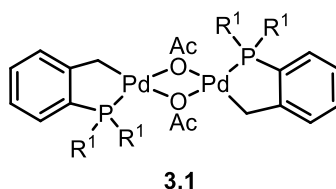


Figure 50: Herrmann's catalyst.

Phosphapalladacycles possess different properties to the aminopalladacycles described in Chapter 2, due to the lower basicity and the larger atomic radius of the phosphorus atom.¹⁴⁷ In contrast to the nitrogen atom,¹⁴⁸ phosphorus can also act as a π -acceptor, binding more strongly to some transition metals. A traditional description of the electronic interaction of a phosphorus–transition metal bond (M–P) involves two components:

- The σ component consists of donation of electrons from the phosphine ligand lone pair to an empty orbital, of σ pseudosymmetry, on the metal, M;
- The π component describes the back-donation from the filled orbitals on the metal, into empty orbitals, of a π pseudosymmetry, belonging to the phosphine ligand.¹⁴⁸

Ab initio molecular orbital calculations have been performed by Marynick and co-workers on simple phosphines (PR_3 with $\text{R} = \text{H}, \text{F}, \text{CH}_3$) to assess the nature of the LUMOs of phosphine ligands. They showed that the π -acceptor orbitals on the phosphorus consist of a doubly degenerate pair of orbitals of π symmetry, where not just the d orbitals of the phosphorus, but also the antibonding orbitals P–R σ^* are involved.¹⁴⁹ The σ^* orbitals mix into the phosphorus 3d orbitals generating the π -acceptor orbital as illustrated in Figure 51.¹⁴⁸

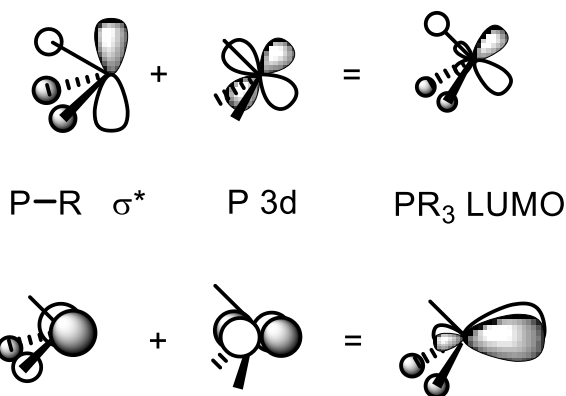


Figure 51: Mixing of P–R σ^* (phosphine) and P 3d orbitals resulting in the π -acceptor LUMOs on phosphorus.

A more electron withdrawing substituent R therefore increases the 3p character in the σ^* orbital, lowering its energy. A scale of π -acidity can be written as $\text{PF}_3 > \text{P(OAr)}_3 > \text{P(OR)}_3 > \text{PAr}_3 > \text{PR}_3$ where R is an alkyl group.¹⁵⁰

In this chapter the synthesis of fluorinated diphenylbenzylphosphines **3.2–3.5** and their relevant chloride-bridged and acetate-bridged phosphapalladacycles will be taken into consideration (Figure 52).

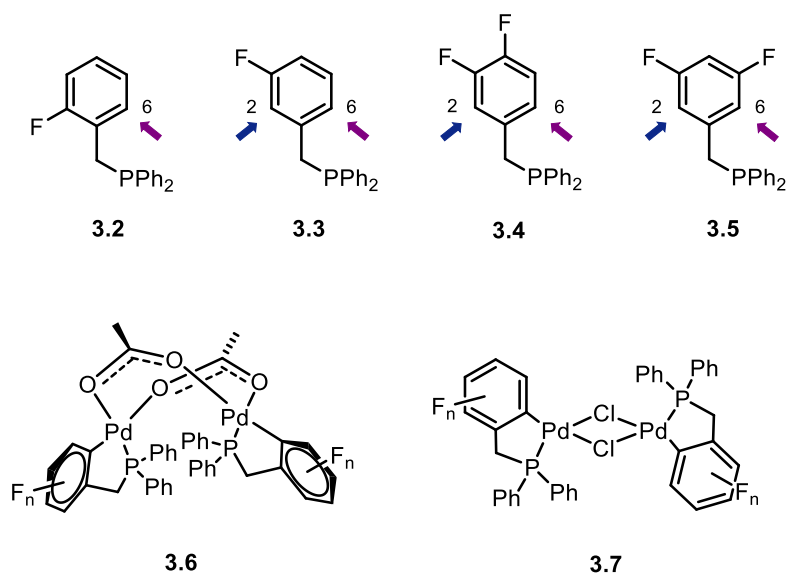


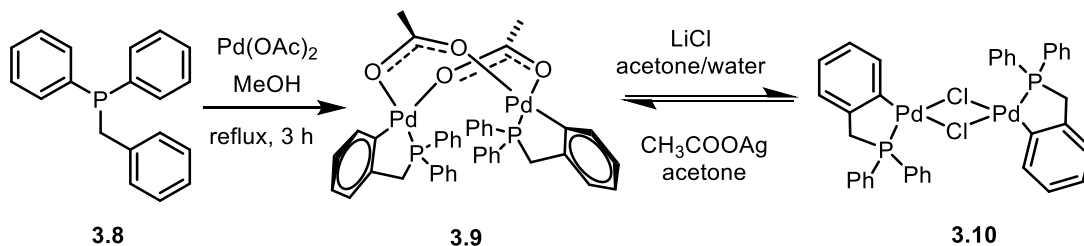
Figure 52: Fluorinated acetate-bridged and chloride-bridged palladacycles.

3.1.1 Synthesis of fluorinated phosphapalladacycles

As discussed in Chapter 1 there are several methods to synthesise palladacycles; hereafter only direct cyclometallation reactions and transmetallacyclisation reactions of tertiary phosphines at Pd will be discussed.

3.1.1.1 Direct reactions

The synthesis of acetate-bridged phosphapalladacycle **3.9** from diphenylbenzylphosphine **3.8**, was first reported by Hiraki and co-workers¹⁰⁰ *via* the direct reaction of the tertiary phosphine with Pd(OAc)₂. Due to the difficulties of purification of palladacycle **3.9**, they converted the impure product *via* a metathesis reaction to the chloride-bridged palladacycle **3.10**, and after a recrystallisation with chloroform, they convert the bridge back to the acetate yielding only 21% of the product **3.9** (Scheme 47).



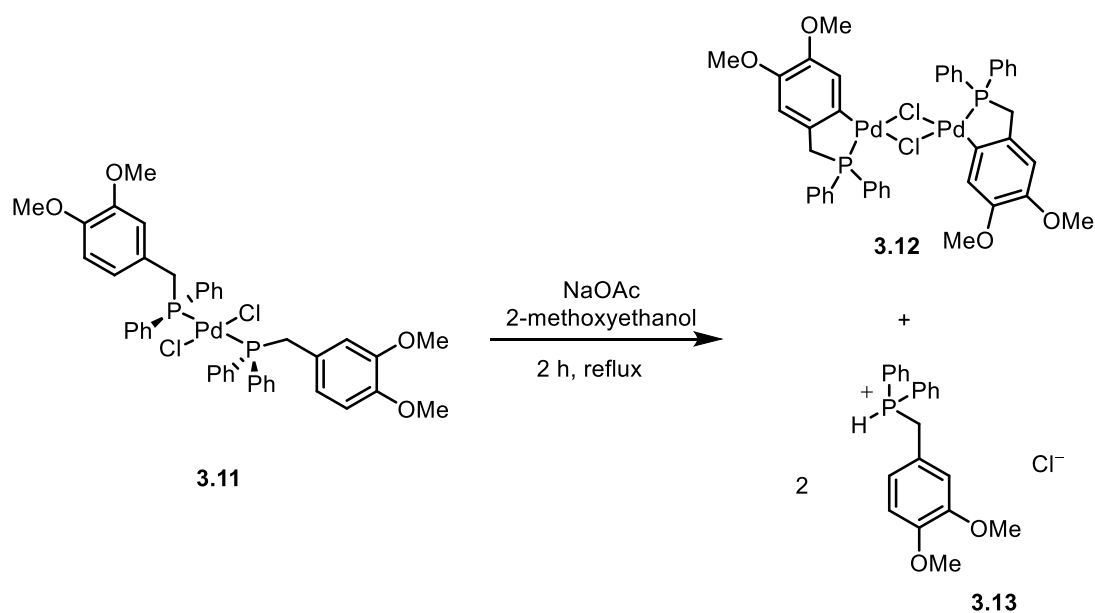
Scheme 47: Synthesis of palladacycles 3.9 and 3.10 (Hiraki *et al.*).

Later Shaw and co-workers reported an extensive study on the cyclometallation at platinum and palladium of tertiary benzylphosphines, noting the difficulty of employing phosphines that do not contain bulky groups on the phosphorus atom, such as the diphenylbenzylphosphine **3.8**.¹⁵¹⁻¹⁵² They also showed that the inclusion of *tert*-butyl groups on tertiary phosphines promotes the internal metal–carbon bond formation.¹⁰⁵ Although the mechanism of this kind of reaction is not fully understood,¹⁵³ the authors made some observations concerning the factors that could have an effect on the cyclometallation at transition metals of these substrates, based on their experimental results:

- *Steric hindrance*: the promotion of cyclometallation by bulky pre-ligands on the phosphorus atom can be explained using thermodynamic arguments. From a thermodynamic point of view, bulky ligands are not strongly bound to the metal in the phosphine–metal complex such as complex **3.10** (Scheme 47) due to their interactions with the other ligands in the *cis*-position (*e.g.* the Cl atoms in **3.10**). When the ligand cyclometallates, the *cis* ligand is eliminated, resulting in a stronger interaction between the phosphorus and the metal. From an entropic point of view the metallation is favoured by bulky ligands because only a small amount of rotational entropy is lost on cyclometallation due to the already restricted rotation around the P–M bond, while if the ligand is less hindered the loss of entropy is large and the P–M bond strength decreases.

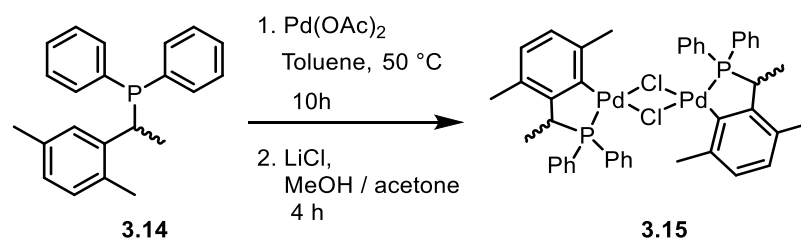
- *Ring size*: while for an amino ligand the cyclometallation reaction occurs only if a five-membered ring is formed,¹⁵⁴ tertiary phosphines are able to undergo cyclometallation to form five-, four- or even three-membered rings.¹⁵⁵

These observations were confirmed by the same researchers a few years later in a report concerning the entropic effects on formation of large macrocycles and cyclometallation reactions¹⁵⁶ and the influence of the Thorpe–Ingold effect, also called “gem-dimethyl effect”, in the synthesis of smaller rings.¹⁵⁷ Soon after, they also showed that while di(*tert*-butyl)benzylphosphine is readily metallated, the same is not true for di(*tert*-butyl)(*o*-tolyl)- and (*tert*-butyl)-di(*o*-tolyl)phosphine. This suggests that the difference is due to electronic rather than steric effects, considering that all three systems have similar steric bulk, and should cyclometallate, forming a 5-membered ring.¹⁰² Later they managed to synthesise complex **3.12** (Scheme 48)¹⁵⁸ starting from complex **3.11** in 2-methoxyethanol and using sodium acetate, known as an agent to promote cyclometallation.¹⁵⁹



Scheme 48: Synthesis of palladacycle 3.8 (Shaw *et al.*).

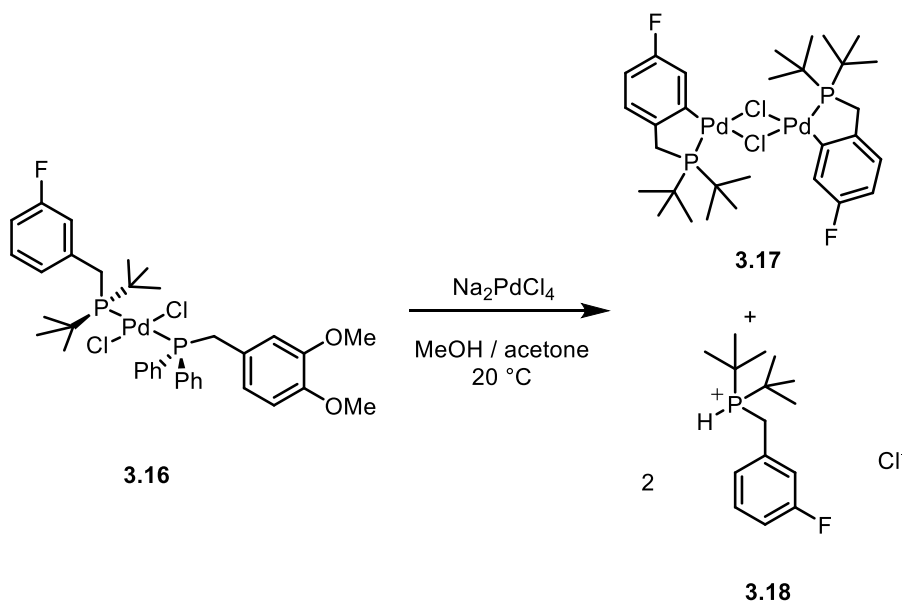
Leung and co-workers have reported the synthesis of a similar palladacycle (**3.15**)¹⁶⁰ reacting the racemic phosphine **3.14** directly with Pd(OAc)₂ followed by chloride metathesis with LiCl (Scheme 49).



Scheme 49: Synthesis of palladacycle 3.15 (Leung *et al.*).

It is clear that electronic effects play a role in the cyclopalladation reactions of these two phosphines. In internal metallation at iridium it has already been shown that electron-donating groups on the aromatic ring of analogues of triphenylphosphine, affect the rate of *ortho*-metallation, *e.g.* for complexes such as [IrCl{P(C₆H₄X)₃}₃] the rate of cyclometallation increases in the order X = F < H < OMe < Me.¹⁶⁰

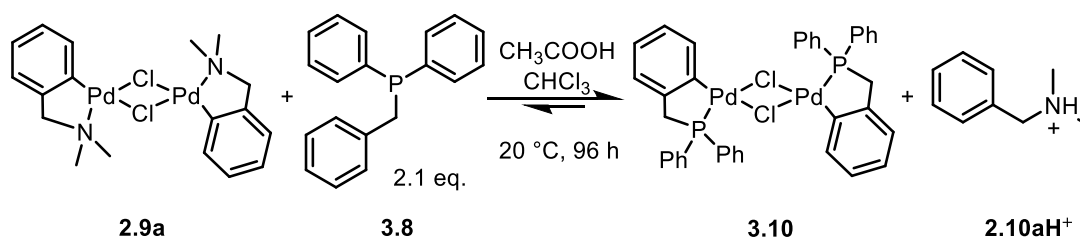
Vrieze and co-workers reported that bulky fluorinated tertiary phosphines (cyclohexyl and *t*-butyl groups on the phosphorus) could activate the C–H *ortho* to the fluorine atom in cyclometallation reactions at Ir and Rh and the one *para* to fluorine for reactions of the same substrates at Pd.¹⁵³ The authors attributed the difference in regioselectivity to a difference in mechanism, suggesting a nucleophilic mechanism for reaction at Ir(I) and Rh(I) and an electrophilic one for reaction at Pd(II). The regiochemistry of the C–H activation reactions was determined by 1D ¹⁹F-NMR spectroscopy, which for these kind of compounds is not very explanatory, as shown in Chapter 2 for amino-type palladacycles. Also the mechanisms have not been validated with further experiments and they only rely on the electrophilic or nucleophilic behaviour of the metal. (Scheme 50).¹⁵³



Scheme 50: Synthesis of fluorinated palladacycle 3.17.

3.1.1.2 Transmetallation reactions

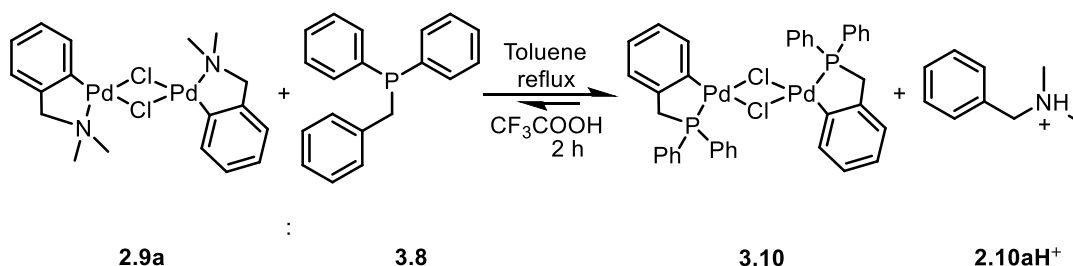
Due to the aforementioned issues with the direct reaction of diphenylbenzylphosphines to form the acetate- and chloride-bridged phosphapalladacycle, the procedure reported by Ryabov and co-workers using a ligand-exchange reaction from the chloride-bridged palladacycle **3.10**, with the tertiary phosphine **3.8**, was taken into consideration as possible alternative.¹⁶¹



Scheme 51: Synthesis of palladacycle 3.10 by ligand-exchange reaction.

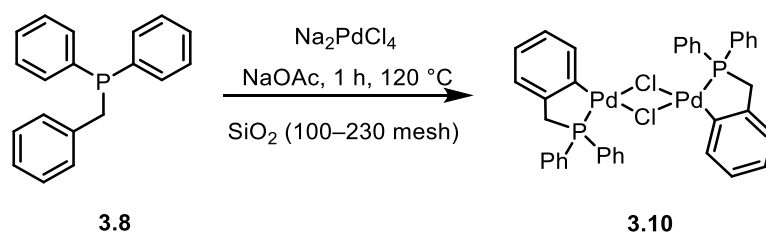
Ryabov and co-workers reported that exchange could be achieved between a nitrogen and a phosphorus ligand, as shown in Scheme 51, or between two different nitrogen ligands or two different phosphorus ligands.^{64,114} Later they studied the kinetics, thermodynamics and mechanism of these reactions⁶⁴ and concluded that the exchange between ligands takes place due to acidolysis of the starting palladacycle. The mechanism was described as a two-step dissociative process in which the Pd–N bond is cleaved in the first step followed by Pd–C bond cleavage. The reaction can be viewed as an equilibrium that is shifted towards the formation of a complex with the ligand containing the strongest electron donating group.

Pfeffer and co-workers improved the yield of this transmetallacyclisation reaction using trifluoroacetic acid in toluene instead of acetic acid in methanol (Scheme 52)¹¹⁵ obtaining palladacycle **3.10** as the main product along with the protonated amine **2.10aH⁺**.



Scheme 52: Improved synthesis of palladacycle 3.10 by ligand-exchange reaction.

Finally Smoliakova and co-workers reported the synthesis of non-fluorinated phosphapalladacycle **3.10** from diphenylbenzylphosphine (**3.8**) in a solvent-free system using silica gel as a support.¹⁶² They also confirmed the structure of the compound **3.10** *via* full characterisation data and crystallographic analysis that had not been previously reported.



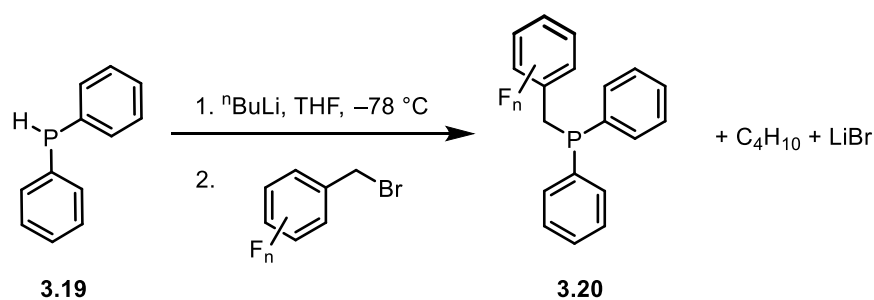
Scheme 53: Synthesis of palladacycle 3.10 in a solvent-free system.

In this chapter an investigation into the effects of fluorine substituents in the regioselectivity of intramolecular C–H activation reactions of fluorinated benzylphosphines at palladium is described. The resulting fluorinated phosphine-derived palladacycles are, in fact, closer systems to those calculated theoretically by Perutz and co-workers on intermolecular arylation reactions of fluoroaromatics described earlier (see Chapter 2).⁶⁸

The aim was to explore whether an *ortho* fluorine effect could be observed in intramolecular C–H activation reactions of fluorinated diphenylbenzylphosphines at Pd as reported experimentally by Vrieze and co-workers for similar substrates (Scheme 50).¹⁵³

3.1.2 Fluorinated benzylphosphines

Tertiary phosphines are a versatile class of compounds used as ligands in the synthesis of transition metal complexes and as reagents in organic transformations.¹⁶³ General synthetic methodologies for the synthesis of tertiary phosphines include reactions of halo-phosphines with organometallic reagents such as Grignards or organolithiums,^{164–165} or reactions of phosphides with aryl halides catalysed by transition metals.¹⁶⁶ Both of these methods are widely used for the synthesis of aromatic phosphines, but the synthesis of benzylic phosphines has not been extensively studied and in particular, only a limited number of fluorinated tertiary phosphines with diphenyl groups on the phosphorus atom are reported, and those that are are not fully characterised.^{153,167} The syntheses of all fluorinated benzylphosphines **3.2–3.5** reported in this chapter were based on the synthesis of diphenylbenzylphosphine **3.8** reported by Freitag and co-workers (Scheme 54)¹⁶⁸ using slightly different conditions for each substrate.



Scheme 54: Synthesis of fluorinated diphenylbenzylphosphines.

3.2 Results

3.2.1 Syntheses of fluorinated benzylphosphines

Four different systems were chosen to study (**3.2**–**3.5** in Figure 53): **3.2** and **3.5** are monofluorinated and difluorinated benzylphosphines respectively, presenting just one possibility for the C–H activation (C-6 in **3.2** and equivalent positions C-2 and C-6 for **3.5**), while **3.3** and **3.4** are monofluorinated and difluorinated benzylphosphines respectively, offering two possibilities for the attack at C-2 and C-6.

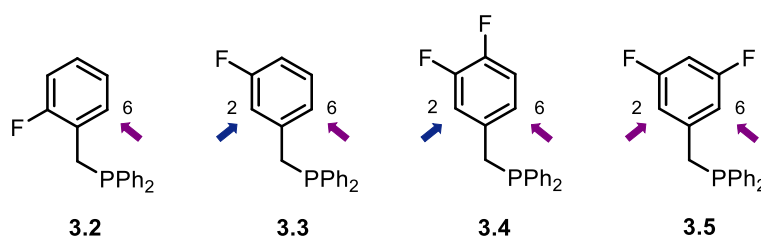
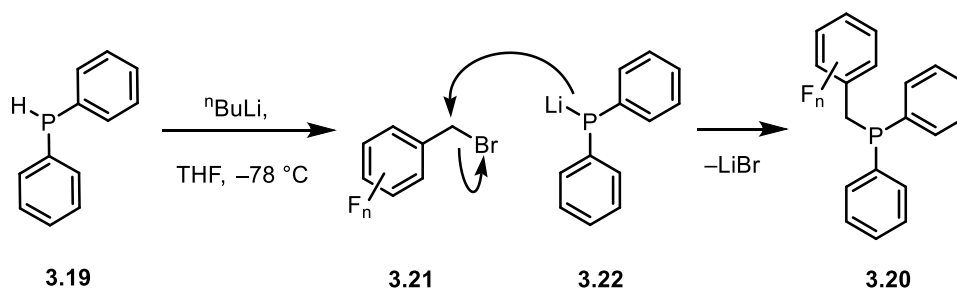


Figure 53: Fluorinated benzylphosphines synthesised and used in this study.

Substrates **3.3**¹⁵³ and **3.5**¹⁶⁷ were already used in the literature as ligands but no characterisation data or synthetic procedures were reported. All these fluorinated benzyldiphenylphosphines (**3.2**–**3.5**) were synthesised as reported in Scheme 54.

The reaction of lithium diphenylphosphide, **3.22**, with the appropriate benzyl bromides is expected to proceed via an S_N2 mechanism (Scheme 55).



Scheme 55: S_N2 mechanism for the synthesis of fluorinated tertiary phosphines.

The deprotonation of the colourless diphenylphosphine (**3.19**) with ⁿBuLi, in THF at -78°C , produced a bright red/orange solution corresponding to the lithium phosphide (**3.22**), which reacts with the relevant fluorobenzylbromide giving LiBr and the corresponding product (**3.20**). All of the benzylphosphines were handled as air sensitive compounds.

The spectroscopic data for 2-fluoro-diphenylbenzylphosphine (**3.2**) are taken as representative of this series of substrates and discussed in detail below. The ¹H-NMR spectrum (Figure 54) run in C₆D₆, shows two multiplets at δ 7.40–7.33 and 7.06–7.01 corresponding to the aromatic protons of the two equivalent phenyl rings. It also shows two multiplets centered at δ 6.91 and 6.76 and one triplet of doublets at δ 6.66 ($J = 7.5, 1.6$ Hz) belonging to the four aromatic protons in the fluorinated benzyl ring coupled to the fluorine atom. The methylene protons resonate at δ 3.34 as a singlet, not showing a coupling with the phosphorus atom as observed for the non-fluorinated diphenylbenzylphosphine **3.8**.¹⁶⁸

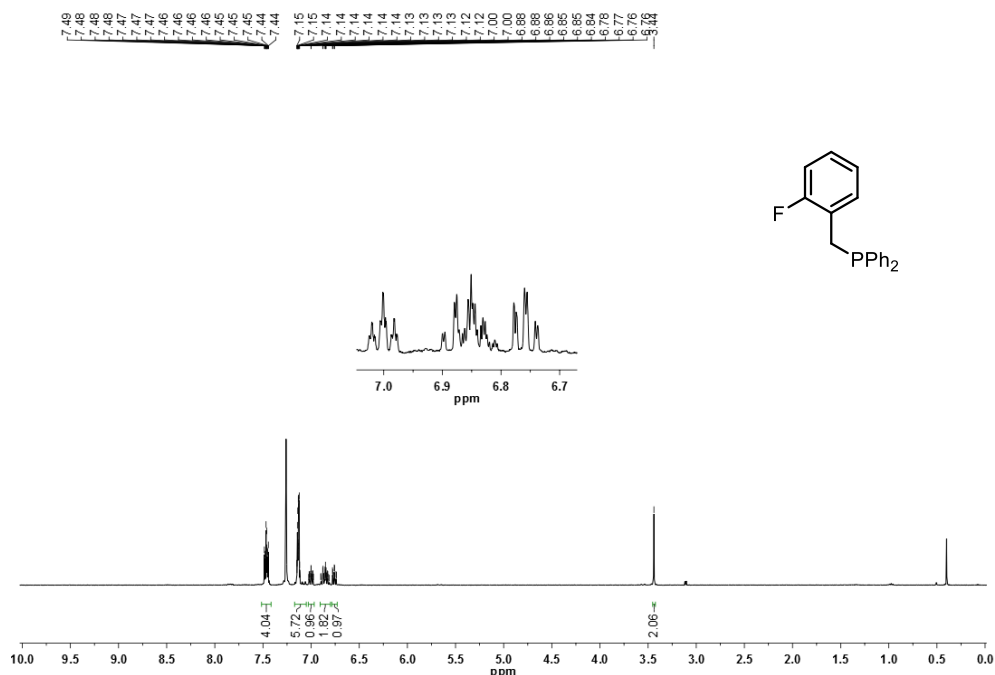


Figure 54: ¹H-NMR spectrum of 3.2 in C₆D₆ at 294 K (400 MHz).

The ^{31}P -NMR spectrum (Figure 55) shows a doublet due to the coupling with the fluorine ($^4J_{\text{P-F}} = 13.2 \text{ Hz}$) at $\delta -10.91$, again in a range consistent with literature value for diphenylbenzylphosphine **3.8**.

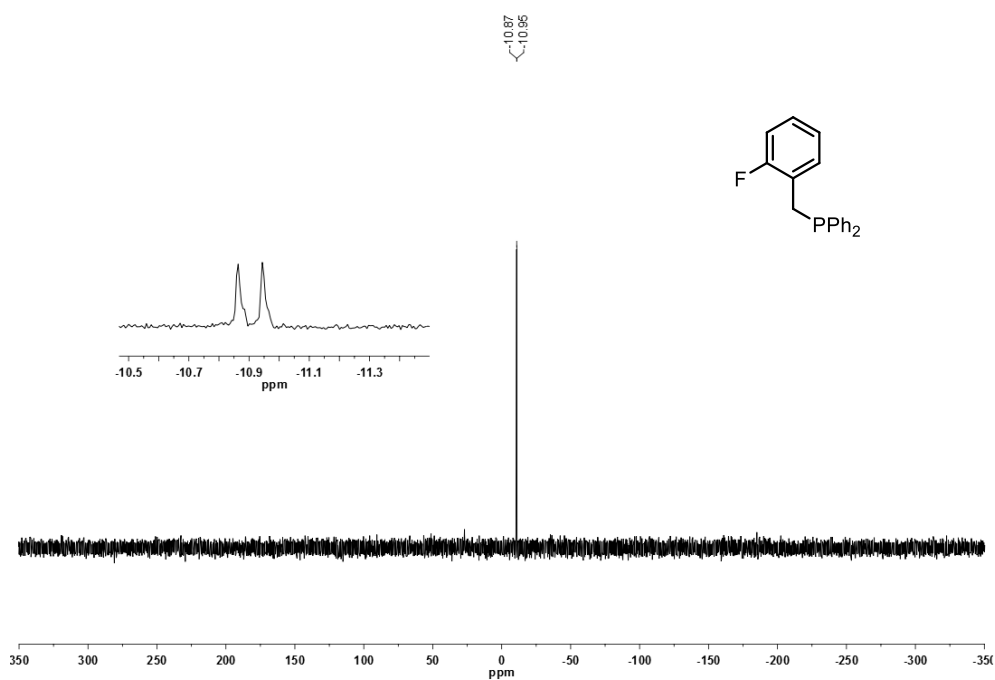


Figure 55: ^{31}P -NMR spectrum of **3.2** in C_6D_6 at 294 K (162 MHz).

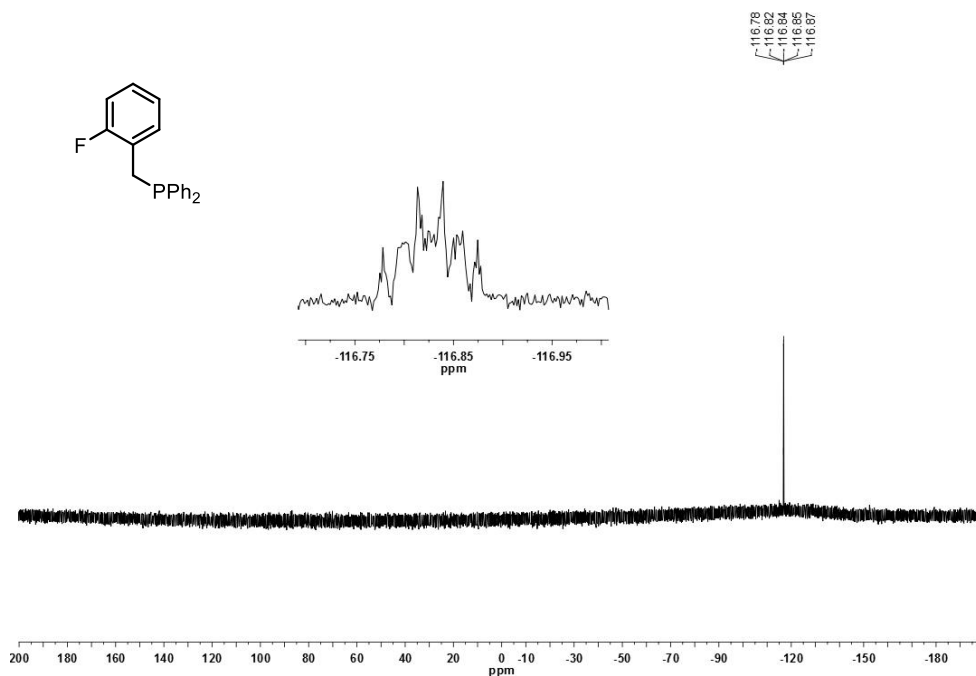


Figure 56: ^{19}F -NMR spectrum of **3.2** in C_6D_6 at 294 K (376 MHz).

The fluorine atom on the benzyl ring resonates as a multiplet centered at $\delta -116.84$ in the ^{19}F -NMR spectrum of **3.2** (Figure 56) due to the coupling with the aromatic protons

and with the phosphorus. The ^{13}C -NMR spectrum (Figure 57) was run in CDCl_3 , to avoid the overlap of the residual benzene signal with the aromatic protons of the two equivalent phenyl groups, which resonate as two doublets at δ 133.1 ($J = 18.8$ Hz) and 128.5 ($J = 6.6$ Hz), a doublet at δ 115.4 ($J = 22.2, 1.4$ Hz) and as a singlet at δ 129.1. The spectrum also shows a doublet of doublets at δ 161.0 for the carbon bonded to the fluorine ($J = 245.4, 4.3$ Hz) and four doublets of doublets at δ 131.4 ($J = 7.8, 4.3$ Hz), 127.8 ($J = 8.1, 2.6$ Hz), 124.8 ($J = 15.3, 8.3$ Hz) and 123.9 ($J = 3.5, 1.7$ Hz) respectively for the non-equivalent *ortho*- and *meta*-carbons and a doublet at δ 138.1 ($J = 15.0$ Hz) for the quaternary carbon *ortho* to F. High resolution ESI mass spectrometry confirmed the identity of compound **3.2** as the m/z value found for $[M+H]^+$ was 295.1053 (calculated for $\text{C}_{19}\text{H}_{17}\text{FP}$ 295.1046 $[M-H]^+$, $\Delta = -0.6$ mDa).

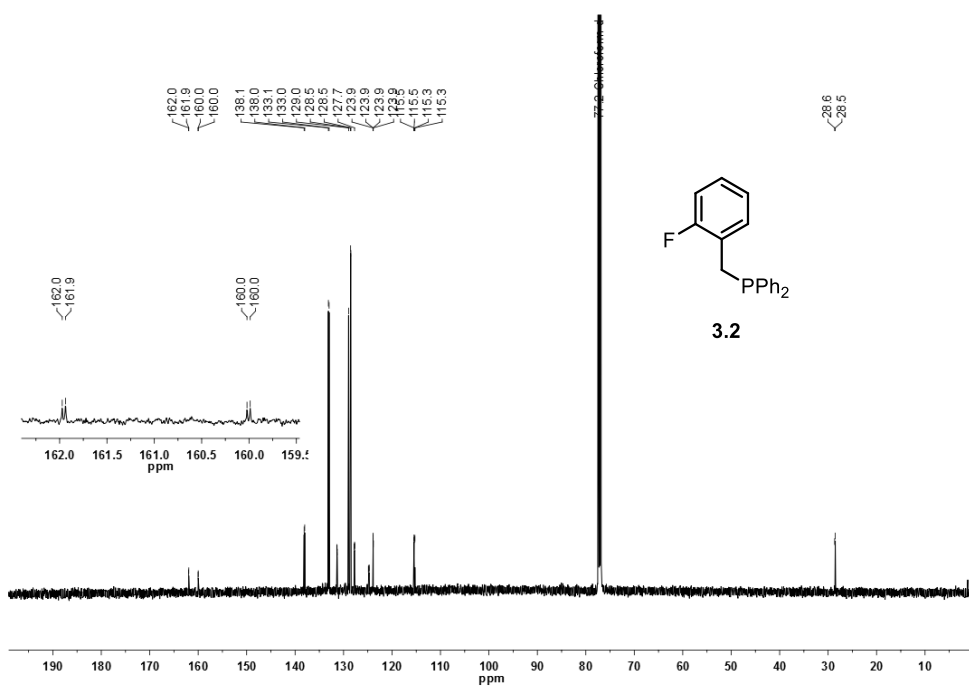


Figure 57: ^{13}C -NMR spectrum of **3.2** in CDCl_3 at 298 K (126 MHz).

Procedures for the synthesis and characterisation of the other fluorinated phosphines were similar to those of **3.2** and their spectroscopic data are reported in Table 14 and Table 15.

Table 14: NMR Data (δ (J/Hz)) for tertiary diphenylbenzylphosphines 3.8 and 3.3–3.5.

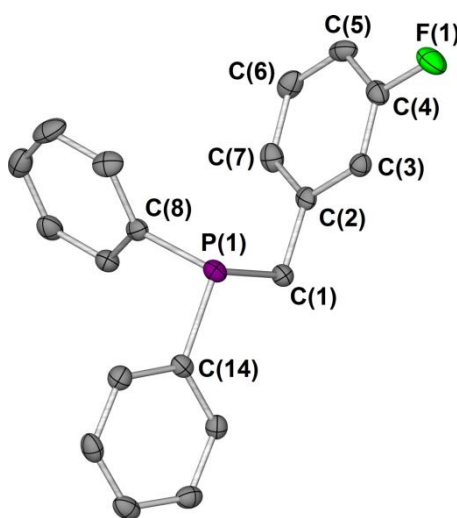
Compound	δ ($^{31}\text{P}\{^1\text{H}\}$) / ppm	δ (^1H) / ppm	δ (^{19}F) / ppm
3.8 ^a CDCl ₃	-10.00 (s)	7.12–7.47 (m, 15H), 3.33 (s, 2H)	-
3.3 CDCl ₃	-9.94 (s)	7.43–7.36 (m, 4H), 7.15–7.11 (m, 6H), 6.91–6.81 (m, 2H), 6.78 (m, 1H), 6.73 (ddd, $J = 9.7, 2.4, 1.2$ Hz, 1H), 3.20 (s, 2H)	-113.47 (m)
3.4 C ₆ D ₆	-10.0 (s)	7.27 (m, 4H), 7.05 (m, 6H), 6.64 (ddt, $J = 11.2, 7.6, 1.7$ Hz, 1H), 6.55 (dt, $J = 10.2, 8.4$ Hz, 1H), 6.41 (ddd, $J = 5.9, 3.7, 1.7$ Hz, 1H), 2.99 (s, 2H)	-138.09 – -138.18 -141.63 – -141.73
3.5 C ₆ D ₆	-9.16 (s)	7.24 (m, 4H), 7.02 (m, 6H), 6.42 (m, 2H), 6.32 (m, 1H), 2.94 (s, 2H)	-110.30– -110.40

^areference ¹⁶⁸

Table 15: ^{13}C -NMR Data (δ (J/Hz)) in CDCl_3 for the tertiary diphenylbenzylphosphines 3.2–3.5

Compound	δ (^{13}C) / ppm
3.2	161.0 (dd, $J = 245.4, 4.3$ Hz), 138.1 (d, $J = 15.0$ Hz), 133.1 (d, $J = 18.8$ Hz), 131.4 (dd, $J = 7.8, 4.3$ Hz), 129.0 (s), 128.5 (d, $J = 6.6$ Hz), 127.8 (dd, $J = 8.1, 2.6$ Hz), 124.8 (dd, $J = 15.3, 8.3$ Hz), 123.9 (dd, $J = 3.5, 1.7$ Hz), 115.4 (dd, $J = 22.2, 1.4$ Hz), 28.6 (d, $J = 16.2$ Hz)
3.3	163.2 (dd, $J = 245.2, 1.9$ Hz), 140.7 (dd, $J = 8.4, 7.7$ Hz), 138.7 (d, $J = 16.3$ Hz), 133.3 (d, $J = 18.8$ Hz), 129.9 (dd, $J = 8.4, 1.6$ Hz), 129.0 (s), 128.7 (d, $J = 6.4$ Hz), 125.3 (dd, $J = 6.8, 2.8$ Hz), 116.6 (dd, $J = 21.4, 6.6$ Hz), 113.1 (dd, $J = 21.0, 2.6$ Hz), 36.1 (dd, $J = 17.2, 1.9$ Hz)
3.4	150.4 (ddd, $J = 247.3, 12.7, 1.8$ Hz), 149.1 (ddd, $J = 245.9, 12.7, 3.0$ Hz), 138.4 (d, $J = 16.0$ Hz), 135.0 (ddd, $J = 9.0, 5.8, 3.9$ Hz), 133.2 (d, $J = 18.7$ Hz), 129.1 (s), 128.7 (d, $J = 6.5$ Hz), 125.5 (td, $J = 6.3, 3.5$ Hz), 118.3 (dd, $J = 17.2, 6.6$ Hz), 117.0 (d, $J = 17.6$ Hz), 35.34 (dd, $J = 17.2, 1.0$ Hz)
3.5	162.9 (ddd, $J = 247.7, 13.2, 1.6$ Hz), 137.5 (d, $J = 14.8$ Hz), 134.5 (t, $J = 12.9$ Hz), 133.0 (d, $J = 18.7$ Hz), 129.2 (s), 128.7 (d, $J = 6.6$ Hz), 112.2 (m), 101.6 (td, $J = 25.3, 2.2$ Hz), 36.2 (d, $J = 17.1$ Hz)

Compounds **3.3** and **3.5** were crystallised in air by slow evaporation of a saturated solution of the compound in MeOH at 2 °C. Compound **3.3** crystallised as the phosphine (Figure 58), whilst **3.5** crystallised as its phosphine oxide (Figure 59).

**Figure 58:** Molecular structure of compound **3.3**. Hydrogen atoms were omitted for clarity; thermal ellipsoids shown with probability of 50%.

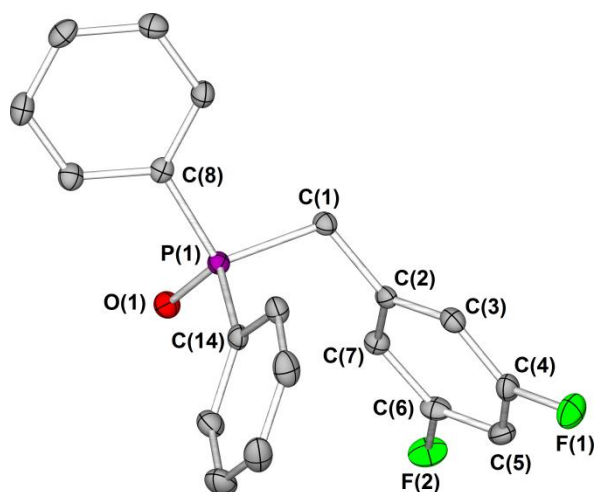


Figure 59: Molecular structure of compound 3.5 in the oxide form. Hydrogen atoms were omitted for clarity; thermal ellipsoids shown with probability of 50%.

Table 16: Selected distances (Å) and angles (°) in fluorinated phosphines 3.3 and 3.5 oxide.

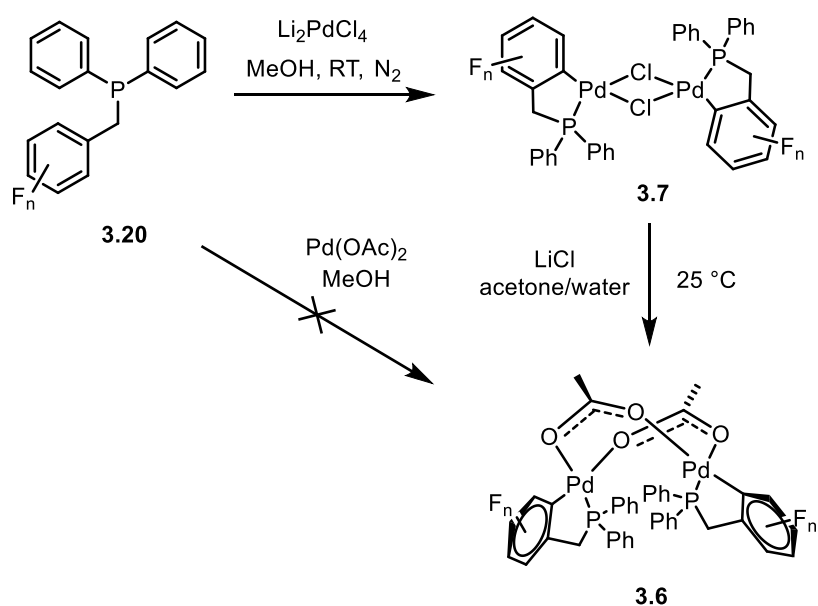
Bond Length / Å	3.3	3.5
C(1)–P(1)	1.8603(19)	1.8117(18)
C(8)–P(1)	1.838(2)	1.8061(18)
C(14)–P(1)	1.8352(19)	1.8045(19)
C(n)–F(n)	C(4)–F(1) 1.364(2)	C(4)–F(1) 1.362(2) C(6)–F(2) 1.358(2)
P(1)–O(1)	-	1.4905(13)
Bond Angle / °	3.3	3.5
C(n)–P(n)–C(n)	C(8)–P(1)–C(1) 99.33(9) C(14)–P(1)–C(1) 103.26(9)	C(8)–P(1)–C(1) 106.41(8) C(14)–P(1)–C(1) 106.45(8)
C(2)–C(1)–P(1)	108.05(13)	112.20(12)
O(1)–P(1)–C(1)	-	114.01(8)
O(1)–P(1)–C(8)	-	111.64(8)
O(1)–P(1)–C(14)	-	111.81(8)

3.2.2 Synthesis of fluorinated palladacycles

The study of the fluorinated phospho-palladacycles started with the selection of a model reaction, the synthesis of the acetate-bridged phosphapalladacycle **3.9** from

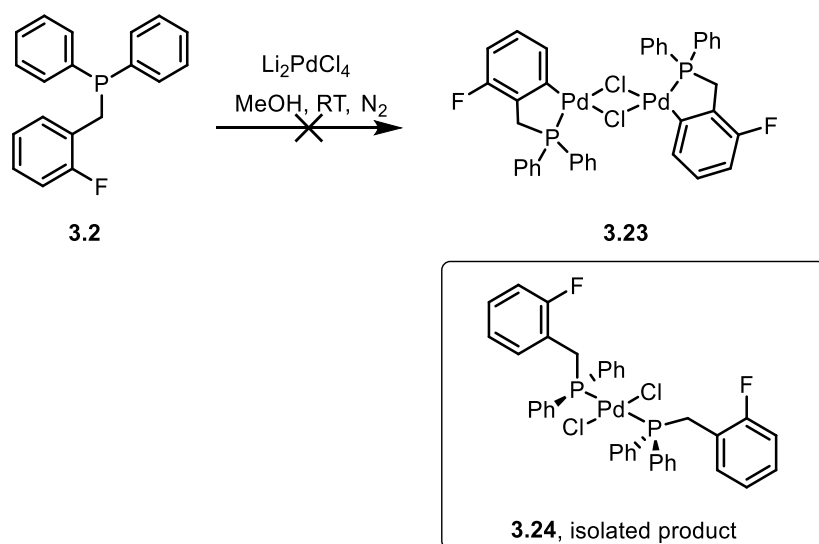
diphenylbenzylphosphine **3.8** reported by Hiraki and co-workers¹⁰⁰ via direct reaction of the tertiary phosphine with Pd(OAc)₂ (model reaction with fluorinated substrates in Scheme 56). In our hands the reaction performed first in methanol as in the Hiraki procedure and then in acetonitrile, according to the study by Fairlamb and co-workers,^{109,122} gave a mixture of products that were not possible to separate by flash chromatography (30:70, hexane/ethyl acetate).

Due to the difficulty in obtaining the acetate-bridged product using a direct reaction, the synthesis of chloride-bridged palladacycles using Li₂PdCl₄, followed by the conversion to acetate-bridged palladacycles by reaction with silver acetate was considered as a viable alternative (Scheme 10).¹⁰⁰



Scheme 56: Synthesis of palladacycles 3.6 and 3.7 (based on Hiraki *et al.* method).

The methodology was tested directly with fluorinated substrate **3.2** to form the fluorinated chloride-bridged palladacycle **3.23** (Scheme 57) using Li₂PdCl₄ as source of palladium.



Scheme 57: Failed synthesis of palladacycle 3.23 along with the unexpected product 3.24.

The product was not the expected palladacycle **3.23**, but the monomeric complex **3.24**, that was crystallised by slow diffusion of a saturated solution of the compound in CDCl_3 (Figure 60).

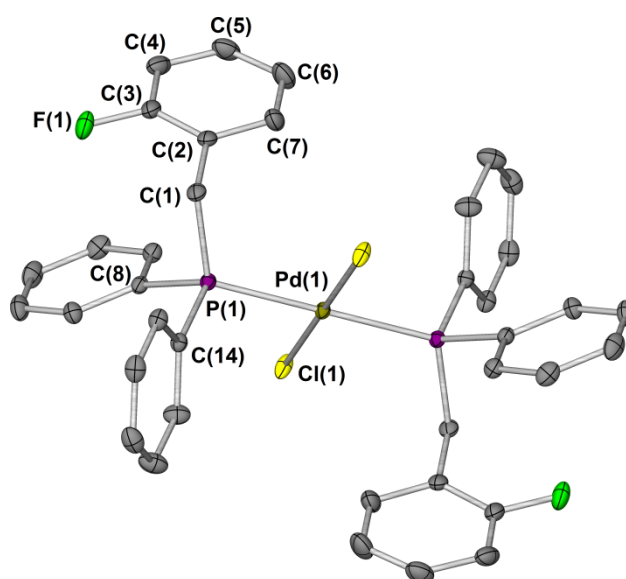
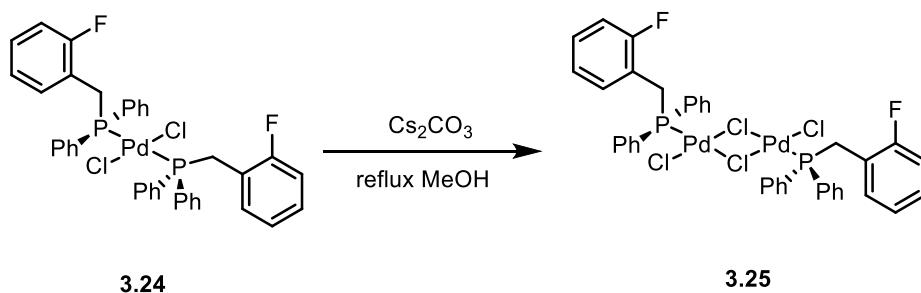


Figure 60: Molecular structure of complex 3.24. Hydrogen atoms were omitted for clarity; thermal ellipsoids shown with probability of 50%.

The monomeric complex **3.24** was reacted with caesium carbonate in refluxing methanol to attempt the cyclometallation reaction, but the dimeric non-cyclometallated compound **3.25** was the only product obtained (Scheme 58).



Scheme 58: Attempted at cyclometallation reaction from monomer 3.24.

The dimeric complex **3.25** shows a broad singlet at δ 29.74 in the ^{31}P -NMR spectrum shifted to high frequency with respect to the monomeric complex **3.24** (δ 20.91) and a multiplet at δ -113.03 in the ^{19}F -NMR spectrum with a chemical shift almost identical to the monomeric compound **3.24** (δ -113.07). LIFDI mass spectrometry confirmed the formation of the dimeric product **3.25** giving the molecular ion (minus two molecules of HCl) as the only peak with a characteristic isotope pattern of a dinuclear palladium compound ($m/z = 869.90$).

As previously discussed Shaw and co-workers reported an extensive study of direct cyclometallation reactions with non-bulky phosphines and in particular they managed to synthesise palladacycle **3.12** (Figure 61)¹⁵⁸ in 2-methoxyethanol using sodium acetate starting from the monomeric complex **3.11**.¹⁵⁹

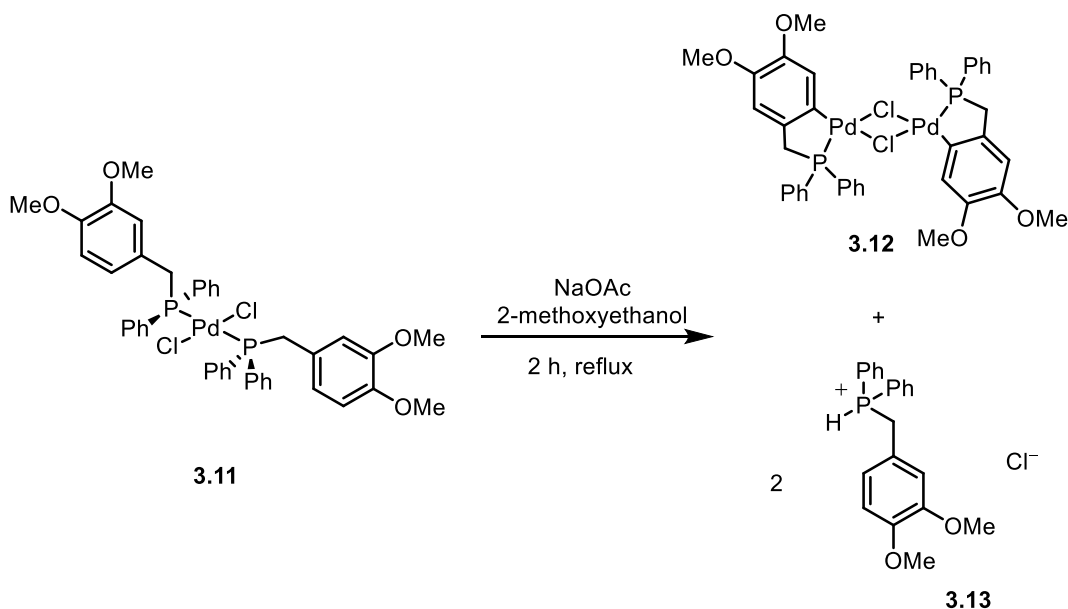
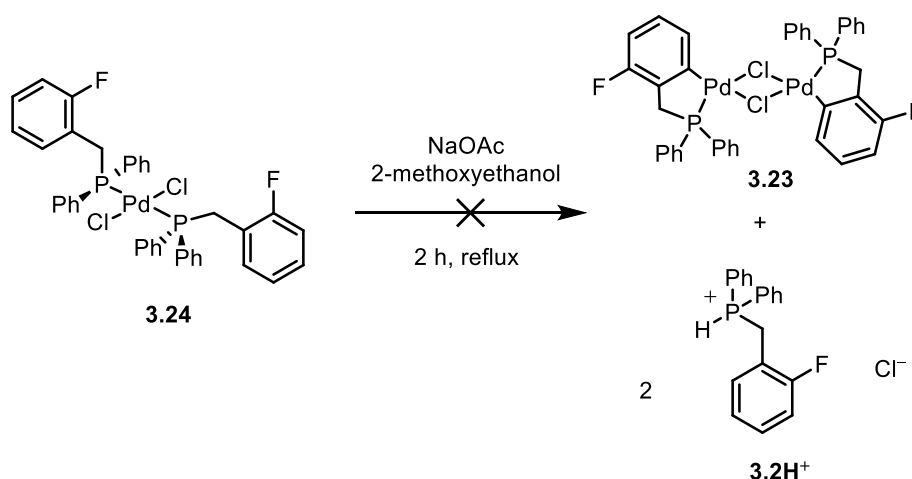


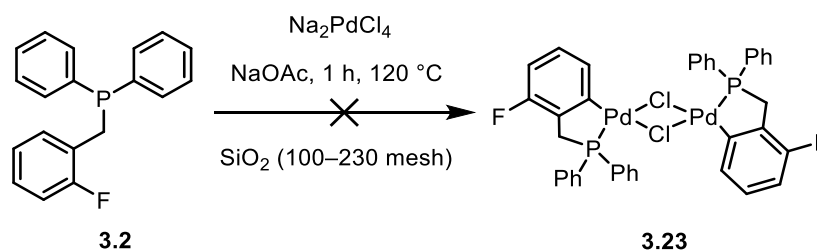
Figure 61: Palladacycle 3.12 synthesised by Shaw *et al.*

The same reaction conditions were used with fluorinated complex **3.24**, but the expected cyclometallated product (**3.23**) was not obtained (Scheme 59). The only species detected by NMR spectroscopy was complex **3.25** along with the starting material.



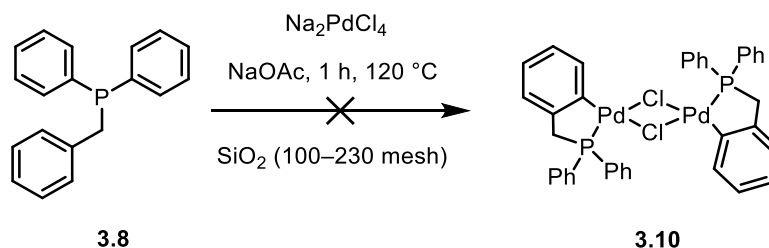
Scheme 59: Attempted synthesis of palladacycle **3.23** using the procedure of Shaw *et al.*

The next attempt was to use the procedure of Smoliakova and co-workers (see section 3.1), which employs silica gel in a solvent-free system.¹⁶² This reaction was attempted using 2-fluoro-diphenylbenzylphosphine (**3.2**) once again (Scheme 60). The use of different types of silica (200–425 and 100–230 mesh) and both sodium and lithium tetrachloropalladate were tested; in all the attempts the monomeric complex **3.24** and the dimeric complex **3.25** (the same obtained from the reaction in Scheme 58) were the only products and no cyclometallation was observed.



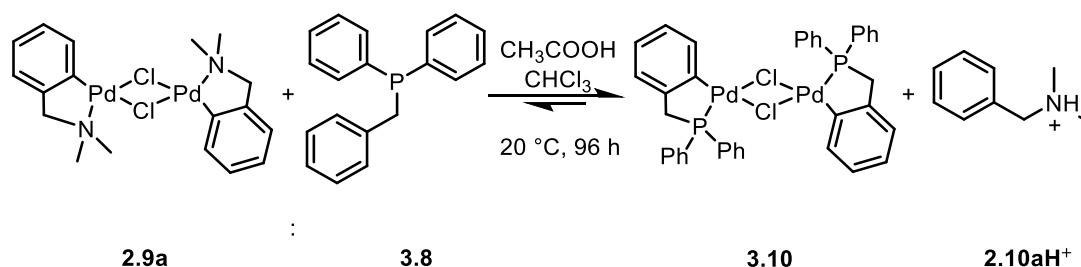
Scheme 60: Attempted synthesis of palladacycle **3.23** using the method of Smoliakova *et al.*

The reaction with the non-fluorinated diphenylbenzylphosphine **3.8** was also attempted to validate their method (Scheme 61) but no cyclometallation product (**3.10**) was obtained using both different types of silica (200–425 and 100–230 mesh).



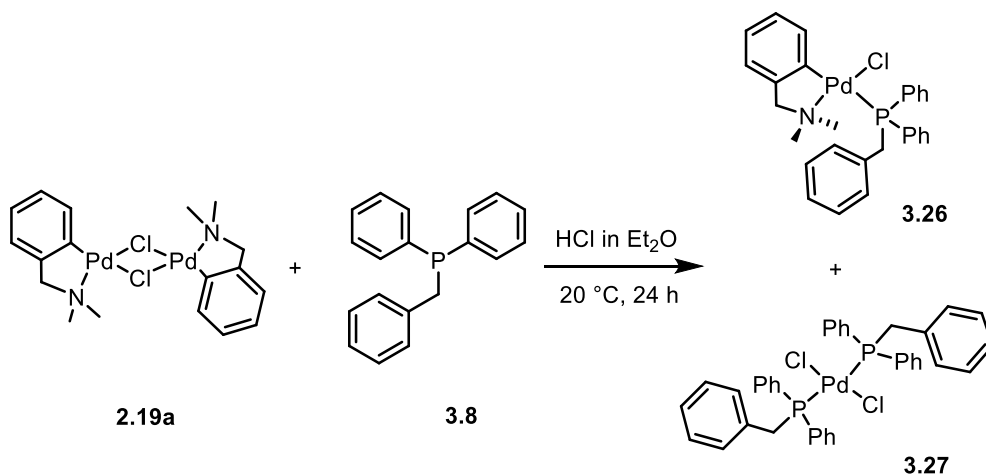
Scheme 61: Failed synthesis of palladacycle **3.10** (Smoliakova *et al.*).

Due to the difficulties in obtaining the fluorinated palladacycles **3.23** by direct reactions, the transcyclometallation method from the aminopalladacycles studied by Ryabov and co-workers was considered as an alternative.¹⁶¹



Scheme 62: Synthesis of palladacycle **3.10** reported by Ryabov *et al.*

The amino-type chloride-bridged palladacycle (**2.9a**) was synthesised as reported in Chapter 2. The presence of acetic acid in the ligand exchange reaction (Scheme 62) led to the formation of a mixture of acetate- and chloride-bridged palladacycles so it was changed to hydrochloric acid (1 M in diethyl ether). The reaction was monitored by TLC (50:50 EtOAc/petrol) and after 24 hours all the starting material was consumed. However, the product of the reaction was not the expected phospho-palladacycle **3.10**, but a mixture of two products: the heteropalladacycle **3.26** where the amino ligand was still cyclometallated and the phosphine substrate coordinated to the metal, and the monomeric dichloro-diphenylbenzylphosphine palladium complex **3.27** (Scheme 63).



Scheme 63: Transmetalation reaction following the procedure of Ryabov *et al.*

The mixture was separated by flash chromatography, allowing isolation and characterisation of the pure compounds **3.26** and **3.27**. In the ³¹P-NMR spectrum, the heterocomplex **3.26** (Scheme 63) in CDCl₃ showed a broad signal at δ 38.33 due to the small coupling with the methylene protons. The ¹H-NMR spectrum showed three signals at δ 7.58 (m), 7.30 (td, $J = 7.8, 2.0$ Hz) and 7.09 (m) for the aromatic protons of the coordinated phosphine, and three

sets at δ 7.41 (td, $J = 7.4, 1.7$ Hz), 6.92 (d, $J = 6.4$ Hz) and 6.77 (td, $J = 7.3, 0.9$ Hz) for the aromatic protons of the cyclometallated amine. The methylene protons of the amino-ligand resonate as a doublet at δ 4.03 ($J = 11.9$ Hz; overlap of two doublets) while the methylene protons of the phosphine ligand resonate at δ 3.98 and show a small splitting (d, $J = 1.92$ Hz) due to a coupling with the phosphorus. Two singlets at δ 1.85 correspond to the two methyl groups of the amino-ligand. Mass spectra were recorded by the LIFDI method¹³⁶ resulting in the molecular ion with a characteristic isotope pattern for a monomeric Pd species ($m/z = 551.07$). A single crystal of the heterocomplex **3.26** was grown by slow diffusion of hexane into a solution of the compound in chloroform (Figure 62).

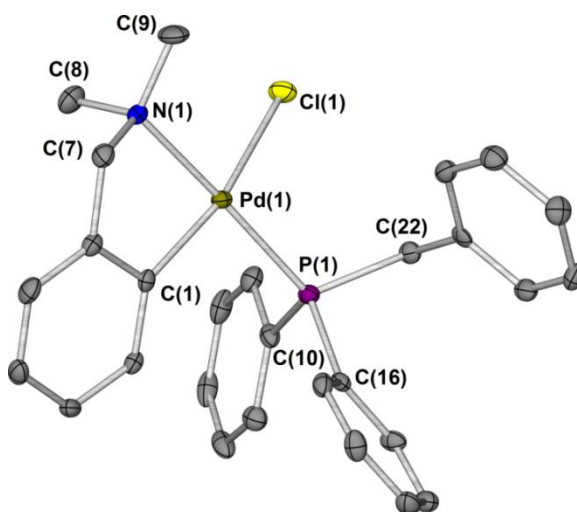


Figure 62: Molecular structure of complex **3.26**. Hydrogen atoms were omitted for clarity; thermal ellipsoids shown with probability of 50%.

The monomeric dichloro-diphenylbenzylphosphine palladium complex **3.27** (Scheme 63) showed two multiplets at δ 7.51 and 7.08 in the ¹H-NMR spectrum for the *ortho* and *meta* aromatic protons on the two phenyl rings and a doublet of doublets at δ 7.17 ($J = 9.2, 4.1$ Hz) for the *para* hydrogen. The benzyl aromatic protons resonate at δ 7.43 (t, $J = 7.4$ Hz) and 7.33 (t, $J = 7.5$ Hz), while the methylene protons at 3.95 (t, $J = 4.1$ Hz). LIFDI mass spectrometry¹³⁶ used to analysed the complex, showed the molecular ion with characteristic isotope pattern for a monomeric Pd species ($m/z = 728.05$). A single crystal suitable for X-ray analysis of the monomer **3.27** was grown by slow diffusion of hexane into a solution of the compound in chloroform (Figure 63).

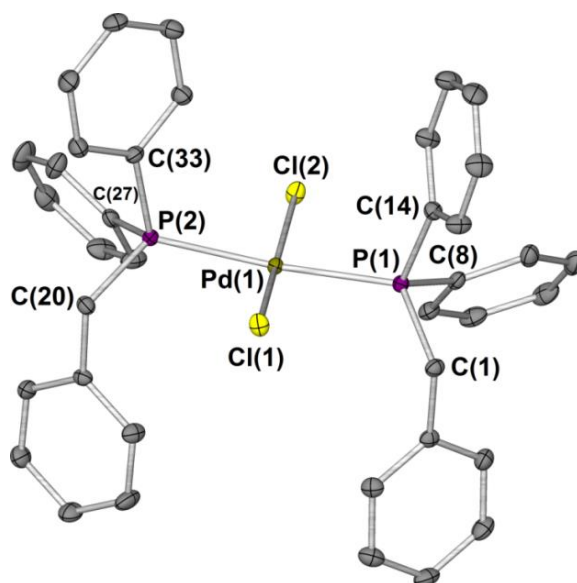


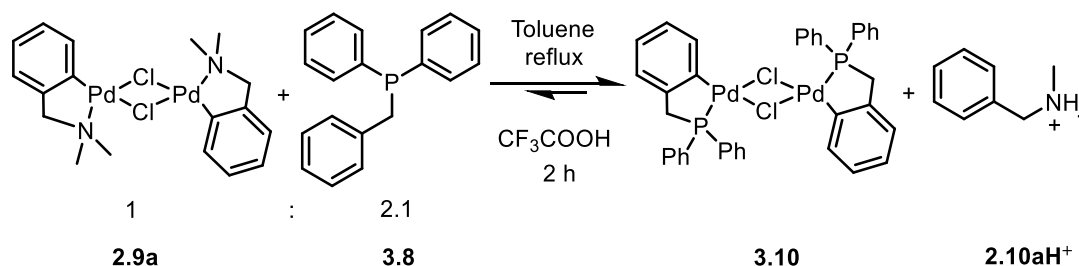
Figure 63: Molecular structure of complex 3.27. Hydrogen atoms were omitted for clarity; thermal ellipsoids shown with probability of 50%.

Table 17: Selected distances (Å) and angles (°) complexes 3.26 and 3.27

Bond Length / Å	3.26	3.27
C(1)–Pd(1)	2.004(3)	-
Cl(1)–Pd(1)	2.4234(7)	2.2946(4)
Cl(2)–Pd(1)	-	2.2967(4)
P(1)–Pd(1)	2.2506(7)	2.3154(4)
P(2)–Pd(1)	-	2.3273(4)
N(1)–Pd(1)	2.143(2)	-
Bond Angle	3.26	3.27
C(1)–Pd(1)–P(1)	94.88(8)	119.92(6)
Cl(1)–Pd(1)–C(1)	166.14(7)	-
P(1)–Pd(1)–Cl(1)	92.65(3)	87.518(15)
Cl(1)–Pd(1)–P(2)	-	90.626(15)
Cl(2)–Pd(1)–P(1)	-	91.081(15)
N(1)–Pd(1)–Cl(1)	91.07(6)	-
C(1)–Pd(1)–N(1)	81.83(10)	-

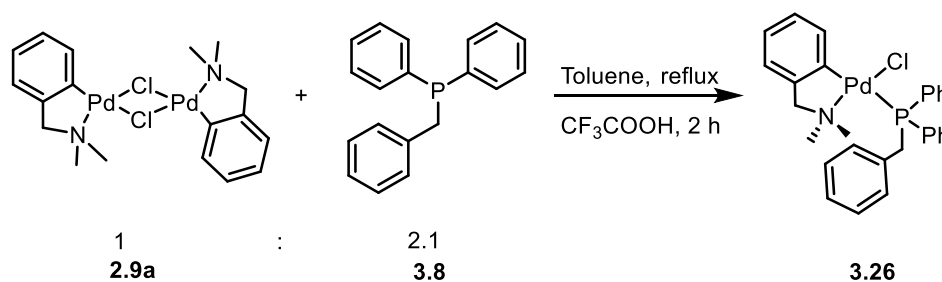
Since palladacycle **3.10** could not be obtained using the modified Ryabov method, an alternative was sought in the literature. Pfeffer and co-workers have reported an

improvement in the yield of this reaction by using trifluoroacetic acid in toluene (Scheme 64).¹¹⁵



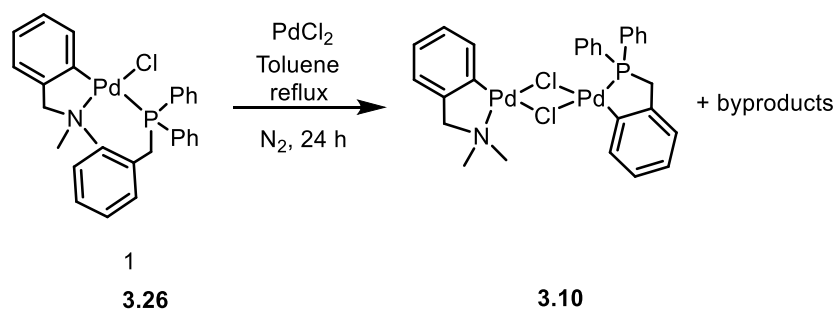
Scheme 64: Synthesis of palladacycle 3.10 by Pfeffer *et al.*

Following the reaction conditions reported in the paper, it was possible to observe complete consumption of starting material after two hours by TLC. However, the isolated product was not the palladacycle **3.10** but the monomer **3.26** (Scheme 65), which is thought to be a possible intermediate in the overall formation of the palladacycle **3.10**.



Scheme 65: Formation of monomer 3.26 instead of palladacycle 3.10.

The monomer **3.26** was reacted with PdCl_2 in toluene at reflux in an attempt to obtain the phosphapalladacycle **3.10** (Scheme 66).

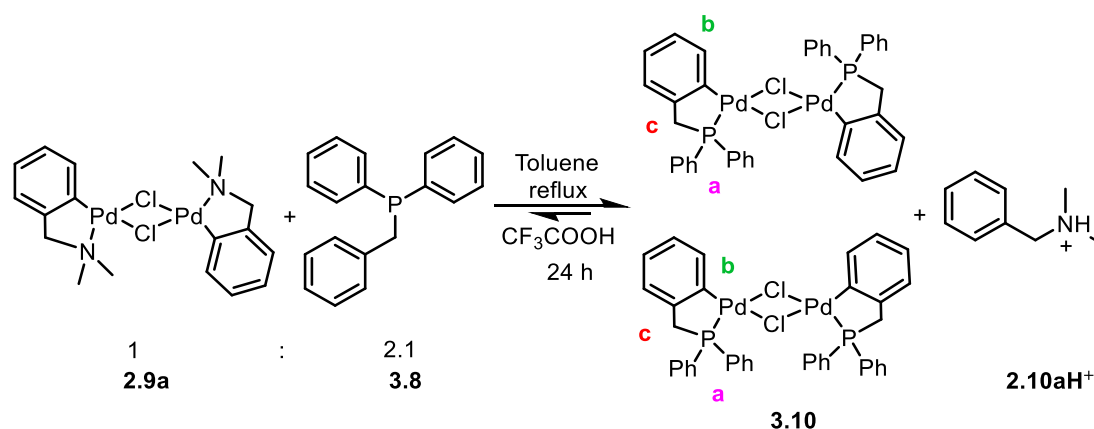


Scheme 66: Synthesis of palladacycle 3.10 from monomer 3.26

After work-up the crude reaction mixture was analyzed by LIFDI mass spectrometry and ^{31}P - and ^1H -NMR spectroscopies. The LIFDI mass spectrum showed the presence of several Pd-containing compounds ($m/z = 553.98, 692.95, 835.94, 871.95$). This was confirmed by the ^{31}P NMR spectrum, which showed three signals at $\delta 29.12, 31.81$ and 56.70 . All of the

species in the mass spectrum possessed the typical isotope pattern of Pd₂ (the signal at 692.94 showed the exact isotope pattern hypothesised for **3.10** confirming that **3.26** is in fact a reaction intermediate).

In an attempt to obtain the palladacycle **3.10** as the only product, the reaction between the chloride-bridged palladacycle **2.9a** and diphenylbenzylphosphine (**3.8**) was extended to 24 hours (Scheme 67), which led to full conversion to the expected product.



Scheme 67: Synthesis of palladacycle 3.10

After isolation of the product **3.10**, the ³¹P-NMR spectrum recorded in CDCl₃, showed two singlets at δ 55.71 and 56.08 in ratio 2:3, while Smoliakova *et al.* and co-workers reported one singlet at δ 55.95.¹⁶² The μ₂-Cl-bridged-palladacycles can exist in two possible geometrical isomers, *syn* and *anti*, depending on the relative positions of the Pd–C bonds,¹⁶⁹ giving an explanation for the two signals detected in the ³¹P-NMR spectrum. The LIFDI mass spectrum showed the correct isotope pattern for the hypothesized product C₃₈H₃₂Cl₂P₂Pd₂ (**3.10**) at *m/z* = 833.94, and despite the ¹H-NMR signals differing slightly from the reported values¹⁶² they are consistent with the hypothesised structure (Table 18 and 6).

Table 18: ^1H -NMR signals of palladacycle 3.10 (500 MHz in CDCl_3 at 300 K).

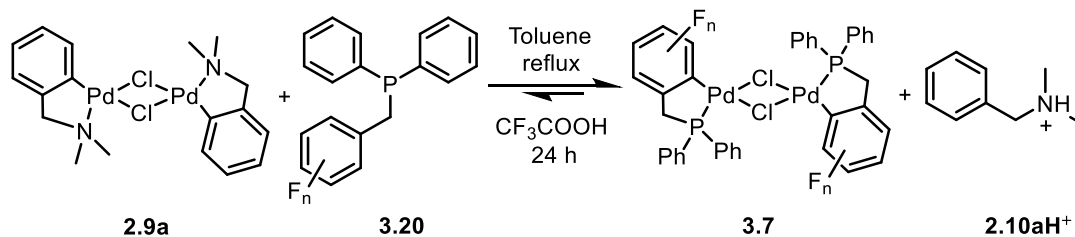
$\delta (^1\text{H}) / \text{ppm}$		
Assignment (Scheme 67)	Experimental 500 MHz, $\delta (J / \text{Hz})$	Literature values ¹⁶² 500 MHz, $\delta (J / \text{Hz})$
a <i>aromatic phenyl rings</i>	7.77 (m) 7.46 (m)	7.74 (br. s) 7.64 (br. s) 7.56 (br. s) 7.35 (m) 7.26 (d, $^3J_{\text{H-H}} = 7.9 \text{ Hz}$) 7.01 (d, $^3J_{\text{H-H}} = 7.9 \text{ Hz}$)
b <i>aromatic benzyl ring</i>	6.96 (m)	6.90 (br. s)
c <i>methylene protons</i>	3.82 (d, $J = 12.3, 2\text{H}$)	3.81 (d, $J = 15, 2\text{H}$)

Table 19: ^{31}P -NMR signals of palladacycle 3.10 (202 MHz in CDCl_3 at 300 K)

$\delta (^{31}\text{P}) / \text{ppm}$	
Experimental 202 MHz, $\delta (J / \text{Hz})$	Literature values ¹⁶² 202 MHz, $\delta (J / \text{Hz})$
55.71 (s)	55.95
56.08 (s)	

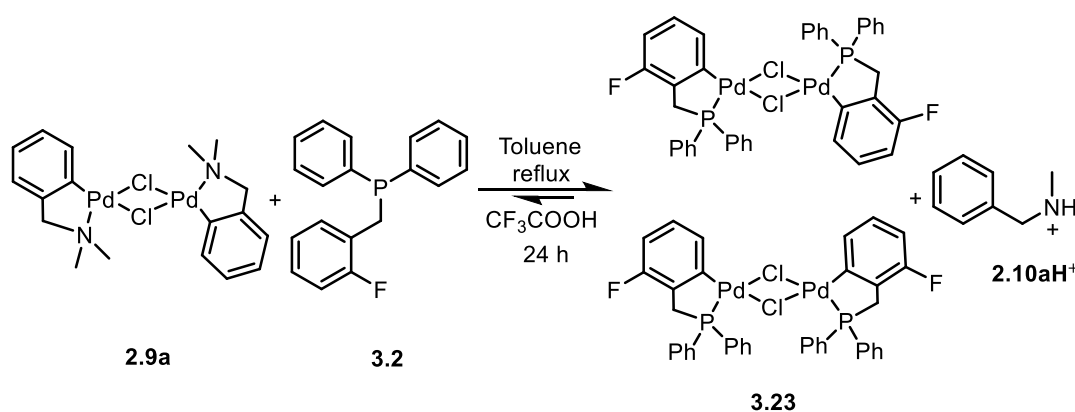
3.2.2.1 Fluorinated chloride-bridged phosphapalladacycles

The aim of the synthesis of fluorinated phosphapalladacycles was to assess the regioselectivity of the intramolecular C–H activation reactions and compare it with that for tertiary fluorinated benzylamines (Chapter 2). All the fluorinated phosphapalladacycles were synthesised using the optimised conditions of the exchange reaction (Scheme 68) (also referred to as a transcyclometallation reaction) reported by Pfeffer and co-workers.¹¹⁵



Scheme 68: Synthesis of fluorinated palladacycles (general scheme).

The reaction between complex **2.9a** and 2-fluoro-diphenylbenzylphosphine **3.2**, in toluene at reflux for 24 hours, gave palladacycle **3.23** in 43% yield along with the protonated substrate **2.10aH⁺** (Scheme 69).



Scheme 69: Synthesis of palladacycle 3.23.

Whereas the free phosphine **3.2** shows a single resonance in the ¹H-NMR spectrum at δ 3.34 for the methylene protons, **3.23** exhibits two doublets at δ 3.83 and 3.84 ($J = 11.8$ Hz) representing the *syn* and *anti* isomeric forms. The aromatic protons of the benzylic group resonate as a multiplet at δ 6.77–6.67 and as three doublets of doublets at δ 6.87 ($J = 13.8, 7.8$ Hz), 6.99 ($J = 12.7, 7.8$ Hz) and 7.66 ($J = 7.8, 4.5$ Hz). The phenyl protons of the phosphino-ligand resonate at δ 7.39–7.32 (m), 7.52–7.40 (m), 7.70 (dd, $J = 12.0, 7.7$ Hz) and 7.82 (dd, $J = 11.8, 7.7$ Hz), values consistent with the reported data for the non-fluorinated palladacycle **3.10**.¹⁶² It is also possible to observe the two isomeric forms (*syn* and *anti*) in the ³¹P-NMR spectrum, which shows two sets of singlets at δ 58.8 and 58.4 (ratio 1.4:1 by integration) and in the ¹⁹F-NMR spectrum where the two isomers resonate as two multiplets at δ -110.58 and -110.70.

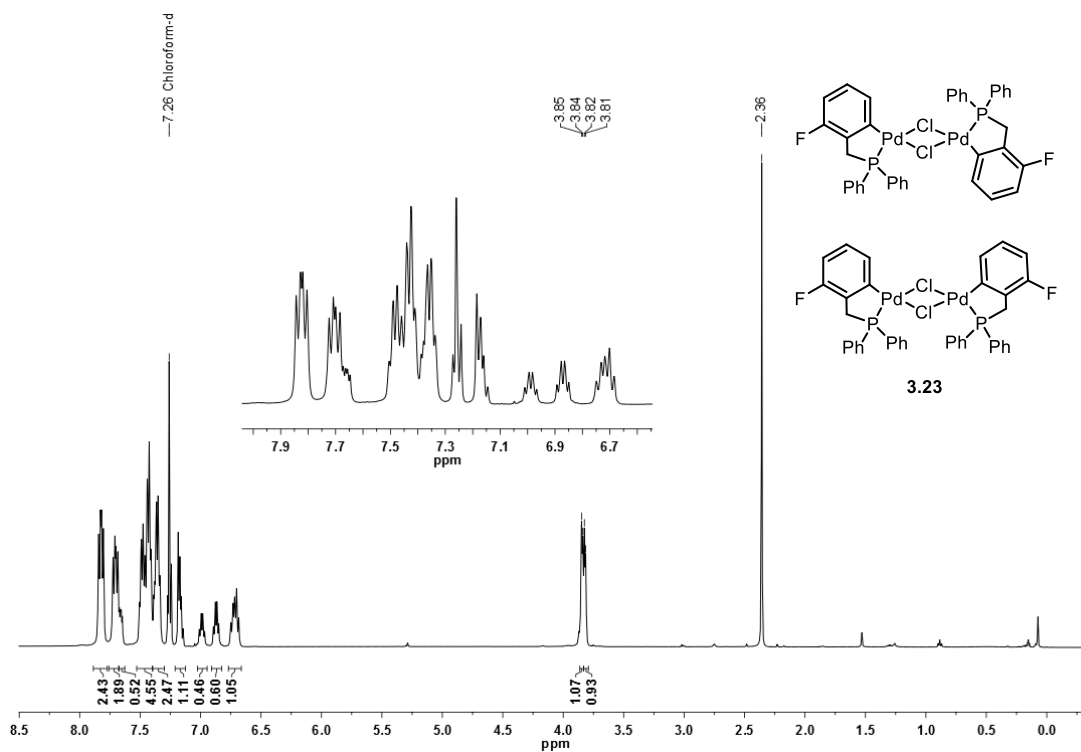


Figure 64: ^1H -NMR spectrum of palladacycle 3.23 in CDCl_3 at 298 K (500 MHz).

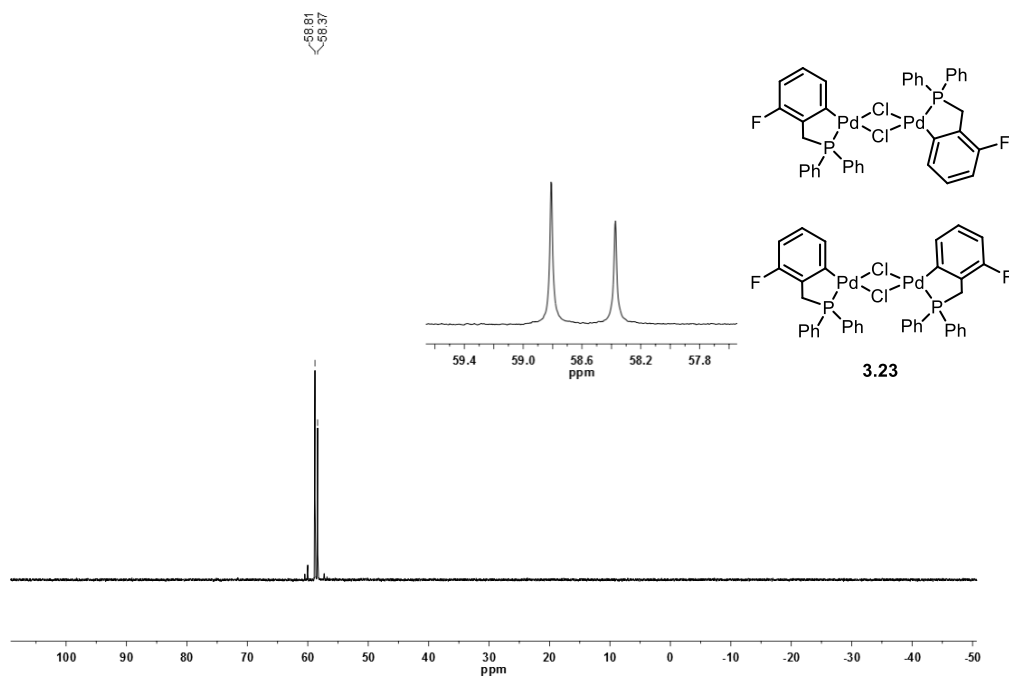


Figure 65: ^{31}P -NMR spectrum of palladacycle 3.23 in CDCl_3 at 298 K (202 MHz).

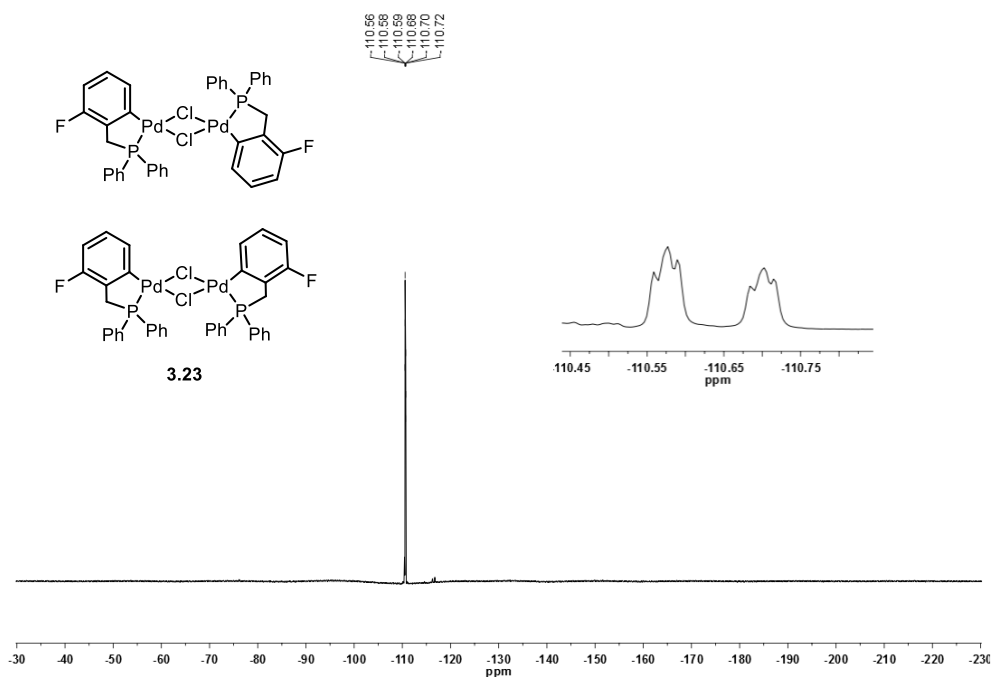


Figure 66: ^{19}F -NMR spectrum of palladacycle **3.23** in CDCl_3 at 298 K (471 MHz).

A single crystal of palladacycle **3.23** was obtained by slow evaporation of a saturated solution of the complex in toluene.

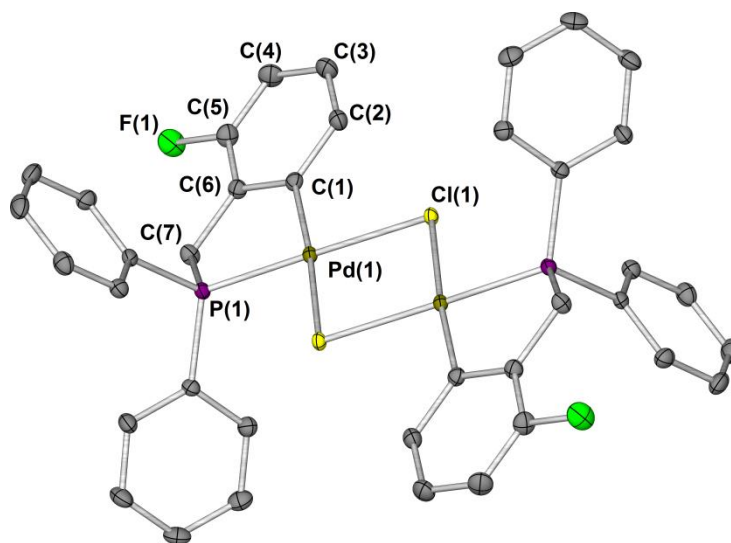
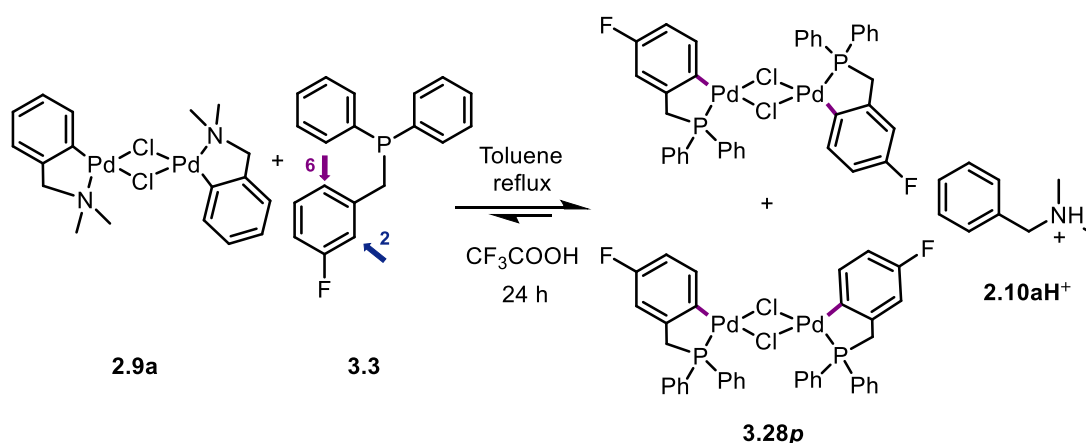


Figure 67: Molecular structure of palladacycle **3.23**. Hydrogen atoms were omitted for clarity; thermal ellipsoids shown with probability of 50%.

The reaction of **2.9a** with 3-fluoro-diphenylbenzylphosphine **3.3** (Scheme 70) allowed an examination of the regioselectivity of the cyclopalladation reaction since the substrate **3.3** offers a choice between the C-2 position or C-6 position (Scheme 70) for C–H activation.



Scheme 70: Synthesis of palladacycle 3.28 (regioselectivity *para* to F).

Two different products **3.28p** and **3.28o** in Figure 68 could have been formed due to the two sites available (blue and purple bonds) for the C–H activation.

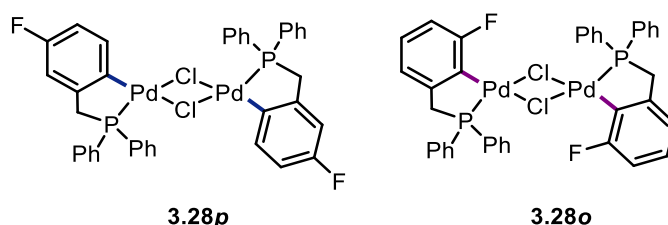


Figure 68: Possible isomers of palladacycle 3.28 (Scheme 70).

From the NMR spectroscopic data it was possible to deduce that the reaction gave exclusively palladacycle **3.28p** in 84% and the protonated substrate **2.10H⁺**, meaning that the cyclometallation occurs only in the position *para* to the fluorine atom (C-6). The ¹⁹F-NMR spectrum exhibits two multiplets at –118.6 and –118.5 ppm in ratio 1:1.5 and the ³¹P-NMR spectrum shows two singlets at 55.0 and 54.6 ppm for the two geometrical isomers.

A ¹H-¹H-COSY NMR spectrum (Figure 69) of palladacycle **3.28p** clarified the correlation between the six benzyl protons and allowed assignment of the correct signals to the two species, indicated in Figure 69 with the green circles and the purple triangles. Unfortunately it was not possible to ascertain which signals correspond to the *syn* isomer and which the *anti*, but it is possible to observe in the expansion of the aromatic region that the patterns of the multiplets form similar pairs of resonances and in one case (6.83 ppm) the multiplets overlap perfectly to form one signal.

A ¹H-³¹P-HSQC NMR experiment was performed making it possible to correlate the two singlets in the ³¹P-NMR (55.0 ppm and 54.5 ppm) with the two methylene protons at 3.79 and 3.78, respectively.

A proton-decoupled proton ($^1\text{H}\{^1\text{H}\}$)-NMR experiment¹⁷⁰ of palladacycle **3.28** (Figure 71) was run on a 700 MHz NMR instrument, in an attempt to get additional information by removing the coupling between aromatic protons and clarify the coupling with fluorine and phosphorus atoms. This experiment uses the method of slice-selective excitation developed by Zangger and co-workers.¹⁷⁰⁻¹⁷¹ When a linear gradient is applied, different parts of an NMR sample show different magnetic field strengths so when a combination of different 180° pulses is then applied, the signals become either off-resonance or on-resonance. By collecting a series of data it is possible to suppress the homonuclear coupling in the region of interest. In this study the aromatic region between 6.5–6.9 ppm was analysed and the spectrum shows only the coupling between proton and fluorine atoms. The coupling constants observed were both 9 Hz for the doublets at 6.61 ppm and 6.83 ppm, which both correspond to the same geometrical isomer. As reported for fluorobenzenes¹⁷²⁻¹⁷⁴ and for parafluorotoluene,¹⁷⁵ the coupling constant *ortho*- $J_{\text{H-F}}$ is ~ 9 Hz, the *meta*- $J_{\text{H-F}}$ is around 5 Hz and the *para*- $J_{\text{H-F}}$ close to 0.

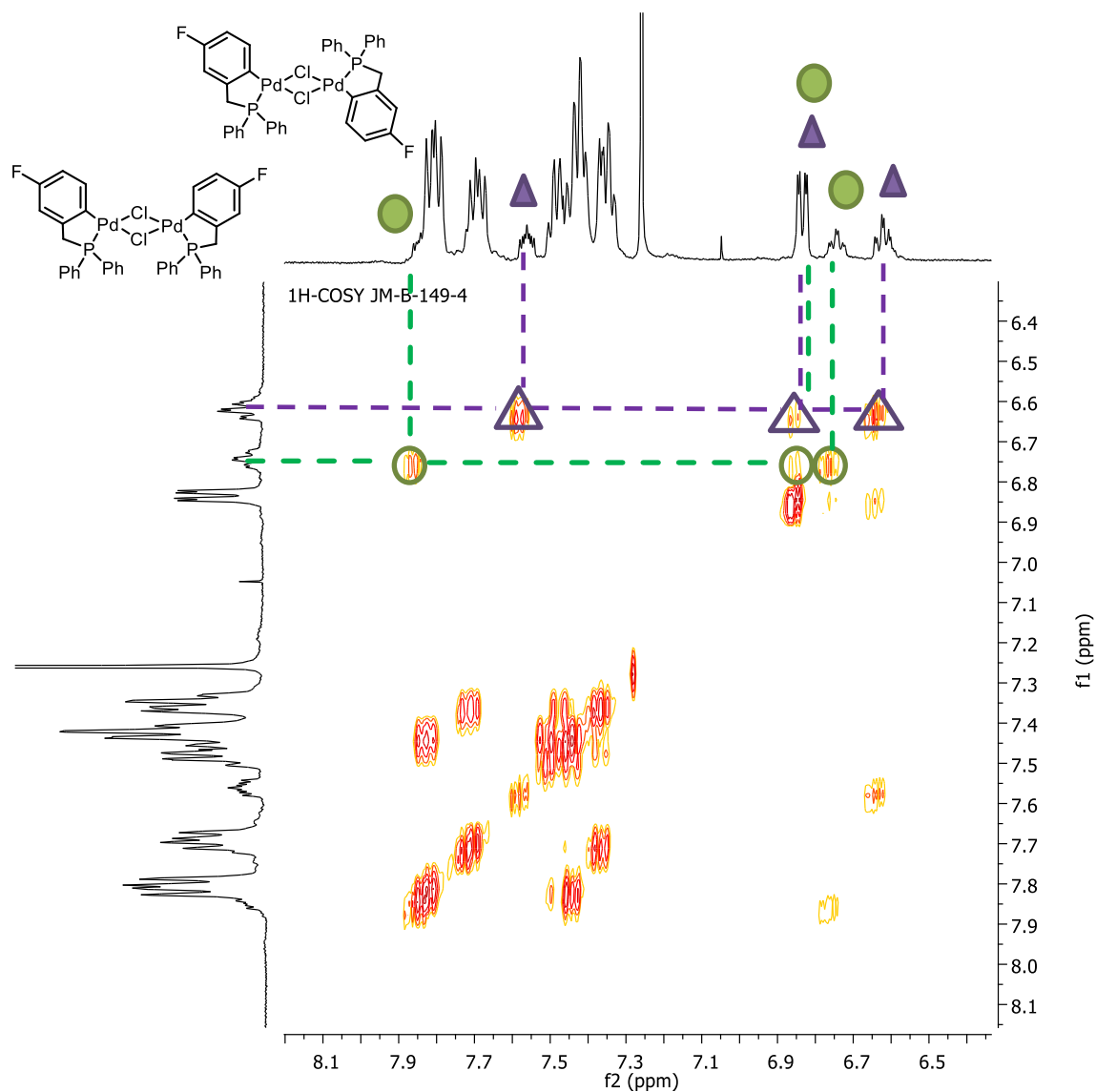


Figure 69: Expansion of aromatic region in ^1H - ^1H -COSY NMR spectrum of palladacycle **3.28** at 298 K (500 MHz) in CDCl_3 .

From the data obtained two protons showed coupling constants of 9 Hz and the only possibility is that there are two protons *ortho* to the fluorine atom, which corresponds to the geometry of the *para* isomer **3.28p** shown in Figure 70.

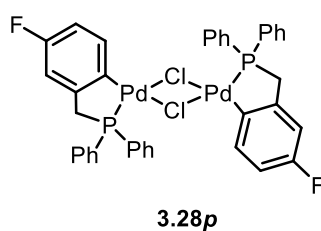


Figure 70: *para* isomer (palladacycle **3.28p**).

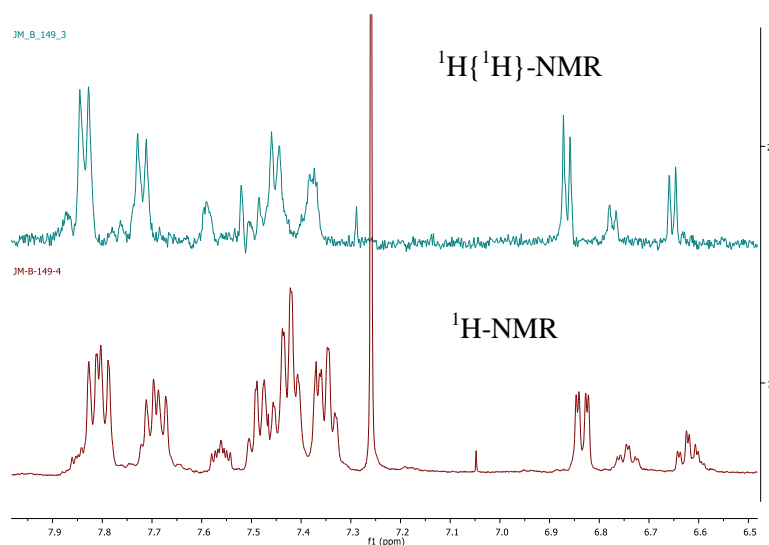


Figure 71: $^1\text{H}\{^1\text{H}\}$ -NMR (700 MHz) spectrum (above) and ^1H -NMR spectrum (below) of palladacycle **3.28p** at 298 K (700 MHz) in CDCl_3 .

A single crystal of the palladacycle **3.28p** was grown by slow evaporation of the complex in toluene, confirming the *para*-selectivity (Figure 72).

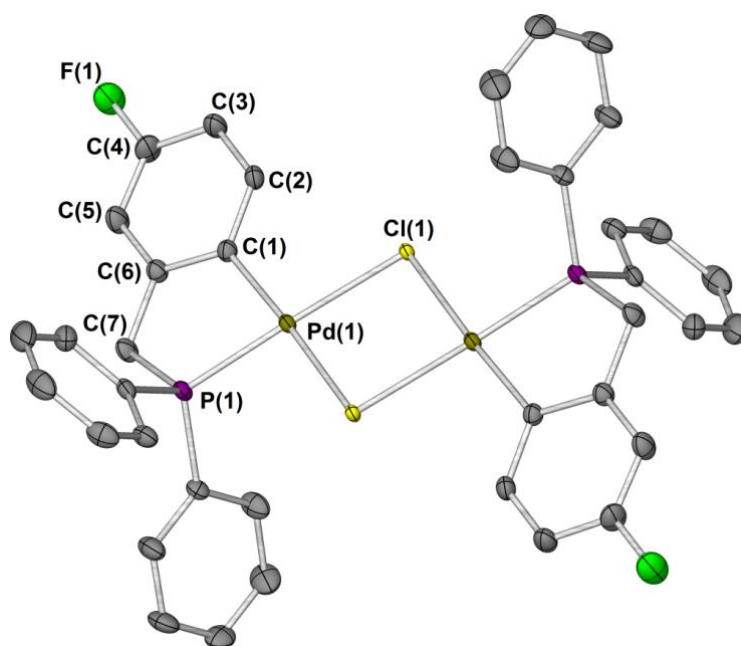


Figure 72: Molecular structure of palladacycle **3.28p**. Hydrogen atoms were omitted for clarity; thermal ellipsoids shown with probability of 50%.

Palladacycle **3.29** was synthesised in an identical fashion, and crystallised by slow evaporation of a saturated solution of the complex in chloroform, while **3.30** was synthesised and crystallised following the same procedures used for **3.23** (Figure 74 and Figure 75). Their NMR signals are reported in Table 20 and a crystallographic analysis is given in section 3.4.

Table 20: NMR spectroscopic data for complexes 3.10, 3.23 and 3.28–3.30.

Compound	δ ($^{31}\text{P}\{\text{H}\}$) / ppm	δ (^1H) / ppm	δ (^{19}F) / ppm
3.10 ^a	55.95	7.74 (br s, 4H), 7.64 (br s, 4H), 7.56 (br s, 1H), 7.35 (m, 5H), 7.26 (d, $J = 7.9$ Hz, 1H), 7.01 (d, $J = 7.9$ Hz, 1H), 6.90 (br s, 2H), 3.81 (d, $J = 15$ Hz, 2H)	-
3.23	58.81 58.37	7.82 (dd, $J = 11.8, 7.7$ Hz, 5H, Ph), 7.70 (dd, $J = 12.0$ Hz, 3H, Ph), 7.66 (dd, $J = 7.8, 4.5$ Hz, 1H, benzyl), 7.52–7.40 (m, 8H, Ph), 7.39–7.32 (m, 4H, Ph), 6.99 (dd, $J = 12.7, 7.8$ Hz, 1H, benzyl), 6.87 (dd, $J = 13.8, 7.8$ Hz, 1H, benzyl), 6.77–6.67 (m, 2H benzyl), 3.84 (d, $J = 11.8$ Hz, 2H, <i>major isomer</i>), 3.83 (d, $J = 11.8$ Hz, 2H, <i>minor isomer</i>)	-110.58 (m, <i>minor isomer</i>) -110.70 (m, <i>major isomer</i>)
3.28 ^p	54.99 54.59	7.85 (m, 1H, benzyl), 7.81 (m, 4H, Ph), 7.73–7.65 (m, 3H, Ph), 7.56 (m, 1H, benzyl), 7.52–7.39 (m, 10H, Ph), 7.39–7.31 (m, 5H, Ph), 6.84 (dd, $J = 9.6, 2.8$ Hz, 2H, benzyl), 6.74 (td, $J = 8.9, 2.8$ Hz, 1H, benzyl), 6.62 (td, $J = 9.0, 2.7$ Hz, 1H, benzyl), 3.79 (d, $J = 12.1$ Hz, 2H, CH ₂ , <i>major isomer</i>), 3.78 (d, $J = 12.4$ Hz, 2H, CH ₂ , <i>minor isomer</i>)	-118.65 (m, <i>minor isomer</i>) -118.54 (m, <i>major isomer</i>)
3.29	56.28 53.89	7.50 (m, 10H, Ph), 6.50 (m, 2H, benzyl), 3.85 (d, $J = 12.64$ Hz, <i>major isomer</i> , CH ₂); 3.49 (d, $J = 12.6$ Hz, <i>minor isomer</i> , CH ₂)	-116.10 (m, <i>minor and major isomer</i>)
3.30 ^p	54.54 54.07	7.90–7.61 (m, 6 H), 7.60–7.33 (m, 14H), 7.23–7.16 (m, 2H, <i>minor and major isomers</i>), 6.99–6.89 (m, 2H, <i>minor and major isomers</i>), 3.76 (d, $J = 12.2$ Hz, 4H, <i>minor and major isomers</i> , CH ₂).	-140.66, -142.52 (m, <i>minor isomer</i>), -141.24, -142.72 (m, <i>major isomer</i>).

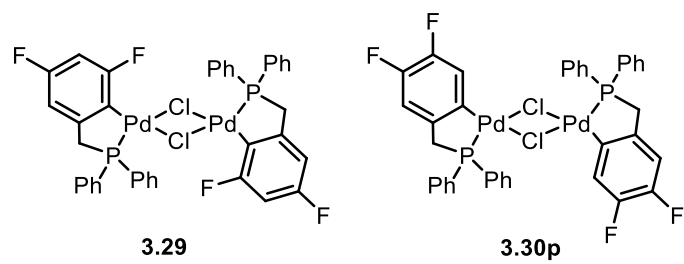


Figure 73: Palladacycles 3.29 and 3.30p.

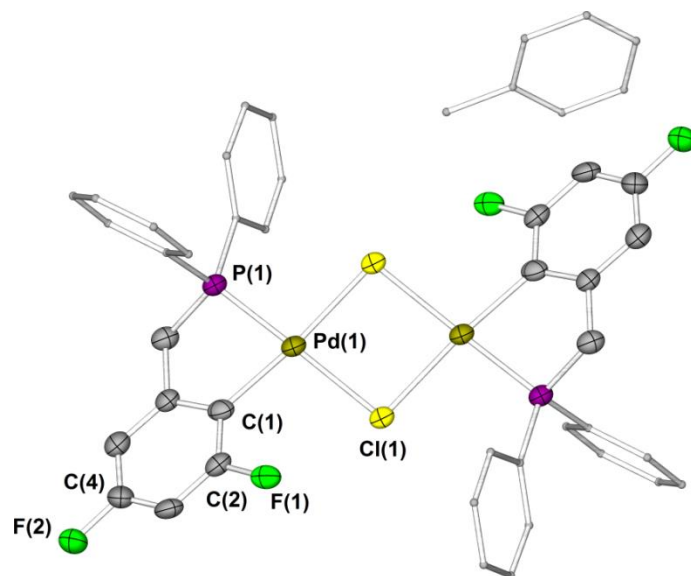


Figure 74: Molecular structure of palladacycle 3.29 along with a molecule of toluene in the unit cell. Hydrogen atoms were omitted for clarity; thermal ellipsoids shown with probability of 50%.

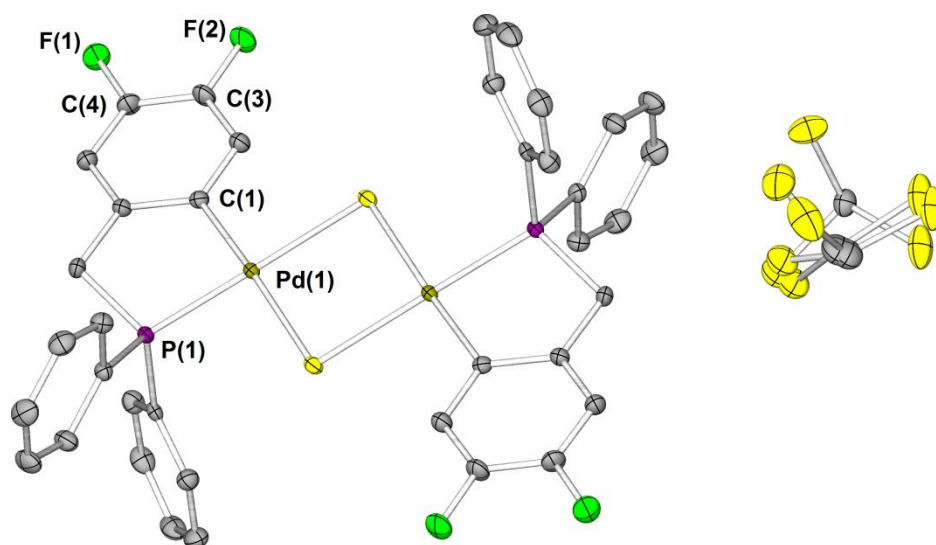
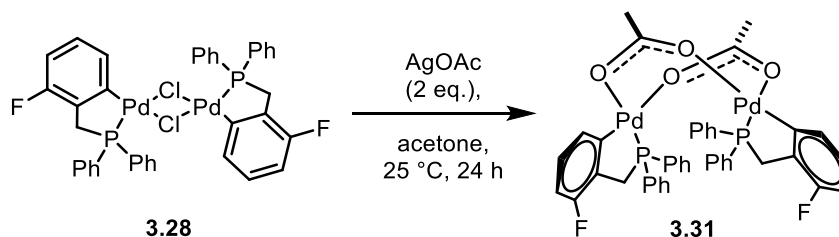


Figure 75: Molecular structure of palladacycle **3.30p** along with disordered molecule of chloroform. Hydrogen atoms were omitted for clarity; thermal ellipsoids shown with probability of 50%.

3.2.2.2 Fluorinated acetate-bridged phosphapalladacycles

Chloride-bridged palladacycle **3.28** was reacted in acetone at 25 °C with silver acetate (Scheme 41) to give the relevant acetate-bridged palladacycle **3.31**, showing a possible new route for the formation of acetate-bridged palladacycles, as observed for the amino-palladacycle systems.¹²²



Scheme 71: Bridge halide conversion reaction from **3.28** to **3.31**.

The structure was confirmed by the X-ray diffraction analysis of a single crystal obtained by slow evaporation of a saturated solution of the complex in chloroform (Figure 76).

Palladacycle **3.31** shows in the ³¹P-NMR spectrum a broad singlet at δ 53.71 and in the ¹⁹F-NMR spectrum a multiplet centered at δ -112.50 due to the presence in solution of the geometrical isomer *trans* only. As for the amino-palladacycles, presented in Chapter 2, acetate-bridged palladacycles of tertiary amines or phosphines show no formation of the *cis* isomer, due to the steric hindrance of the phenyl groups bound to the phosphorus.

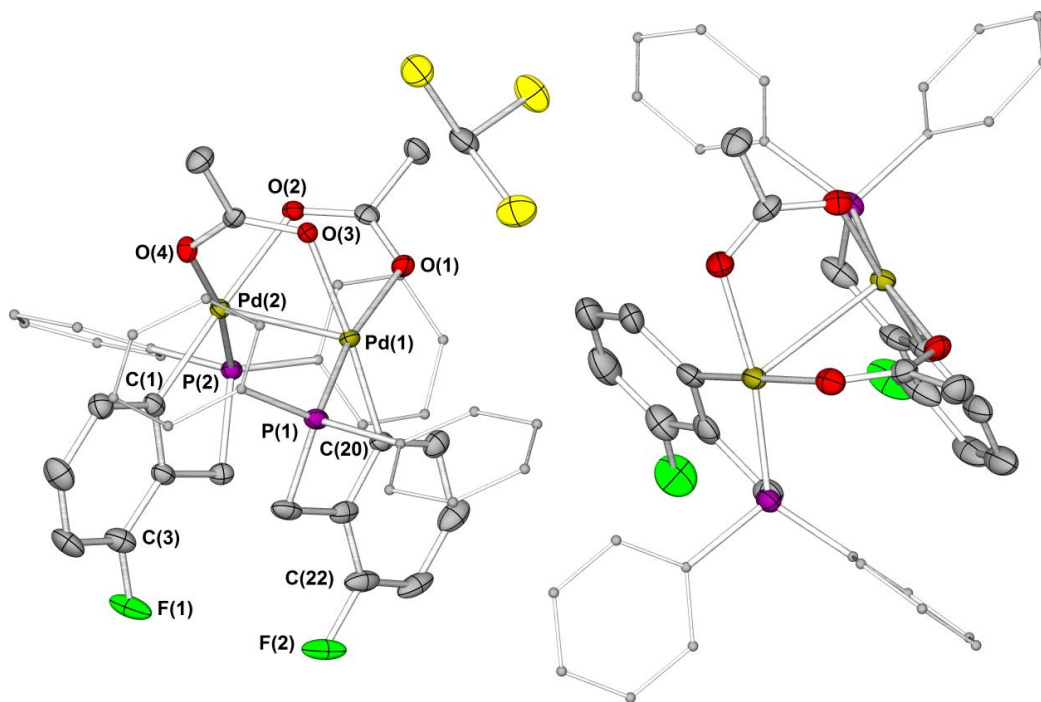


Figure 76: Molecular structure of palladacycle 3.31. Hydrogen atoms were omitted for clarity; thermal ellipsoids shown with probability of 50%.

The $^1\text{H-NMR}$ spectrum shows three multiplets (δ 7.54–7.39, 7.36–7.21, 7.21–7.07) for the phenyl protons and a doublets of doublets of doublets (δ 6.77, $J = 7.5, 4.3, 1.0$ Hz) and a multiplet at δ 6.68–6.52 for the benzylic protons; the methylene protons resonate as a triplet at δ 3.21 ($J = 15.3$ Hz) and a doublet of doublets at 2.83 ($J = 15.3, 9.7$ Hz). The equivalent methyl groups of the acetate bridge resonate as a singlet at 1.96. LIFDI mass spectrometry also confirmed the formation of palladacycle **3.31** with the molecular ion being the only peak ($m/z = 918.0127$).

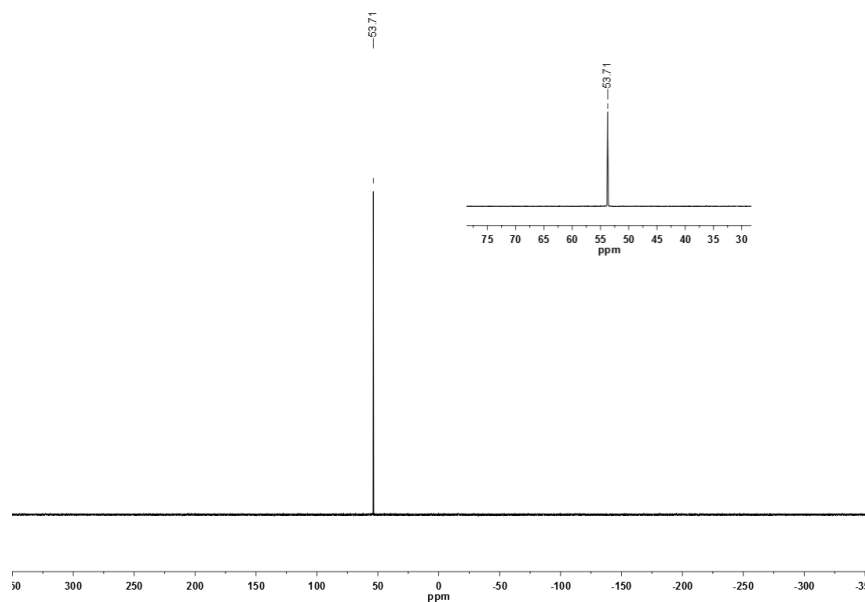


Figure 77: ^{31}P -NMR spectrum of palladacycle 3.31 in CDCl_3 at 294K (162 MHz).

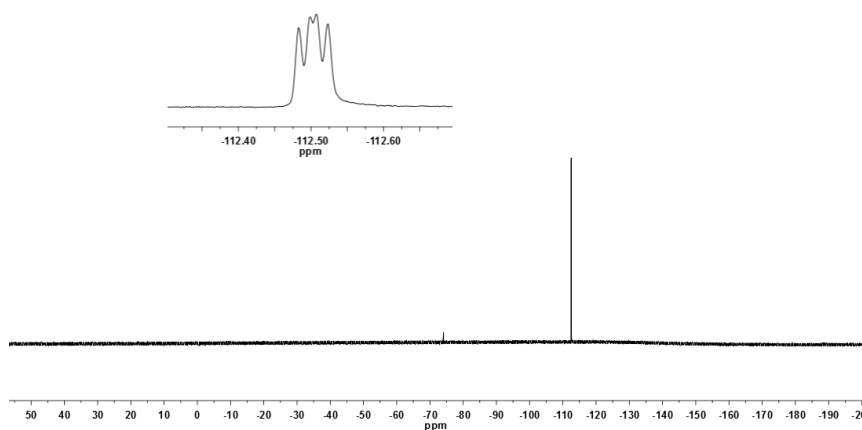


Figure 78: ^{19}F -NMR spectrum of palladacycle 3.31 in CDCl_3 at 294K (471 MHz).

3.3 Discussion

In this chapter several different cyclometallation reactions at palladium have been investigated and, as reported by Shaw and co-workers, tertiary phosphines that do not contain bulky groups on the phosphorus atom do not cyclometallate in direct reactions.¹⁵² The only method that has been found to successfully obtain fluorinated phosphapalladacycles from fluorinated diphenylbenzylphosphines (**3.2–3.5**) is the transcyclometallation reaction between an amino chloride-bridged palladacycle (**2.9a**) and the relevant fluorinated phosphine in the presence of trifluoroacetic acid. This study shows

that a fluorinated substrate (**3.3**) with the possibility of cyclometallating *via* C–H activation with Pd *ortho* to F (position C-2, Scheme 70) or *para* to F (position C-6, Scheme 70) shows complete regioselectivity toward the *para* position. The regioselectivity, as observed for fluorinated benzylamines in Chapter 2, derives from the structural features of the product obtained. The formation of isomers **3.28o** and **3.30o** (from attack on position C-2) is disfavoured presumably by electronic and steric repulsion between the lone pair of the fluorine atom and the lone pair of the chlorine atom; due to the planar structure (confirmed by X-ray crystallography), the fluorinated ring cannot twist and the electronic repulsion dominates the regioselectivity.

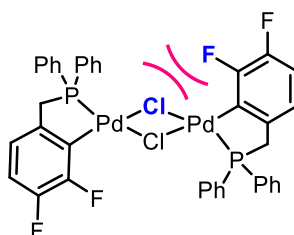


Figure 79: Representation of the electronic repulsion in palladacycle 3.30o.

The mechanisms of intramolecular C–H activation reactions of tertiary phosphines have not been well studied in the past several decades, but investigations at different transition metals has divided their reactions into electrophilic and nucleophilic mechanisms.¹⁷⁶ Vrieze and co-workers investigated the reaction of metal halides (Ir, Rh, Pd and Pt) with tertiary benzylphosphines and discovered that the reactivity increases in the order Pt(II) ~ Pd(II) << Rh(I) < Ir(I). They also assessed the differences in regioselectivity and in reaction mechanism of the different transition metals by reacting the metal halides with two fluorinated phosphines **3.32** and **3.33** (Figure 80) presenting two choices for the C–H activation reactions.

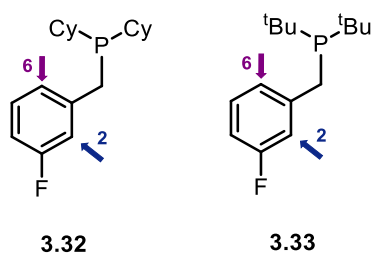


Figure 80: Fluorinated tertiary phosphines 3.32 and 3.33 used by Vrieze *et al.* to assess the regioselectivity of C–H activation at different transition metals.

They hypothesised that for iridium and rhodium the mechanism was nucleophilic due to the formation of 80% of the *ortho* isomer (C–H activation at position 2), the metal atom is the negative center and is oxidized from M^{n+} to $M^{(n+2)+}$. They also investigated the behaviour of

Pd toward the same cyclometallation reaction suggesting that in this case the mechanism was electrophilic,¹⁷⁷ due to the formation of 100% of *para* isomer (C–H activation in position 6),¹⁵³ such that the metal attacks the aromatic ring acting as an electrophilic center.

As mentioned previously, Vrieze and co-workers' paper lacks mechanistic investigation and despite the fact that the experimental results are consistent with their explanation, it is not possible to confirm an electrophilic mechanism without further investigations. Our observations are, however, consistent with their hypothesis since we also observe complete *para* selectivity, and although the Pd source differs, since in this case the phosphapalladacycle formation is *via* a transcyclometallation reaction, it would suggest that an electrophilic mechanism is also operating here.

3.4. Crystallographic analysis of chloride-bridged phosphapalladacycles

As reported by Smoliakova *et al.* for the non-fluorinated phosphapalladacycle **3.10**¹⁶² the X-ray crystal structures of all the fluorinated palladacycles exhibit a square planar geometry with an *anti* configuration where the two phosphorus atoms are *trans* to each other. The same geometry was observed in the analogous amino-palladacycles (Chapter 2) and in chloride-bridged dimers with chiral phosphines.¹⁶⁰ The main bond lengths reported in Table 21 are all similar to those reported for the non-fluorinated palladacycle **3.10**.¹⁶²

Table 21: Selected distances (Å) and angles (°) in chloride-bridged palladium dimer structures

Bond length / Å	3.10^a	3.23	3.28_p	3.29	3.30
C(1)–Pd(1)	2.009(2)	2.0071(17)	2.006(3)	2.027(7)	1.998(2)
Cl(1)–Pd(1)	2.4393(5)	2.4457(4)	2.4499(6)	2.4233(15)	2.4135(5)
Cl(n)–Pd(1)	2.4267(5)	2.4368(4)	2.4457(6)	2.4148(16)	2.4149(5)
P(1)–CH₂	1.832(2)	1.8263(17)	1.827(3)	1.812(7)	1.810(2)
P(1)–Pd(1)	2.1953(5)	2.1949(4)	2.1867(7)	2.1937(17)	2.1854(6)
C(n)–F(n)	-	C5–F1 1.355(2)	C4–F1 1.359(3)	C2–F1 1.362(8) C4–F2 1.364(8)	C4–F1 1.351(3) C3–F2 1.346(3)
Bond Angle / °	3.10^a	3.23 (B-144)	3.28_p	3.29	3.30
C(1)– Pd(1)–P(1)	82.04(6)	82.40(5)	82.59(8)	79.62(19)	82.44(7)
Cl(n)– Pd(1)–Cl(1)	97.75(6)	85.946(13)	85.69(2)	85.65(5)	85.402(59)
P(1)–Pd(1)– Cl(n)	178.283(18) 95.1049(19)	178.211(16) 94.591(15)	176.77(3) 94.53(2)	174.05(7) 95.19(6)	179.36(2) 94.89(2)

^a as reported in ref ¹⁶²

The bond angles between Cl(n)–Pd(1)–Cl(1) are smaller in the fluorinated palladacycles (average 85°) compared to the non-fluorinated one (97°).

3.5 Summary

This chapter describes the synthesis and full characterisation of fluorinated diphenylbenzylphosphines **3.2–3.5** and their respective fluorinated chloride-bridged phosphapalladacycles **3.23** and **3.28–3.30**.

Due to various electronic and steric factors the direct reactions of these fluorinated phosphines to obtain phosphapalladacycles either with Pd(OAc)₂ or Li₂PdCl₄ did not give the cyclometallated products. The only method found to obtain these products was the transcyclometallation reaction from the amino-chloride-bridged palladacycle **2.19a** and the relevant phosphine in the presence of trifluoroacetic acid.

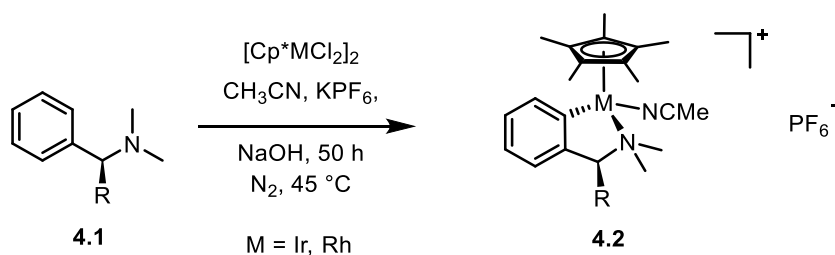
The effect of fluorine substituents on the regioselectivity of intramolecular C–H activation reactions was studied. For substrates such as **3.3** and **3.4**, where two possible C–H bonds could be activated, the cyclopalladation reactions occur regioselectively *para* to the fluorine atom. The resulting products were analysed in detail by NMR spectroscopy, mass spectrometry and X-ray crystallography. The crystallographic analysis showed that the position of the fluorine substituents on the ring does not have a marked effect on the geometry of the palladacycles, behaviour similar to that observed for chloride-bridged palladacycle with amino-ligands (Chapter 2). However, it does have an effect on the regioselectivity, disfavours the formation of the *ortho* isomer, feasibly due to the repulsion between the lone pair of the fluorine atom and of the chlorine atom, resulting in the exclusive formation of the *para* isomer. More general conclusions are given in Chapter 6.

Chapter 4: C-H activation reactions of benzylamines at Ir, Rh and Ru

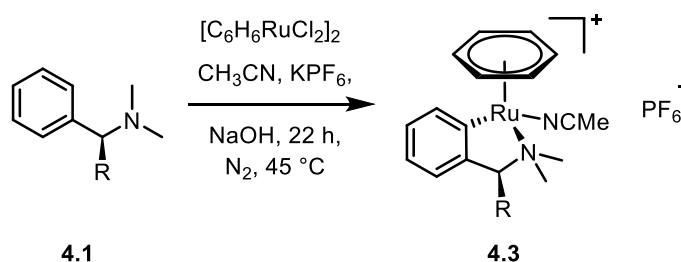
4.1 Introduction

Despite the success of palladium catalysis in organic synthesis and its application in the pharmaceutical and agrochemical industries, there is considerable scope and potential for the development of catalysis using other kinds of metallacycles such those containing cobalt,¹⁷⁸⁻¹⁷⁹ ruthenium¹⁸⁰⁻¹⁸¹ and rhodium.¹⁸²⁻¹⁸³ The synthesis of such complexes has historically required forcing conditions, such as strong bases and acids or mercury reagents, to provide a driving force for the C–H activation process.^{116,184-185}

Pfeffer and co-workers reported in 2001 the synthesis of metallacycles at Ir, Ru and Rh using tertiary, secondary and primary amines as substrates (**4.2** in Scheme 72), along with NaOH as a base and acetonitrile as the solvent of the reaction (Scheme 72 and Scheme 73).^{119-120,186}



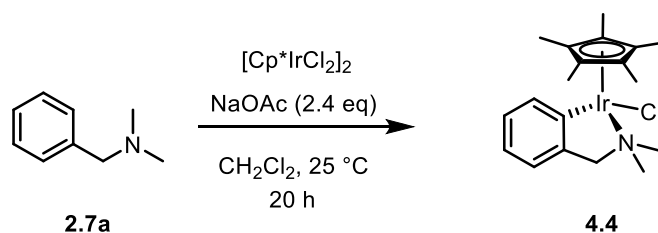
Scheme 72: General cyclometallation reaction of amines at Ir and Rh (Pfeffer *et al.*).



Scheme 73: General cyclometallation reaction of amines at Ru (Pfeffer *et al.*).

The mechanism of the reaction was not investigated by the authors, but they hypothesised that the reaction proceeds *via* an electrophilic aromatic substitution ($\text{S}_{\text{E}}\text{Ar}$) mechanism. This is consistent with the fact that the more electrophilic cationic Ru or Rh complexes could only be cyclometallated in the presence of a strong base such as NaOH.¹¹⁷

Davies and co-workers later reported a new and efficient method to promote C–H activation at Ir using NaOAc, which acts as both a base and co-ligand (Scheme 74).¹¹⁷

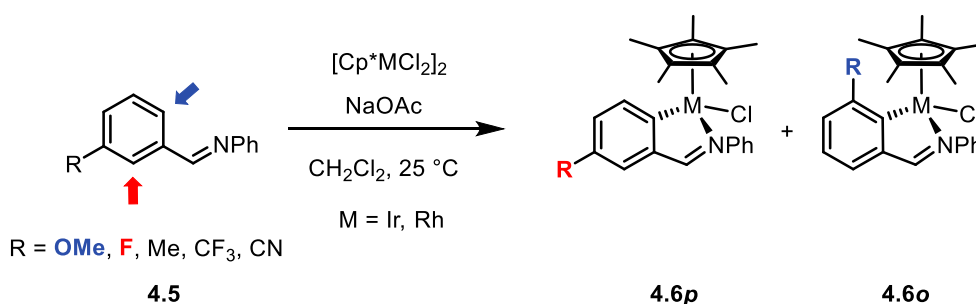


Scheme 74: Cyclometallation reaction at Ir of amine 2.17a (Davies *et al.*).

The same reaction attempted at Rh and Ru however did not afford the desired metallacycles and the only product obtained, at Rh, was the complex $[\text{Rh}(\text{OH}_2)(\eta^1\text{-O}_2\text{CMe})_2\text{Cp}^*]$ with no coordination of the nitrogen ligand (**2.7a**) observed. The higher reactivity of IrCp^* than Rh toward C–H activation has already been observed for benzoate complexes.¹⁸⁷

The two possible reaction mechanisms proposed for the C–H activation reaction to form the metallacycle at Ir(III) were oxidative addition of the aryl C–H bond to give an Ir(IV) cation, followed by reductive elimination of HX (X = Cl or OAc), or electrophilic aromatic substitution ($\text{S}_{\text{E}}\text{Ar}$). The two mechanisms would of course require different sources of metal: electrophilic mechanisms are favoured by electron-poor metal centres whilst the opposite is true for oxidative addition mechanisms. The failure of the cyclometallation reactions at Rh and Ru is therefore more consistent with an electrophilic mechanism, due to the good σ -donor, but poor π -acceptor properties of these metals. Later Davies and co-workers reported computational and experimental studies of the C–H activation reaction at Ir of *N,N*-dimethylbenzylamine (**2.7a**) to validate their first hypothesis, but unexpectedly they showed that a completely different mechanism was involved, and that the reaction in fact proceeds *via* an AMLA mechanism, as for cyclometallation of the same ligand at palladium.⁹⁴ They proposed a two-step process involving the initial displacement of the acetate ($\kappa^2\text{-}\kappa^1$) followed by C–H bond cleavage. Performing synthetic studies in parallel with the computational ones, no simple correlation between reactivity and computed C–H activation barriers was observed, suggesting that the C–H bond cleavage is not the rate determining step.⁶⁷

Due to the limited substrate scope of Davies' method (activation of amines, imines and oxazolines only), Jones and co-workers decided to investigate the reactivity and scope of functionalised imines (**4.5**) and phenylpyridines at Ir and Rh to assess how electronic factors could affect the C–H activation processes.¹¹⁶



Scheme 75: Cyclometallation reaction of phenylimines at Ir and Rh (Jones *et al.*).

They reported that reactions with the same substrate at Ir were 2–4 times faster than at Rh and that those with electron-donating groups on the aromatic ring were faster than those with electron-withdrawing substituents, further supporting an electrophilic activation mechanism (S_EAr). They also investigated the regioselectivity of these reactions, reacting Ir and Rh complexes with *meta*-substituted phenylimines (Scheme 75). The regioselectivity was particularly sensitive to steric effects, giving preference to the isomer with the R group in the *para* position, **4.6p**. In the case of R = F the major isomer formed was the one with the fluorine atom *ortho* to the metal, **4.6o** (2.3:1 for Ir and 8.5:1 for Rh), an effect which can be attributed to the *ortho* fluorine effect already discussed in intermolecular reactions at palladium (Chapter 2).

In this chapter an investigation into the effects of fluorine substituents on the regioselectivity of intramolecular C–H activation reactions of fluorinated benzylamines at iridium, rhodium and ruthenium is described.

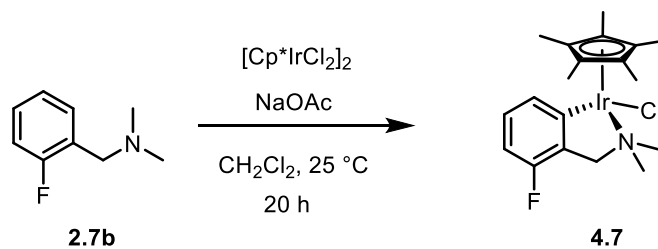
The aim was to explore whether an *ortho* fluorine effect could be observed in intramolecular C–H activation reactions of fluorinated dimethylbenzylamines at Rh, Ru and Ir, as reported experimentally by Jones for fluorinated imines at Rh and Ir,¹¹⁶ and to assess whether a change in reaction conditions, using the Pfeffer (NaOH and KPF_6)¹¹⁻¹³ and Davies (NaOAc) methods,¹¹⁷ would lead to a change in regioselectivity resulting from the reactions proceeding *via* different mechanisms.

4.2 Results and discussion

4.2.1 Reactions at Ir

The study of intramolecular C–H activation reactions of fluorinated benzylamines began with the reaction of the 2-fluoro-*N,N*-dimethylbenzylamine (**2.7b**) with the iridium complex $[Cp^*IrCl_2]_2$ at 25 °C in dichloromethane. The reaction conditions used were the same as

those developed by Davies and co-workers¹¹⁷ for the non-fluorinated ligand **2.7a** (Scheme 76), using NaOAc as a base, and metallacycle **4.7** was obtained in 68% isolated yield.



Scheme 76: Cyclometallation reaction at Ir of 2.7b following Davies' method.

The ¹H- and ¹⁹F-NMR spectra of **4.7** are consistent with those reported for the non-fluorinated Ir metallacycle **4.4**.¹¹⁷ The ¹H-NMR spectrum run in CDCl₃ shows three different signals for the three aromatic protons at δ 7.35 (d, $J = 7.5$ Hz), 6.99 (dd, $J = 13.9, 7.6$ Hz) and 6.55 (m) and two coupled doublets for the diastereotopic CH₂ protons at δ 4.27 (d, $J = 13.3$ Hz) and 3.54 (dd, $J = 13.3, 1.1$ Hz) where the low frequency doublet shows an additional splitting due to the coupling with the fluorine atom. The two methyl groups resonate as two singlets at δ 3.07 and 2.90 while the methyl groups of the Cp* are at δ 1.63. The ¹⁹F-NMR spectrum of **4.7** shows a doublet of doublets at δ -117.48 ($J = 9.7, 6.0$ Hz), slightly changed from that of the free amine **2.7b** (δ -118.6), but with a substantial reduction in the ³J_{H-F} of 6.0 Hz (15.9 Hz in the free substrate **2.7b**).

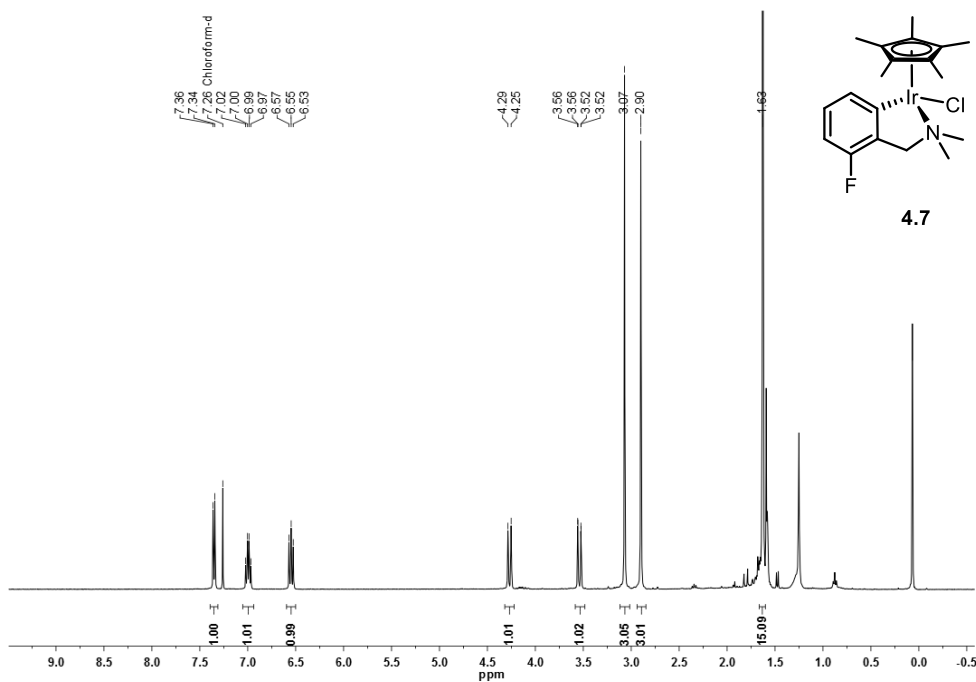


Figure 81: ¹H-NMR of 4.7 in CDCl₃ at 298 K (400 MHz).

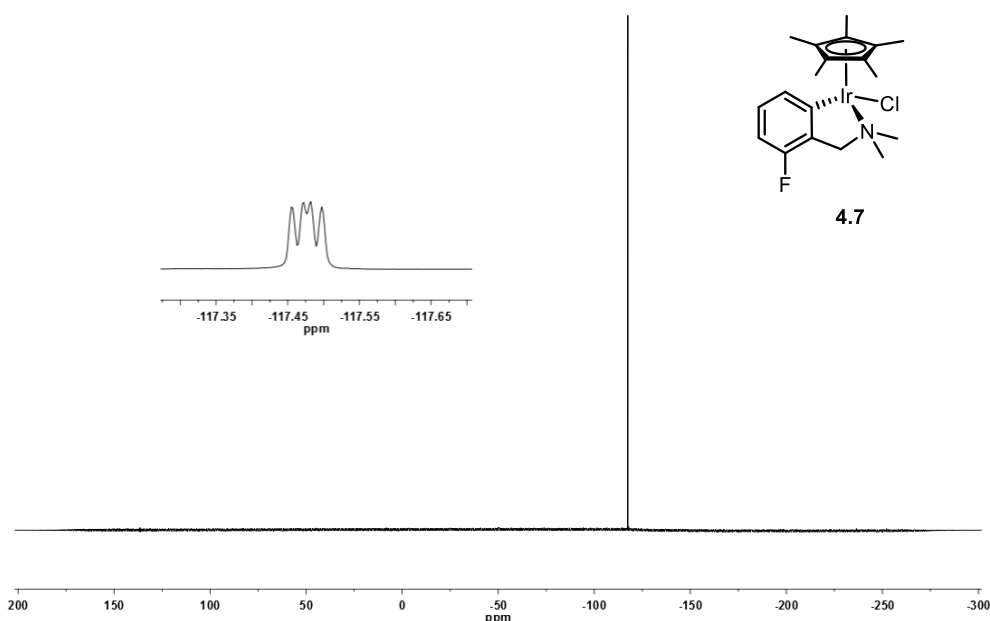
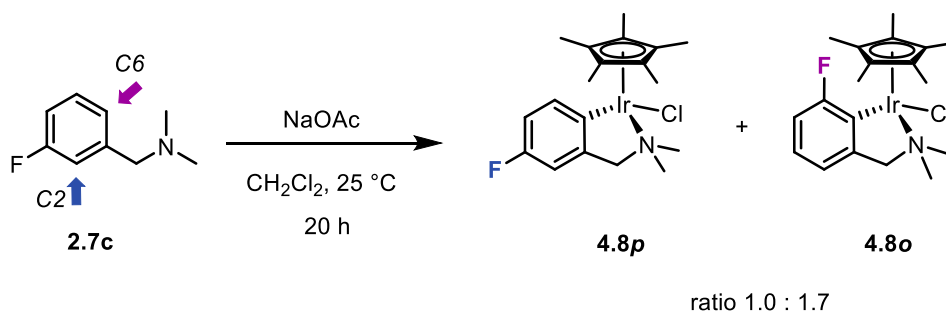


Figure 82: ^{19}F -NMR of **4.7** in CDCl_3 at 298 K (376 MHz).

The effect of the fluorine on the regioselectivity of C–H activation at Ir was tested with the key substrate **2.7c**, which presents two possibilities for attack at C-2 and C-6 (red and blue arrows respectively in Scheme 77) such that the C–H activation can occur *ortho* or *para* to the fluorine atom, respectively.



Scheme 77: Cyclometallation reaction at Ir of **2.7c** following Davies' method.

The reaction yielded a mixture of isomers **4.8o** and **4.8p** (49% overall yield) in the ratio *ortho/para* of 1.7 : 1.0. The ^{19}F -NMR spectrum of the product mixture shows two signals for the *para* and *ortho* isomers at δ -123.78 (td, $J = 9.7, 6.3$ Hz) and -94.21 (m) respectively while the ^1H -NMR spectrum shows two sets of signals for the two isomers (Table 22). It is possible to assign to the minor isomer as the *para* (**4.8p**) due to the low field doublet of doublets in the ^1H -NMR spectrum at δ 7.49 which corresponds to the proton at C-2 (see integration in the ^1H -NMR spectrum in Figure 83).

Table 22: $^1\text{H-NMR}$ signals of the two isomeric forms *ortho* and *para* of **4.8**.

$\delta (^1\text{H}) / \text{ppm}$	
<i>ortho</i> isomer	<i>para</i> isomer
-	7.49 (dd, $J = 8.3, 6.3$ Hz)
6.87–6.77 (m)	6.87–6.77 (m)
6.77–6.67 (m)	6.77–6.67 (m)
4.08 (d, $J = 12.8$ Hz)	4.38 (d, $J = 13.0$ Hz)
3.52 (d, $J = 12.9$ Hz)	3.20 (d, $J = 12.4$ Hz)
3.02 (s)	3.04 (s)
2.77 (s)	2.87 (s)
1.65 (d, $J = 0.7$ Hz)	1.62 (s)

The results indicate a preference for the *ortho* isomer, **4.8_o**, and, due to the mechanism presumably being an AMLA as proposed by Davies and co-workers,⁶⁷ there is a similarity in behaviour to the intermolecular C–H functionalisation reactions at Pd studied by Fagnou *et al.* experimentally²⁰ and by Perutz *et al.* computationally.⁶⁸ Interestingly the same substrate in intramolecular reaction at Pd showed no selectivity for the *ortho* isomer (*ortho/para* = 1:1) due to electronic and steric factors (Chapter 2),¹²² effects which are not relevant in the iridium system due to the completely different geometry of the metallacycle **4.8**.

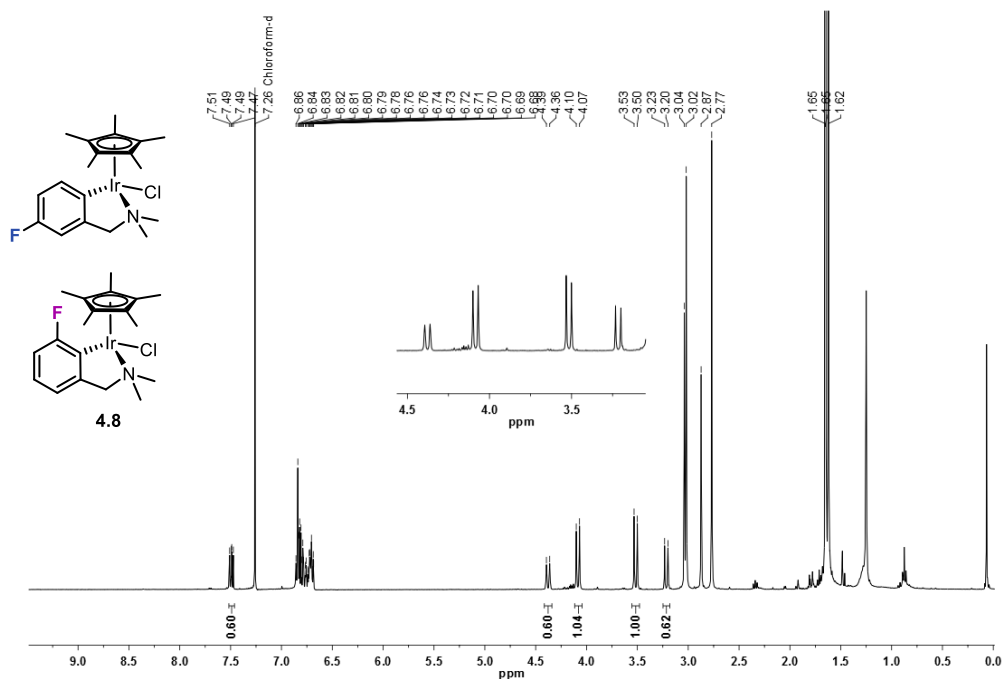


Figure 83: $^1\text{H-NMR}$ spectrum of mixture of isomers **4.8** in CDCl_3 at 298 K (400 MHz).

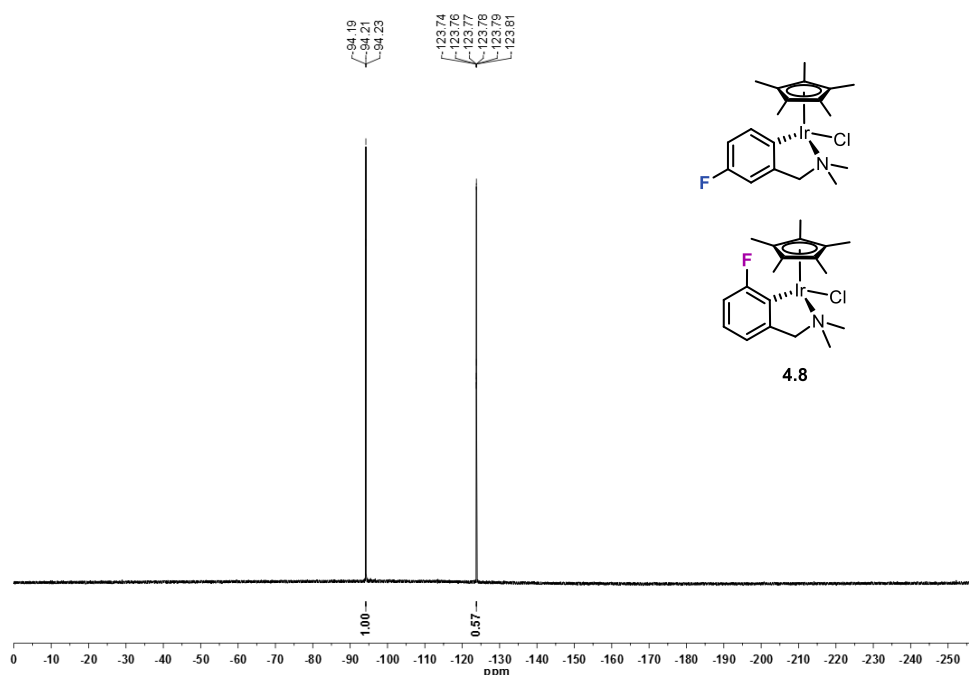
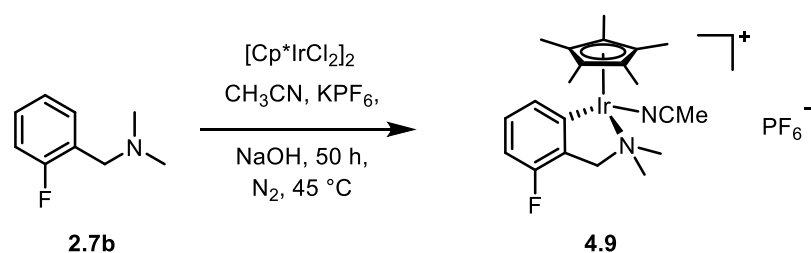


Figure 84: ^{19}F -NMR spectrum of mixture of isomers **4.8** in CDCl_3 at 298 K (376 MHz).

The structures of the iridium metallacycles have been reported by Jones *et al.*¹¹⁶ for phenylpyridines and by Pfeffer *et al.* for primary benzylamines.¹²⁰ While they both show the Cp^* in a *pseudo*-axial position, all the other features (bond angles and bond lengths) differ depending on the substrate, so a common analysis cannot be conducted.

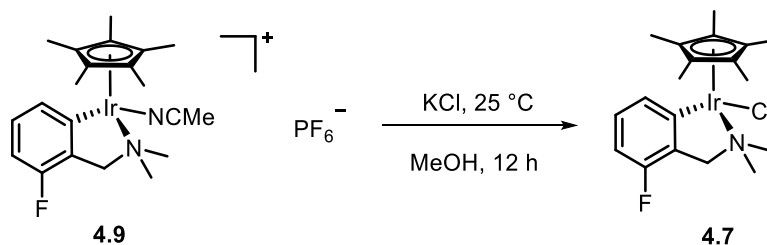
To assess if the regioselectivity with the same substrate **2.7c** could be different in reactions proceeding *via* a different mechanisms, the Pfeffer method, using NaOH as base instead of NaOAc, was used to synthesise the positively charged Ir metallacycle **4.13**, which could then be converted to Ir metallacycle, **4.11**, by a metathesis reaction (Scheme 81). The method was first employed with substrate **2.7b** (Scheme 78).



Scheme 78: Cyclometallation reaction at Ir of **2.7b** following the Pfeffer method.

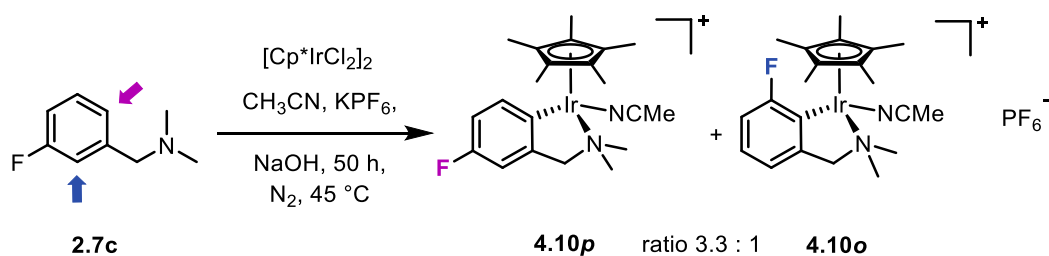
The iridium complex obtained, **4.9**, is a half sandwich Ir(III) complex, positively charged with PF_6^- as a counter anion. The iridium has a *pseudo*-tetrahedral geometry, is coordinated to the nitrogen atom of the fluorinated benzylamine and has an acetonitrile ligand that in CD_3CN at room temperature shows a fluxional exchange. A ^1H -NMR spectrum of the crude

reaction mixture was run to confirm the formation of the product **4.9**, which was then converted, without being isolated, to metallacycle **4.7** by reaction with KCl in MeOH (Scheme 79), showing matching data with the same metallacycle **4.7** obtained by Davies' method.

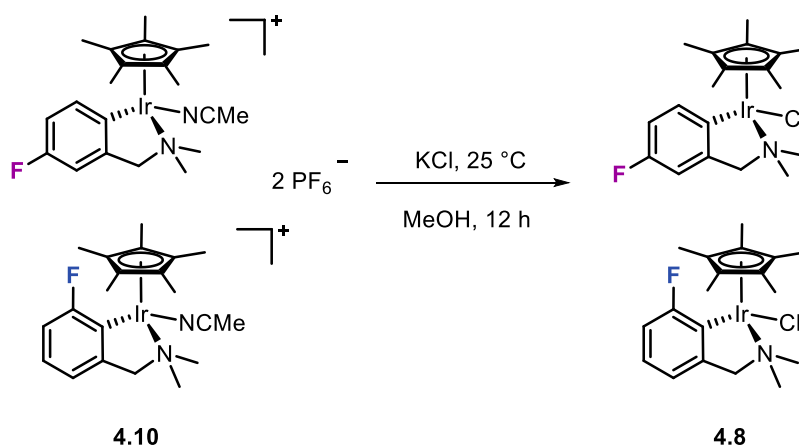


Scheme 79: Conversion of metallacycle 4.9 to metallacycle 4.7 with KCl.

Pfeffer and co-workers reported this conversion reaction under nitrogen,¹⁸⁶ but metallacycle **4.9** is not air-sensitive either in solution or in solid state. The only significant observation was the slow conversion of metallacycle **4.7** back to metallacycle **4.9** in CD₃CN after 48 hours as observed by ¹H-NMR spectroscopy. Once tested with substrate **2.7b**, the method was applied to the key substrate **2.7c** to assess the regioselectivity in the intramolecular C–H activation reaction (Scheme 80 Scheme 81).



Scheme 80: Cyclometallation reaction at Ir of 2.7c following Pfeffer method.



Scheme 81: Conversion of metallacycle 4.10 to metallacycle 4.8 with KCl.

The ^1H - and ^{19}F -NMR spectra of the product in CD_3CN showed that the reaction produced metallacycle **4.8** along with some by-products, but the interesting detail is the different ratio between *ortho* and *para* isomers being 3.3:1.0 (calculated by integration of the protons in the CH_2 group), considerably different from the one obtained using Davies' method (sample run in CDCl_3 , ratio 1.7:1.0) (Figure 85).

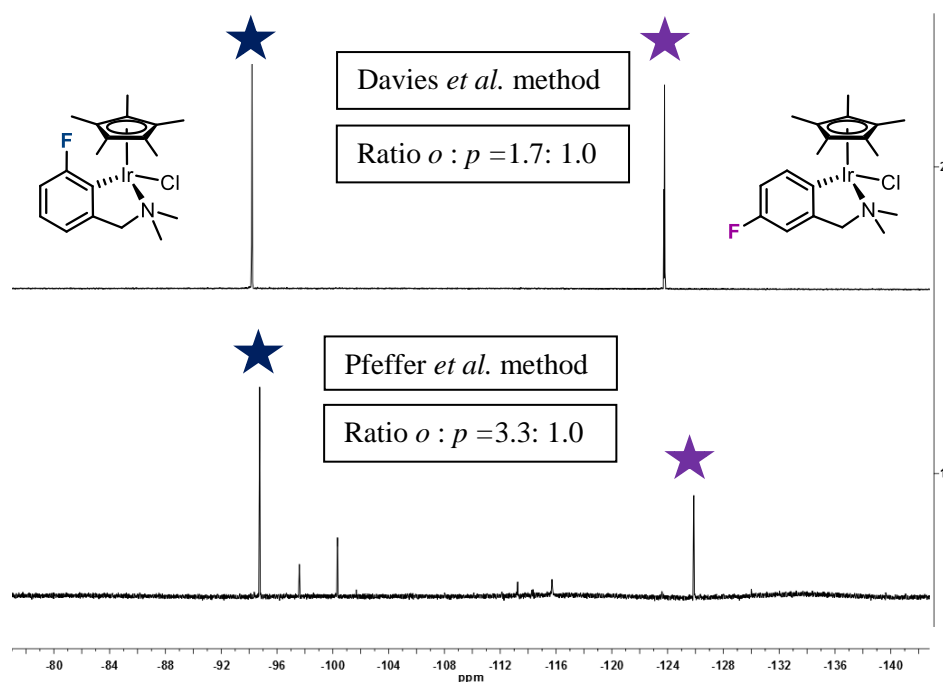
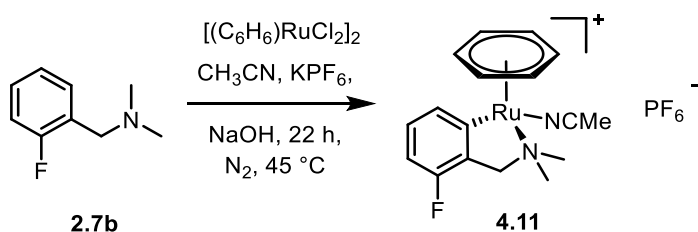


Figure 85: Comparison ^{19}F -NMR spectra of metallacycle **4.8 obtained via different syntheses.**

The difference in ratio could feasibly be attributed to a presumed difference in mechanism, A_{MLA} in the Davies' method versus $\text{S}_{\text{E}}\text{Ar}$ in the Pfeffer's method, but further investigation is needed to confirm this hypothesis. On the C–H activation at Ir using NaOH, the base is not coordinated to the metal and an electrophilic mechanism where the Wheland intermediate is formed is possible. It is also true, as reported by Davies and co-workers by density functional calculation of the electrophilic C–H activation at Ir, that other possible mechanisms are feasible depending upon the ligand present on the metal. Poorly orientated ligands, which cannot act as proton acceptors, undergo C–H activation at Ir *via* an oxidative addition mechanism while heteroatoms co-ligands, having lone pairs, undergo σ -bond metathesis, because the electronic participation of the metal on the four-centered mechanism is less required.¹¹⁸ A computational investigation should be performed on the system where NaOH is used, to better understand the type of mechanism and in the case of an electrophilic one, if the C–H activation is the rate determining step.

4.2.2 Reactions at Ru

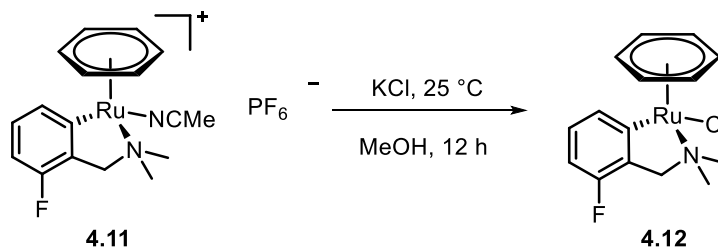
The only method reported to synthesise Ru metallacycles with benzylamines is that of Pfeffer and co-workers discussed previously for Ir, using NaOH as a base, and is suggested to proceed *via* an electrophilic aromatic substitution mechanism.¹¹⁹ As already shown by Davies *et al.*¹¹⁷ C–H activation at Ru with NaOAc gives the complex [RuCl(O₂CMe)(*p*-cymene)], but not cyclometallation products. Substrate **2.7b** was therefore reacted with [(C₆H₆)RuCl₂]₂ in acetonitrile at 45 °C for 50 hours, in the presence of NaOH, to obtain metallacycle **4.11** in 74% isolated yield.



Scheme 82: Synthesis of metallacycle **4.11** by the Pfeffer's method.

The ¹H-NMR spectrum of **4.11** (Figure 86) run in CD₃CN shows for the three aromatic protons a doublet at δ 7.72 ($J = 7.5$ Hz), a triplet of doublets at δ 7.11 ($J = 7.8, 5.6$ Hz) and a multiplet at δ 6.70. It also shows a singlet at δ 5.67 for the η^6 -benzene ring and two doublets for the diastereotopic CH₂ protons at δ 3.62 ($J = 14.0$ Hz) and δ 3.54 ($J = 14.0, 1.4$ Hz), where the high field doublet shows an additional splitting due to the coupling with the fluorine atom. The two methyl groups resonate at δ 3.03 and 2.86 as two singlets. The ¹⁹F-NMR spectrum shows a multiplet centered at $-\delta$ 117.34, slightly different from the free substrate **2.7b** (δ $-\delta$ 118.10).

Complex **4.11** was then converted to metallacycle **4.12** in 55% isolated yield using the same method as that used for the iridium complexes.



Scheme 83: Conversion of metallacycle **4.11** to metallacycle **4.12** with KCl.

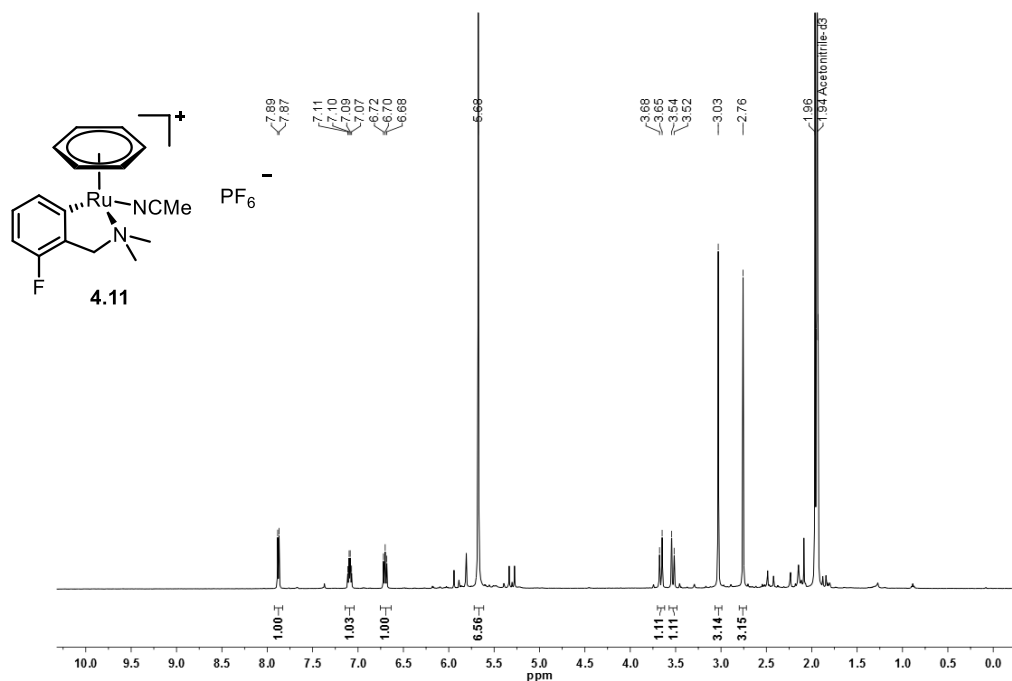
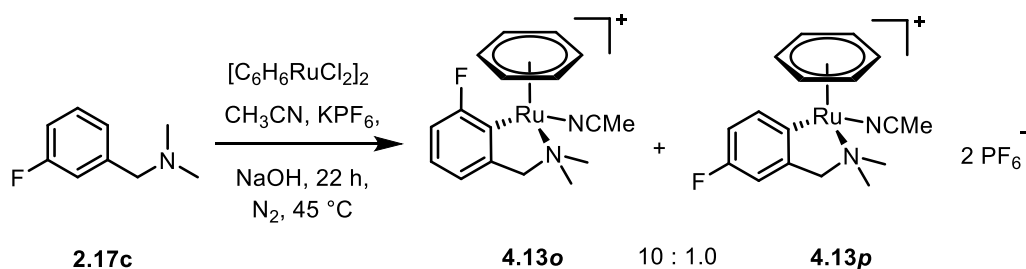


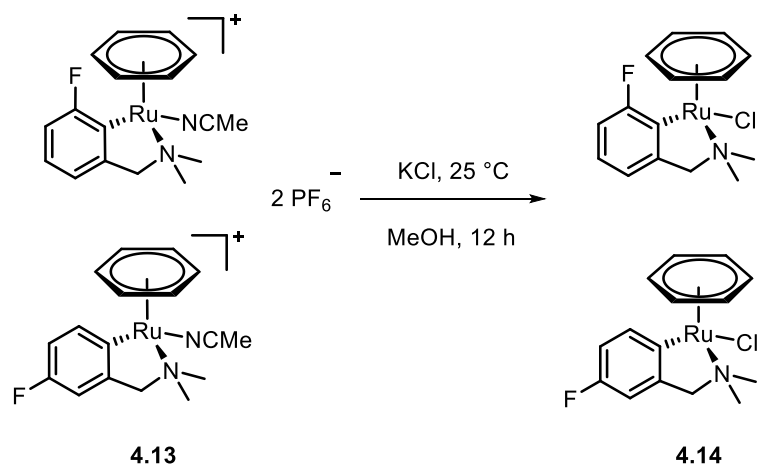
Figure 86: $^1\text{H-NMR}$ spectrum of **4.11** in CD_3CN at 298 K (500 MHz).

To assess the regioselectivity of the C–H activation reaction at Ru, substrate **2.7c** was reacted with $[(\text{C}_6\text{H}_6)\text{RuCl}_2]_2$ following the same method described above and metallacycle **4.13** was obtained in 63% isolated yield (Scheme 84). As in the case of the equivalent iridium metallacycle **4.8**, two regioisomers, **4.13o** and **4.13p**, were formed, this time in the ratio *ortho* : *para* = 10 : 1.0.



Scheme 84: Synthesis of metallacycle **4.13** by Pfeffer *et al.* method.

The mixture of isomers of **4.13** was then converted to metallacycles **4.14o** and **4.14p** (Scheme 85), which showed retention of the ratio between the regioisomers observed previously (Figure 87).



Scheme 85: Conversion of metallacycle 4.13 to metallacycle 4.14 with KCl.

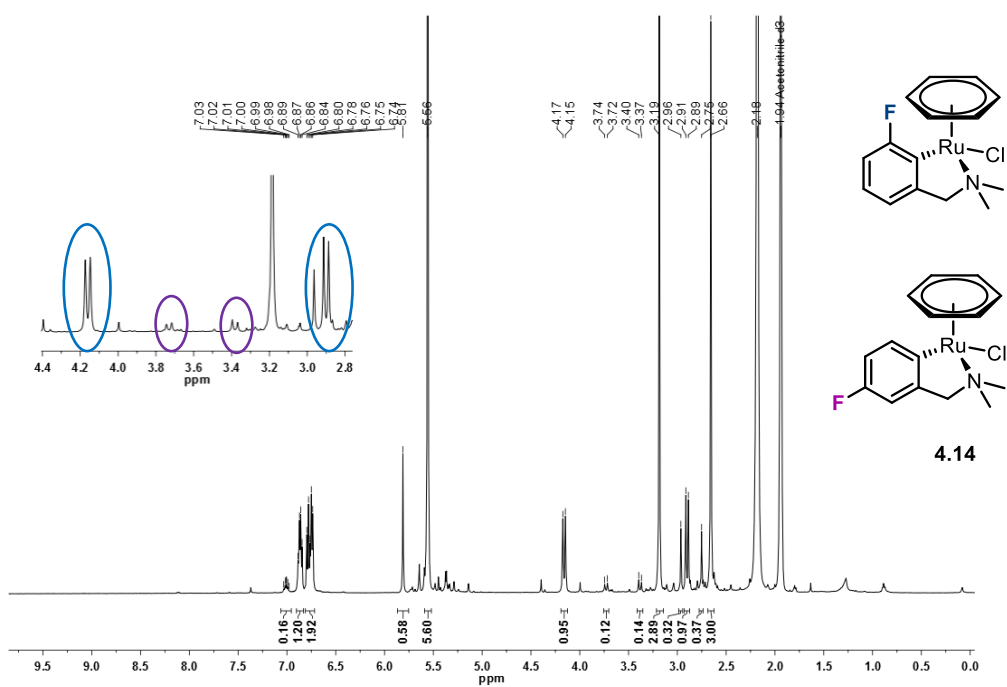


Figure 87: ¹H-NMR spectrum of 4.14 in CD₃CN at 298 K (500 MHz).

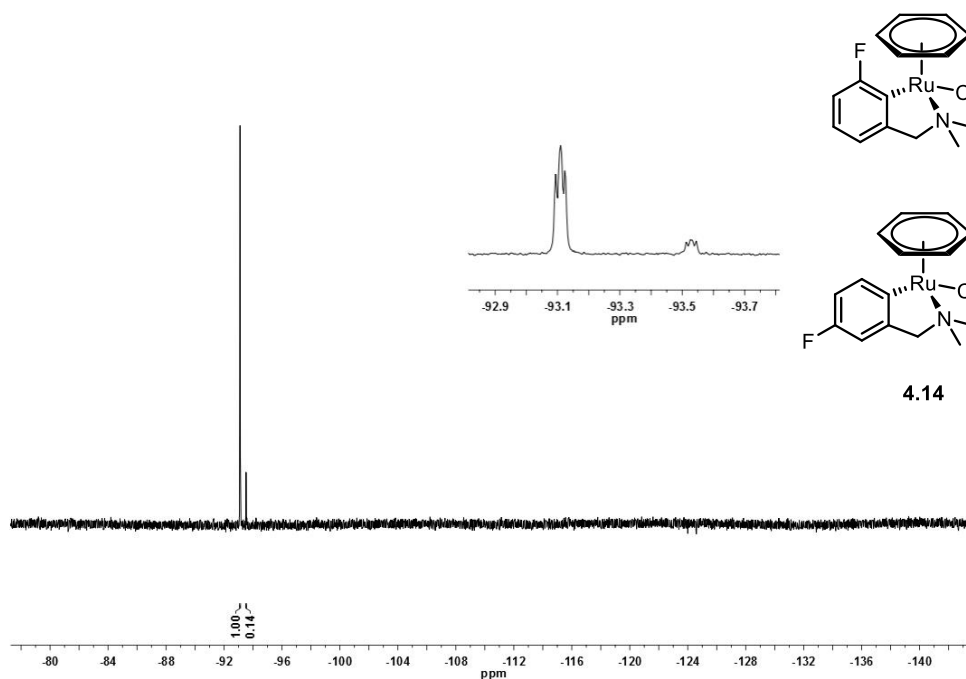
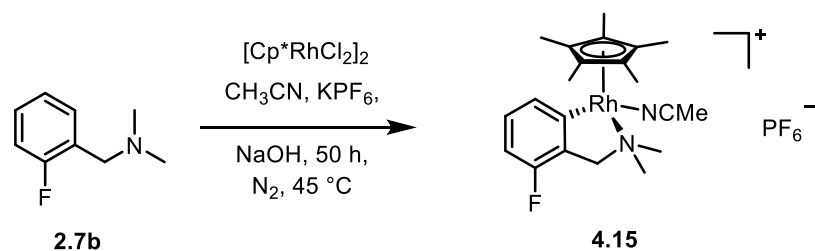


Figure 88: ^{19}F -NMR spectrum of **4.14** in CD_3CN at 298 K (471 MHz).

As reported by Pfeffer and co-workers the role of NaOH is not fully understood but is necessary to obtain the cyclometallated product. Interestingly the source of Ru can change the outcome of the reaction, the *p*-cymene complex is not in fact able to cyclometallate tertiary amines and this could be consistent with an electrophilic mechanism being the *p*-cymene ligand less electrophilic than the benzene-ligand on the Ru centre.¹²¹

4.2.3 Reactions at Rh

The only method reported to synthesise Rh metallacycles with benzylamines is that of Pfeffer and co-workers.¹²⁰ As already shown by Davies *et al.*¹¹⁷ and confirmed by Jones *et al.*,¹¹⁶ C–H activation at Rh with NaOAc is substrate specific and does not work for tertiary benzylamines. The synthesis with fluorinated substrates was attempted, but the desired products could not be obtained by this method. Therefore, as for the synthesis of iridium complexes, the substrate **2.7b** was reacted with $[\text{Cp}^*\text{RhCl}_2]_2$ in acetonitrile at 45 °C for 50 hours in the presence of NaOH and protected from light to obtain metallacycle **4.15** in a 69% isolated yield.



Scheme 86: Synthesis of metallacycle 4.15 by Pfeffer *et al* method.

The $^1\text{H-NMR}$ spectrum of **4.15** (Figure 89) run in CDCl_3 shows a doublet at δ 7.35 ($J = 7.5$ Hz), a doublet of doublets at δ 7.05 ($J = 13.5, 7.6$ Hz), a triplet at δ 6.59 ($J = 9.0$ Hz) for the three aromatic protons and the characteristic two doublets for the diastereotopic CH_2 protons at δ 4.02 ($J = 13.4$ Hz) and δ 3.49 ($J = 13.3$ Hz). The two methyl groups resonate at δ 2.75 and 2.76 as two singlets and the methyl groups of the Cp^* resonate as a singlet at δ 1.59.

The same reaction was attempted with substrate **2.7c** to assess the regioselectivity, but the reaction gave a complex mixture of products from which the isomeric ratio could not be determined, and the attempted purification of the products failed. Further experiments need to be performed.

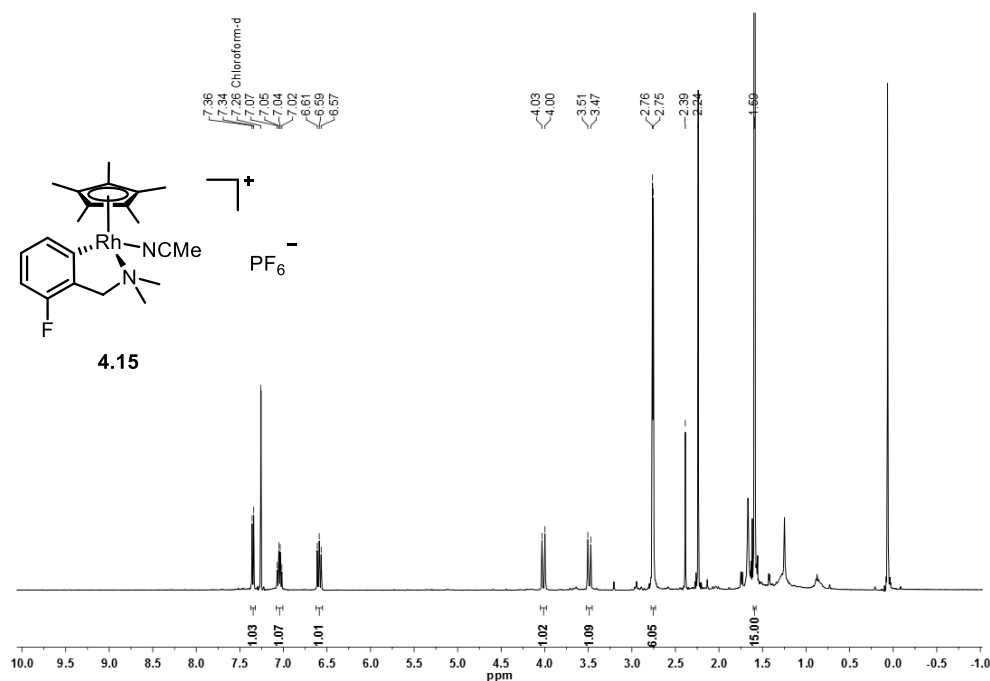


Figure 89: $^1\text{H-NMR}$ spectrum of 4.15 in CDCl_3 at 298 K (400 MHz).

4.3 Summary

This chapter describes the synthesis and characterisation of Ir, Ru and Rh metallacycles (**4.7–4.14**) with fluorinated benzylamines **2.7b** and **2.7c** via intramolecular C–H activation reactions.

Two different methods were used in the synthesis of Ir metallacycles, and for substrate **2.7c**, offering two possibilities for the C–H activation reaction, the regioselectivity observed, *ortho* to fluorine, seems to be dependent from the method used (*ortho/para* ratio of 1.7 : 1.0. using NaOAc as a base versus 3.3:1.0 using NaOH).

Jones and co-workers, having used NaOAc in the reactions at Ir and Rh of phenylimines (**4.5**) suggested that the mechanism was an S_EAr while Davies *et al.* reported computational and experimental studies of *N,N*-dimethylbenzylamine (**2.7a**) suggesting an AMLA mechanism. Pfeffer *et al.* did not report any mechanistic investigation for their method, but the different results obtained would be consistent with an electrophilic aromatic substitution (S_EAr) mechanism. This could explain the different *ortho/para* ratios obtained and the fact that reactions with Rh proceed with the Pfeffer method (as for the Jones system) using a strong base, but not with the Davies procedure using the weaker base NaOAc.

In the case of Ru and Rh a comparison between methods could not be carried out due to the difficulty in synthesising Ru and Rh metallacycles using NaOAc, as reported by Davies and co-workers and confirmed by Jones *et al.*¹¹⁶

The Ru metallacycle with substrate **2.7c** gave a preference for the *ortho* isomer, the (ratio *ortho/para* of 10:1.0) which was determined by ¹H-NMR spectroscopy, but a crystal structure analysis would help to confirm that the major isomer is the one with the metal *ortho* to the fluorine atom.

More general conclusions are given in Chapter 6.

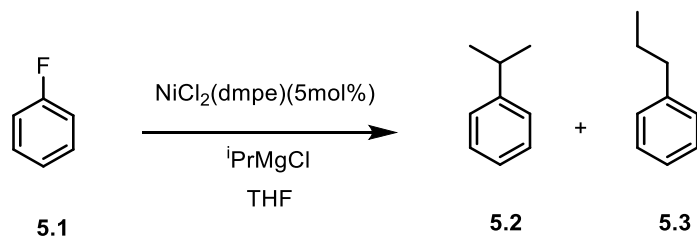
Chapter 5: C–F activation experiments at Ni(0), Pd(0) and Pt(0)

5.1 Catalytic C–F functionalisation at Pd(0)

5.1.1 Introduction

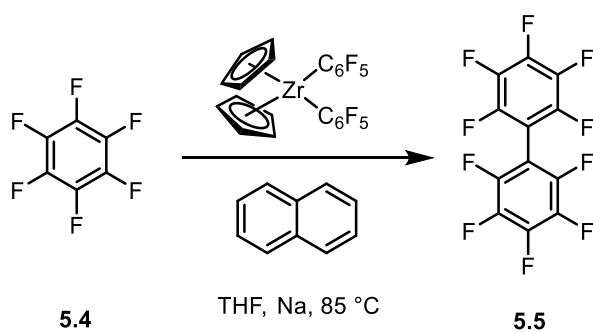
The introduction of partially fluorinated aromatic fragments *via* selective C–F activation at transition metals holds much potential for the synthesis of pharmaceutical and agrochemical building blocks.¹⁸⁸ The abundance of relatively cheap polyfluoroarenes make them attractive alternatives to using heavier halogens or preactivated organometallic substrates.¹⁸⁹ Despite the progress in stoichiometric C–F activation reactions there are few examples of C–C bond formation *via* catalytic C–F activation, presumably due to the difficulty of breaking the C–F bond with its very high bond dissociation energy.¹⁹⁰

Kumada and co-workers reported the first example of a catalytic C–C bond formation in 1973, using a Ni(II) phosphine complex as a catalyst in the presence of a Grignard reagent to functionalise a monofluorobenzene, forming the desired isopropylbenzene (**5.2**), but also noting that isomerization reactions were taking place (*e.g.* the formation of **5.3** in Scheme 87).^{188,190-191}



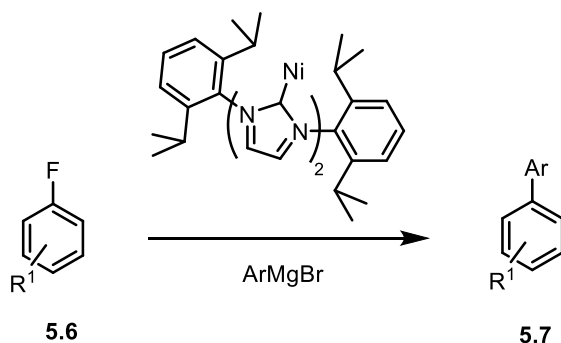
Scheme 87: First example of catalytic C–C bond formation using Ni(II) complex (Kumada *et al.*).

The first catalytic C–C bond formation with a polyfluoroarene was then reported by Jones and co-workers in 1999, using a Zr complex as the catalyst (Scheme 88).¹⁹²

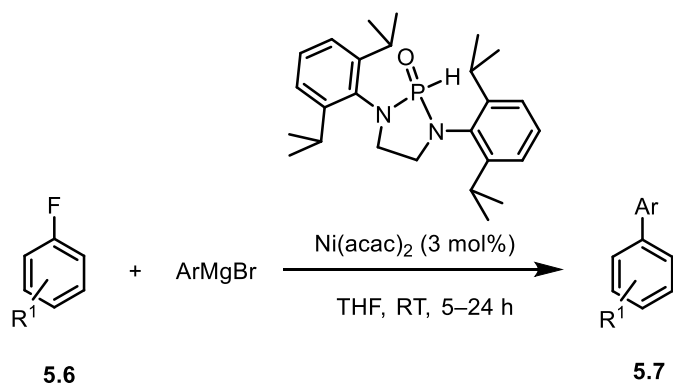


Scheme 88: First catalytic C–C bond formation with a polyfluoroarene (Jones *et al.*).

Group 10 transition metal catalysts (Ni, Pd and Pt) are the most frequently used in the development of catalytic cross coupling reactions of fluoroaromatics. The Herrmann group reported a Ni-catalysed Kumada reaction of functionalised monofluoroarenes using an *N*-heterocyclic carbene (Scheme 89),¹⁹³ and a few years later Ackermann reported a similar reaction using the cheaper Ni(acac)₂ supported with an unusual phosphine oxide ligand, to functionalise aryl and alkyl Grignard reagents (Scheme 90).¹⁹⁴

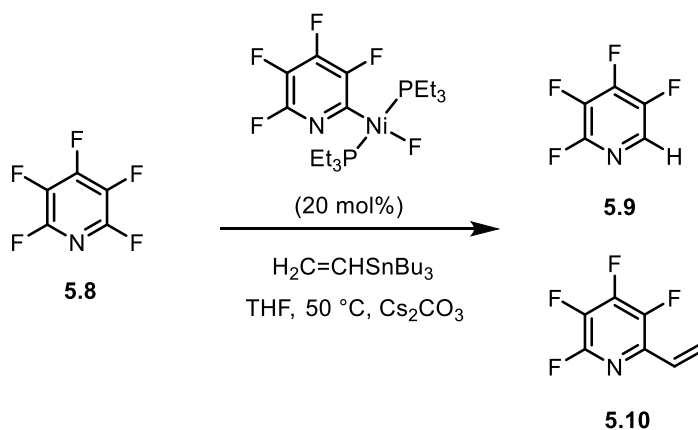


Scheme 89: Functionalisation of monofluoroarene with Ni(II) and *N*-heterocyclic carbene ligand (Herrmann *et al.*).



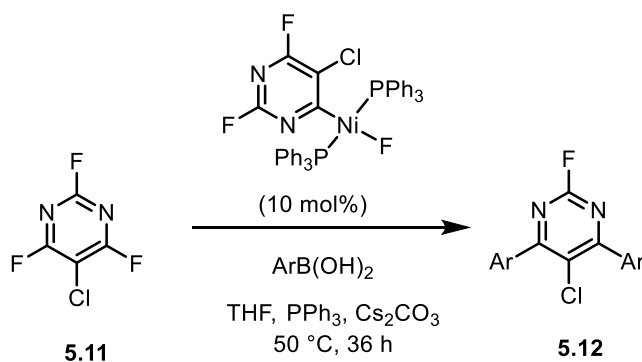
Scheme 90: Functionalisation of monofluoroarene with Ni(II) with phosphine oxide ligand (Ackermann *et al.*).

Perutz and co-workers, after extensive studies on stoichiometric C–F activation reactions at Ni(0),¹⁹⁵⁻¹⁹⁶ developed the first Ni(II) cross-coupling reaction of a polyfluoroarene (Scheme 91).¹⁹⁷



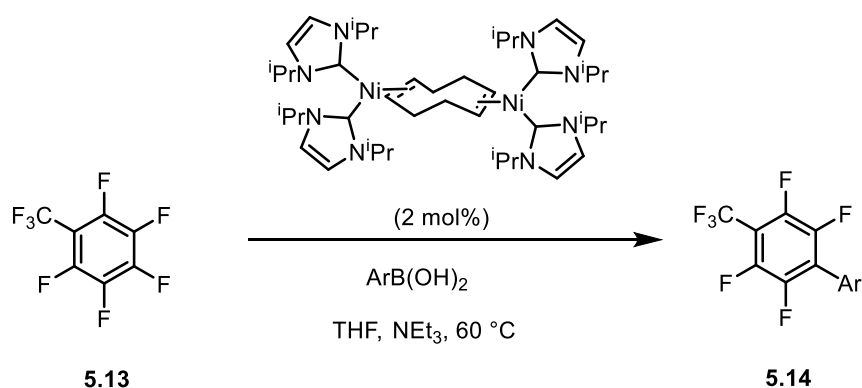
Scheme 91: Stoichiometric C–F activation reactions at Ni(0) of perfluoropyridine (Perutz *et al.*).

The Ni fluoride complex used was able to catalyse the regioselective C–F functionalisation *ortho* to the nitrogen atom of a pentafluoropyridine (5.8) in the presence of a vinyl tin reagent. Interestingly, in a similar manner, Braun and co-workers later reported the first example of selective C–F functionalisation in the presence of a weaker chlorine–carbon bond (Scheme 92).¹⁹⁸



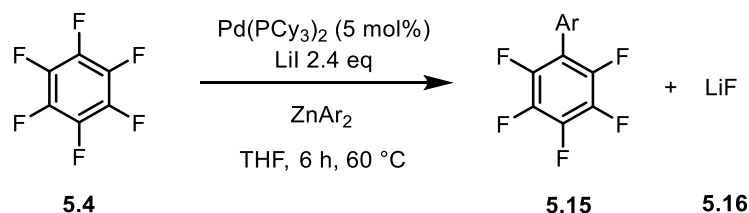
Scheme 92: Selective C–F functionalisation in the presence of a weaker chlorine–carbon bond (Braun *et al.*).

The first example of a Ni(0) Suzuki cross-coupling reaction was reported in 2006 by Radius and co-workers on perfluoroarenes, using a Ni(0) carbene complex previously used by the same group in stoichiometric C–F activation reactions of hexafluorobenzene (Scheme 93).¹⁹⁹



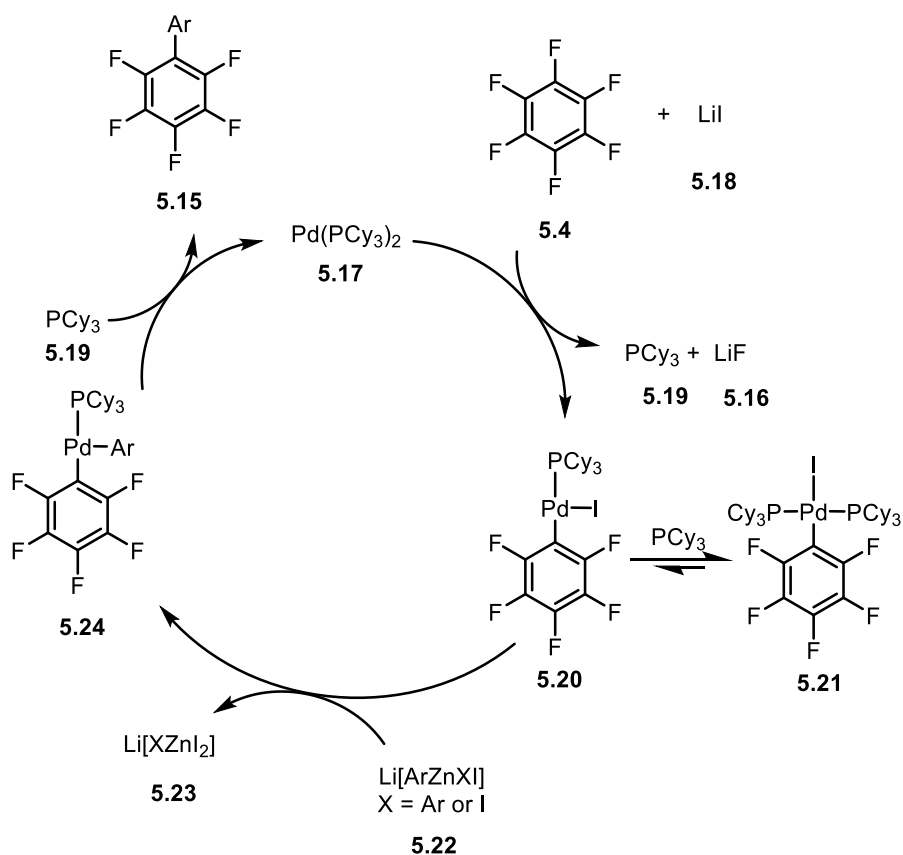
Scheme 93: First example of a Ni(0) Suzuki cross-coupling reaction (Radius *et al.*).

Despite the extensive use of Pd in catalysis, few examples of Pd-catalysed cross coupling reactions *via* C–F activation are reported.¹⁹⁰ Ogoshi and co-workers reported the first example of a Pd(0) catalysed functionalisation of hexafluorobenzene in the presence of diarylzinc compounds (generated *in situ* from zinc dichloride and an arylmagnesium bromide) to obtain pentafluorophenyl derivatives (Scheme 94).²⁰⁰



Scheme 94: Pd(0)-catalysed functionalisation of hexafluorobenzene (Ogoshi *et al.*).

The presence of LiI in the reaction mixture helps the abstraction of the fluorine atom by forming the thermodynamically favourable LiF as a by-product, along with the functionalised fluoroaromatic. The substrate scope of the reaction includes electron-donating and electron-withdrawing substituents on the aryl group and different fluoroaromatics including pentafluoropyridine and perfluoronaphthalene. The mechanism (Scheme 95) proposed by Ogoshi *et al.* starts with the oxidative addition of hexafluorobenzene (**5.4**) to the Pd(PCy₃)₂ (**5.17**) with the dissociation of one PCy₃ ligand (**5.19**) and the exchange at Pd of a fluorine for an iodine atom. The transmetalation step with the diaryl zinc generated *in situ* (**5.23**) leads to the final step where the reductive elimination of the product (**5.15**) regenerates the catalyst (**5.17**).



Scheme 95: Ogoshi's proposed mechanism for catalytic C–F activation of hexafluorobenzene.

The aim of the study reported hereafter, performed in collaboration with Stefanie Federle (Erasmus student from Heidelberg University) was to assess if the method developed by Ogoshi *et al.* could be applied to functionalise fluorinated *N,N*-dimethylbenzylamines *via* C–F bond activation, and if this kind of activation could be obtained regioselectively.

5.1.2 Results and discussion

The substrates considered for the catalytic C–F activation at Pd(0) were 2,6-difluoro-*N,N*-dimethylbenzylamine (5.25), 3,4-difluoro-*N,N*-dimethylbenzylamine (2.7e) and 2,3,4,5,6-pentafluoro-*N,N*-dimethylbenzylamine (5.26), shown in Figure 90.

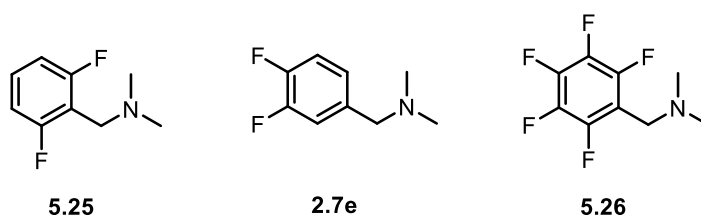
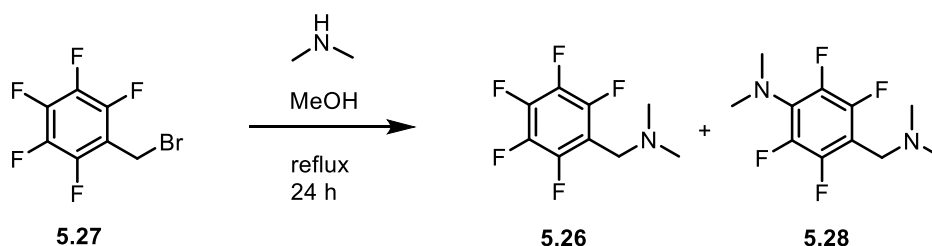


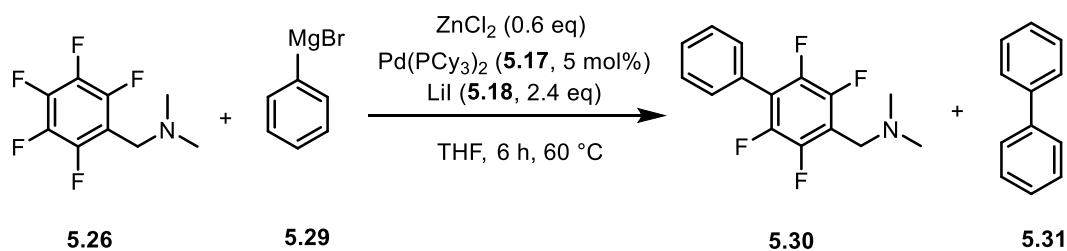
Figure 90: Fluorinated substrates considered for the catalytic C–F activation at Pd(0).

Substrates **5.25** and **2.7e** were synthesised as described in Chapter 2, following the procedure developed by Liu and co-workers.¹²⁶ The synthesis of substrate **5.26**, following the same reaction conditions, gave predominantly the by-product **5.28** due to a second nucleophilic substitution, *para* to the benzylic arm, from the excess of dimethylamine (Scheme 96).



Scheme 96: Formation of expected product 5.26 along with byproduct 5.28.

Following this result, the reaction conditions were altered: a temperature of 25 °C was used instead of 65 °C and the reaction time was decreased from 24 to 4 hours; this led to the successful isolation of **5.26** in 82% yield. Compound **5.26** was a suitable candidate for testing the method used by Ogoshi *et al.* due to the similarity of the substrates (**5.26** and hexafluorobenzene, **5.4**) both having a perfluorinated aromatic ring. The reaction was performed using the same stoichiometry used in their report (see Scheme 97), but after 6 hours the presence of the starting material **5.26** was still evident along with the formation of biphenyl **5.30** as by-product.



Scheme 97: Cross coupling reaction of 5.26 using Ogoshi's conditions.

After a brief preliminary catalytic screening, the amount of PhMgBr/ZnCl₂ was increased from 0.6 to 1 eq, the amount of Pd complex **5.17** from 5 to 7 mol% and the amount of LiI from 2.4 to 4 mol%. After 6 hours at 60 °C, using these ratios of reagents, the product **5.30** was obtained in 28% isolated yield as a yellow solid along with biphenyl **5.31** (56% yield w.r.t PhMgBr) following purification by flash chromatography (CH₂Cl₂:methanol, 100:1). The ¹⁹F-NMR spectrum of **5.30**, in CDCl₃, shows only two signals at δ -144.52 (dd, *J* = 23.0, 13.1 Hz) and -142.93 (dd, *J* = 23.0, 13.1 Hz) validating the hypothesis that the C–F functionalisation is regioselective *para* to the benzylic arm. The regioselectivity was also

confirmed by X-ray crystallography of a single crystal obtained by slow evaporation of a saturated solution of the product **5.30** in CDCl₃ (Figure 91).

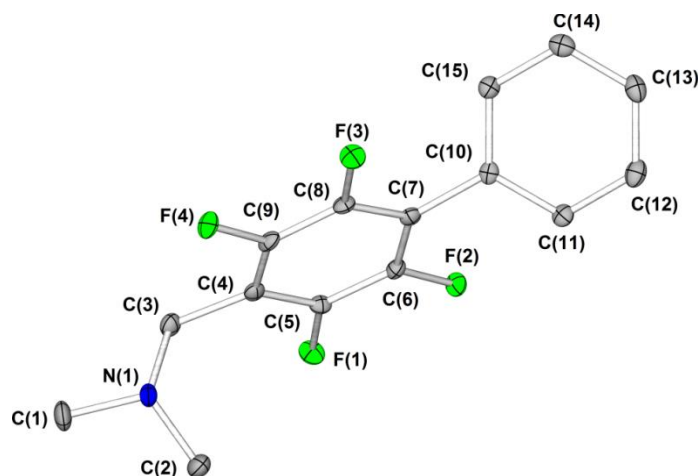
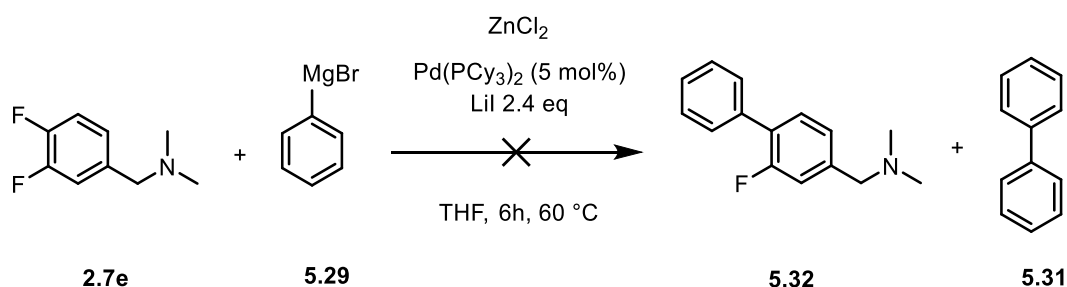


Figure 91: Molecular structure of palladacycle 5.30. Hydrogen atoms were omitted for clarity; thermal ellipsoids shown with probability of 50%. Selected bond lengths(Å): C(5)–F(1): 1.350(3), C(6)–F(2): 1.353(3), C(8)–F(3): 1.346(3), C(9)–F(4): 1.346(3), C(7)–C(10): 1.482(4); selected bond angles (°): C(15)–C(10)–C(7): 119.6(2), C(11)–C(10)–C(7): 121.1(2), F(4)–C(9)–C(4): 119.8(2), F(1)–C(5)–C(4): 119.7(2).

The reaction was also carried out in the absence of ZnCl₂, using only the Grignard reagent to test the transmetalation step; after 6 hours under these conditions only 25% of the starting material was converted to **5.30** (vs. full consumption of starting material in presence of ZnCl₂, as measured by integration of ¹⁹F-NMR signals of starting material and product), indicating that the transmetalation step is faster in the presence of Zn. The reaction was also carried out without the Pd complex (**5.17**) and in this case after 24 hours no product was observed.

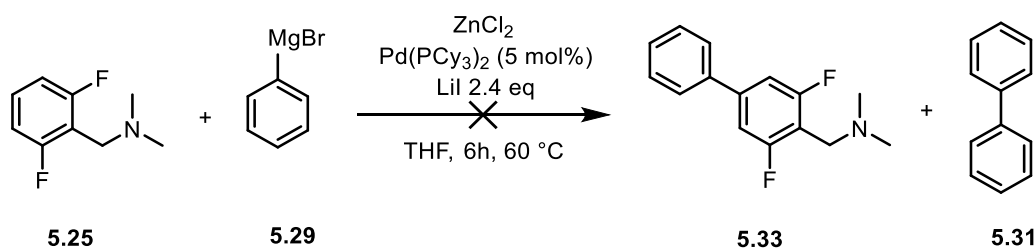
Since the functionalisation occurred *para* to the benzylic arm, it is possible to exclude the coordination of the Pd to the nitrogen atom in the first step of the catalytic cycle, as this would lead to an *ortho* functionalisation. The *para* position is presumably favoured by the nucleophilic palladium atom, being the least electron-rich position in the ring.

Following the regioselective C–F functionalisation obtained with the perfluorobenzylamine **5.26**, the reaction was attempted with the difluorinated substrate **2.7e** having one of the fluorines *para* to the benzyl arm; this substrate would also allow the catalytic process to be tested for C–H versus C–F activation.



Scheme 98: Attempted C–F functionalisation reaction of 2.7e following the Ogoshi method.

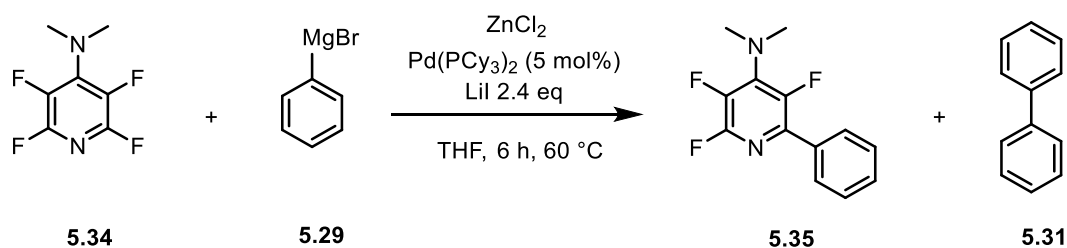
The reaction with substrate **2.7e** under the same conditions used previously (Scheme 98) did not take place even after 24 hours, and only the starting material **2.7e** along with the biphenyl **5.31** was recovered, with no C–H or C–F activation products detected. The reaction with substrate **5.25** was then attempted (Scheme 99) to check if a regioselective C–H functionalisation reaction *para* to the benzylic arm could be obtained. Similarly for substrate **2.7e**, no cross-coupling products were detected.



Scheme 99: Attempted C–H functionalisation reaction of 5.25 following the Ogoshi method.

It is possible that the two difluorinated substrates (**5.25** and **2.7e**) did not react under the Ogoshi conditions due to the higher electron density of the aromatic ring; the nucleophilic palladium is less inclined to attack these aromatic carbons, which are much less electrophilic compared to those in the perfluorinated substrates used by Ogoshi.

The method was then tested on a different amine, 4-*N,N*-dimethylamino-2,3,5,6-tetrafluoro-pyridine **5.34**, synthesised by reaction of *N,N*-dimethylamine with pentafluoropyridine, **5.8**, at 0 °C.²⁰¹



Scheme 100: C–F functionalisation reaction of 5.34 following Ogoshi method.

In Ogoshi's paper, the reaction with pentafluoropyridine, **5.8**, gave two products, with the C–F activation occurring *ortho* and *para* to nitrogen with a ratio of the two isomeric products of 1: 3.8 respectively.²⁰⁰ The experiment with substrate **5.34** was performed to test if a complete *ortho* selectivity could be obtained by blocking the *para* position with the dimethylamine group.

The desired product was indeed obtained, but in a low yield (Figure 92, blue stars indicate the product against starting material in the ¹⁹F-NMR spectrum) and even after 24 hours the conversion was just 10% (as calculated from the ¹⁹F-NMR spectrum, using C₆F₆ as internal standard). This could again be due to the electron-donating character of the dimethylamine which makes the aromatic ring more electron-rich and disfavours the C–F functionalisation by the nucleophilic palladium.

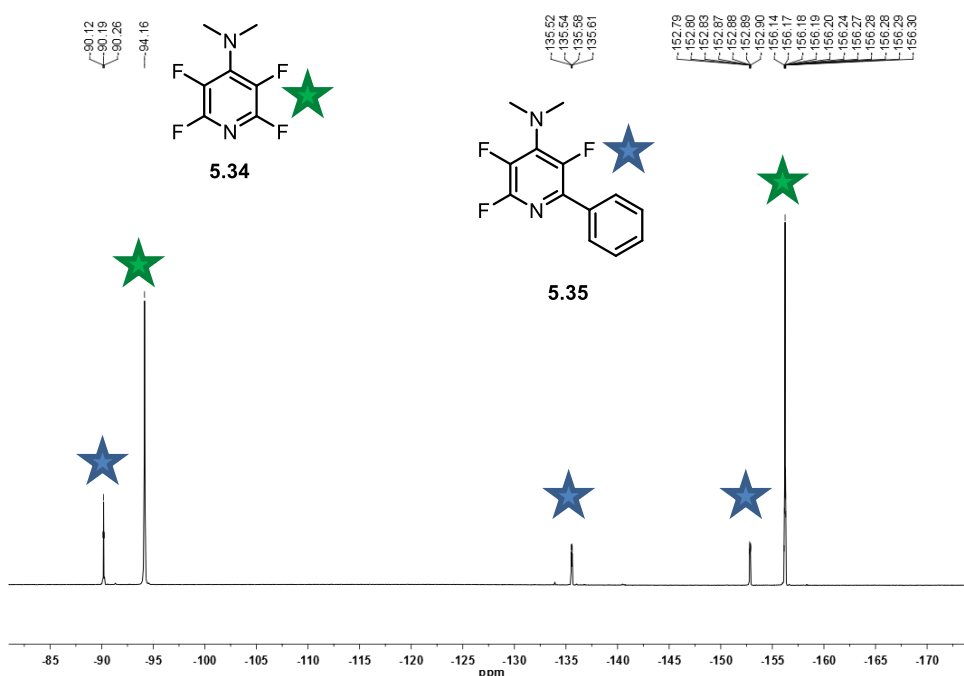


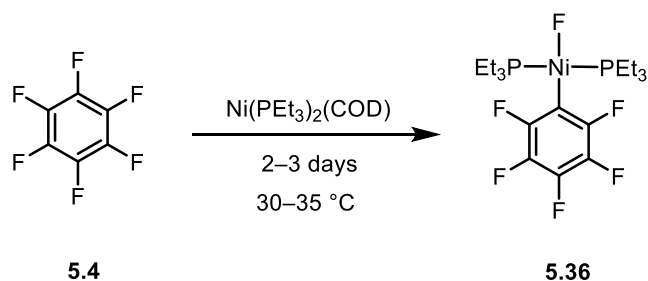
Figure 92: ¹⁹F-NMR spectrum of reaction in Scheme 100. Blue stars indicate signals arising from compound **5.35** while green stars indicate the starting material **5.34**.

This brief study has shown that it is possible to expand the substrate scope of Ogoshi's C–F activation reaction to substrates containing tertiary amine groups, and to obtain the products regioselectively. However, the failure of reactions with substrates **2.7e** and **5.25** and slow reaction with compound **5.34** suggests that the electron-deficiency of the aromatic ring is crucial for efficient reaction and thus reducing the number of fluorine atoms or adding electron-donating groups to the ring hinders the reaction dramatically.

5.2 Stoichiometric C–F activation attempts of fluorinated benzylamines and benzylphosphines at Ni(0) and Pt(0)

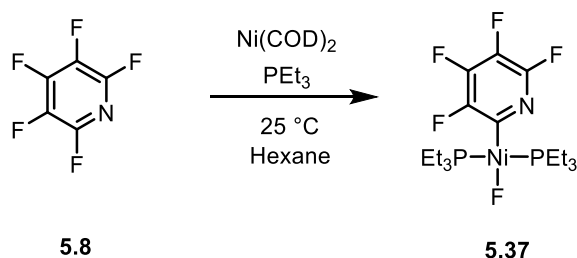
5.2.1 Introduction

Stoichiometric transition metal C–F activation reactions have been extensively studied and reviewed.^{188,190,202-203} Fahey and Mahan reported in 1977, the first example of a stoichiometric C–F activation reaction at Ni(0) of hexafluorobenzene **5.4** (Scheme 101) to obtain the Ni(II) complex **5.36**, however they were only able to characterise their product using IR spectroscopy and elemental analysis, as paramagnetic impurities made NMR experiments impossible. The yield was also very low (7%) and the reaction time long (2–3 days).²⁰⁴



Scheme 101: First example of a stoichiometric C–F activation reaction at Ni(0) of hexafluorobenzene (Fahey and Mahan).

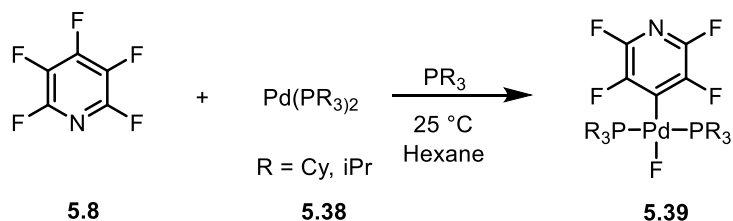
Perutz and Braun subsequently reported the C–F activation reactions at Ni(0) of fluorinated heterocycles obtaining chemospecific C–F activation over C–H activation, in substrates such as tetrafluoropyridine and regioselective activation *ortho* to the nitrogen atom of the pyridine ring (**5.8** in Scheme 102). They were able to isolate the product **5.37** and fully characterise it by NMR spectroscopy and X-ray crystallography.^{195-196,205-206}



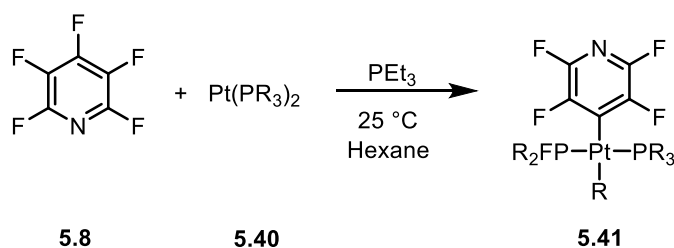
Scheme 102: C–F activation reactions at Ni(0) of fluorinated heterocycles (Perutz and Braun).

In the Perutz group, selective C–H over C–F functionalisation of fluoroaromatics has also been studied at Pd(0) and Pt(0).^{34,207} Interestingly the regioselectivity obtained for pentafluoropyridine **5.8** was different from that observed for Ni(0) reactions. The substrate

was activated in the *para* position to the nitrogen atom for Pd(0) reactions (**5.40** in Scheme 103) and in the case of Pt(0) reactions an additional P–C bond activation reaction took place (forming **5.41** in Scheme 104). This difference in reactivity is believed to derive from a nucleophilic substitution process similar to that exhibited by Rh(I) complexes.²⁰⁸

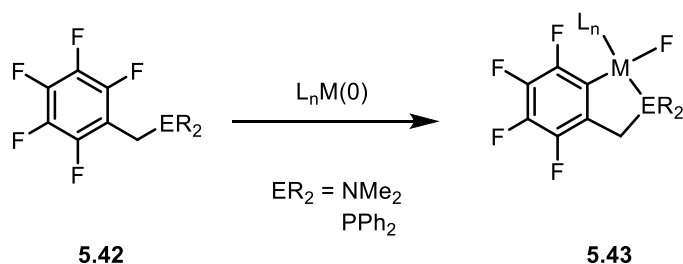


Scheme 103: C–F activation reactions at Pd(0) of fluorinated pyridine (Perutz *et al.*).



Scheme 104: C–F activation reactions at Pt(0) of fluorinated pyridine (Perutz *et al.*).

The aim of the preliminary study described in this section was the investigation of C–F activation reactions of fluorinated *N,N*-dimethylbenzylamines and fluorinated benzylphosphines with two different metals, Ni(0) and Pt(0).



Scheme 105: General scheme of C–F activation reactions of fluorinated substrates M(0).

5.2.2 Results and discussion

5.2.2.1 Reaction of fluorinated *N,N*-dimethylbenzylamines at Ni(0)

The behaviour of this type of substrate towards C–H and C–F functionalization at Ni(0) has not been investigated to date. To begin with, the two substrates **5.26** and **5.25**

(Figure 93) were chosen following the results obtained with the catalytic process at Pd(0) discussed above.

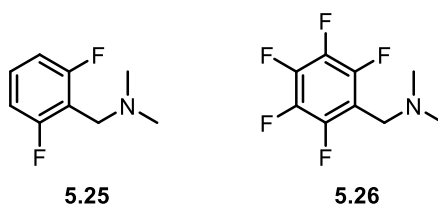


Figure 93: Substrates 5.25 and 5.26 used in the attempted C–F activation reactions at Ni(0).

Both substrates were reacted with Ni(1,5-COD)₂ and PEt₃ in hexane at room temperature, as reported by Perutz and co-workers for the fluorinated pyridines.²⁰⁹ Substrate **5.26** can only undergo C–F functionalisation, while **5.25** can undergo either C–F or C–H functionalisation.

Substrate **5.26** was reacted with Ni(1,5-COD)₂ and PEt₃ in a ratio of 2:2:1 but the main product observed was the complex Ni(1,5-COD)(PEt₃)₂, **5.44**, which crystallised from benzene/hexane (Figure 94). The molecular structure was thus determined by X-ray crystallography.

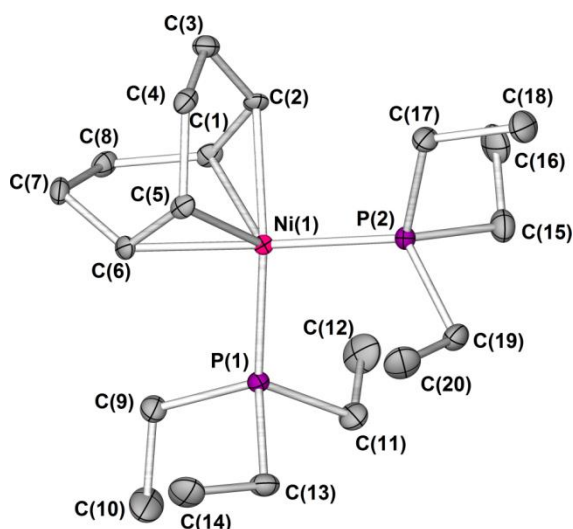
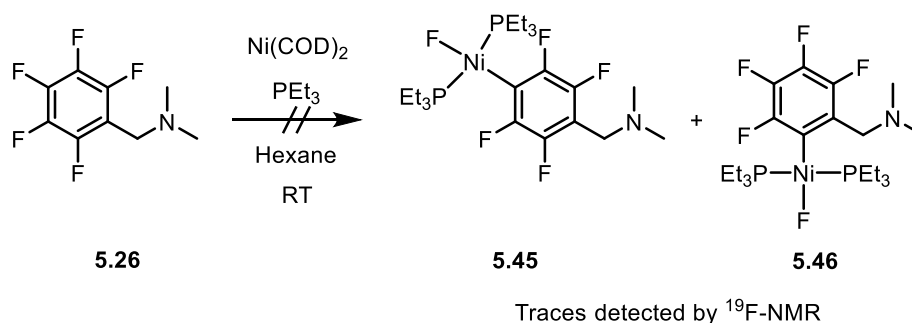


Figure 94: X Molecular structure of palladacycle 5.44. Hydrogen atoms were omitted for clarity; thermal ellipsoids shown with probability of 50%. Selected bond lengths (Å): Ni(1)–P(1): 2.1717(7), Ni(1)–P(2): 2.1786(7), Ni(1)–C(1): 2.095(2), Ni(1)–C(2): 2.092(2), Ni(1)–C(5), Ni(1)–C(6): 2.096(2); selected bond angles (°): Ni(1)–P(1)–P(2): 103.26(3), C(2)–N(1)–P(2): 95.43(7), C(6)–N(1)–P(1): 95.62(6), N(1)–P(2)–C(17): 114.18(8), N(1)–P(1)–C(9): 116.84(8).

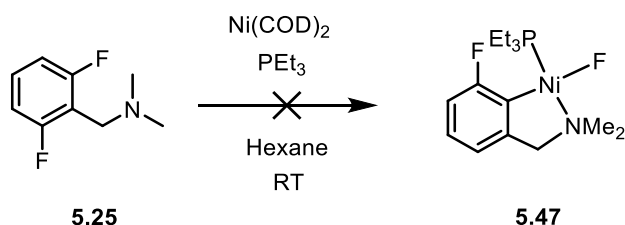
A signal at $\delta -371.0$ in the ¹⁹F-NMR spectrum indicated the formation of a small quantity of metal fluoride complex, presumably **5.45** or **5.46** in Scheme 106. This value is in fact consistent with that one reported for the C–F functionalization of hexafluorobenzene at Ni(0) ($\delta -390.33$ in C₆D₆)¹⁹⁵ but despite a change in reaction conditions (time, temperature) it was not possible to isolate or to increase the conversion to the desired product. Changing

the ratio between substrate, PEt_3 and Ni to 1.2 : 2.2 : 1, did not lead to the detection of the characteristic signal of an Ni–F species.



Scheme 106: Reaction of Ni(0) with fluorinated benzylamine 5.26.

The reaction attempted with substrate **5.25** did not proceed and the starting material was fully recovered along with $\text{Ni}(\text{COD})(\text{PEt}_3)_2$, **5.44**.

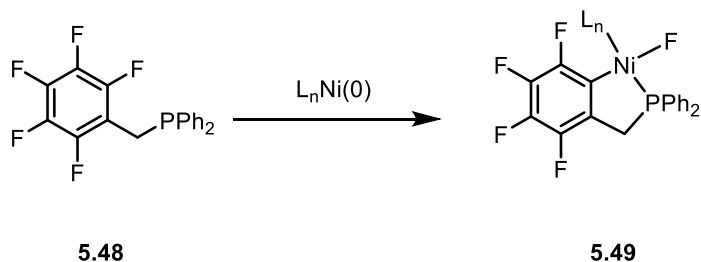


Scheme 107: Reaction of Ni(0) with fluorinated benzylamine 5.25.

The lack of reactivity of fluorinated *N,N*-dimethylbenzylamines **5.25** and **5.26** at Ni(0) could be attributed to the lower energy of the lone pair on the nitrogen atom of the tertiary amine compared to the phosphorus atom. $\text{Ni}(1,5\text{-COD})_2$ in fact reacts rapidly with two PEt_3 ligands, forming the Ni(0) complex $\text{Ni}(\text{PEt}_3)_2$ and the fluorinated benzylamines are then presumably not able to displace the phosphine ligands to form complex **5.47**. This study needs further expansion and the reaction of $\text{Ni}(1,5\text{-COD})_2$ directly with the tertiary amines could be attempted to circumvent this problem.

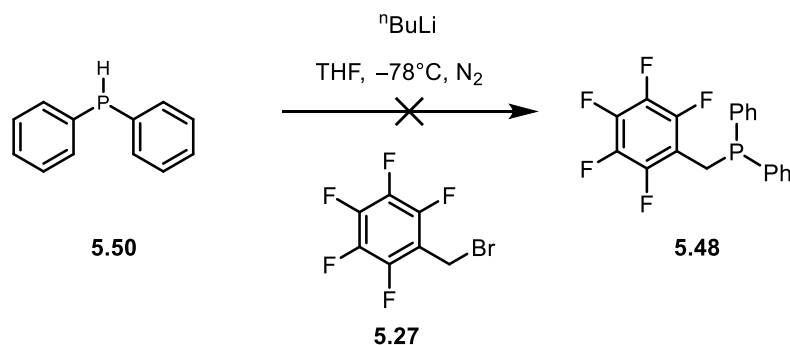
5.2.2.2 Reactions of fluorinated benzylphosphines at Pt(0)

Due to the lack of reactivity of fluorinated benzylamines at Ni(0), a phosphine analogue of 2,3,4,5,6-pentafluoro-benzylamine **5.26** was prepared to attempt the cyclometallation reaction at Ni(0) *via* C–F activation (Scheme 108).



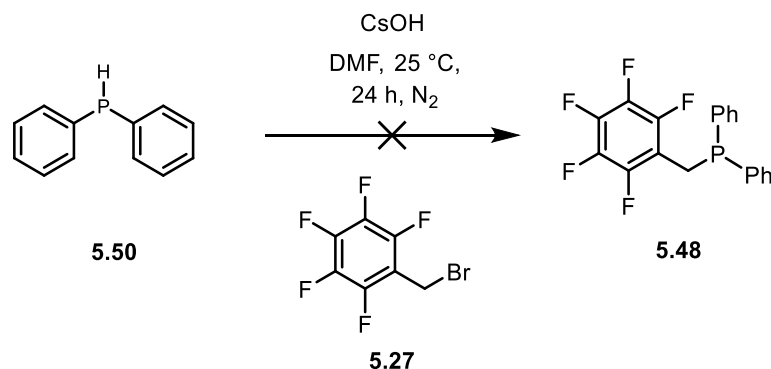
Scheme 108: Desired reaction of Ni(0) with fluorinated benzylphosphine 5.48.

Due to the electronic properties of the substrate (diphenyl-pentafluorobenzylphosphine, **5.48**) the procedure used for the synthesis of the other fluorinated phosphines described in Chapter 3 could not be used (Scheme 109) and resulted in unwanted aromatic substitution reactions on the fluorinated ring.



Scheme 109: Attempted synthesis of 5.48 via nucleophilic substitution using ⁿBuLi as a base.

The next attempt was based on a procedure used by Honaker²¹⁰ and co-workers for the synthesis of tertiary phosphines using CsOH as a base to deprotonate the diphenylphosphine **5.50** followed by reaction with the relevant halide **5.27** (Scheme 110).

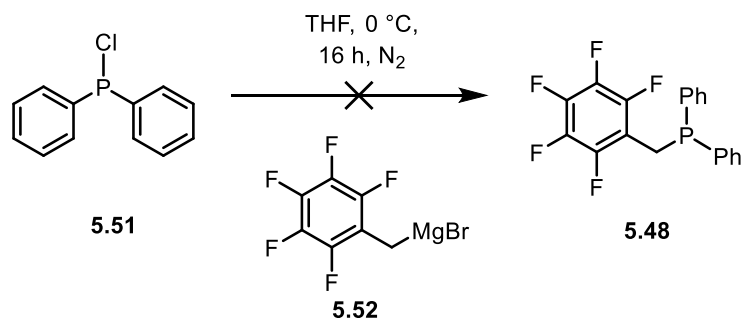


Scheme 110: Attempted synthesis of 5.48 via nucleophilic substitution using CsOH as a base.

This method looked promising since it was used by Ahn and co-workers¹⁶⁷ for the synthesis of 3,5-difluoro-diphenylbenzylphosphine, **3.5**, although no experimental data were reported

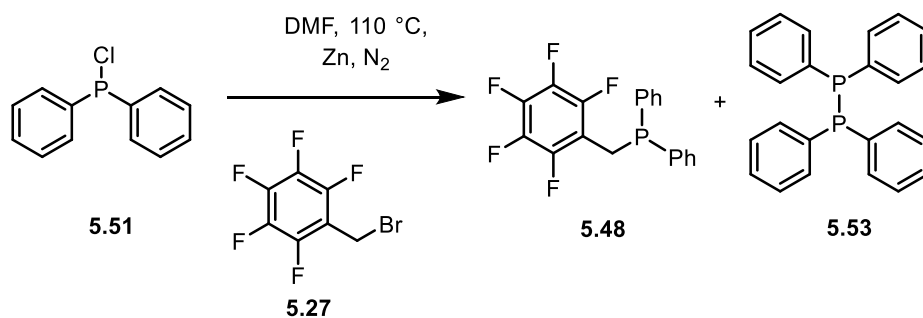
for this compound. When the experiment was attempted for the same substrate and for substrate **5.48**, both reactions were unsuccessful.

The synthesis of aromatic phosphines is frequently performed using Grignard reagents,¹⁶⁴ and so in a similar manner, diphenyl-chlorophosphine (**5.51**) was reacted in THF at 0 °C with the *in situ* generated pentafluorobenzyl Grignard reagent **5.49**. The attempt was unsuccessful probably due to the non-formation of the Grignard itself owing to the highly electron-deficient benzylic ring.



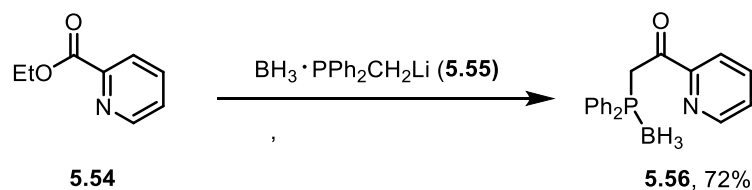
Scheme 111: Attempted synthesis of 5.48 using Grignard reagent.

Another method attempted was the Ni-catalysed cross coupling reaction for the synthesis of tertiary phosphines developed by Ager and co-workers.²¹¹ The reaction, between chlorodiphenylphosphine **5.51** and pentafluorobenzylbromide **5.27** is reported to take place in the presence of zinc, which acts as transmetallating agent forming Ph_2PZnCl , and also reduces the Ni(II) to Ni(0) (Scheme 112). However in this case the main product of the reaction was the result of the homocoupling of the chlorodiphenylphosphine **5.53**, and the fluorinated phosphine **5.48** was formed only in a very small quantity.



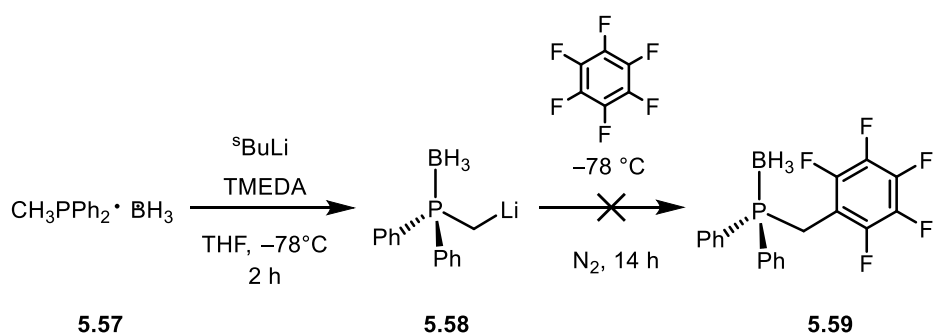
Scheme 112: Attempted synthesis of 5.48 using Ni-catalysed cross coupling reaction.

Drury and co-workers reported the synthesis of several chiral N, P aromatic ligands by the reaction between diphenylmethylphosphine borane (**5.55**)²¹² and the relevant nucleophile (Scheme 113).²¹³



Scheme 113: Synthesis of pyridyl phosphine 5.56.

The synthesis could potentially be a good method for the synthesis of pentafluoro-diphenylphosphine (**5.48**) using hexafluorobenzene, **5.4**, as the electrophile. The diphenylmethylphosphine borane **5.57**, synthesised as reported by Wagner and co-workers,²¹² was treated with ^sBuLi-TMEDA complex, followed by reaction with hexafluorobenzene at $-78\text{ }^\circ\text{C}$ (Scheme 114).



Scheme 114: Attempted synthesis of 5.59 following Drury *et al.* method.

The borane group was found to be labile under the reaction conditions and the result was a mixture of boron-containing and non-boron-containing species. This instability could be due to the highly electron withdrawing properties of the fluorinated benzylic group. Moreover, due to the high acidity of the benzylic protons of **5.48**, the major product of the reaction, after the removal of the remaining borane, was the di-substituted diphenyl([dipentafluorophenyl]methyl)phosphine **5.60** (Figure 95), due to further deprotonation of the product (**5.48**) present in the same vessel as the lithiated species (**5.58**).

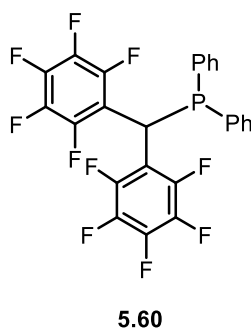
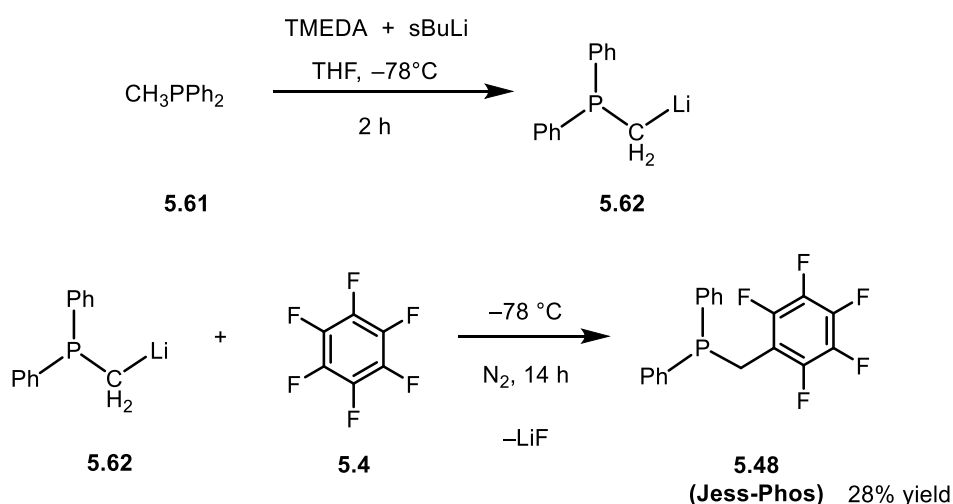


Figure 95: Byproduct 5.60 of reaction in Scheme 114.

Despite the formation of the by-product **5.60**, the reaction successfully gave the target product **5.48**, so the reaction conditions were modified in order to obtain only the monobenzyl perfluorinated phosphine (**5.48**). The synthesis was carried out directly from methyldiphenylphosphine (**5.61**) without forming the intermediate borane species, and the lithiated species **5.62** was transferred by cannula into the THF solution of hexafluorobenzene (**5.4**) to avoid the formation of the byproduct **5.60**.



Scheme 115: Successful synthesis of 5.47, also called Jess-phos.

The reaction successfully gave the monosubstituted phosphine (**5.48**) with some impurities that were removed by precipitation of the reaction mixture with hexane followed by sublimation under vacuum at room temperature. The $^{31}\text{P}\{^1\text{H}\}$ -NMR spectrum (Figure 96) of the product **5.48** shows a triplet of doublets at $\delta -10.6$ ppm with a $^4J_{\text{P-F}}$ of 21 Hz. The triplet shows another small splitting corresponding to the coupling with the fluorine *para* to the benzylic arm ($^6J_{\text{P-F}} = 4.6$ Hz).

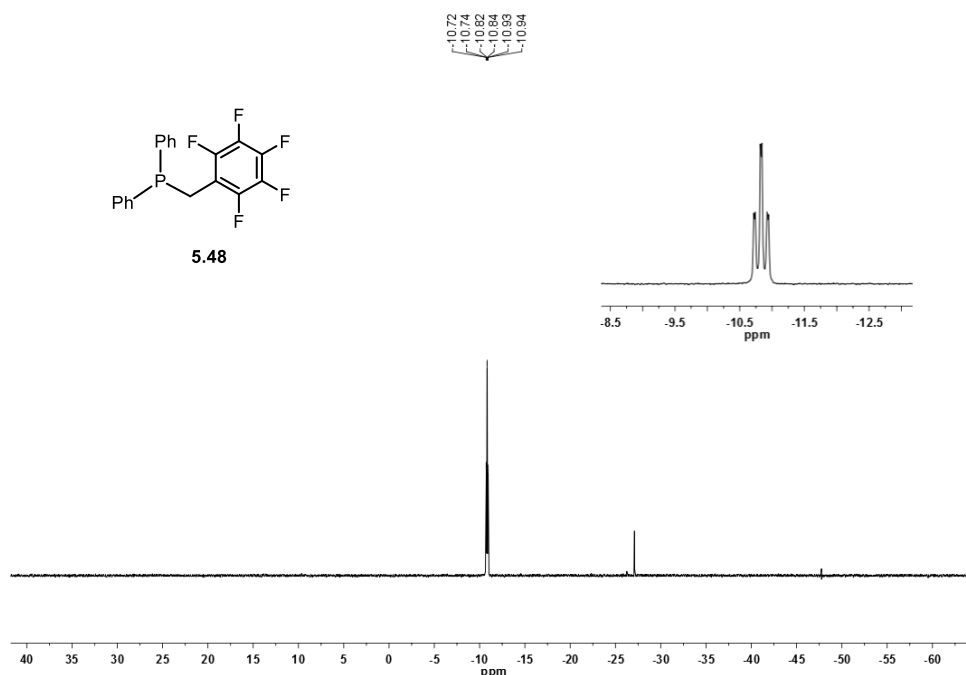


Figure 96: $^{31}\text{P}\{^1\text{H}\}$ -NMR spectrum of 5.48 in C_6D_6 at 298 K (202 MHz).

The ^{19}F -NMR spectrum (Figure 97) shows three signals for the three different fluorine environments around the aromatic ring at δ -141.9 , -157.8 and -163.5 , two of them showing second order couplings. The integration between the three fluorine signals is 2:2:1 indicating that the signal at δ -157.8 is the fluorine in *para* to the benzylic group, confirmed by its splitting being a triplet of doublets with a $^3J_{\text{F-F}} = 21.4$ Hz with the fluorine in *ortho* and a $^6J_{\text{P-F}} = 4.6$ Hz with the phosphorus atom. $^4J_{\text{F-F}}$ couplings in perfluoroaromatics are known to be very small.²¹⁴

The ^1H -NMR spectrum (Figure 98) shows a broad singlet at δ 3.08 for the benzylic protons and two multiplets for the aromatic protons of the phenyl rings. The $^{13}\text{C}\{^1\text{H}\}$ -NMR spectrum shows the characteristic signals of the fluorinated ring at δ 145.2 (dtt, $^1J_{\text{C-F}} = 247$ Hz, $^2J_{\text{C-F}} = 11.7$ Hz, $^3J_{\text{C-F}} = 3.8$ Hz), 139.7 (dm, $^1J_{\text{C-F}} = 254$ Hz) and 137.7 (dm, $^1J_{\text{C-F}} = 248$ Hz) and the typical signals of the phenyl rings bonded to phosphorus at δ 137.4 (d, $^1J_{\text{C-P}} = 16.3$ Hz), 133.1 (d, $^2J_{\text{C-P}} = 19.7$ Hz), 129.5 (s), 128.8 (d, $^3J_{\text{C-P}} = 6.8$ Hz), 112.3 (tdd, $^2J_{\text{C-F}} = 18$ Hz, $^3J_{\text{C-F}} = 3.3$ Hz, $^3J_{\text{C-P}} = 9$ Hz, C_{ipso}), while the CH_2 group resonates at δ 23.1 (d, $^1J_{\text{C-P}} = 20.9$ Hz).

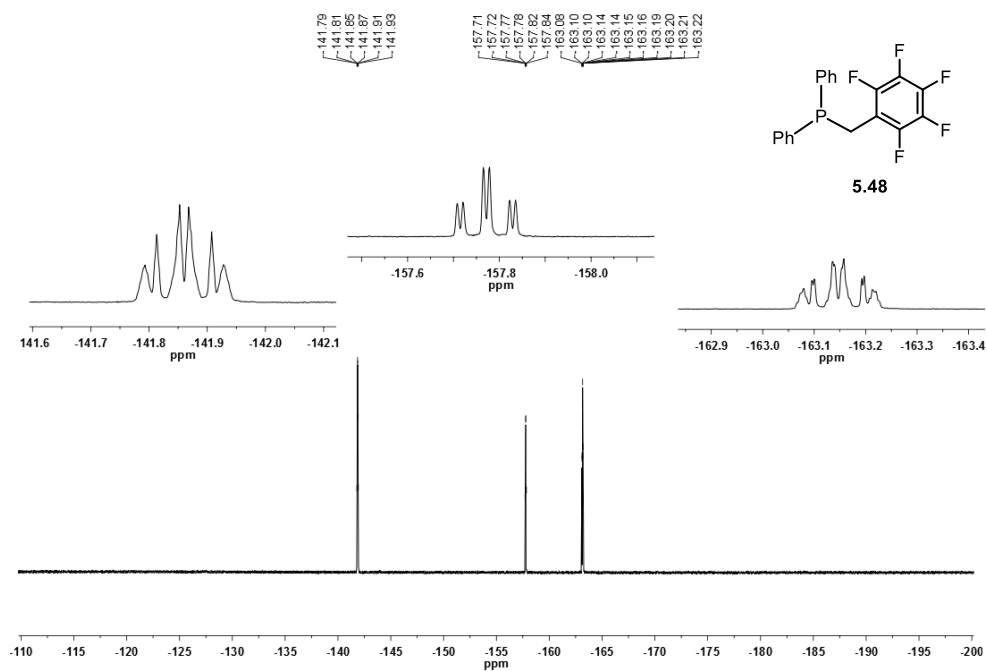


Figure 97: ^{19}F -NMR spectrum of **5.48** in C_6D_6 at 298 K (471 MHz).

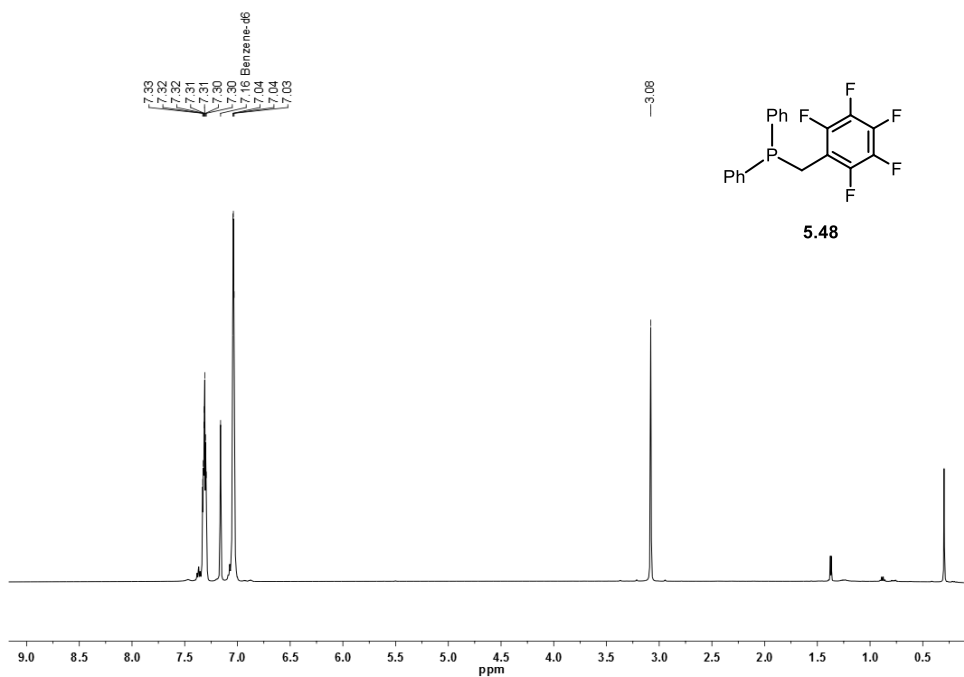


Figure 98: ^1H -NMR spectrum of **5.48** in C_6D_6 at 298 K (500 MHz).

A single crystal of the oxide form of **5.48** was obtained by slow evaporation of a solution of the substrate in benzene (Figure 99).

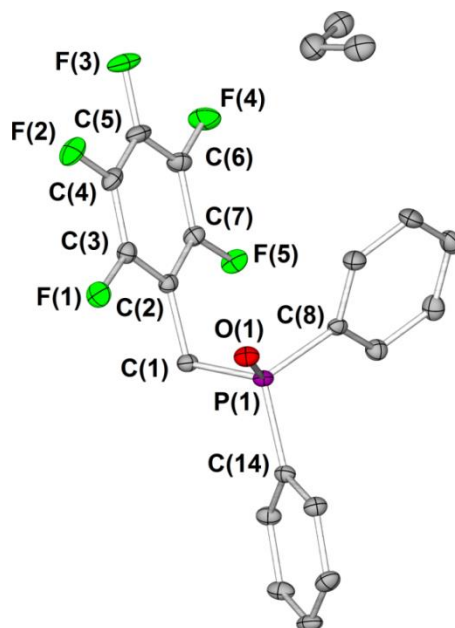
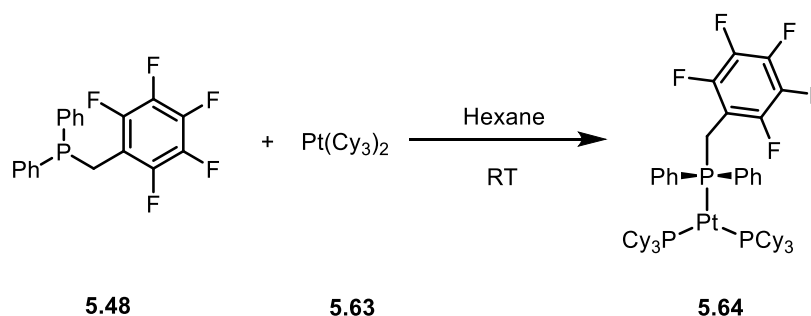


Figure 99: Molecular structure of phosphine 5.48 in the oxide form. Hydrogen atoms were omitted for clarity; thermal ellipsoids shown with probability of 50%. Selected bond lengths (Å): C(3)–F(1): 1.3346(15), C(4)–F(2): 1.3361(15), C(5)–F(3): 1.3393(15), C(6)–F(4): 1.3388(16), C(7)–F(5): 1.3399(15), C(1)–P(1): 1.8263(13), O(1)–P(1): 1.4836(9); selected bond angles (°): C(2)–C(1)–P(1): 108.63(9), F(1)–C(3)–C(2): 120.23(11), F(5)–C(7)–C(2): 119.95 (11).

5.2.2.3 Reaction of phosphine 5.48 at Pt(0)

The diphenylpentafluorobenzylphosphine (**5.48**) was reacted in an NMR tube with a source of platinum(0), Pt(PCy₃)₂ (**5.63**)²¹⁵ (ratio 1.5:1) at room temperature, and the reaction mixture analysed by ³¹P{¹H}-, ¹⁹F- and ¹⁹⁵Pt{¹H}-NMR spectroscopy. The major product of the reaction was characterised as the Pt(0) complex **5.64** shown in Scheme 116.



Scheme 116: Synthesis of complex 5.64.

The ¹⁹⁵Pt{¹H}-NMR spectrum was run as a 2D experiment (¹⁹⁵Pt-¹H-HSQC-NMR spectroscopy in Figure 101) and shows a quartet in the Pt spectrum with correlation to the benzylic protons of the substrate **5.48** coordinated to the Pt ($\delta -4458.4$ correlates with $\delta 3.5$). The quartet has a coupling constant of ¹J_{P-Pt} of 4406 Hz matching with the coupling constant between the triplet at $\delta 61.36$ (corresponding to the coordinated pentafluorobenzylphosphine) and its Pt satellites in the ³¹P{¹H}-NMR spectrum (shown in

Figure 102). There are another three signals in the $^{31}\text{P}\{^1\text{H}\}$ -NMR spectrum, two belonging to the non-coordinated fluorinated phosphine **5.48** (δ -10.61), non-coordinated tricyclohexylphosphine **5.19** (δ 9.67) and a doublet at δ 43.55 corresponding to tricyclohexylphosphine coordinated to the Pt in compound **5.63** (starting material). The ratio calculated by integration of the $^{31}\text{P}\{^1\text{H}\}$ -NMR spectrum shows a ratio of 1 : 2.5 : 1.4.

There is also a minor species detected by ^{195}Pt - ^1H -HSQC-NMR spectroscopy where another quartet at δ -4479.1 correlates with a signal in the ^1H -NMR spectrum at δ 3.3. Due to the multiplicity it must be bonded to three phosphines, and the likely possibility is the complex **5.65** in Figure 100.

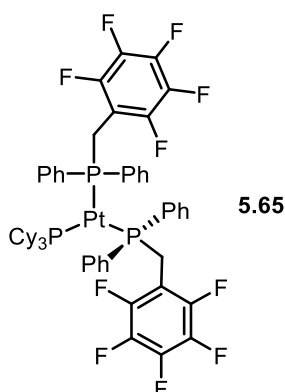


Figure 100: Presumed structure of the minor complex (**5.65**) obtained from the reaction in Scheme 116.

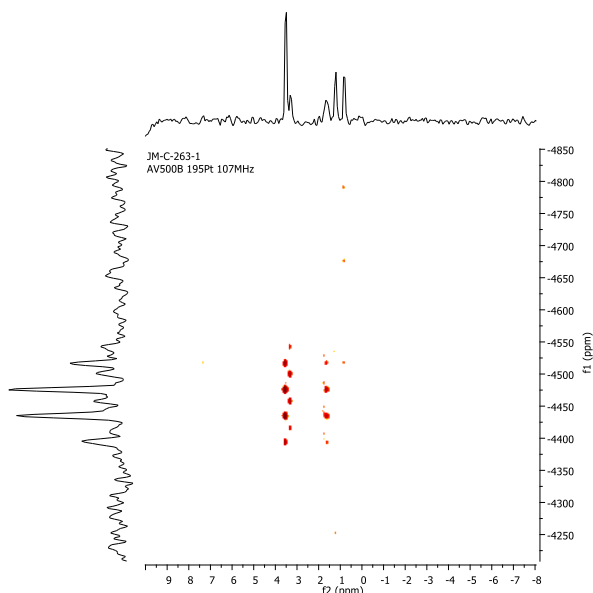


Figure 101: ^{195}Pt - ^1H - HSQC-NMR spectrum of reaction in Scheme 116 at 298 K in C_6D_6 (107/500 MHz), ^1H decoupled in ^{195}Pt dimension (y-axis).

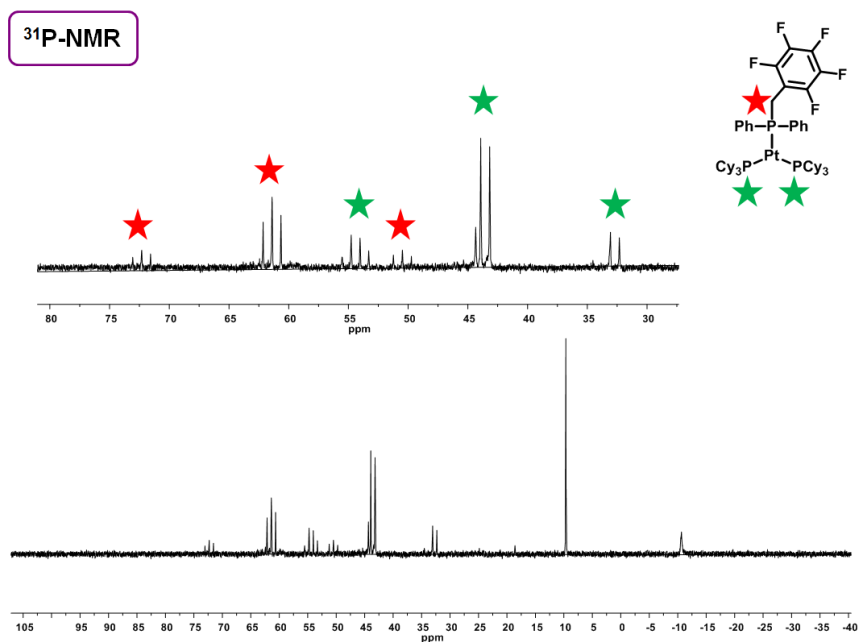


Figure 102: $^{31}\text{P}\{^1\text{H}\}$ -NMR spectrum of the products resulting from the reaction in Scheme 116 at 298 K in C_6D_6 (202 MHz).

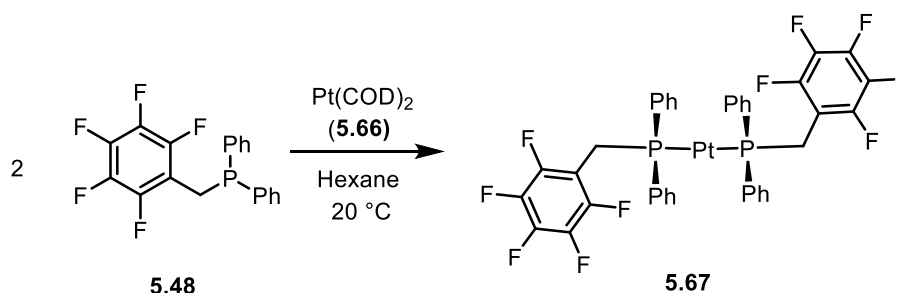
The ^{19}F -NMR spectrum shows two sets of signals corresponding respectively to the fluorine of the free pentafluorobenzylphosphine (**5.48**) (δ -142.36, -159.05, -164.25) and to the substrate coordinated to the Pt in complex **5.64** (δ -139.46, -160.01, -164.70).

The behaviour of substrate **5.48** toward C–F activation at Pt(0) suggests that the fluorinated phosphine coordinates less strongly to Pt than the PCy_3 and hence it is not able to displace the latter phosphine from the metal centre. This is not surprising given the strongly electron withdrawing nature of the perfluorinated benzyl ring, which will both lower the energy of the phosphorus lone pair, and increase the π -acceptor ability of the vacant orbitals on the phosphine (see section 3.1).

The 14-electron complex $\text{Pt}(\text{PCy}_3)_2$ is very reactive toward C–F oxidative addition of fluorinated species as reported by Stone *et al.*²¹⁶ and Perutz and co-workers^{207,215} and due to the labile PCy_3 ligands, can easily react with silanes²¹⁷ and borane sources.²¹⁸ However, as far as the author is aware, no direct reactions with tertiary phosphines have been reported. Further investigation is needed and a possible experiment to promote the cyclometallation reaction could be the reaction of substrate **5.48** directly with the source of Pt(0) in conjunction with the increase the temperature and of the reaction time to assess a possible C–F activation. The addition of LiI as reported in catalytic C–F activation reactions at Pd in section 5.1.2 to promote C–F activation could similarly be an interesting further experiment.

The source of platinum could also be changed, for instance trying the reaction between $[\text{Pt}(1,5\text{-COD})_2]$, **5.66**,²¹⁶ directly with phosphine **5.48** to form the 14-electron

complex **5.67**. A similar reaction was reported by Stone and co-workers for the synthesis of **5.63** and $[\text{Pt}(\text{PMe}(t\text{-Bu})_2)_2]$, which can be heated to promote cyclometallation or further reacted with borane or silane sources to obtain novel Pt complexes.²¹⁶



Scheme 117: Proposed synthesis of Pt complex 5.67.

The study could also be extended to the other fluorinated phosphines (described in Chapter 3) to investigate C–H versus C–F activation reactions at Pt(0).

5.3 Conclusions

The first part of this Chapter (section 5.1) described the cross-coupling reaction *via* C–F functionalisation of fluorinated *N,N*-dimethylbenzylamines **2.7e**, **5.25**, **5.26** and 4-*N,N*-dimethyl-2,3,5,6-tetrafluoro-pyridine **5.34** using the Pd(0) precursor $\text{Pd}(\text{PCy}_3)_2$ (**5.17**) as a catalyst in the presence of a Grignard reagent and ZnCl_2 . Whilst the perfluorinated substrate **5.26** undergoes C–F functionalisation, the reaction with difluorinated substrates **5.25** and **2.7e** do not proceed, potentially due to the aromatic rings being too electron-rich to react with the nucleophilic palladium source. In the case of 2,3,4,5,6-pentafluoro-*N,N*-dimethylbenzylamine (**5.26**) the C–F activation occurs regioselectively *para* to the benzylic arm, presumably due to the lower electron density of the C-4 carbon atom in the aromatic perfluorinated ring, preferred by the nucleophilic palladium. The reaction with 4-*N,N*-dimethylamino-2,3,5,6-tetrafluoro-pyridine (**5.34**) proceeds slowly *ortho* to the ring nitrogen due to the additional steric bulk in the *para* position. The slow reaction and low conversion observed is presumably due to the additional electron density in the aromatic ring from the nitrogen atom.

The study could be further extended by testing a trifluorinated substrate or changing the substrate from fluorinated amines to fluorinated phosphine oxides, due to their different electronic behaviour towards the metal.

The second part of this chapter (section 5.2) described a preliminary study of C–F activation reactions of fluorinated *N,N*-dimethylbenzylamines (**5.25** and **5.26**) at Ni(0),

followed by the synthesis of 2,3,4,5,6-pentafluorodiphenylbenzylphosphine (**5.48**, **Jess-Phos**) and its reaction with a source of Pt(0).

The reaction at Ni(0) of fluorinated benzylamines **5.25** and **5.26** did not give any C–H or C–F activation product, potentially due to the poor coordinating properties of the nitrogen atom compared to the phosphorus atoms of the two PEt₃ ligands bound to the metal centre. The system reaction conditions need to be improved and the phosphine ligands replaced by some which are less strongly coordinating.

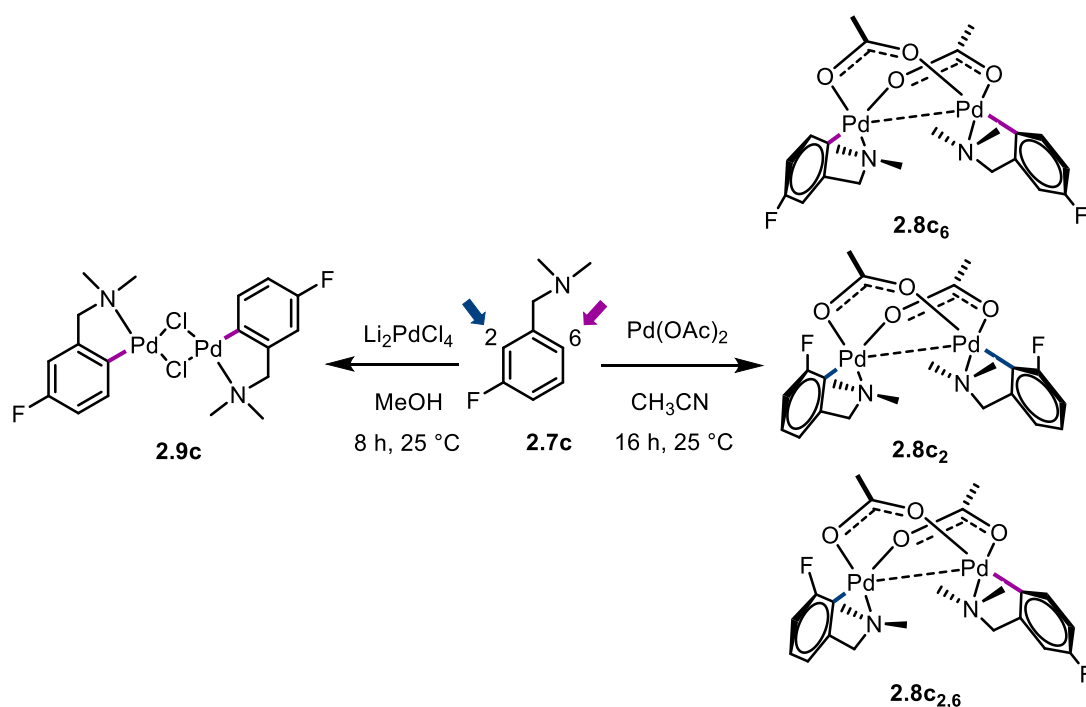
The reaction at Pt(0) of substrate **5.48** did not give any C–F or P–C activation product, with the substrate in fact simply binding to the metal centre without displacing the PCy₃ phosphine ligands coordinated to the metal. Further investigation is needed to fully understand the behaviour of these novel and interesting substrate towards C–F activation. More general conclusions are given in Chapter 6.

Chapter 6: Conclusions and Future Work

6.1 Conclusions

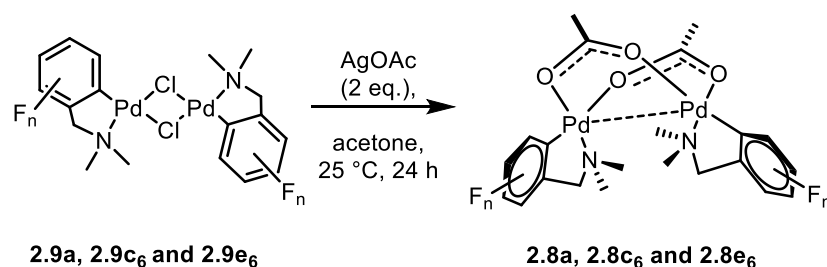
The work described in this thesis has explored the effects of fluorine substituents on the regioselectivity of intramolecular C–H activation reactions of fluorinated substrates at transition metals.

Fluorinated benzylamines **2.7a–f** were reacted with two different sources of palladium, Pd(OAc)₂ and Li₂PdCl₄, to give fluorinated acetate- and chloride-bridged palladacycles (**2.8a–f** and **2.9a–f**, respectively), which were fully characterised using a range of techniques. Substrates **2.7c** and **2.7e** do not exhibit any regioselectivity for the C–H activation reactions when reacted with Pd(OAc)₂ *via* a proposed CMD mechanism, while they exhibit complete regioselectivity *para* to fluorine when reacted with Li₂PdCl₄ to give palladacycles **2.9c₆** and **2.9e₆** as the only products *via* a hypothesised S_EAr mechanism (Scheme 118).



Scheme 118: Reactivity of substrate **2.7c** towards C–H bond activation at Pd(OAc)₂ and Li₂PdCl₄.

The two chloride-bridged *para* isomers, **2.9c₆** and **2.9e₆**, could then be converted to acetate-bridged palladacycles **2.8c₆** and **2.8e₆** by reaction with silver acetate with complete retention of regioselectivity.



Scheme 119: Bridge conversion reaction to acetate-bridged palladacycle with retention of regioselectivity.

Fluorinated substrates in intermolecular reactions at Pd are known to give *ortho* selective C–H functionalisation reactions when proceeding *via* a CMD mechanism,²⁰ so the lack of regioselectivity in the acetate-bridged palladacycle formation (reported in this study) indicates that an additional effect is involved in controlling the regioselectivity. This phenomenon could be linked to steric and electronic repulsion between the fluorine and oxygen lone pairs. A detailed crystallographic analysis revealed that the geometry of the clamshell shape of the acetate-bridged palladacycles is in fact affected by the position and the number of fluorine atoms on the ring; for example palladacycle **2.8d**, where activation must occur *ortho* to fluorine, shows a large twist of the aromatic ring due to the repulsion between the oxygen and fluorine lone pairs. It is this repulsion that could be responsible for the lack of regioselectivity in the other palladacycles, by opposing the *ortho* fluorine effect.

In the case of chloride-bridged palladacycles, where the mechanism is presumed to be an S_EAr process, and regioselectivity *para* to fluorine is observed, the rigidity of the planar structure does not permit the same twist that is observed for acetate-bridged palladacycles. Electronic and steric repulsions therefore dominate the regioselectivity, disfavouring the formation of the *ortho* isomer and leading to exclusive formation of the *para* isomer.

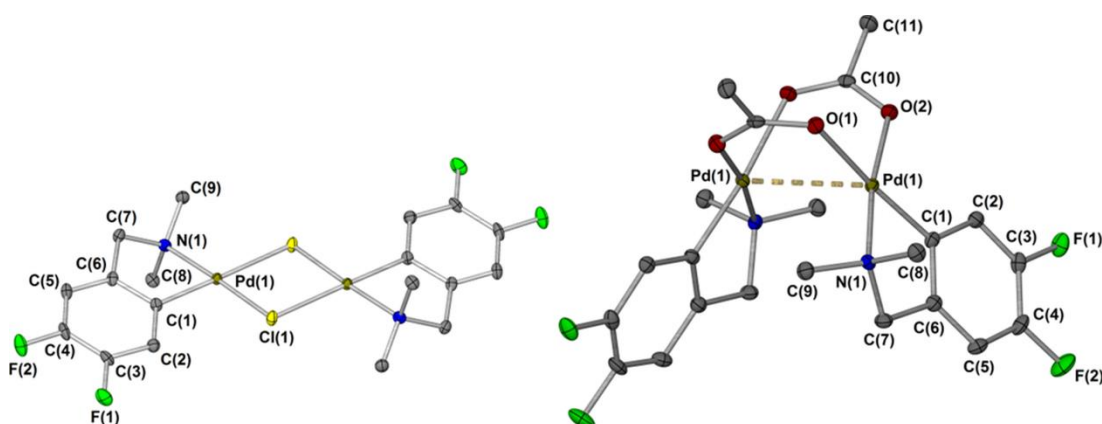
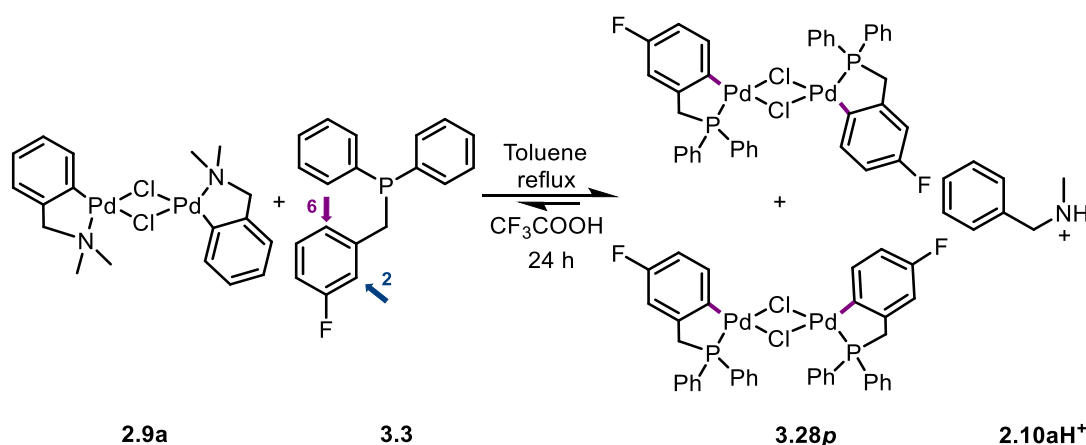


Figure 103: Comparison between the molecular geometries of the molecular structures of clam shell palladacycle **2.8e₆** and planar **2.9e₆**.

Although this behaviour diverges from similar C–H activation reactions, which proceed *via* an $S_{\text{E}}\text{Ar}$ mechanism at Rh reported by Jones *et al.*,¹¹⁶ it is possible that the differences in substrate and metal could lead to a different mechanism or to a different rate determining step of the same mechanism. The hypothesis of steric and electronic repulsions was also supported by reacting the chlorinated 3-chloro-*N,N*-dimethylbenzylamine, **2.7g**, with the same two sources of palladium and observing in both cases 100% regioselectivity *para* to chlorine, even in the case of the acetate-bridged palladacycle, **2.8g**, due to the chlorine atom being larger than fluorine and the absence of any *ortho* fluorine effect.

The effect of fluorine substituents on C–H activation reactions of fluorinated diphenylbenzylphospines **3.2–3.5** has also been investigated. Fluorinated phosphines were synthesised in-house and due to their lack of reactivity toward the direct reactions at Pd, assumed to be partly due to the lack of a significant Thorpe–Ingold effect, the C–H activation reactions were studied *via* transcyclometallation reactions (selected example in Scheme 120).



Scheme 120: Transcyclometallation reaction example of substrate **3.3** gives regioselectively *para* isomer **3.28p**.

For substrates **3.3** and **3.4** the cyclopalladation reactions to form chloride-bridged palladacycles **3.28** and **3.30** occur regioselectively *para* to fluorine similarly to the chloride-bridged amino system. The structures of these palladacycles are also rigid, without the possibility of twisting to minimise steric interactions (Figure 104). Therefore in substrates **3.3** and **3.4**, where two possible C–H bonds could be activated, the *ortho* isomers, where the fluorine atoms are pointing toward the chlorine atom of the bridge, are disfavoured.

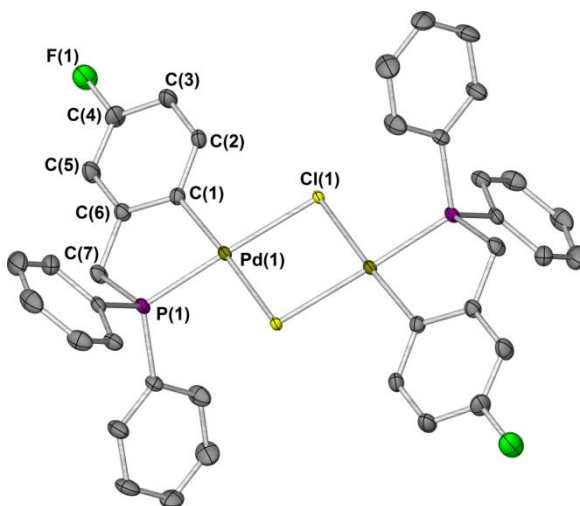
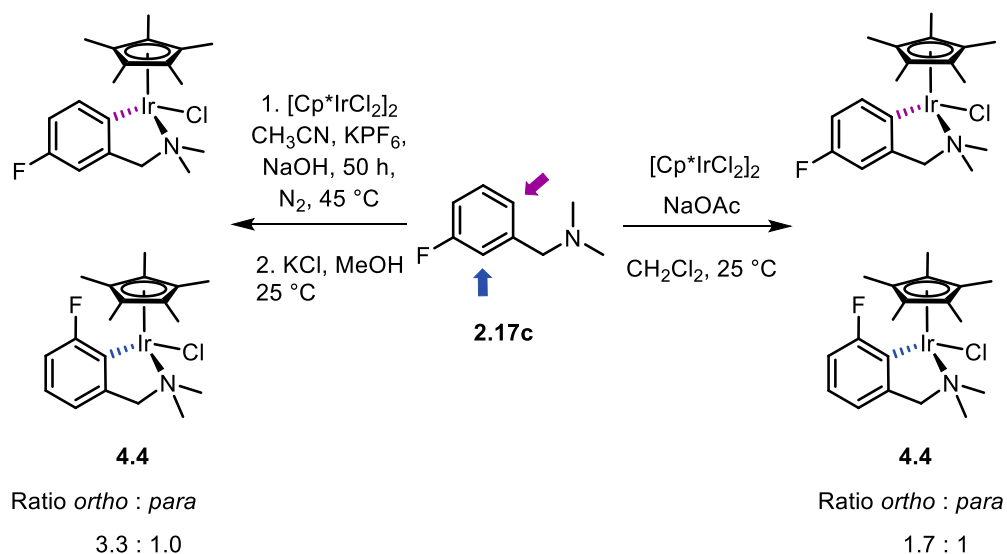


Figure 104: Molecular structure of palladacycle 3.28p (planar structure).

The effect of fluorine atoms on the regioselectivity of intramolecular reactions at Ir, Rh and Ru was also investigated for fluorinated benzylamines **2.7b** and **2.7c**. Two different methods were used in the metalation reactions at Ir to form the same metallacycle **4.4** and a difference in regioselectivity was observed. The ratio between *ortho* and *para* isomers was 3.3 : 1.0 using NaOH as a base while it was 1.7 : 1 when using NaOAc.

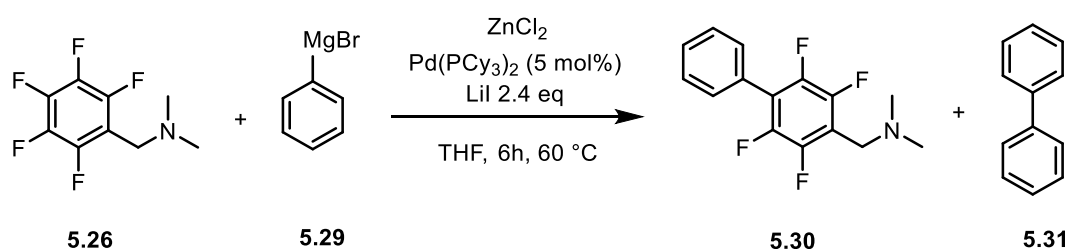


Scheme 121: Comparison between the two methods to obtain Ir metallacycle 4.4.

This difference in regioselectivity could potentially be due to the operation of two different proposed mechanisms, S_EAr and CMD. This could also explain why just one of the two methods is successful with Rh and Ru. All three metals show a preference for the formation of the *ortho* isomer, where the metal is *ortho* to the fluorine atom, in cyclometallation reactions with substrate such as **2.7c**, where two positions are available for the C–H activation. This is in contrast to the reactions with Pd, but can be explained in part by the

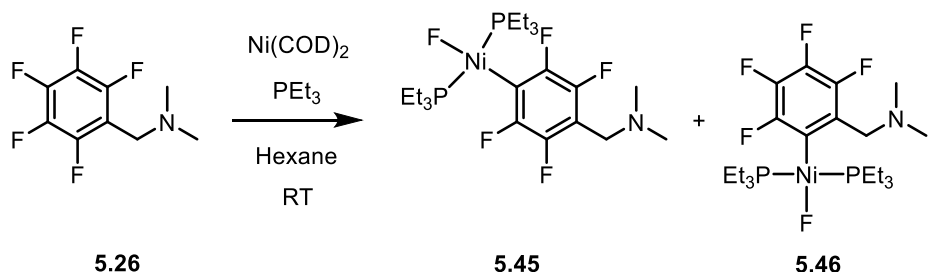
completely different geometries of the complexes, with the Ir, Rh and Ru compounds being pseudotetrahedral around the metal, leading to minimal steric interaction between the *ortho* fluorine and the other ligands. Crystal structure determination of these complexes would be useful to confirm the favoured regioselectivity beyond doubt.

Preliminary results were obtained in catalytic C–F functionalisation reactions at Pd(0) of benzylamines **2.7e**, **5.25** and **5.26** and fluoropyridine **5.34** conducted in the presence of a Grignard reagent and ZnCl₂. C–F activation could be obtained only with perfluorinated substrates (**5.26** and **5.34**) and does not proceed for difluorinated ones (**2.7e** and **5.25**). In the case of **5.26** the functionalisation is regioselective *para* to the benzyl arm, presumably due to the lower electron density of the *para* position in the ring, attacked by the nucleophilic source of palladium. In the case of **5.34** where the *para* position was blocked by the dimethylamine group, the C–F functionalisation occurs *ortho* to the nitrogen atom but only in poor yield.



Scheme 122: Cross-coupling reaction via catalytic C–F activation reaction at Pd(0).

Preliminary studies were also performed towards stoichiometric C–F activation reactions of fluorinated benzylamines at Ni(0). These were found to only give trace amounts of the expected fluoride complexes, and this is proposed to be due to the poor coordinating properties of these ligands, which are not able to displace the triethylphosphine ligands of the complex Ni(PEt₃)₂ and thus unable to coordinate to the metal.

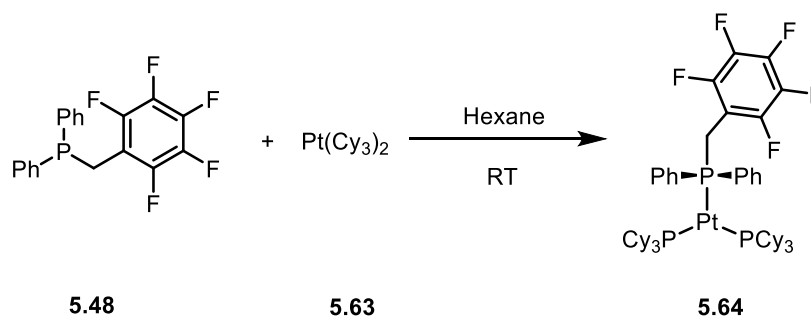


trace amounts detected by ¹⁹F-NMR spectroscopy

Scheme 123: Attempted stoichiometric C–F activation reaction of 5.26 at Ni(0).

Stoichiometric C–F activation reactions at Pt(0) were also attempted using the novel ligand pentafluoro-diphenylbenzylphosphine, **5.48**, but the only product observed was

the Pt complex **5.64**, where substrate **5.48** coordinates to the metal centre, without displacing the other two PCy₃ ligands.



Scheme 124: Stoichiometric attempted C–F activation reaction of **5.48** at Pt(0).

6.2 Future work

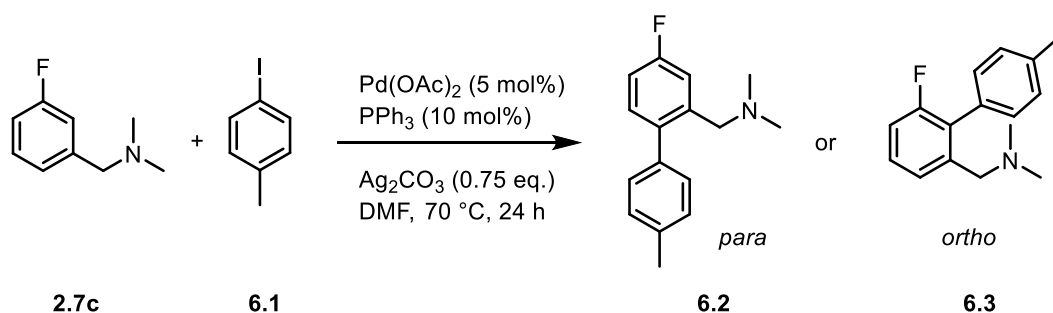
6.2.1 Biological tests on fluorinated palladacycles

After the preliminary biological tests performed on palladacycles **2.9c** and **2.9e** it would be interesting to expand the study to the remaining fluorinated amino- and phosphapalladacycles to observe if the presence of the fluorine can improve their anti-cancer activity, in line with the extensive studies on fluoroaromatics as pharmaceutical drugs.^{50,142-143} Moreover an investigation into the difference in anticancer properties between acetate- (**2.8b–f**) and chloride-bridged (**2.9b–f**) palladacycles could be performed. Similar studies have been reported with fluorinated aromatic amino acids²¹⁹ and with non-fluorinated monomers obtained from palladacycles with non-fluorinated benzylamine **2.7a** reacting with triphenylphosphine or pyridine.¹⁴¹

6.2.2 Investigation of catalytic activity of fluorinated phospho- and amino-palladacycles

Due to the extensive use of palladacycles in catalytic processes⁸² such as carbonylation reactions¹³⁵ and Heck, Suzuki¹³⁰⁻¹³¹ and Stille cross-coupling,⁸⁴ it would be interesting to assess the catalytic activity of the novel fluorinated palladacycles **2.8a–g** and **2.9a–g** synthesised in this study. Following the different selectivities obtained in the amino-palladacycle systems toward C–H activation, the investigation of intermolecular C–H functionalisation reactions using the fluorinated palladacycles as precatalysts could lead to different regioselectivity in the cross-coupled products. The study could begin with the stoichiometric reactions of substrate **2.7c** and iodotoluene using Pd(OAc)₂ (Scheme 125) and

Li_2PdCl_4 as catalysts to form the palladacycles *in situ* and compare their catalytic behaviour and regioselectivity.



Scheme 125: Proposed stoichiometric C–H functionalisation reaction of 2.7c with iodotoluene to assess regioselectivity in cross-coupling reactions.

6.2.3 Electrochemistry and UV-studies of acetate-bridged palladacycles

Bercaw and co-workers have investigated both computationally and experimentally the acetate-bridged and chloride-bridged palladacycles obtained from a 2-phenylpyridine ligand to assess the d^8 – d^8 interactions existing between the Pd atoms in the resulting complexes, thus confirming the hypothesis that an interaction between the d orbitals is present in the clamshell-type complexes.¹²⁷

A similar investigation, using UV-studies and cyclic voltammetry could be performed using the fluorinated acetate-palladacycles with amine and phosphine ligands to assess how the presence of fluorine atoms on the ring affects the electronic interactions between the d^8 orbitals at Pd of these complexes. A comparison between amino- and phosphino-systems could also be performed.

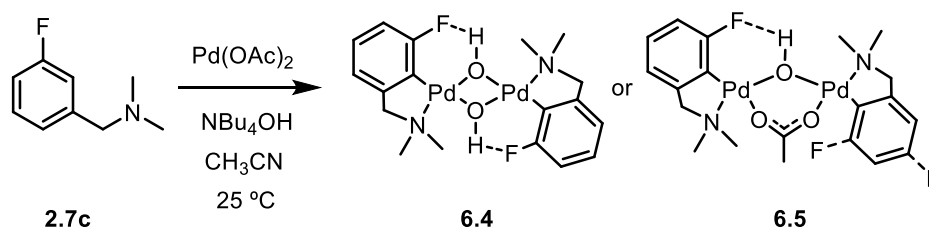
6.2.4 Cyclometallation reactions at Ir, Ru and Rh of fluorinated benzylphosphines

As discussed earlier for the fluorinated *N,N*-dimethylbenzylamines **2.7c** and **2.7e**, the C–H activation reactions at Ir, Ru and Rh could be attempted with the novel fluorinated benzylphosphines **3.2–3.5** to assess if a different regioselectivity could be obtained for substrates having two possible choices toward C–H activation, as for substrate **3.3**.

It would also be interesting to attempt transcyclometallation reactions starting from the metallacycle obtained from Ir, Ru and Rh with amino-ligands (**2.7a–g**) to form the relevant metallacycles with a phosphino ligand, using the Pfeffer method as reported in Chapter 3 at Pd(II) for the synthesis of fluorinated phospho-palladacycles **3.28–3.30**.¹¹⁵

6.2.5 Synthesis of hydroxyl-bridged and bromine-bridged palladacycles

Following the extensive studies of halogen and hydrogen bonding carried out in the Perutz group,²²⁰⁻²²¹ it would be interesting to synthesise hydroxyl-bridged palladacycles to assess whether a hydrogen bond, between the hydrogen of the hydroxyl group bridge and the fluorine substituent of the aromatic ring, could lead to a regioselective C–H activation *ortho* to fluorine (Scheme 126). Similar studies have been reported by Strauss *et al.* for functionalised arenes²²² and by Gouverneur and co-workers in fluorinated carbohydrates.²²³



Scheme 126: Cyclometallation reaction of substrate **2.7c** forming *in situ* OH-bridged palladacycles **6.4** and **6.5**.

In the Fairlamb group the crystal structure of a fluorinated hydroxyl-bridged palladacycle (shown below) has been obtained while studying the direct transmetalation between palladacycles and arylboronic acids, and by analysing the packing of the crystal structure it is possible to observe a short contact between the fluorine atom (F(6)) and the hydrogen of the bridging OH group which could correspond to a hydrogen bond (Figure 105).¹³¹

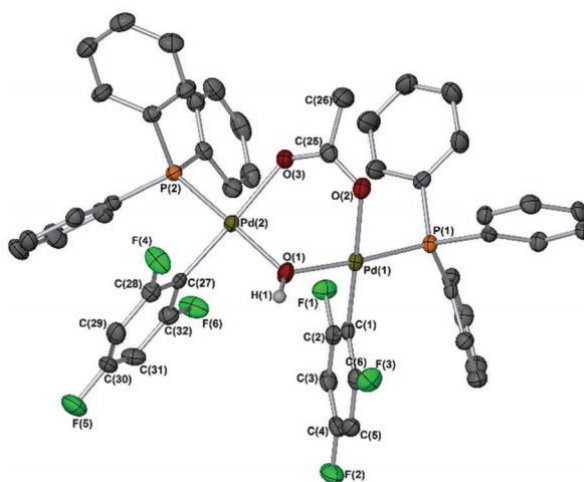


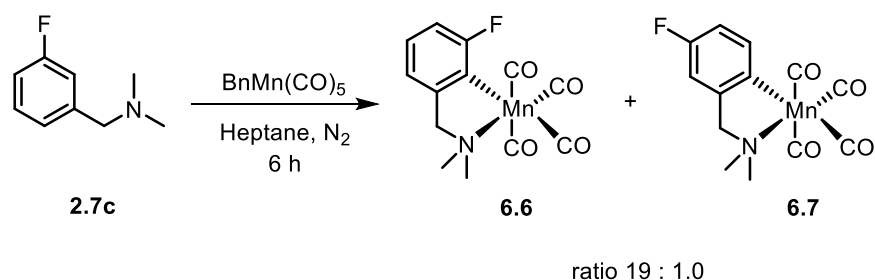
Figure 105: Molecular structure of dinuclear hydroxyl-bridged palladacycle **6.5** reported by Fairlamb *et al.*¹³¹ (Image taken with permission from ref. 131. Copyright 2014, RSC.)

Palladacycle **6.4** could be obtained directly as shown in Scheme 126 or *via* a bridge-conversion reaction starting from the chloride- or acetate-bridged palladacycles reacting with

NBu₄OH in acetone and water.²²⁴ The regioselectivity could then be compared between the two different methods.

6.2.6 Cyclometallation of fluorinated benzylamines at Mn

Preliminary results of the C–H activation reaction of substrate **2.7c** have been obtained at Mn, leading to a regioselective product **6.6** (95%), where the metal is *ortho* to the fluorine atom.²²⁵



Scheme 127: Cyclometallation reaction of **2.7** at Mn leading to the formation of **6.6** (95%).

A crystal structure confirming the regioselectivity has been obtained (Figure 106).

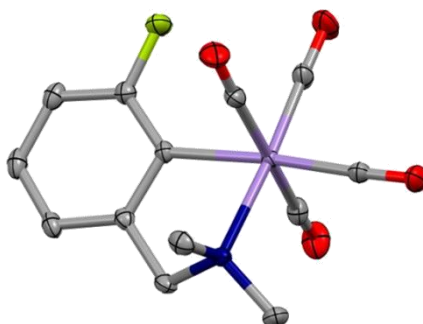


Figure 106: Molecular structure of Mn complex **6.6**. Hydrogen atoms were omitted for clarity; thermal ellipsoids shown with probability of 50%.

The hypothesised mechanism of the cyclometallation at Mn is the σ -bond metathesis (σ -CAM) and some preliminary DFT calculations concerning the suggested mechanism have been performed (Dr Jason Lynam), but further investigation is needed. The possibility of using Mn complexes as precatalysts for cross coupling reactions is also being explored. It would be interesting to test the behaviour of phosphine ligands such as **3.3** and compare the regioselectivity obtained with the amino-system.

Chapter 7: Experimental Section

7.1 General experimental techniques

7.1.1 Solvent and Reagents

Reagents were purchased from Fluorochem, Alfa Aesar or Sigma-Aldrich and used without further purification unless otherwise specified. Pd(OAc)₂ (>99.9%) was obtained from Precious Metals Online. Dry toluene and benzene were obtained by distillation over potassium. THF, diethyl ether, dichloromethane and acetonitrile were obtained from a Pure Solv MD-7 solvent machine and further dried by distillation using standard procedures. All dry solvents were stored under Ar in ampoules fitted with Young's PTFE stopcocks. Deuterated solvents were dried over CaH₂ (chloroform and acetonitrile) or potassium (benzene and toluene), distilled under high vacuum, and stored in small ampoules under Ar. The reactions discussed in Chapter 2 were carried out under an atmosphere of air while all others were performed under an argon or nitrogen atmosphere either in a glovebox or using standard Schlenk line techniques and oven- or flame-dried glassware.

7.1.2 Melting Points

Melting points were determined using a Stuart SMP3 melting point apparatus and a temperature ramp of 4 °C min⁻¹.

7.1.3 Nuclear Magnetic Resonance Spectroscopy

¹H, ¹³C, ¹⁹F, ³¹P and ¹¹B-NMR spectra were recorded on Jeol ECS400 (400, 100, 376, 162 and 128 MHz, respectively) or on a Bruker AMX500 (500, 126 and 471, 202 MHz, respectively) as specified in the text. ¹⁹⁵Pt was recorded on a Bruker AMX500 (108 MHz). ¹³C, ³¹P and ¹⁹F-NMR spectra were obtained with ¹H decoupling. ¹⁹F-NMR spectra were externally referenced to CFCl₃, while ¹H and ¹³C were referenced using the chemical shifts of residual protiated and deuterated solvent respectively (CHCl₃, δ 7.26 for ¹H and CDCl₃ δ 77.16 for ¹³C). ³¹P-NMR spectra were referenced externally to H₃PO₄. Chemical shifts are reported in parts per million (ppm). Spectra were recorded at 298 K unless otherwise stated. Multiplicities are described as (s) singlet, (d) doublet, (t) triplet, (q) quartet, (m) multiplet, (app) apparent and (br) broad. Multiplets are reported as a range when two or more resonances/environments overlap; when the multiplet contains a single resonance (*i.e.* one environment) the centrepoint of the multiplet is reported only. Spectra were processed using MestReNova software and exported as JPEG images into the appropriate document where

required. Copies of the NMR spectra for all compounds are given in Appendix III (CD attached).

7.1.4 X-ray Crystallography

X-ray crystallographic data were collected on an Agilent SuperNova diffractometer with MoK α radiation ($\lambda = 0.71073 \text{ \AA}$) or CuK α radiation ($\lambda = 1.54184 \text{ \AA}$) at 110.00(10) K. The structures were solved and refined using Olex2²²⁶ implementing SHELX algorithms and the Superflip²²⁷⁻²²⁹ structure solution program. All non-hydrogen atoms were refined anisotropically. Hydrogen atoms were placed at calculated positions and refined using a “riding model”. Structures were solved by Charge Flipping, Patterson or direct methods and refined with the ShelXL²³⁰ package using full matrix least squares minimization. Crystallographic parameters are given in Appendix II. Data were collected, processed and analysed by the author where specified.

7.1.5 Infrared Spectroscopy

Infrared spectra were recorded using a Unicam RS 10000E FTIR instrument. They were carried out as thin layer film or ATR averaging 64 scans at 1 cm^{-1} resolution. Absorption maxima are reported in wavenumbers (cm^{-1}) and are described as (br) broad, (m) medium, (s) strong and (w) weak. Far-IR spectra were recorded using a Bruker Tensor 37.

7.1.6 Mass Spectrometry

Liquid Injection Field Desorption/Ionisation (LIFDI)¹³⁶ and Electron Impact (EI) mass spectrometry were performed on a Waters GCT Premier mass spectrometer. Electrospray Ionisation (ESI) mass spectrometry was performed on a Bruker Daltonics microTOF spectrometer with an Agilent series 1200 LC with less than 5 ppm error for all HRMS values. Mass spectrometric data are quoted as an m/z ratio along with the relative peak height in parentheses (base peak = 100). In all cases the m/z ratio of the most abundant isotope combination is quoted. High resolution mass spectra (HRMS) are reported with error less than 5 ppm.

7.1.7 Elemental Analysis

Elemental analysis was carried out by Elemental Microanalysis Ltd (Exeter, UK) using a Dumas combustion method or by Dr Graeme McAllister using an Exeter Analytical CE-440 Elemental Analyser with the percentages reported as an average of two runs.

7.1.8 Chromatographic methods

Flash column chromatography was ordinarily performed using Merck 60 silica gel (particle size 40–63 μm). Thin layer chromatography (TLC) was carried out using Merck aluminium backed 5554 plates and relevant spots were visualised by ultraviolet light ($\lambda_{\text{max}} = 254 \text{ nm}$) and then stained with a solution of potassium permanganate and heated. Retention factors (R_f) are reported along with the solvent system used in parentheses.

7.1.9 Waste and disposal

All pyrophoric materials were quenched with a saturated solution of iodine in ethanol. All solid, sharps and solvent wastes were disposed following the protocol developed by the Chemistry Department in the University of York.

7.2 General Procedures

7.2.1 General procedure A: Synthesis of fluorinated benzylamines

The fluorinated *N,N*-dimethylbenzylamines were synthesized following the procedure reported by Liu and co-workers.¹²⁶ The appropriate fluorinated benzyl bromide (1 mmol, 1 eq.) was added to a solution of dimethylamine in MeOH (2 M, 3 mL, 3 eq.) in a sealed tube and heated at 65 °C for 24 hours. After cooling to room temperature, the resultant yellow solution was concentrated under reduced pressure. The residue was dissolved in water (10 mL) and the pH was adjusted to 12 by addition of 1 M aq. NaOH. The solution was then extracted with diethyl ether (3 \times 15 mL) and the combined organic layers dried over MgSO_4 , filtered and evaporated to afford the product as a colourless oil which was used without further purification.

7.2.2 General procedure B: Synthesis of fluorinated amino-derived acetate-bridged palladacycles from $\text{Pd}(\text{OAc})_2$

The fluorinated chloride-bridged amino-derived palladacycles were synthesized using a modified version of the literature procedure reported by Heck and co-workers.¹⁰⁴ To a solution of $\text{Pd}(\text{OAc})_2$ (1 eq.) in acetonitrile (20 mL mmol^{-1}) was added the relevant fluorinated *N,N*-dimethylbenzylamine (1.2 eq.) and the reaction mixture was stirred for 14 hours at 25 °C. The resulting green-to-yellow solution was filtered through cotton wool and reduced *in vacuo*. The residue was triturated with diethyl ether and dried to obtain the

desired product which was used without further purification. Single crystals suitable for X-ray analysis were grown by slow diffusion of hexane into a saturated solution in chloroform.

7.2.3 General procedure C: Synthesis of fluorinated amino-derived chloride-bridged palladacycles from Li_2PdCl_4

The fluorinated chloride-bridged amino-derived palladacycles were synthesized using a modified version of the literature procedure reported by Cope and co-workers.⁹⁷ To a solution of lithium (or potassium) tetrachloropalladate (1 eq.) in methanol (25 mL mmol^{-1}) was added the relevant fluorinated *N,N*-dimethylbenzylamine (2 eq.). The initially clear red reaction mixture rapidly turned slightly orange and after about 10 min at room temperature a yellow solid began to precipitate. After stirring for 6 hours, the yellow product was isolated by filtration, washed with MeOH and dried *in vacuo* and could be used without further purification. Single crystals suitable for X-ray analysis could be grown by slow diffusion of hexane into a saturated solution of the compound in chloroform.

7.2.4 General procedure D: Synthesis of fluorinated amino-derived acetate-bridged palladacycles from chloride-bridged palladacycles

The fluorinated acetate-bridged palladacycles were synthesized from chloride-bridged palladacycles using a modified version of the procedure reported by Cotton and co-workers.²³¹ To a solution of chloride-bridged amino-derived palladacycle (1 eq.) in acetone (100 mL mol^{-1}) was added silver acetate (2 eq.). The reaction mixture was stirred for 24 hours at 25 °C. The resulting greenish solution was filtered through Celite to remove the excess silver acetate, and reduced to dryness *in vacuo* to obtain the product as a green powder, which was not purified further.

7.2.5 General procedure E: Synthesis of fluorinated amino-derived chloride-bridged palladacycles from acetate-bridged palladacycles

The fluorinated chloride-bridged amino-derived palladacycles were synthesized from the appropriate acetate-bridged amino-derived palladacycles as reported by Hiraki and co-workers.¹⁰⁰ To a solution of acetate-bridged amino-derived palladacycle (1 eq.) in a solution of H_2O /acetone (1:20, 0.34 mL mol^{-1}), was added lithium chloride (8 eq.). The reaction mixture was stirred for 24 hours at 25 °C. The resulting yellow solution was filtered through

Celite and evaporated to obtain a yellow powder, which was washed with H₂O to remove the excess lithium chloride and dried *in vacuo* to afford the desired compound.

7.2.6 General procedure F: Synthesis of fluorinated diphenylbenzylphosphines

The fluorinated diphenylbenzylphosphines were synthesized following the procedure reported by Freitag and co-workers.¹⁶⁸ ⁿBuLi (2.5 M, 4.2 mL, 10.5 mmol) was added dropwise to a solution of diphenylphosphine (10 mmol, 1.74 mL) in dry THF (20 mL) in a Schlenk tube at -78 °C. The colourless solution immediately turned red/orange and was stirred for a further 30 mins at -78 °C. It was then warmed to room temperature and stirred for another 30 min, before being cooled once again to -78 °C. The relevant distilled fluorinated benzylbromide (12 mmol) was added dropwise, and the solution turned from red to yellow to colourless. It was stirred at -78 °C for 30 mins then allowed to warm to room temperature over 12 hours. The solvent was removed under reduced pressure and the residue treated with dry CH₂Cl₂ (20 mL), the precipitated LiCl was then removed by filtration under N₂ using a filter stick. The solvent was removed under reduced pressure and the residue washed with dry MeOH. The resulting white precipitate was dried *in vacuo* and stored in the glove box for further use.

7.2.7 General procedure G: Synthesis of fluorinated phosphino-derived chloride-bridged palladacycles

The fluorinated chloride-bridged palladacycles were synthesised using a modified version of the procedure reported by Pfeffer and co-workers.¹¹⁵ All reactions were performed under an inert atmosphere using standard Schlenk techniques. Palladacycle di- μ -chloro-bis-[*o*-dimethylaminomethyl-phenyl-*C,N*] dipalladium(II) (**2.9a**) (144 mg, 0.26 mmol) was pre-dried in a Schlenk tube, and transferred to a glove box, where the relevant fluorinated phosphine (0.56 mmol) was added along with dry toluene (20 mL). The Schlenk tube was removed from the glovebox and CF₃COOH (0.21 mmol from a stock solution 0.02 M in dry toluene) was added. The reaction mixture immediately changed colour from green to orange and was then stirred at 110 °C for 24 hours. Whilst still hot, the mixture was opened to air and filtered through Celite to remove traces of metallic Pd(0). The volume of solvent was reduced *in vacuo* to one half and the mixture cooled to 0 °C to leading to the formation of a yellow precipitate. The precipitate was filtered and washed with cold toluene to afford the fluorinated chloride-bridged palladacycles which were not purified further. Single crystals suitable for X-ray analysis were grown in air by slow evaporation the compound in toluene or CHCl₃.

7.2.8 General procedure H: Synthesis of fluorinated amino-iridacycles

The products were synthesised according to the procedure of Davies and co-workers.¹¹⁷ In a Schlenk tube a mixture of $[\text{Cp}^*\text{IrCl}_2]_2$ (1 eq.),²³² NaOAc (2.4 eq.) and the relevant fluorinated benzylamine (2.5 eq) was stirred at room temperature for 20 h in dry CH_2Cl_2 (100 mL mol⁻¹). The resulting mixture was filtered through Celite and the solvent removed under reduced pressure. The remaining solid was washed with hexane, under Ar, to remove the excess ligand and dried *in vacuo*, affording the product as an orange powder.

7.2.9 General procedure I: Synthesis of fluorinated amino metallacycles (L = CH₃CN)

The products were synthesised according to the procedure of Pfeffer and co-workers.¹²⁰ In a Schlenk tube a solution of $[\text{Cp}^*\text{MCl}_2]_2$ (M = Ir, Rh, Ru)²³²⁻²³³ (1 eq.), NaOH (2 eq.), KPF₆ (4 eq.) and the relevant fluorinated benzylamine (1.2 eq.) in CH_3CN (100 mL mol⁻¹) was shielded from light and stirred at 45 °C for 50 hours. Hexane (8 mL) was added and the resulting suspension was stirred for 2 h, under Ar, to remove the excess ligand. The layers were separated and the CH_3CN layer was concentrated *in vacuo* to afford the desired metallacycle.

7.2.10 General procedure J: Synthesis of fluorinated amino metallacycles (L = Cl)

Metallacycles obtained from general procedure I were reacted with KCl (13 eq.) in dry MeOH (10 mL mmol⁻¹) at room temperature for 16 hours as reported by Pfeffer and co-workers.¹²⁰ After this time, the solvent was removed under reduced pressure to afford the desired metallacycle.

7.2.11 General procedure K: Cross-coupling reactions with Pd(0)

Zinc chloride (81.1 mg, 0.6 mmol) was suspended in dry THF (5 mL) in a Schlenk tube and phenylmagnesium bromide (3 M in Et₂O, 0.4 mL, 1.2 mmol) was added. The mixture was stirred until complete dissolution of the zinc chloride was observed. In another Schlenk tube, a solution of lithium iodide (321.2 mg, 2.4 mmol), the relevant fluorinated substrate (1 mmol) and $[\text{Pd}(\text{PCy}_3)_2]$ ²³⁴ (33.3 mg, 0.05 mmol, 5 mol%) in dry THF (3 mL) was prepared and cannula-transferred into the zinc chloride solution. The mixture was stirred for 6 hours

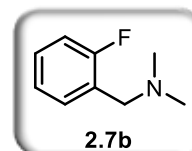
at 60 °C, then HCl (1 M, 15 mL) was added and the aqueous phase was extracted with diethylether (3 × 5 mL). The combined organic layers were dried over MgSO₄, filtered and evaporated to afford a brown solid, which was purified by flash chromatography.

7.3 Synthetic procedures and Compound Data

7.3.1 Compounds in Chapter 2

N,N-Dimethyl-2-fluorobenzylamine (2.7b)

The *title compound* was prepared according to General Procedure A, on a 3.3 mmol scale, as a colourless oil (505.6 mg, 74%).



¹H NMR (400 MHz, CDCl₃) δ 7.36 (td, $J = 7.5, 1.7$ Hz, 1H), 7.25 (m, 1H), 7.11 (td, $J = 7.5, 1.2$ Hz, 1H), 7.04 (ddd, $J = 9.6, 8.2, 1.1$ Hz, 1H), 3.52 (s, 2H), 2.28 (s, 6H).

¹³C NMR (101 MHz, CDCl₃) δ 161.6 (d, $J = 246.3$ Hz), 131.8 (d, $J = 4.5$ Hz), 129.1 (d, $J = 8.1$ Hz), 124.0 (d, $J = 3.6$ Hz), 115.4 (d, $J = 22.3$ Hz), 56.7, 56.6, 45.3.

¹⁹F NMR (376 MHz, CDCl₃) δ -118.10 (m).

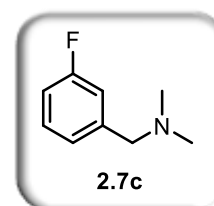
HRMS (ESI) m/z 154.1031 (100%, [$M+H$]⁺), (calculated for C₉H₁₃FN 154.1027, $\Delta = 0.5$ mDa).

IR (ATR, ν cm⁻¹): 1618 (w), 1587 (m), 1490.1 (s), 1456 (s), 1367 (m), 1259 (m), 1228 (s), 1218 (s), 1176 (m), 1151 (w), 1097 (m), 1020 (m, br), 941 (w), 862 (w), 835 (m), 756 (s), 663 (w).

Lab book reference number: JM-A-9

N,N-Dimethyl-3-fluorobenzylamine (2.7c)

The *title compound* was prepared according to General Procedure A, on a 2 mmol scale, as a colourless oil (245 mg, 80%).



¹H NMR (500 MHz, CDCl₃) δ 7.27 (m, 1H), 7.08 (d, $J = 7.6$ Hz, 1H), 7.10–7.02 (m, 2H), 6.95 (td, $J = 8.3, 1.8$ Hz, 1H), 3.43 (s, 2H), 2.25 (s, 6H).

¹³C NMR (126 MHz, CDCl₃) δ 163.1 (d, $J = 245.5$ Hz), 141.6 (d, $J = 6.8$ Hz), 129.8 (d, $J = 8.2$ Hz), 124.7 (d, $J = 2.8$ Hz), 116.0 (d, $J = 21.2$ Hz), 114.1 (d, $J = 21.1$ Hz), 63.9 (d, $J = 1.8$ Hz), 45.4.

¹⁹F NMR (376 MHz, CDCl₃) δ -113.70 (m).

HRMS (ESI) m/z 154.1029 (100%, [$M+H$]⁺), (calculated for C₉H₁₃FN 154.1027, difference $\Delta = 0.3$ mDa).

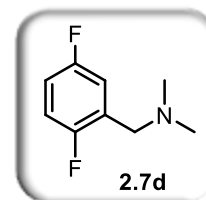
IR (ATR, ν cm^{-1}): 2925 (m, br), 2854 (m), 2819.5 (m), 2777 (m), 2362 (w), 2337 (w), 1733 (w), 1616.1 (w), 1591 (m), 1486 (m), 1456 (m), 1456 (m), 1363 (w), 1259 (s), 1174 (w), 1132 (w), 1097 (m), 1031 (m).

All data are in accordance with the literature.¹²⁶

Lab book reference number: JM-A-6

***N,N*-Dimethyl-2,5-difluorobenzylamine (2.7d)**

The *title compound* was prepared according to General Procedure A, on a 2 mmol scale, as a colourless oil (218.4 mg, 64%).



¹H NMR (400 MHz, CDCl_3) δ 7.09 (ddd, $J = 8.8, 5.7, 3.2$ Hz, 1H), 6.98 (td, $J = 9.0, 4.5$ Hz, 1H), 6.91 (m, 1H), 3.46 (d, $J = 1.2$ Hz, 2H), 2.27 (s, 6H).

¹³C NMR (101 MHz, CDCl_3) δ 158.8 (dd, $J = 241.9, 2.3$ Hz), 157.3 (dd, $J = 241.8, 2.4$ Hz), 127.4 (dd, $J = 17.1, 7.3$ Hz), 117.6 (dd, $J = 24, 4.9$ Hz), 116.3 (dd, $J = 25.4, 8.6$ Hz), 115.1 (dd, $J = 24.1, 8.7$ Hz), 56.4 (t, $J = 1.4$ Hz), 45.3.

¹⁹F NMR (376 MHz, CDCl_3) δ -119.46 (m, 1F), -124.33 (dtd, $J = 13.7, 9.1, 4.9$ Hz, 1F).

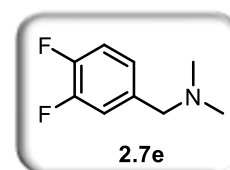
HRMS (ESI) m/z 172.0932 (100%, $[M+H]^+$), (calculated for $\text{C}_9\text{H}_{12}\text{F}_2\text{N}$ 172.0938, difference $\Delta = 0.6$ mDa).

IR (ATR, ν cm^{-1}): 2977 (m), 2946 (m), 2860 (m), 2821 (m), 2775 (m), 1737 (w), 1596 (w), 1494 (s), 1458 (m), 1435 (m), 1367 (m), 1265 (m), 1240 (m), 1191 (m), 1135 (m), 1097 (w), 1031 (m), 979 (w), 954 (w), 883 (m), 842 (m), 812 (m), 723 (m).

Lab book reference number: JM-A-40

***N,N*-Dimethyl-3,4-difluorobenzylamine (2.7e)**

The *title compound* was prepared according to General Procedure A, on a 5 mmol scale, as a colourless oil (546.2 mg, 64%).



¹H NMR (500 MHz, CDCl_3) δ 7.14 (m, 1H), 7.08 (m, 1H), 7.00 (m, 1H), 3.35 (s, 2H), 2.22 (s, 6H).

¹³C NMR (126 MHz, CDCl_3) δ 150.4 (dd, $J = 247.7, 12.7$ Hz), 149.6 (dd, $J = 246.8, 12.7$ Hz), 136.3 (dd, $J = 5.2, 3.9$ Hz), 124.8 (dd, $J = 6.2, 3.5$ Hz), 117.8 (d, $J = 17.1$ Hz), 117.0 (d, $J = 17.1$ Hz), 63.4 (d, $J = 1.1$ Hz), 45.4.

¹⁹F NMR (376 MHz, CDCl_3) δ -138.4 (dddd, $J = 19.5, 11.5, 8.1, 1$ Hz, 1F), -140.4 (dddd, $J = 17.9, 10.6, 7.8, 4.5$ Hz).

HRMS (ESI) m/z 172.0936 (100%, $[M+H]^+$), (calculated for $C_9H_{12}F_2N$ 172.0932, difference $\Delta = 0.4$ mDa).

Lab book reference number: JM-A-81

***N,N*-Dimethyl-3,5-difluorobenzylamine (2.7f)**

The *title compound* was prepared according to General Procedure A, on a 5 mmol scale, as a colourless oil (646 mg, 76%).

1H NMR (400 MHz, $CDCl_3$) δ 6.91–6.80 (m, 2H), 6.68 (tt, $J = 8.7$, 2.2 Hz, 1H), 3.38 (s, 2H), 2.23 (s, 6H).

^{13}C NMR (101 MHz, $CDCl_3$) δ 163.1 (dd, $J = 247.9$, 12.7 Hz), 143.4 (t, $J = 8.7$ Hz), 111.7–111.4 (m), 102.5 (t, $J = 25.4$ Hz), 63.7 (t, $J = 2.1$ Hz), 45.5.

^{19}F NMR (376 MHz, $CDCl_3$) δ -110.55 (m).

HRMS (ESI) m/z 172.0939 (100%, $[M+H]^+$), (calculated for $C_9H_{12}F_2N$ 172.0932, difference $\Delta = -0.6$ mDa).

Lab book reference number: JM-B-124

***N,N*-Dimethyl-3-chlorobenzylamine (2.7g)**

The *title compound* was prepared according to General Procedure A, on a 6.6 mmol scale, as a colourless oil (771 mg, 69%).

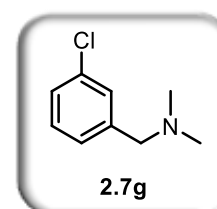
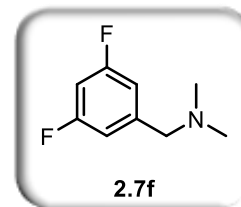
1H NMR (400 MHz, $CDCl_3$) δ 7.32 (m, 1H), 7.24 (m, 2H), 7.19 (m, 1H), 3.39 (s, 2H), 2.24 (s, 6H).

^{13}C NMR (126 MHz, $CDCl_3$) δ 141.3, 134.3, 129.7, 129.2, 127.4, 127.3, 63.9, 45.5.

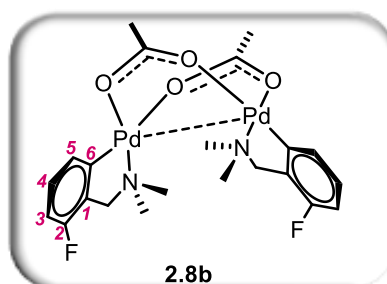
HRMS (ESI) m/z 170.0727 (100%, $[M+H]^+$), (calculated for $C_9H_{13}ClN$ 170.0731, difference $\Delta = 0.4$ mDa).

All data are in accordance with the literature.²³⁵

Lab book reference number: JM-C-204



Representative compound numbering for acetate-bridged palladacycles



Di- μ -acetato-bis-[*o*-dimethylaminomethylphenyl-*C,M*] dipalladium(II) (2.8a)

The *title compound* was prepared according to General Procedure B, on a 0.26 mmol scale, to afford the product as green powder (78 mg, 91%).

M.p. 197–199 °C (dec.) (lit. 210–211 °C).¹⁰⁴

¹H-NMR (500 MHz, CDCl₃) δ 7.02 (d, J = 7.1 Hz, 2H), 6.97 (t, J = 7.3 Hz, 2H), 6.89 (t, J = 7.2 Hz, 2H), 6.84 (d, J = 7.2 Hz, 2H), 3.58 (d, J = 13.7 Hz, 2H, RCH₂N), 3.09 (d, J = 13.7 Hz, 2H, RCH₂N), 2.80 (s, 6H, NCH₃), 2.06 (s, 6H, NCH₃), 2.05 (s, 6H, CH₃CO).

¹³C NMR (126 MHz, CDCl₃) δ 180.9 (CO), 147.2 (Aromatic), 144.1 (Aromatic), 132.3 (Aromatic), 124.8 (Aromatic), 124.4 (Aromatic), 121.2 (Aromatic), 72.3 (CH₂), 52.7 (NCH₃), 51.3 (NCH₃), 24.7 (CH₃CO).

IR (ATR, ν cm⁻¹): 1727 (w), 1588 (m), 1569 (m), 1412 (s), 1345 (w), 1260 (s), 1072 (m, br), 1020 (s, br), 799 (s), 737 (s), 680 (m).

LRMS (LIFDI) m/z 599.94 (100%, [M]⁺).

All data are in accordance with the literature.¹²⁴

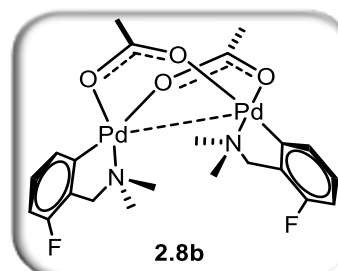
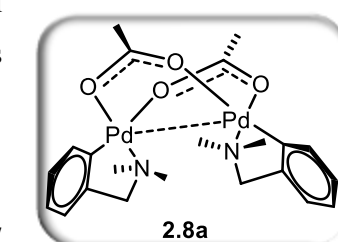
Lab book reference number: JM-A-3

Di- μ -acetato-bis-[*o*-dimethylaminomethyl-2-fluorophenyl-*C,M*] dipalladium(II) (2.8b)

The *title compound* was prepared according to General Procedure A, on a 0.27 mmol scale, to afford the product as yellow powder (72.8 mg, 85%).

M.p. 190–193 °C (dec.).

¹H NMR (400 MHz, CDCl₃) δ 6.91 (td, J = 7.8, 5.6 Hz, 2H, H-4), 6.79 (d, J = 7.4 Hz, 2H, H-5), 6.71 (ddd, J = 9.5, 8.1, 0.9 Hz, 2H, H-3), 3.50 (d, J = 14.1 Hz, 2H, CHH'), 3.45 (dd, J = 14.3, 1.4 Hz, 2H, CHH'), 2.83 (s, 6H, NCH₃), 2.07 (s, 6H, NCH₃), 2.06 (s, 6H, CH₃CO).



¹³C NMR (126 MHz, CDCl₃) δ 181.2 (CO), 156.4 (d, J = 250.2 Hz, C-2), 148.8 (C-6), 132.6 (d, J = 10.1 Hz, C-1), 127.8 (d, J = 2.9 Hz, C-5), 126.3 (d, J = 6.4 Hz, C-4), 111.1 (d, J = 20.2 Hz, C-3), 67.7 (CH₂), 52.9 (NCH₃), 51.6 (NCH₃), 24.6 (CH₃CO).

¹⁹F NMR (471 MHz, CDCl₃) δ -115.01 (dd, J = 9.7, 5.5 Hz).

IR (ATR, ν cm⁻¹): 1601 (m), 1576 (s), 1558 (s), 1455 (m), 1410 (s), 1345 (m), 1232 (s), 1127 (w), 986 (w), 874 (m), 844 (m), 769 (s), 678 (s).

LRMS (LIFDI) m/z 636.02 (100%, [M]⁺).

CHN Anal. Calcd for C₂₂H₂₈F₂N₂O₄Pd₂: C, 41.58; H, 4.39; N, 4.22. Found: C, 41.59; H, 4.44; N, 4.51.

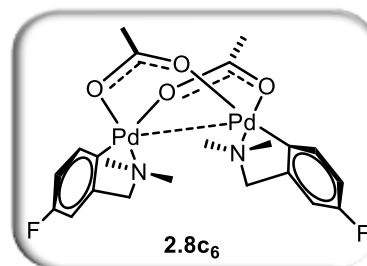
Lab book reference number: JM-A-25

Di- μ -acetato-bis-[*o*-dimethylaminomethyl-3-*p*-fluorophenyl-*C,N*] dipalladium(II) (2.8c₆)

The *title compound* was prepared according to General Procedure D, on a 0.17 mmol scale, to afford the product as yellow powder (105.4 mg, 98%).

M.p. 191–195 °C (dec.).

¹H NMR (500 MHz, CDCl₃) δ 6.95 (dd, J = 8.3, 6.2 Hz, 2H, H-1), 6.71–6.61 (m, 4H, H-2, H-4), 3.52 (d, J = 13.9 Hz, 2H, CHH'), 3.09 (d, J = 13.9 Hz, 2H, CHH'), 2.79 (s, 6H, NCH₃), 2.06 (s, 6H, NCH₃), 2.05 (s, 6H, CH₃CO).



¹³C NMR (126 MHz, CDCl₃) δ 181.1 (CO), 161.3 (d, J = 240.6 Hz, C-3), 147.7 (d, J = 6.2 Hz, C-1), 137.2 (d, J = 2.5 Hz, C-6), 133.0 (d, J = 6.8 Hz, C-5), 111.5 (d, J = 19.7 Hz, C-4), 108.6 (d, J = 21.4 Hz, C-2), 72.0 (CH₂), 52.7 (NCH₃), 51.3 (NCH₃), 24.6 (CH₃CO).

¹⁹F NMR (471 MHz, CDCl₃) δ -119.31 (td, J = 9.6, 6.2 Hz).

LRMS (LIFDI) m/z 636.00 (100%, [M]⁺).

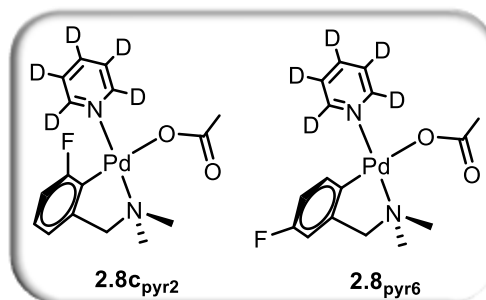
CHN Anal. Calcd for C₂₂H₂₈F₂N₂O₄Pd₂·0.2AgCl: C, 39.8; H, 4.25; N, 4.22. Found: C, 39.87; H, 4.26; N, 3.97.

Lab book reference number: JM-B-171

Acetato-*O*-[*o*-dimethylaminomethyl-3-fluorophenyl-*C,N*](pyridine-*d*₅)palladium(II)

(**2.8c_{pyr2}** and **2.8c_{pyr6}**)

A portion of the mixture of isomers of di- μ -acetato-bis-[*o*-dimethylaminomethyl-3-fluorophenyl-*C,N*] dipalladium(II) (**2.8c**) was dissolved in pyridine-*d*₅ to obtain a mixture the two isomers of **2.8c_{pyr}** in a 1:1 ratio.



¹H NMR (400 MHz, CDCl₃): δ 7.07 (td, $J = 5.5, 7.7$ Hz, 1H), 6.92–6.88 (m, 2H), 6.77 (m, 1H), 6.65 (t, $J = 8.4$ Hz, 1H), 6.28 (dd, $J = 8.4, 6.2$ Hz, 1H), 3.93 (s, 2H), 3.86 (s, 2H), 2.84 (s, 6H), 2.76 (s, 6H), 2.19 (s, 6H).

¹⁹F NMR (376 MHz, CDCl₃) δ -100.98 (dd, $J = 8.7, 5.4$ Hz), -119.88 (dd, $J = 15.9, 9.6$ Hz).

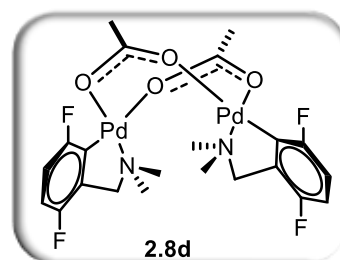
Lab book reference number: JM-A-18-P

Di- μ -acetato-bis-[*o*-dimethylaminomethyl-2,5-*o,m*-difluorophenyl-*C,N*] dipalladium(II)

(**2.8d**)

The *title compound* was prepared according to General Procedure B, on a 0.26 mmol scale, to afford the product as yellow/green powder (70.2 mg, 78%).

M.p. 187–190 °C (dec.).



¹H NMR (400 MHz, CDCl₃) δ 6.67 (td, $J = 8.7, 3.7$ Hz, 2H, H-3), 6.51 (td, $J = 7.7, 4$ Hz, 2H, H-4), 3.76 (dd, $J = 14.4, 1.8$ Hz, 2H, CHH'), 3.54 (d, $J = 14.4$ Hz, 2H, CHH'), 2.83 (s, 6H, NCH₃), 2.23 (s, 6H, NCH₃), 2.00 (s, 6H, CH₃CO).

¹³C NMR (126 MHz, CDCl₃) δ 182.2 (CO), 163.6 (dd, $J = 235.5, 1.8$ Hz, C-5), 153.1 (dd, $J = 244.9, 2.2$ Hz, C-2), 134.7 (dd, $J = 15.1, 12.4$ Hz, C-1), 127.9 (d, $J = 36.9$ Hz, C-6), 114.5 (dd, $J = 31.5, 7.6$ Hz, C-4), 112.1 (dd, $J = 23.4, 8.6$ Hz, C-3), 69.0 (CH₂), 52.8 (NCH₃), 51.9 (NCH₃), 23.6 (d, $J = 2.1$ Hz, CH₃CO).

¹⁹F NMR (376 MHz, CDCl₃) δ -111.12 (ddd, $J = 20.9, 7.6, 3.6$ Hz, 2F), -121.08 (m, 2F).

IR (ATR, ν cm⁻¹): 1590 (s), 1571 (s), 1458 (s), 1418 (s, br), 1349 (m), 1213 (s), 1023 (m), 972 (m), 838 (s), 805 (s), 727 (s), 683 (m).

LRMS (LIFDI) m/z 672.02 (100%, [M]⁺).

CHN Anal. Calcd for C₂₂H₂₆F₄N₂O₄Pd₂: C, 39.36; H, 3.90; N, 4.17. Found: C, 38.99; H, 3.91; N, 4.31.

Lab book reference number: JM-A-41

Di- μ -acetato-bis-[*o*-dimethylaminomethyl-3,4-*p,m*-difluorophenyl-*C,N*] dipalladium(II)
(2.8e)

The *title compound* was prepared according to General Procedure D, on a 0.16 mmol scale, to afford the product as yellow powder (102 mg, 95%).

M.p. 188–190 °C (dec.).

^1H NMR (500 MHz, CDCl_3) δ 6.78–6.72 (m, 4H, H-2, H-5), 3.58 (d, $J = 13.8$ Hz, 2H, CHH'), 3.13 (d, $J = 13.8$ Hz, 2H, CHH'), 2.79 (s, 6H, NCH_3), 2.11 (s, 6H, NCH_3), 2.06 (s, 6H, CH_3CO).

^{13}C NMR (126 MHz, CDCl_3) δ 181.6 (CO), 148.3 (dd, $J = 243.2, 13.7$ Hz, C-3), 146.7 (dd, $J = 250.6, 12.1$ Hz, C-4), 142.0 (dd, $J = 4.8, 3.7$ Hz, C-6), 138.9 (dd, $J = 3.7, 2.9$ Hz, C-1), 120.0 (d, $J = 14.7$ Hz, C-5), 110.3 (d, $J = 17.5$ Hz, C-2), 72.0 (CH_2), 52.6 (NCH_3), 51.5 (NCH_3), 24.6 (CH_3CO).

^{19}F NMR (471 MHz, CDCl_3) δ -140.92 (m, 2F), -143.94 (ddd, $J = 19.7, 10.7, 8.8$ Hz, 2F).

LRMS (LIFDI) m/z 672.00 (100%, $[\text{M}]^+$).

CHN Anal. Calcd for $\text{C}_{22}\text{H}_{26}\text{F}_4\text{N}_2\text{O}_4\text{Pd}_2 \cdot 0.1\text{AgCl}$: C, 38.54; H, 3.82; N, 4.09. Found: C, 38.56; H, 3.85; N, 3.92.

Lab book reference number: JM-B-170

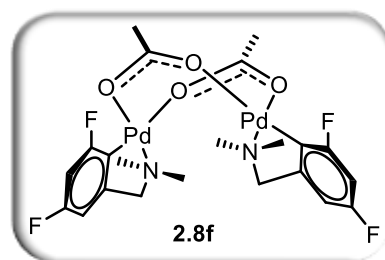
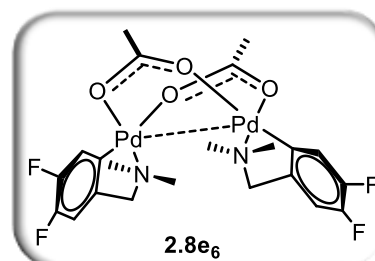
Di- μ -acetato-bis-[*o*-dimethylaminomethyl-3,5-difluorophenyl-*C,N*] dipalladium(II)
(2.8f)

The *title compound* was prepared according to General Procedure A, on a 0.26 mmol scale, to afford the product as yellow powder (71 mg, 82%).

M.p. 205–208 °C (dec.).

^1H NMR (400 MHz, CDCl_3) δ 6.54 (dd, $J = 8.4, 2.4$ Hz, 2H, H-2), 6.34 (m, 2H, H-4), 3.56–3.46 (m, 4H, CHH' , CHH'), 2.80 (s, 6H, NCH_3), 2.18 (s, 6H, NCH_3), 2.00 (s, 6H, CH_3CO).

^{13}C NMR (126 MHz, CDCl_3) δ 182.1 (CO), 167.7 (dd, $J = 242.6, 11.2$ Hz, C-5), 161.4 (dd, $J = 243.2, 11.9$ Hz, C-3), 150.1 (dd, $J = 17.2, 8.2$ Hz, C-6), 119.1 (dd, $J = 34.3, 3.2$ Hz, C-1), 105.1 (dd, $J = 21.1, 3.3$ Hz, C-2), 101.6 (dd, $J = 32.2, 23.7$ Hz, C-4), 73.5 (d, $J = 3.1$ Hz, CH_2), 52.6 (NCH_3), 51.6 (NCH_3), 23.7 (d, $J = 1.7$ Hz, CH_3CO).



^{19}F NMR (376 MHz, CDCl_3) δ -100.81 (m, 2F), -116.37 (dd, $J = 17.6, 8.2$ Hz, 2F).

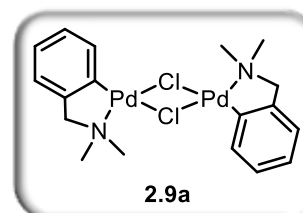
LRMS (LIFDI) m/z 671.99 (100%, $[\text{M}]^+$).

CHN Anal. Calcd for $\text{C}_{22}\text{H}_{26}\text{F}_4\text{N}_2\text{O}_4\text{Pd}_2$: C, 39.36; H, 3.90; N, 4.17. Found: C, 39.28; H, 3.89; N, 3.90.

Lab book reference number: JM-B-125

Di- μ -chloro-bis-[*o*-dimethylaminomethyl-phenyl-*C,N*] dipalladium(II) (2.9a)

The *title compound* was prepared according to General Procedure D, on a 1.69 mmol scale, to afford the product as yellow powder (462 mg, 46%).



M.p. 173–175 °C (dec.) (lit. 183–185 °C).⁹⁷

^1H NMR (500 MHz, CDCl_3) δ 7.17 (dd, $J = 19.3, 7.6$ Hz, 2H), 6.99–6.94 (m, 2H), 6.87 (t, $J = 6.8$ Hz, 4H), 3.93 (s, 4H), 2.87 (s, 6H), 2.84 (s, 6H).

IR (ATR, ν cm^{-1}): 1738 (w), 1578 (w), 1447 (m), 1259 (s). 1095 (s, br), 1043 (s), 1017 (s, br), 982 (m), 861 (m), 799 (s), 733 (s), 698 (m).

Far-IR (ATR, ν cm^{-1}): 516.04 (m), 498.64 (w), 477.33 (w), 422.85 (m), 398.60 (w), 368.37 (w), 329.15 (m), 280.00 (m), 265.76 (m), 247.08 (s), 244.39 (m), 232.86 (w), 217.42 (s).

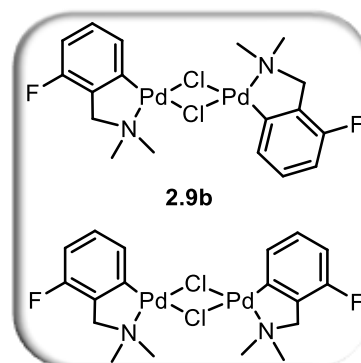
LRMS (LIFDI) m/z 551.96 (100%, $[\text{M}]^+$).

All data are in accordance with the literature.⁹⁷

Lab book reference number: JM-B-163

Di- μ -chloro-bis-[*o*-dimethylaminomethyl-2-*m*-fluorophenyl-*C,N*] dipalladium(II) (2.9b)

The *title compound* was prepared according to General Procedure C, on a 0.26 mmol scale, to afford the product in a mixture of geometrical isomers (*syn* and *anti*) as a yellow powder (74 mg, 86%).



M.p. 180–182 °C (dec.).

^1H NMR (500 MHz, CDCl_3) δ 6.94 (dd, $J = 20.1, 7.7$ Hz, 2H), 6.70 (dd, $J = 13.6, 4.9$ Hz, 2H), 6.87 (td $J = 7.9, 5.6$ Hz, 2H), 4.01 (d, $J = 2.3$ Hz, 4H), 2.88 (s, 6H), 2.86 (s, 6H).

^{13}C NMR (126 MHz, CDCl_3) δ 156.1 ($J = 249.6, 2.4$ Hz), 144.9 (d, $J = 13.12$ Hz), 132.8 (t, $J = 11.1$ Hz), 128.8 (dd, $J = 67.6, 2.9$ Hz), 126.5 (dd, $J = 13.4, 6.6$ Hz), 111.6 (d, $J = 20.2$ Hz), 68.6 (d, $J = 22.3$ Hz), 53.3, 53.0.

¹⁹F NMR (376 MHz, CDCl₃) δ -113.97 (m).

LRMS (LIFDI) *m/z* 587.92 (100%, [M]⁺).

CHN Anal. Calcd for C₁₈H₂₂F₂N₂Cl₂Pd₂: C, 36.76; H, 3.77; N, 4.76. Found: C, 36.63; H, 3.64; N, 4.40.

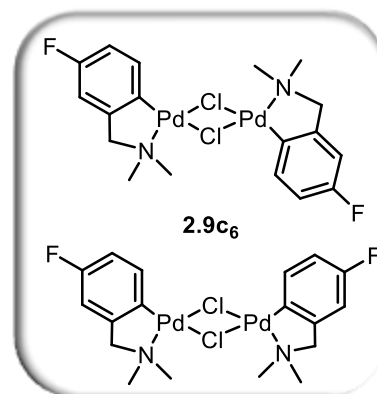
Lab book reference number: JM-B-198

Di-μ-chloro-bis-[*o*-dimethylaminomethyl-3-*p*-fluorophenyl-*C,N*] dipalladium(II) (2.9c₆)

The title compound was prepared according to General Procedure C, on a 0.77 mmol scale, to afford the product in a mixture of geometrical isomers (*syn* and *anti*) as a yellow powder (171 mg, 76%).

M.p. 174.4–176.2 °C (dec).

¹H NMR (500 MHz, CDCl₃) δ 7.17–6.98 (m, 2H), 6.65 (d, *J* = 9.2 Hz, 4H), 3.90 (br s, 4H), 2.86 (s, 6H), 2.83 (s, 6H).



¹³CNMR (126 MHz, CDCl₃) δ 161.4 (d, *J* = 241.5 Hz, major isomer), 161.4 (d, *J* = 241.6 Hz, minor isomer), 147.6 (d, *J* = 6.3 Hz, major isomer), 147.6 (d, *J* = 6.5 Hz, minor isomer), 136.1 (d, *J* = 2.2 Hz, major isomer), 136.0 (d, *J* = 2.2 Hz, minor isomer), 134.3 (d, *J* = 7.0 Hz, minor isomer), 133.8 (d, *J* = 6.9 Hz, major isomer), 112.0 (d, *J* = 9.8 Hz, major isomer), 111.9 (d, *J* = 9.8 Hz, minor isomer), 109.0 (s, major isomer), 108.8 (s, minor isomer), 73.2 (d, *J* = 2.6 Hz, major isomer), 73.0 (d, *J* = 2.9 Hz, major isomer), 53.1 (s, major isomer), 52.8 (s, minor isomer).

¹⁹F NMR (471 MHz, CDCl₃) δ -119.01 (m, minor isomer), -119.10 (m, major isomer).

Far-IR (ATR, ν cm⁻¹): 576.72 (m), 553.97 (w), 518.76 (w), 441.67 (m), 427.53 (m), 337.55 (m), 316.09 (s), 274.60 (m), 255.36 (w), 252.25 (w), 239.54 (s), 215.26 (s), 196.34 (m).

LRMS (LIFDI) *m/z* 587.89 (100%, [M]⁺).

CHN Anal. Calcd for C₁₈H₂₂F₂N₂Cl₂Pd₂: C, 36.76; H, 3.77; N, 4.76. Found: C, 36.61; H, 3.77; N, 4.53.

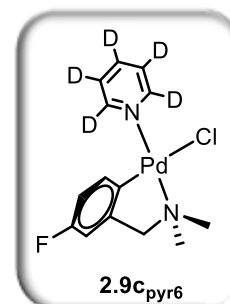
Lab book reference number: JM-B-167, JM-B-179

**Chloro-κO-[*o*-dimethylaminomethyl-3-*p*-fluorophenyl-*C,N*](pyridine-*d*₅)palladium(II)
(**2.9c_{pyr}**)**

A portion of di-μ-chloro-bis-[*o*-dimethylaminomethyl-3-*p*-fluorophenyl-*C,N*] dipalladium(II) (**2.19c₆**) was dissolved in pyridine-*d*₅ to obtain the *title compound*.

¹H NMR (500 MHz, CDCl₃) δ 6.93 (dd, *J* = 9.6, 2.5 Hz, 1H), 6.78 (t, *J* = 7.8 Hz, 1H), 6.27–6.17 (m, 1H), 3.91 (s, 2H), 2.94 (s, 6H).

¹⁹F NMR (471 MHz, CDCl₃): δ -119.35–-119.46 (dd, *J* = 16.4, 10.3 Hz).



Lab book reference number: JM-B-168-P

**Di-μ-chloro-bis-[*o*-dimethylaminomethyl-2,5-*o,m*-difluorophenyl-*C,N*] dipalladium(II)
(**2.9d**).**

The *title compound* was obtained according to General Procedure C, with a reaction time of 1 week, on a 0.1 mmol scale, to afford the product in a mixture of geometrical isomers (*syn* and *anti*) as a yellow product (21 mg, 67%).

M.p. 172.9–174 °C (dec.).

¹H NMR (500 MHz, CDCl₃) δ 6.66 (qd, *J* = 8.5, 3.6 Hz, 2H), 6.52 (m, 2H), 4.05 (d, *J* = 4.1 Hz, 4H), 2.77 (s, 6H), 2.75 (s, 6H).

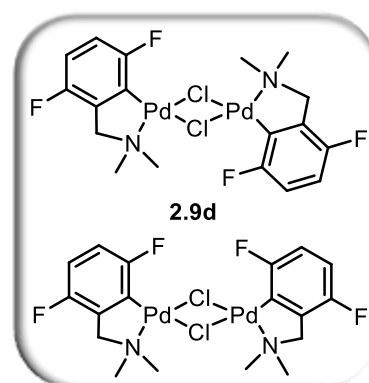
¹³C NMR (126 MHz, CDCl₃, *major isomer*) δ 162.3 (dd, *J* = 239.3, 19.6 Hz), 152.7 (d, *J* = 244.6 Hz), 134.2 (m), 126.8 (m), 114.7 (m), 112.4 (m), 69.4 (d, *J* = 9.3 Hz), 53.1, 52.7.

¹⁹F NMR (376 MHz, CDCl₃, *minor and major isomers*) δ -102.94 (ddd, *J* = 20.0, 7.7, 3.6 Hz), -105.75 (ddd, *J* = 20.1, 7.9, 3.6 Hz), -120.49 (m), -120.90 (m).

LRMS (LIFDI) *m/z* 623.94 (100%, [M]⁺).

CHN Anal. Calcd for C₁₈H₂₀F₄N₂Cl₂Pd₂: C, 34.64; H, 3.23; N, 4.49. Found: C, 34.49; H, 3.16; N, 4.25.

Lab book reference number: JM-D-306



Di- μ -chloro-bis-[*o*-dimethylaminomethyl-3,4-*p,m*-difluorophenyl-*C,N*] dipalladium(II) (2.9e₆**)**

The *title compound* was prepared according to General Procedure C, on a 0.77 mmol scale, to afford the product in a mixture of geometrical isomers (*syn* and *anti*) as a yellow powder (171 mg, 71%).

M.p. 178.6–180.2 °C.

¹H NMR (400 MHz, CDCl₃) δ 6.92 (ddd, $J = 19.1, 10.6, 8.6$ Hz, 2H), 6.74 (dd, $J = 10.6, 7.6$ Hz, 2H), 3.88 (s, 4H), 2.85 (s, 6H), 2.82 (s, 6H).

¹⁹F NMR (376 MHz, CDCl₃): δ -140.22 (m, *major isomer*), -140.55 (m, *minor isomer*), -143.50 (m, *major isomer*), -143.67 (m, *minor isomer*).

HSQC NMR (500, 126 MHz): δ (6.92, 121.1), (6.74, 109.9), (3.88, 72.5), (2.85, 52.6).

Far-IR (ATR, ν cm⁻¹): 520.26 (w), 466.51 (w), 439.59 (m), 374.08 (m), 319.81 (s), 278.79 (m), 263.58 (m), 236.05 (m), 211.74 (w), 180.23 (w).

LRMS (LIFDI) m/z 623.89 (100%, [M]⁺).

CHN Anal. Calcd for C₁₈H₂₀F₄N₂Cl₂Pd₂: C, 34.64; H, 3.23; N, 4.49. Found: C, 34.64; H, 3.19; N, 4.28

Lab book reference number: JM-B-167, JM-B-179

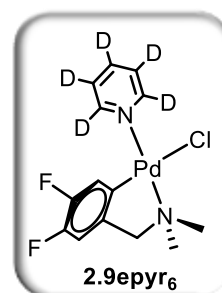
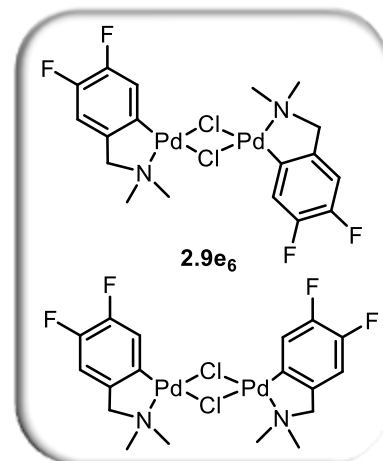
Chloro- κ -[*o*-dimethylaminomethyl-3,4-difluorophenyl-*C,N*](pyridine-*d*₅)palladium(II) (2.9epy₆**)**

A portion of di- μ -chloro-bis-[*o*-dimethylaminomethyl-3,4-*p,m*-difluorophenyl-*C,N*] dipalladium(II) (**2.19e₆**) was dissolved in pyridine-*d*₅ to obtain the *title compound*.

¹H NMR (500 MHz, CDCl₃) δ 7.03–6.96 (m, 1H), 6.04 (t, $J = 9.5$ Hz, 1H), 3.88 (s, 2H), 2.94 (s, 6H).

¹⁹F NMR (471 MHz, CDCl₃): δ -142.41 (m), -145.06 (m).

Lab book reference number: JM-B-167-P



Dichloropalladium-bis-2,4-difluoro-*N,N*-dimethylbenzylamine (2.28d)

The *title compound* was prepared according to general procedure C, on a 0.29 mmol scale, to afford the product as an orange powder (111 mg, 73%).

M.p 132.0–135.4 °C (dec.).

¹H NMR (500 MHz, CDCl₃) δ 8.77 (ddd, $J = 8.8, 5.5, 3.2$ Hz, 2H), 7.12 (ddd, $J = 14.3, 7.3, 3.7$ Hz, 4H), 3.90 (s, 4H), 2.60 (s, 12H).

¹³C NMR (126 MHz, CDCl₃) δ 158.4 (dd, $J = 242.4, 2.2$ Hz), 157.9 (dd, $J = 243.70, 2.5$ Hz), 123.1 (dd, $J = 16.62, 8.12$ Hz), 120.5 (dd, $J = 24.9, 3.7$ Hz), 117.6 (dd, $J = 24.1, 8.9$ Hz), 116.8 (dd, $J = 26.1, 8.6$ Hz), 60.1, 54.0 (d, $J = 0.6$ Hz).

¹⁹F NMR (376 MHz, CDCl₃) –118.22 (m), –121.50 (m).

HRMS (ESI) m/z 483.0453 (100%, [$M+H-Cl$]⁺), (calculated for C₁₈H₂₂F₄N₂PdCl 483.0441, difference $\Delta = -1.2$ mDa).

CHN Anal. Calcd for C₁₈H₂₂F₄N₂Cl₂Pd: C, 41.60; H, 4.27; N, 5.39. Found: C, 41.28; H, 4.14; N, 5.13.

Lab book reference number: JM-C-292

Di- μ -chloro-bis-[*o*-dimethylaminomethyl-3-*p*-chlorophenyl-*C,M*] dipalladium(II) (2.8g₆)

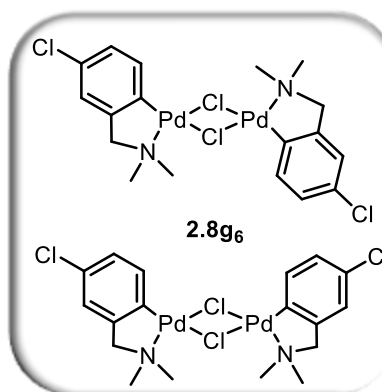
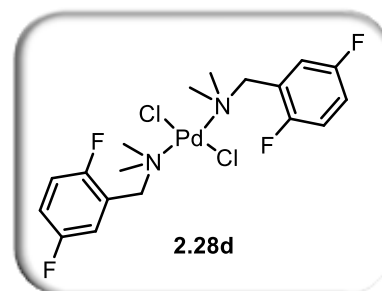
The *title compound* was prepared according to General Procedure C, on a 0.12 mmol scale, to afford the product in a mixture of geometrical isomers (*syn* and *anti*) as a dark green powder (23.8 mg, 63%).

M.p. 178.5–179.6 °C (dec).

¹H NMR (400 MHz, CDCl₃) δ 7.08 (m, 2H) 6.90–6.85 (m, 4H), 3.89 (s, 4H), 2.85 (s, 6H), 2.82 (s, 6H).

¹³C NMR (100 MHz, CDCl₃) δ , 148.2 (s, *major* isomer), 148.1 (s, *minor* isomer), 140.5 (s, *major* isomer), 140.4 (s, *minor* isomer), 134.6 (s, *minor* isomer), 134.1 (s, *major* isomer), 131.6 (s, *minor* isomer), 130.9 (s, *major* isomer), 125.2 (s, *minor* isomer), 125.1 (s, *major* isomer), 121.7 (s, *major* and *minor* isomers), 73.0 (s, *minor* isomer), 72.9 (s, *major* isomer), 53.1 (s, *major* isomer), 52.8 (s, *minor* isomer).

LRMS (LIFDI) m/z 621.82 (100%, [M]⁺).

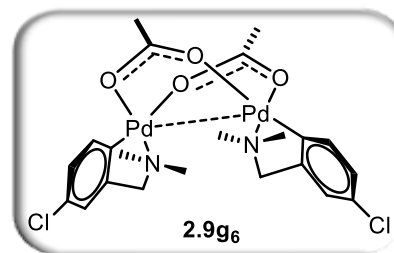


CHN Anal. Calcd for $C_{18}H_{22}N_2Cl_4Pd_2 \cdot CH_3OH$: C, 33.88; H, 3.63; N, 4.39. Found: C, 33.69; H, 3.40; N, 4.23.

Lab book reference: JM-C-209

Di- μ -acetato-bis-[*o*-dimethylaminomethyl-3-*p*-chlorophenyl-*C,N*] dipalladium(II) (2.9g₆**)**

The *title compound* was prepared according to General Procedure D, on a 0.18 mmol scale, to afford the product as green powder (52.6 mg, 87%).



M.p. 175.8–176.6 °C (dec.).

¹H NMR (400 MHz, $CDCl_3$) δ 6.97–6.87 (m, 2H, H-1), 6.74 (m, 4H, H-2, H-4), 3.55 (d, $J = 13.9$ Hz, 2H, CHH'), 3.10 (d, $J = 13.9$ Hz, 2H, CHH'), 2.78 (s, 6H, NCH_3), 2.08 (s, 6H, NCH_3), 2.05 (s, 6H, CH_3CO).

¹³C NMR (126 MHz, $CDCl_3$) δ 181.2 (CO), 148.8, 141.6, 133.3, 130.2, 124.8, 121.4, 72.0 (CH_2), 52.6 (NCH_3), 51.4 (NCH_3), 24.5 (CH_3CO).

LRMS (LIFDI) m/z 667.97 (100%, $[M]^+$).

CHN Anal. Calcd for $C_{22}H_{28}Cl_2N_2O_4Pd_2$: C, 39.54; H, 4.22; N, 4.19. Found: C, 39.27; H, 4.21; N, 3.95.

Lab book reference: JM-C-208

Biological tests

A2780 ovarian cancer cells were grown in RPMI 1640 medium enriched with 10% FBS and 1% L-glu. They were cultured with 0.25% EDTA-trypsin when 70–80% confluent. Cells were centrifuged for 5 min at 1000 rpm, suspended in 10 mL of medium and counted using a Vi-cell machine (Tot viable cells $1.27 \cdot 10^6$ cells/mL). Cells were diluted in order to have a concentration of 3000 cells per well (236 μ L in 10 mL); 100 μ L of dilute cells suspension were added to each well and the plates were left incubating overnight (21/08/2014).

[Di- μ -chloro-(*p*-3-fluoro-dimethylbenzylamine- *C,N*) dipalladium(II)] (**2.9c₆**) was dissolved in 0.1 mL of DMSO (0.44 %) and medium was added (total volume of 10 mL). The solution was sterilised through a filter and diluted as reported in Table 23. An aliquot (100 μ L) of the prepared solution were added to each well. On the plate two controls were set up (one positive and one negative), and the plate was left incubating for three days.

MTT was dissolved in PBS (around 10.6 mg in 5.5 mL for each plate), filtered through sterilising filters and 50 μL of the solution was added to each well. The plate was left incubating for 2 hours and then centrifuged for 10 mins at 500 rpm. A portion (220 μL) of medium was removed from wells and DMSO (150 μL) was added to dissolve the formazan (precipitate formed after metabolism, see Section 2.5 in Chapter 2). Absorbance was recorded at 540 nm using the plate reader and cell viability plotting as percentage from negative to positive controls. The fitting was done using Origin Functions (Non linear fitting: Growth/ Sigmoidal –Logistic curve) and X_0 on the graphs is the IC_{50} .

All biological tests were carried out in collaboration with Dr Luisa Ciano (member of Paul Walton research group in York).

Table 23: Dilution of compound 2.9c₆ for biological tests

MTT Calculator				Experiment Identifier: JM-C-244						
The Drug and experiment				JM-B-178						
M_r	588.12	g / mol	Mass	4.3	mg	conc range	2 %			
# plates	1		Drug Vol. / well	100	μL	Well Vol.	200 μL			
Vol Req	800	μL	Vol. make	1000	μL	Drug:Well	2			
The Stock Solution		Dilute Solution A		Dilute Solution B						
Volume	10	mL	Volume	5	mL	Volume	5			
Conc. Fact.	1	x	Conc. Fact	0.1	x	Conc Fac	0.2			
Target Conc.	516	μM	Target Con.	51.6	μM	Target Con.	103.2			
Target Mass	3.034699	mg	Vol. Stock	0.355	mL	Vol. A	9.945			
			Vol. PBS	4.645	mL	Vol. PBS	-4.945			
Real Conc.	731.1	μM	Real Conc.	51.9	μM	Real Conc.	103.3			
Vol. Req	1.435	mL	Vol. Req	19.79	mL	Vol. Req	9.945			
Concentrations to test										
2	3	4	5	6	7	8	9	10	11	
258	128	64	32	16	8	4	2	1	0.5	μM
2.412	2.107	1.806	1.505	1.204	0.903	0.602	0.301	0.000	-0.301	
Solution Prep - Stock Solution										
2	3	4	5	6	7	8	9	10	11	
259.556	129.778	65.803	32.901	16.451	9.139	5.484	3.656	1.828	1.828	μM
710	355	180	90	45	25	15	10	5	5	μL
290	645	820	910	955	975	985	990	995	995	μL
Solution Prep - Stock Solution										
2	3	4	5	6	7	8	9	10	11	
258.128	128.091	64.110	32.055	16.092	8.046	4.023	2.076	1.038	0.519	μM
9945	4935	2470	1235	620	310	155	80	40	20	μL
-8945	-3935	-1470	-235	380	690	845	920	960	980	μL

7.3.2 Compounds in Chapter 3

2-Fluoro-diphenylbenzylphosphine (3.2)

The *title compound* was prepared according to General Procedure F, on a 10 mmol scale, as white powder (1.33 g, 45%).

M.p. 76.9–85.9 °C.

¹H NMR (400 MHz, C₆D₆) δ 7.40–7.33 (m, 4H), 7.06–7.01 (m, 6H), 6.91 (m, 1H), 6.76 (m, 2H), 6.66 (td, *J* = 1.6, 7.3 Hz, 1H), 3.34 (s, 2H, CH₂).

³¹P NMR (161.8 MHz, C₆D₆) δ -10.91 (d, *J*_{P-F} = 13.2 Hz).

¹⁹F NMR (376 MHz, C₆D₆) δ -116.84 (m).

¹³C NMR (126 MHz, CDCl₃) δ 161.0 (dd, *J* = 245.4, 4.3, Hz), 138.1 (d, *J* = 15.0 Hz), 133.1 (d, *J* = 18.8 Hz), 131.4 (dd, *J* = 7.8, 4.3, Hz), 129.1 (s), 128.5 (d, *J* = 6.6 Hz), 127.8 (dd, *J* = 8.1, 2.6 Hz), 124.8 (dd, *J* = 15.3, 8.3, Hz), 123.9 (dd, *J* = 3.5, 1.7, Hz), 115.4 (dd, *J* = 22.2, 1.4 Hz), 28.6 (d, *J* = 16.2 Hz).

HRMS (ESI) *m/z* calculated for C₁₉H₁₇FP 295.1046 [*M*-H]⁺, found *m/z* 295.1053 (Δ = -0.6 mDa).

CHN Anal. Calcd for C₁₉H₁₆FP: C, 77.54; H, 5.48; Found: C, 77.76; H, 5.52.

Lab book reference number: JM-B-142, JM-C-316

3-Fluoro-diphenylbenzylphosphine (3.3)

The *title compound* was prepared according to General Procedure F, on a 10 mmol scale, as white powder (1.14 g, 39%).

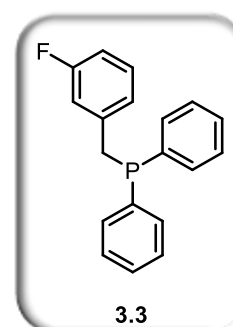
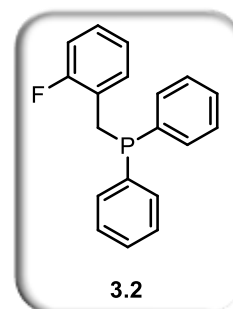
M.p. 57.3–57.8 °C.

¹H NMR (400 MHz, CDCl₃) δ 7.43–7.36 (m, 4H), 7.15–7.11 (m, 6H), 6.91–6.81 (m, 2H), 6.78 (m, 1H), 6.73 (ddd, *J* = 9.7, 2.4, 1.2 Hz, 1H), 3.20 (s, 2H, CH₂).

³¹P NMR (161.8 MHz, C₆D₆) δ -9.94 (s).

¹⁹F NMR (376 MHz, C₆D₆) δ -113.47 (m).

¹³C NMR (126 MHz, CDCl₃) δ 163.2 (dd, *J* = 245.2, 1.9 Hz), 140.7 (dd, *J* = 8.4, 7.7 Hz), 138.7 (d, *J* = 16.3 Hz), 133.3 (d, *J* = 18.8 Hz), 129.9 (dd, *J* = 8.4, 1.6, Hz), 129.0 (s), 128.7



(d, $J = 6.4$ Hz), 125.3 (dd, $J = 6.8, 2.8$ Hz), 116.6 (dd, $J = 21.4, 6.6$, Hz), 113.1 (dd, $J = 21.0, 2.6$ Hz), 36.1 (dd, $J = 17.2, 1.9$ Hz).

HRMS (ESI) calculated for $C_{19}H_{17}FP$ m/z 295.1046 $[M-H]^+$, found m/z 295.1039 $[M-H]^+$ ($\Delta = 0.7$ mDa).

CHN Anal. Calcd for $C_{19}H_{16}F_1P_1$: C, 77.54; H, 5.48; Found: C, 77.12; H, 5.46.

Lab book reference number: JM-B-148, JM-C-317

3,4-Difluoro-diphenylbenzophosphine (3.4)

The *title compound* was prepared according to General Procedure F, on a 10 mmol scale, as white powder (1.74 g, 51%).

M.p. 140.6–147.5 °C.

1H NMR (500 MHz, C_6D_6) δ 7.31–7.24 (m, 4H), 7.10–7.01 (m, 6H), 6.64 (ddt, $J = 11.2, 7.6, 1.7$ Hz, 1H), 6.55 (m, 1H), 6.41 (m, 1H), 2.99 (s, 2H, CH_2).

^{31}P NMR (202.5 MHz, C_6D_6) δ –10.00 (s).

^{19}F NMR (470.6 MHz, C_6D_6) δ –138.14 (m), –141.68 (m),

^{13}C NMR (126 MHz, C_6D_6) δ 150.4 (ddd, $J = 247.3, 12.7, 1.8$ Hz), 149.1 (ddd, $J = 245.9, 12.7, 3.0$ Hz), 138.4 (d, $J = 16.0$ Hz), 135.0 (ddd, $J = 9.0, 5.8, 3.9$ Hz), 133.2 (d, $J = 18.7$ Hz), 129.1 (s), 128.7 (d, $J = 6.5$ Hz), 125.5 (td, $J = 6.3, 3.5$ Hz), 118.3 (dd, $J = 17.2, 6.6$ Hz), 117.0 (d, $J = 17.6$ Hz), 35.3 (dd, $J = 17.2, 1.0$ Hz).

HRMS (ESI) m/z calculated for $C_{19}H_{16}F_2P$ 313.0952 $[M-H]^+$, found m/z 313.0942 $[M-H]^+$ ($\Delta = 1.0$ mDa).

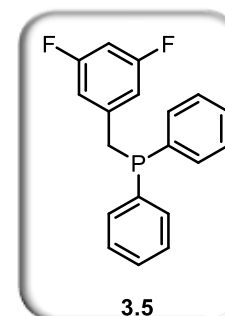
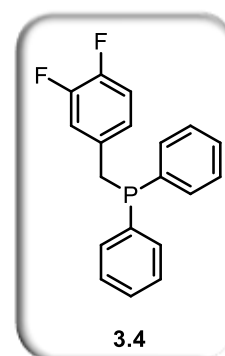
CHN Anal. Calcd for $C_{19}H_{16}F_2P_1$: C, 73.07; H, 4.84; Found: C, 73.76; H, 4.94;

Lab book reference number: JM-C-270-3

3,5-Difluoro-diphenylbenzophosphine (3.5)

The *title compound* was prepared according to General Procedure F, on a 11 mmol scale, as white powder (1.82 g, 53%).

1H NMR (500 MHz, $CDCl_3$) δ 7.41–7.31 (m, 10H), 6.61–6.51 (m, 3H), 3.37 (s, 2H, CH_2).



^{31}P NMR (203 MHz, CDCl_3) δ -8.99 (s).

^{19}F NMR (470.6 MHz, CDCl_3) δ -110.49 (m).

^{13}C NMR (126 MHz, CDCl_3) δ 162.9 (ddd, $J = 247.7, 13.2, 1.6$ Hz), 137.5 (d, $J = 14.8$ Hz), 134.5 (t, $J = 12.9$ Hz), 133.0 (d, $J = 18.7$ Hz), 129.2 (s), 128.7 (d, $J = 6.6$ Hz), 112.2 (m), 101.6 (td, $J = 25.3, 2.2$ Hz), 36.2 (d, $J = 17.1$ Hz).

HRMS (ESI) m/z calculated for $\text{C}_{19}\text{H}_{16}\text{F}_2\text{P}$ 313.0952 $[\text{M}-\text{H}]^+$, found m/z 313.0948 $[\text{M}-\text{H}]^+$ ($\Delta = 0.4$ mDa).

Lab book reference number: JM-C-138, JM-C-291

Di- μ -chloro-bis-[*o*-diphenylphosphinomethyl-2-difluorophenyl-*C,P*] dipalladium(II)
(3.23)

The *title compound* was prepared according to General Procedure G, on a 0.26 mmol scale, to afford the product in a mixture of geometrical isomers (*syn* and *anti*) as a yellow powder (96 mg, 42%).

M.p. 228.0–230.1 °C.

^1H NMR (500 MHz, CDCl_3) δ 7.82 (dd, $J = 11.8, 7.7$ Hz, 5H, Ph), 7.70 (dd, $J = 12.0$ Hz, 3H, Ph), 7.66 (dd, $J = 7.8, 4.5$ Hz, 1H, benzyl), 7.52–7.40 (m, 8H, Ph), 7.39–7.32 (m, 4H, Ph), 6.99 (dd, $J = 12.7, 7.8$ Hz, 1H, benzyl), 6.87 (dd, $J = 13.8, 7.8$ Hz, 1H, benzyl), 6.77–6.67 (m, 2H benzyl), 3.84 (d, $J = 11.8$ Hz, 2H, *minor isomer*), 3.83 (d, $J = 11.8$ Hz, 2H *major isomer*).

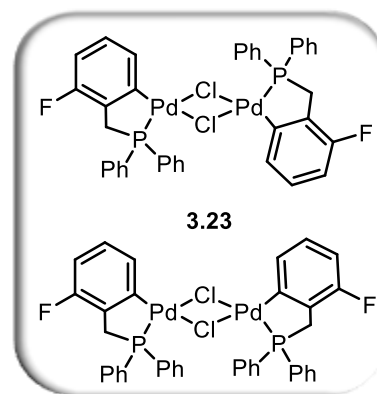
^{31}P NMR (202.5 MHz, CDCl_3) δ 58.81 (s, *major isomer*), 58.37 (s, *minor isomer*).

^{19}F NMR (470.6 MHz, CDCl_3): δ -110.58 (m, *major isomer*), -110.70 (m, *minor isomer*).

LRMS (LIFDI) m/z 869.92 (100%, $[\text{M}]^+$).

CHN Anal. Calcd for $\text{C}_{38}\text{H}_{30}\text{F}_2\text{P}_2\text{Cl}_2\text{Pd}_2 \cdot \text{CHCl}_3 \cdot \text{C}_6\text{H}_6$: C, 50.62; H, 3.49; Found: C, 51.0; H, 3.67. (Single crystal grown in $\text{CHCl}_3/\text{benzene}$)

Lab book reference number: JM-B-144, JM-D-324



Di- μ -chloro-bis-[*o*-diphenylphosphinomethyl-3-*p*-difluorophenyl-*C,P*] dipalladium(II) (3.28*p*)

The *title compound* was prepared according to General Procedure G, on a 0.13 mmol scale, to afford the product in a mixture of geometrical isomers (*syn* and *anti*) as a yellow powder (93 mg, 84%).

M.p. 198.5–199.7°C.

¹H NMR (500 MHz, CDCl₃) δ 7.85 (m, 1H, benzyl), 7.81 (m, 4H, Ph), 7.73–7.65 (m, 3H, Ph), 7.56 (m, 1H, benzyl), 7.52–7.39 (m, 10H, Ph), 7.39–7.31 (m, 5H, Ph), 6.84 (dd, $J = 9.6, 2.8$ Hz, 2H, benzyl), 6.74 (td, $J = 8.9, 2.8$ Hz, 1H, benzyl), 6.62 (td, $J = 9.0, 2.7$ Hz, 1H, benzyl), 3.79 (d, $J = 12.1$ Hz, 2H, CH₂, *major isomer*), 3.78 (d, $J = 12.4$ Hz, 2H, CH₂, *minor isomer*).

¹³C NMR (125.8 MHz, C₆D₆) δ 150.4 (ddd, $J = 247.3, 12.7, 1.8$ Hz), 149.1 (ddd, $J = 245.9, 12.7, 3.0$, Hz), 138.4 (d, $J = 16.0$ Hz), 135.0 (ddd, $J = 9.0, 5.8, 3.9$ Hz), 133.2 (d, $J = 18.7$ Hz), 129.1 (s), 128.7 (d, $J = 6.5$ Hz), 125.5 (td, $J = 6.3, 3.5$ Hz), 118.3 (dd, $J = 17.2, 6.6$ Hz), 117.0 (d, $J = 17.6$ Hz), 35.3 (dd, $J = 17.2, 1.0$ Hz).

³¹P NMR (202.5 MHz, CDCl₃) δ 54.99 (s, *major isomer*), 54.59 (s, *minor isomer*).

¹⁹F NMR (470.6 MHz, CDCl₃): δ -118.52 – -118.60 (m, *minor isomer*), -118.62 – -118.70 (m, *major isomer*).

LRMS (LIFDI) m/z 869.92 (100%, [M]⁺).

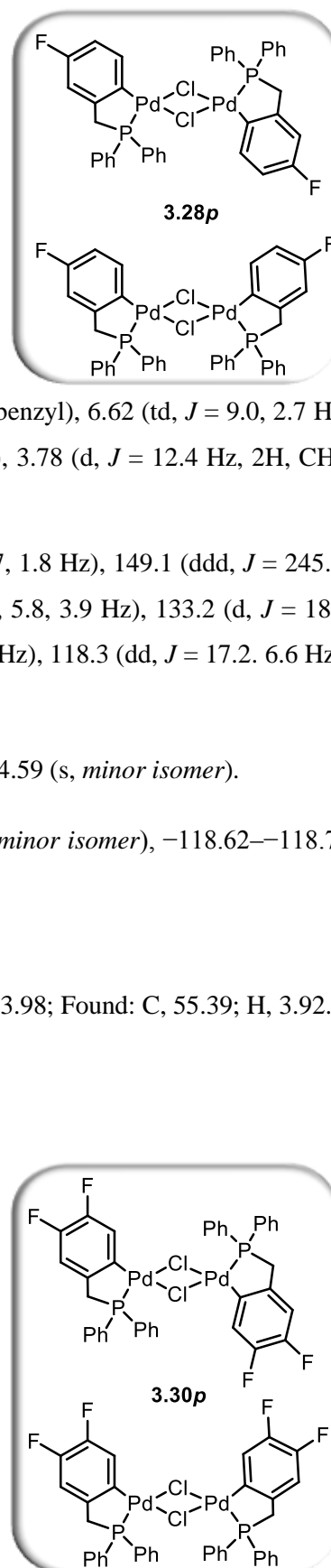
CHN Anal. Calcd for C₃₈H₃₀F₂P₂Cl₂Pd₂·C₇H₈: C, 56.16; H, 3.98; Found: C, 55.39; H, 3.92.

Lab book reference number: JM-B-149, JM-D-323

Di- μ -chloro-bis-[*o*-diphenylphosphinomethyl-3,5-*p,o*-difluorophenyl-*C,P*] dipalladium(II) (3.30*p*)

The *title compound* was prepared according to General Procedure G, on a 0.15 mmol scale, to afford the product in a mixture of geometrical isomers (*syn* and *anti*) as a yellow powder (47 mg, 42%).

M.p. 194.5–195.8 °C.



¹H NMR (500 MHz, CDCl₃) δ 7.90–7.61 (m, 6 H), 7.60–7.33 (m, 14H), 7.23–7.16 (m, 2H, *minor* and *major isomers*), 6.99–6.89 (m, 2H, *minor* and *major isomers*), 3.76 (d, *J* = 12.2 Hz, 4H, *minor* and *major isomers*, CH₂).

³¹P NMR (202.5 MHz, CDCl₃) δ 54.54 (s, *major isomer*), 54.07 (s, *minor isomer*).

¹⁹F NMR (470.6 MHz, CDCl₃): δ -142.61 – -142.79 (m, *major isomer*), -141.14 – -141.31 (m, *major isomer*), -140.66 – -140.75 (m, *minor isomer*), -142.43 – -142.59 (m, *minor isomer*).

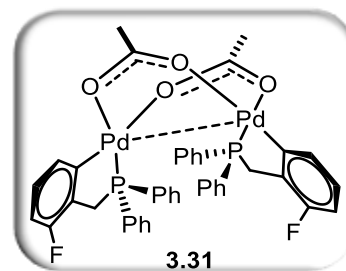
LRMS (LIFDI) *m/z* 905.93 (100%, [M]⁺).

CHN Anal. Calcd for C₃₈H₂₈F₄P₂Cl₂Pd₂·0.65CHCl₃: C, 47.18; H, 2.94; Found: C, 47.25; H, 2.95.

Lab book reference number: JM-D-296, JM-D-322

Di-μ-acetato-bis-[*o*-diphenylphosphinomethyl-2-difluorophenyl-*C,P*] dipalladium(II) (3.31)

The *title compound* was synthesized from chloride-bridged palladacycle **3.23** using a modified version of the procedure reported by Cotton and co-workers (General procedure B).²³¹



To a solution of chloride-bridged amino-derived palladacycle **3.23** (0.034 mmol, 1 eq.) in acetone (100 mL mol⁻¹), was added silver acetate (0.068 mmol, 2 eq.). The reaction mixture was stirred for 24 hours at 25 °C. The resulting yellowish solution was filtered through Celite to remove the excess silver acetate, and reduced to dryness *in vacuo* to obtain the product as yellow powder (23 mg, 68% yield). The product was crystallized by slow diffusion of hexane into a saturated solution in chloroform.

¹H NMR (400 MHz, CDCl₃) δ 7.54–7.39 (m, 6H), 7.36–7.21(m, 6H), 7.21–7.07 (m, 8H), 6.77 (ddd, *J* = 7.5, 4.3, 1.0 Hz, 2H), 6.68–6.52 (m, 4H), 3.21 (t, *J* = 15.3 Hz, 2H, CHH'), 2.83 (dd, *J* = 15.3, 9.7 Hz, 2H, CHH'), 1.96 (s, 6H, CH₃CO).

¹³C NMR (126 MHz, CDCl₃) δ 180.0 (CO), 133.8 (d, *J* = 13.64 Hz), 133.1 (m), 132.7 (d, *J* = 1.5 Hz), 131.9 (d, *J* = 11.0 Hz), 131.02 (d, *J* = 12.0 Hz), 128.4 (m), 127.5 (d, *J* = 6.4 Hz), 111.01 (d, *J* = 21.0 Hz), 24.9 (d, *J* = 3.6 Hz, CH₃CO).

³¹P NMR (161.8 MHz, C₆D₆) δ 53.71.

¹⁹F NMR (471 MHz, CDCl₃) δ -112.50 (m).

HRMS (LIFDI) m/z 918.0127 (100%, $[M]^+$).

Lab book reference number: JM-C-249

7.3.3 Compounds in Chapter 4

$[(\eta^6\text{-C}_{10}\text{H}_{15})\text{Ir}(2\text{F-C}_6\text{H}_3\text{-6-CH}_2\text{NMe}_2)\text{Cl}]$ (4.7)

The *title compound* was prepared according to General Procedure I, on a 0.11 mmol scale, as an orange powder (36.8 mg, 68%).

$^1\text{H NMR}$ (400 MHz, CDCl_3) δ 7.35 (d, $J = 7.5$ Hz, 1H), 6.99 (dd, $J = 13.9, 7.6$ Hz, 1H), 6.55 (m, 1H), 4.27 (d, $J = 13.3$ Hz, 1H), 3.54 (dd, $J = 13.3, 1.1$ Hz, 1H), 3.07 (s, 3H), 2.90 (s, 3H), 1.63 (s, 15H).

$^{19}\text{F NMR}$ (376 MHz, CDCl_3) δ -117.48 (dd, $J = 9.7, 6.0$ Hz).

$^{13}\text{C NMR}$ (126 MHz, CDCl_3) δ 158.4 (d, $J_{\text{C-F}} = 247.0$ Hz, C-2), 155.0 (C-6), 134.0 (d, $J = 9.1$ Hz, C-1), 130.0 (d, $J = 2.5$ Hz, C-4), 127.8 (d, $J = 6.8$ Hz, C-5), 108.8 (d, $J = 20.6$ Hz, C-3), 87.8 (C_5Me_5), 68.1 (NCH₂), 57.7 (NMe), 51.9 (NMe), 9.4 (C_5Me_5).

HRMS (LIFDI) m/z 515.1376 (100%, $[M]^+$).

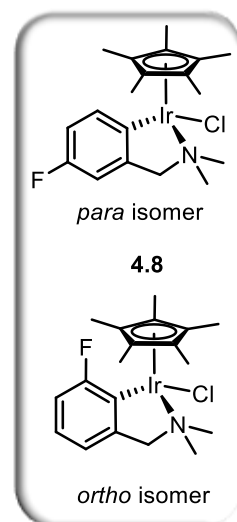
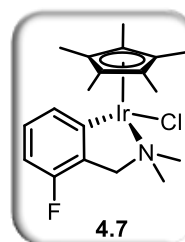
Lab book reference number: JM-D-334

Mixture of isomers of $[(\eta^6\text{-C}_{10}\text{H}_{15})\text{Ir}(3\text{F-C}_6\text{H}_3\text{-6-CH}_2\text{NMe}_2)\text{Cl}]$ (4.8)

The *title compound* was prepared according to General Procedure I, on a 0.11 mmol scale, as an orange powder (27.4 g, 49%, ratio *ortho:para* = 1:0.6).

$^1\text{H NMR}$ (400 MHz, CDCl_3) δ 7.49 (dd, $J = 8.3, 6.3$ Hz, 1H, *ortho* isomer), 6.87–6.77 (m, 4H, *ortho* and *para* isomers), 6.77–6.67, m, 2H, *ortho* and *para* isomers), 4.38 (d, $J = 13.0$ Hz, 1H, NCHH *para* isomer), 4.08 (d, $J = 12.8$ Hz, 1H, NCHH *ortho* isomer), 3.52 (d, $J = 12.9$ Hz, 1H, NCHH, *ortho* isomer), 3.20 (d, $J = 12.4$ Hz, 1H, NCHH, *para* isomer), 3.04 (s, NMe, 3H, *para* isomer), 3.02 (s, NMe, 3H, *ortho* isomer), 2.87 (s, NMe, 3H, *para* isomer), 2.77 (s, NMe, 3H, *ortho* isomer), 1.65 (d, $J = 0.7$ Hz, 15H, *ortho* isomer), 1.62 (s, 15H, *para* isomer).

$^{19}\text{F NMR}$ (376.2 MHz, CDCl_3) δ -123.78 (td, $J = 9.7, 6.3$ Hz, *para* isomer), -94.21 (m, *ortho* isomer).



^{13}C NMR (125.76 MHz, CDCl_3) *ortho* isomer δ 166.7 (d, $J_{\text{C-F}} = 234.5$ Hz, C-5), 150.0 (d, $J = 15.0$ Hz, C-6), 136.8 (d, $J = 39.6$ Hz, C-4), 124.1 (d, $J = 7.8$ Hz, C-2), 117.5 (d, $J = 2.3$ Hz, C-1), 113.3 (d, $J = 29.8$ Hz, C-3), 88.2 (C_5Me_5), 75.0 (d, $J = 1.3$ Hz, NCH_2), 57.5 (NMe), 52.0 (NMe), 9.9 (d, $J = 3.4$ Hz C_5Me_5).

para isomer δ 160.34 (d, $J = 237.8$ Hz, C-3), 149.6 (d, $J = 6.1$ Hz, C-6), 144.6 (d, $J = 3.1$ Hz, C-5), 134.8 (d, $J = 6.3$ Hz, C-1), 113.0 (d, $J = 18.5$ Hz, C-2), 108.8 (d, $J = 20.5$ Hz, C-4), 87.4 (C_5Me_5), 73.3 (d, $J = 2.9$ Hz, NCH_2), 57.3 (NMe), 51.7 (NMe), 9.4 (d, $J = 3.4$ Hz C_5Me_5).

HRMS (LIFDI) m/z 515.1358 (100%, $[\text{M}]^+$).

Lab book reference number: JM-D-333

$[(\eta^6\text{-C}_6\text{H}_6)\text{Ru}(2\text{-F-C}_6\text{H}_4\text{-6-CH}_2\text{NMe}_2)(\text{CH}_3\text{CN})]\text{PF}_6$ (4.11)

The *title compound* was prepared according to General Procedure J, on a 0.1 mmol scale, as a white powder (38.5 mg, 74%).

^1H NMR (500 MHz, CD_3CN) δ 7.88 (d, $J = 7.5$ Hz, 1H), 7.09 (dd, $J = 13.6, 7.6$ Hz, 1H), 6.70 (m, 1H), 5.68 (s, 6H), 3.66 (d, $J = 13.5$ Hz, 1H), 3.53 (d, $J = 14.2$ Hz, 1H), 3.03 (s, 3H), 2.76 (s, 3H).

^{19}F NMR (470.6 MHz, CD_3CN) δ -117.34 (m).

LRMS (LIFDI) m/z 373.06 (100%, $[\text{M}]^+$).

Lab book reference number: JM-D-302-1

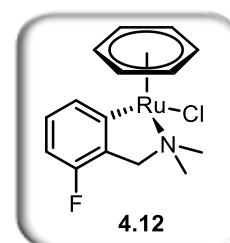
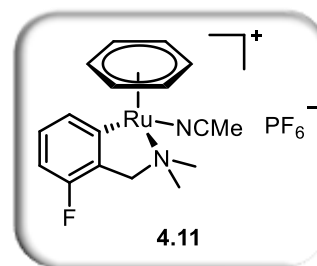
$[(\eta^6\text{-C}_6\text{H}_6)\text{Ru}(2\text{-F-C}_6\text{H}_4\text{-6-CH}_2\text{NMe}_2)\text{Cl}]$ (4.12)

The *title compound* was prepared according to General Procedure J, on a 0.06 mmol scale, as an orange powder (15.5 mg, 55%).

^1H NMR (500 MHz, CD_3CN) δ 7.99 (d, $J = 7.38$ Hz, 1H), 6.99 (m, 1H), 6.53 (dd, $J = 23.9, 15.3$ Hz, 1H), 5.39 (s, 6H), 3.99 (d, $J = 13.3$ Hz, 1H), 3.24 (s, 3H), 3.13 (d, $J = 13.3$ Hz, 1H), 2.66 (s, 3H).

^{19}F NMR (400 MHz, C_6D_6) δ -118.76 (dd, $J = 9.6, 5.7$ Hz).

^{13}C NMR (125.76 MHz, CDCl_3) δ 161.0 (dd, $J = 245.4, 4.3$ Hz), 138.1 (d, $J = 15.0$ Hz), 133.1 (d, $J = 18.8$ Hz), 131.4 (dd, $J = 7.8, 4.3$ Hz), 129.1 (s), 128.5 (d, $J = 6.6$ Hz), 127.8



(dd, $J = 8.1, 2.6$ Hz), 124.8 (dd, $J = 15.3, 8.3$ Hz), 123.9 (dd, $J = 3.5, 1.7$ Hz), 115.4 (d, $J = 22.2, 1.4$ Hz), 28.6 (d, $J = 16.2$ Hz).

HRMS (LIFDI) m/z 367.0053 (100%, $[M]^+$).

Lab book reference number: JM-D-302-2

Mixture of isomers of $[(\eta^6\text{-C}_6\text{H}_6)\text{Ru}(3\text{-F-C}_6\text{H}_4\text{-6-CH}_2\text{NMe}_2)(\text{CH}_3\text{CN})]\text{PF}_6$ (4.13)

The *title compound* was prepared according to General Procedure J, on a 0.10 mmol scale, as a dark orange powder (32.7 mg, 63%, ratio *ortho* : *para* = 10:90).

$^1\text{H NMR}$ (500 MHz, CD_3CN) *ortho* isomer δ 7.01 (m, 1H), 6.87 (m, 2H), 5.81 (s, 6H), 3.73 (d, $J = 13.9$ Hz, 1H), 3.38 (d, $J = 13.9$ Hz, 1H), 2.97 (s, 3H), 2.75 (s, 3H).

para isomer δ 8.01 (dd, $J = 8.2, 6.3$ Hz, 1H), 6.81 (m, 3H), 5.65 (s, 6H), 3.68 (d, $J = 14.0$ Hz, 1H), 3.29 (d, $J = 13.9$ Hz, 1H), 2.98 (s, 3H), 2.73 (s, 3H).

$^{19}\text{F NMR}$ (471MHz, CD_3CN) δ -123.03 (m) *ortho* isomer, -93.55 (m) *para* isomer.

LRMS (LIFDI) m/z 373.06 (100%, $[M]^+$).

Lab book reference number: JM-D-303-1

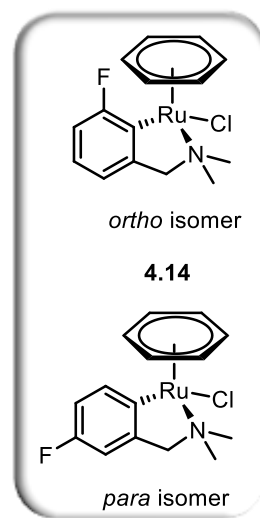
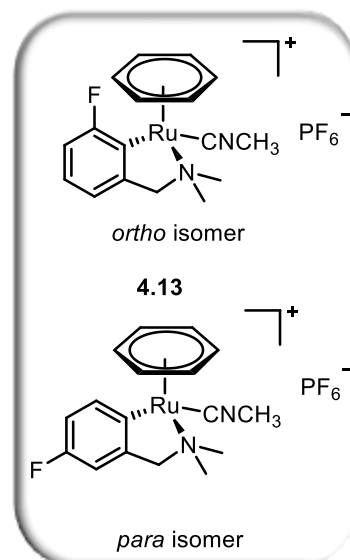
Mixture of isomers of $[(\eta^6\text{-C}_6\text{H}_6)\text{Ru}(3\text{-F-C}_6\text{H}_4\text{-6-CH}_2\text{NMe}_2)\text{Cl}]$ (4.14)

The *title compound* was prepared according to General Procedure J, on a 0.06 mmol scale, as a white powder (14.1 mg, 50%, ratio *ortho:para* = 10:1.0

$^1\text{H NMR}$ (500 MHz, CD_3CN) *ortho* isomer δ 6.87 (dd, $J = 13.4, 7.3$ Hz, 1H), 6.76 (m, 2H), 5.56 (s, 6H), 4.16 (d, $J = 13.0$ Hz, 1H), 3.19 (s, 3H), 2.90 (d, $J = 13.0$ Hz, 1H), 2.66 (s, 3H).

para isomer δ 7.01 (m, 1H), 6.87 (dd, $J = 13.4, 7.3$ Hz, 1H), 6.76 (m, 2H), 5.81 (s, 6H), 3.73 (d, $J = 13.9$ Hz, 1H), 3.38 (d, $J = 14.0$ Hz, 1H), 2.96 (s, 3H), 2.75 (s, 3H).

$^{19}\text{F NMR}$ (470.6 MHz, CD_3CN) δ -93.11 (m) *ortho* isomer. -93.53 (m) *para* isomer.

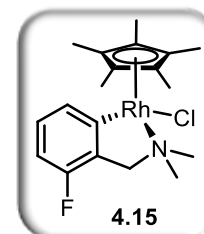


HRMS (LIFDI) m/z 367.0058 (100%, $[M]^+$).

Lab book reference number: JM-D-303-2

$[(\eta^6\text{-C}_{10}\text{H}_{15})\text{Rh}(\text{2-F-C}_6\text{H}_4\text{-6-CH}_2\text{NMe}_2)\text{Cl}]$ (4.15)

The *title compound* was prepared according to General Procedure J, on a 0.06 mmol scale, as a brown powder that was purified by recrystallisation from CH_2Cl_2 /pentane. The filtrate was collected and the solvent removed under reduced pressure to give the product as a dark orange powder (18.4 mg, 69%).



^1H NMR (500 MHz, CDCl_3) δ 7.35 (d, $J = 7.5$ Hz, 1H), 7.05 (d, $J = 13.5, 7.6$ Hz, 1H), 6.59 (t, $J = 8.9$ Hz, 1H), 4.02 (d, $J = 13.4$ Hz, 1H), 3.49 (d, $J = 13.3$ Hz, 1H), 2.76 (s, 3H), 2.75 (s, 3H), 1.59 (s, 15H).

^{19}F NMR (400 MHz, CDCl_3) δ -117.41 (m)

^{13}C NMR (125.76 MHz, CDCl_3) δ 169.4 (d, $J = 33.0$ Hz, C-6), 157.6 (d, $J_{\text{C-F}} = 248.9$ Hz, C-2), 131.7 (d, $J = 9.4$ Hz, C-1), 130.6 (d, $J = 2.7$ Hz, C-4), 127.7 (d, $J = 6.3$ Hz, C-5), 109.4 (d, $J = 20.7$ Hz, C-3), 95.5 (d, $J = 6.6$ Hz, NCH_2), 66.7 (C_5Me_5), 55.1 (NMe), 52.1 (NMe), 9.7 (C_5Me_5).

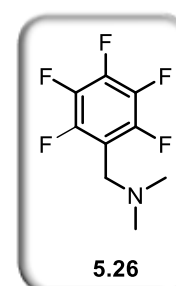
HRMS (LIFDI) m/z 425.0803 (100%, $[M]^+$).

Lab book reference number: JM-C-274-3

7.3.4 Compounds in Chapter 5

2,3,4,5,6-Pentafluoro- N,N -dimethylbenzylamine (5.26)

2,3,4,5,6-Pentafluoro-benzylbromide (0.5 mL, 6.6 mmol) was added to dimethylamine solution (2 M in MeOH, 5 mL, 19.8 mmol) in a sealed tube. The mixture was stirred for 4 hours at 20 °C. The solvent was then removed in *vacuo*, the residue dissolved in H_2O (30 mL) and adjusted to pH 12 with 1 M NaOH. The solution was then extracted with diethylether (3×60 mL), and the organic extracts dried with MgSO_4 and evaporated to obtain the *title compound* as a colourless oil (1.21 g, 82%).



^1H -NMR (500 MHz, CDCl_3) δ 3.64 (t, $J = 1.9$ Hz, 2H), 2.27 (t, $J = 1.0$ Hz, 6H).

^{13}C -NMR (126 MHz, CDCl_3) δ 145.7 (dm $^1J_{\text{C-F}} = 248.0$ Hz, C-3, C-5), 140.7 (dm $^1J_{\text{C-F}} = 252.5$ Hz, C-4), 137.6 (dm, $^1J_{\text{C-F}} = 252.5$ Hz, C-2, C-6), 111.0 (tm, $^1J_{\text{C-F}} = 19.6$ Hz, C-1), 49.7 (d, $^3J_{\text{C-F}} = 0.7$ Hz, NCH_2), 44.8 (s, NMe)

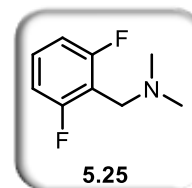
¹⁹F-NMR (470.6 MHz, CDCl₃) δ -141.89 (dd, $J = 22.1, 6.2$ Hz), -155.02 (t, $J = 20.6$ Hz), -162.29 (m).

HRMS (ESI) m/z 226.0650 (100%, $[M+H]^+$), (calculated for C₉H₉F₅N 226.0650, difference $\Delta = -0.5$ mDa).

Lab book reference number SF-A-10 and JM-C-217

***N,N*-Dimethyl-2,6-difluorobenzylamine (5.25)**

The *title compound* **5.25** was prepared according to General Procedure A, on a 6.6 mmol scale, as a colourless oil (658 mg, 58%).



¹H NMR (400 MHz, CDCl₃) δ 7.22 (m, 1H), 6.88 (m, 2H), 3.57 (s, 2H), 2.27 (s, 6H).

¹³C NMR (125 MHz, CDCl₃) δ 162.2 (d, $J_{C-F} = 248.0$ Hz), 129.3 (t, $J = 10.0$ Hz), 113.8 (t, $J = 20.0$ Hz), 111.2 (dd, $J = 26.0, 15.0$ Hz), 49.8, 45.0.

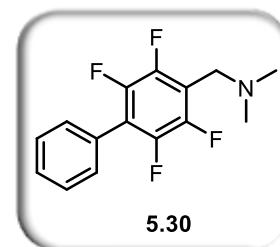
¹⁹F NMR (376 MHz, CDCl₃) δ -114.03 (t, $J = 6.4$ Hz).

HRMS (ESI) m/z 172.0932 (100%, $[M+H]^+$), (calculated for C₉H₁₂F₂N 172.0937, difference $\Delta = -0.5$ mDa).

Lab book reference number: SF-A-17

***N,N*-Dimethyl-2,3,4,5,6-pentafluoropyridine-4-phenylbenzylamine (5.30)**

The *title compound* was prepared according to General Procedure K, on a 1 mmol scale, and isolated after flash chromatography (SiO₂, CH₂Cl₂/MeOH, 10:1) as a yellow/orange powder (37.6 mg, 20%).



R_f: 0.23 (CH₂Cl₂:MeOH, 10:1).

¹H NMR (400 MHz, CDCl₃) δ 7.52–7.43 (m, 5H), 3.71 (s, 2H), 2.34 (s, 6H).

¹³C NMR (125 MHz, CDCl₃) δ 145.9 (dm, $J = 247.0$ Hz), 143.6 (dm, $J = 248.0$ Hz), 130.3 (t, $J = 2.0$ Hz), 129.2, 128.7, 127.7 (t, $J = 2.0$ Hz), 120.2 (t, $J = 17.0$ Hz), 115.2 (t, $J = 19.0$ Hz), 50.0 (t, $J = 2.0$ Hz), 45.0.

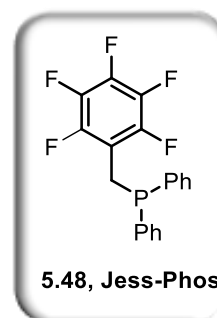
¹⁹F NMR (376 MHz, CDCl₃) δ -142.93 (dd, $J = 23.0, 13.1$ Hz), -144.52 (dd, $J = 23.0, 13.1$ Hz), -162.13 (m).

HRMS (ESI) m/z 284.1060 (100%, $[M+H]^+$), (calculated for C₁₅H₁₄F₄N 284.1057, $\Delta = -1.1$ mDa).

Lab book reference number: SF-A-7C

2,3,4,5,6-Pentafluoro-diphenylbenzylphosphine (Jess-Phos, 5.48)

A solution of TMEDA (1.2 eq, 0.33 mL, 2.4 mmol) in dry THF ((5 mL) was cooled to $-78\text{ }^{\circ}\text{C}$ and *sec*-BuLi (1.3 M in hexane, 1.69 mL, 2.4 mmol, 1.2 eq.) was added dropwise. After the solution has been stirred for 25 mins, a solution of Ph₂PMe (0.37 mL, 2 mmol, 1 eq) in dry THF (5 mL), prepared in the glovebox, was added dropwise. The mixture changed colour from colourless to orange and was left stirring for 2 hours at $-78\text{ }^{\circ}\text{C}$, after which time it was allowed to warm to room



temperature. After 15 mins the solution was cooled to $-78\text{ }^{\circ}\text{C}$ and transferred by cannula dropwise into a solution of C₆F₆ (2.30 mL, 20 mmol, 10 eq) in dry THF (5 mL) at $-78\text{ }^{\circ}\text{C}$. The addition was carefully controlled and slow enough to avoid any temperature rise. Soon after the beginning of the addition, the colourless solution began to change from orange to green and at the end of the addition became blue. The reaction was allowed to warm slowly to room temperature overnight. After 14 hours the orange solution was reduced to one third of its volume before being quenched with dry MeOH (10 mL) at $0\text{ }^{\circ}\text{C}$. The addition of dry hexane (8 mL) led to the formation of a yellow precipitate, which was removed by filtration. The hexane solution was evaporated *in vacuo* and the residue sublimed on in a Schlenk tube under an inert atmosphere using a cold finger filled with liquid nitrogen. The pure product sublimed onto the side of the Schlenk tube and was collected (205 mg, 28%) while the unreacted starting material Ph₂PMe sublimed directly onto the cold finger.

¹H NMR (500 MHz, C₆D₆) δ 7.31–7.04 (m, 10H, phenyl), 3.08 (br s, 2H, PCH₂).

¹³C-NMR (126 MHz, C₆D₆) 145.2 (dtt ¹J_{C-F} = 247 Hz, ²J_{C-F} = 11.7 Hz, ³J_{C-F} = 3.8 Hz), 139.7 (dm ¹J_{C-F} = 251 Hz), 137.7 (dm, ¹J_{C-F} = 249 Hz), 137.4 (d, ¹J_{C-P} = 16.3 Hz), 133.1 (d, ²J_{C-P} = 19.7 Hz), 129.5 (s), 128.8 (d, ³J_{C-P} = 6.8 Hz), 112.3 (tdd, ²J_{C-F} = 18 Hz, ³J_{C-F} = 3.3 Hz, ³J_{C-P} = 9 Hz), 23.1 (d, ¹J_{C-P} = 20.9 Hz).

³¹P NMR (202 MHz, C₆D₆) δ -10.00 (td, ⁴J_{P-F} = 21 Hz, ⁶J_{P-F} = 4.6 Hz).

¹⁹F NMR (471 MHz, C₆D₆) δ -141.9 (tdd *J* = 22.4, 7.5, 3.2 Hz), -157.8 (td *J* = 21.4, 4.6 Hz), -163.5 app td (*J* = 21.1, 6.7, 2.9 Hz).

HRMS (LIFDI) *m/z* (rel%) 366.0591 [*M*]⁺ (100), 366.0597 calcd for C₁₉H₁₂F₅P.

CHN Anal. Calcd for C₁₉H₁₂F₅P₁: C, 62.31; H, 3.30; Found: C, 59.29; H, 3.40. *CHN sample was contaminated during preparation in the glove box. See NMR spectra for purity.*

Lab book reference number: JM-C-258

Appendix I: Published paper

Reprinted with permission from [*Organometallics*, 2015, 34 (17), pp 4376–4386]. Copyright [2016] American Chemical Society.

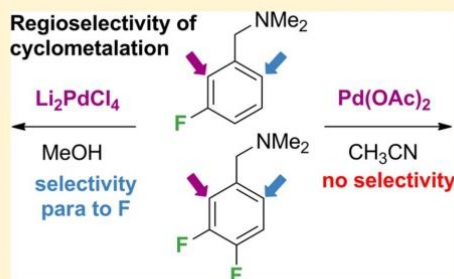
The Role of Fluorine Substituents in the Regioselectivity of Intramolecular C–H Bond Functionalization of Benzylamines at Palladium(II)

Jessica Milani, Natalie E. Pridmore, Adrian C. Whitwood, Ian J. S. Fairlamb,* and Robin N. Perutz*

Department of Chemistry, University of York, Heslington, York YO10 5DD, U.K.

Supporting Information

ABSTRACT: The effect of fluorine substituents on the regioselectivity of intramolecular reactions of mono- and difluorinated *N,N*-dimethylbenzylamines (1a–f) at palladium, to form palladacycles di- μ -acetatobis[*o*-dimethylaminomethyl-*n*-fluorophenyl-*C,N*]dipalladium(II) (2a–f) and di- μ -chlorobis[*o*-dimethylaminomethyl-*n*-fluorophenyl-*C,N*]dipalladium(II) (3a–e), has been investigated. When fluorinated substrates with two sites available for the C–H functionalization (1c and 1e) undergo cyclopalladation via a CMD mechanism (acetate-bridged palladacycles), they do not exhibit regioselectivity. In contrast, the same substrates exhibit complete regioselectivity for the C–H functionalization *para* to fluorine in cyclopalladation reactions that proceed via an S_EAr mechanism (involving chloride-bridged palladacycles). X-ray crystal structures were obtained for all the palladacycles synthesized, and a structural analysis showed that the number and the position of the fluorine atoms on the aromatic ring have a marked effect on the “clamshell” structure of the acetate-bridged palladacycles. By contrast, there is no great variation in the structures of the planar chloride-bridged palladacycles.



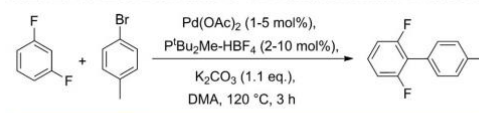
INTRODUCTION

The functionalization of a C–H bond to form a new C–C or C–Y (Y = heteroatom or halide) bond is an inherently efficient method for the construction of useful building blocks for natural products and pharmaceutical drugs.¹ Recent advances have made these reactions viable processes for the synthesis of an eclectic array of compounds,² offering an alternative to traditional cross-coupling reactions that require preactivation of both substrates.³ The control of the regioselectivity of the C–H bond functionalization, however, remains one of the challenges in the field.⁴ Methods employing directing groups⁵ in a proximal position to the target C–H site are widely used due to the high regioselectivity obtained, but they have limitations; for example the functionalization occurs only *ortho* to the directing group,⁵ with some exceptions.⁶ Functional groups, such as fluorine atoms, on the aromatic ring can be used to direct the C–H functionalization, or the C–F bond can itself be activated in a regioselective manner depending on the transition metal used and the mechanism of the catalytic or stoichiometric reaction.⁷

The mechanisms of direct arylation catalyzed by transition metals⁸ have been the subject of considerable debate.⁹ The most extensively studied and reported mechanisms are electrophilic aromatic substitution, S_EAr ,¹⁰ and concerted metalation deprotonation, CMD,¹¹ also known as AMLA(6).^{12,13} Fagnou and co-workers^{11a,14} investigated experimentally the effect of fluorine substituents on aromatic

rings in intermolecular C–H functionalization reactions proceeding via CMD, and Perutz and co-workers¹⁵ have performed DFT calculations on similar reactions (Scheme 1).

Scheme 1. Intermolecular C–H Functionalization Reaction



Competition experiments performed by Fagnou and co-workers^{11a} show that more electron-deficient arenes undergo intermolecular C–H functionalization reactions more rapidly and also that these reactions occur regioselectively *ortho* to fluorine substituents. In the CMD step two transformations occur simultaneously, the formation of a Pd–C bond and the cleavage of the C–H bond. The presence of fluorine, *ortho* to the target site, favors both processes because it can strengthen the Pd–C bond formed as well as increase the acidity of the arene.¹⁵ Several other examples of C–H functionalization of fluoroaromatics, catalyzed by palladium, iridium, and rhodium,

Received: July 14, 2015

Published: August 26, 2015

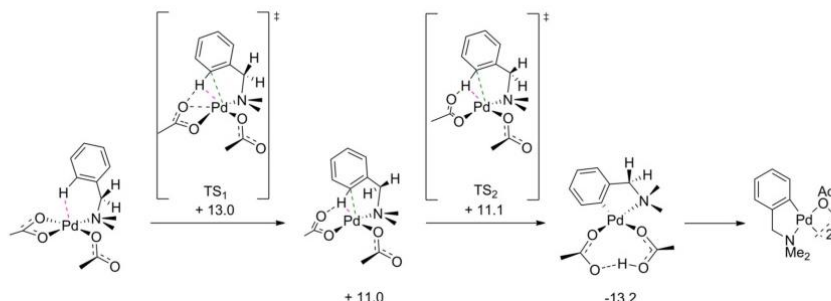
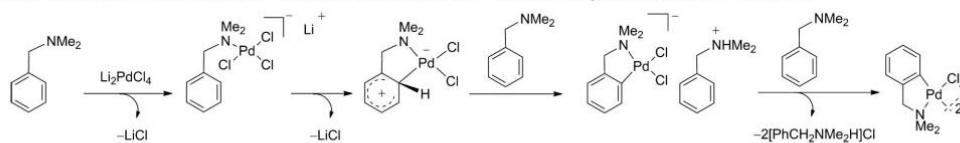


Figure 1. Computational reaction profile (kcal/mol) and bond lengths (Å) for the cyclometalation of Pd(OAc)₂(DMBA-H) proposed by Macgregor et al.¹²

Scheme 2. Proposed Electrophilic Aromatic Substitution for Chloride-Bridged Palladacycle Formation



favor activation *ortho* to the fluorine atom for kinetic or thermodynamic reasons.^{7a,g,h}

Jones and co-workers reported an extensive study on the kinetics, regioselectivity, and mechanism of intramolecular C–H functionalization of phenylimines at iridium and rhodium, showing that the regioselectivity is sensitive to steric effects and also solvent dependent in reaction with iridium. The same reactions are solvent independent with rhodium.¹⁶

Palladacycles in general have been studied extensively and are believed to act as precatalysts in important reactions such as carbonylation reactions¹⁷ and the Heck, Sonogashira,¹⁸ Suzuki,¹⁹ and Stille cross-couplings.²⁰ Cyclopalladation reactions of nonfluorinated tertiary benzylamines have been reported previously,²¹ and their mechanisms investigated.^{12,22} In a catalytic context, applications utilizing benzylamine and related substrates have also been reported.²³ There is strong evidence for the reaction of benzylamines with Pd(OAc)₂ proceeding via a CMD mechanism (Figure 1),¹² while the reaction with lithium tetrachloropalladate has been suggested to proceed via an electrophilic aromatic substitution (S_EAr),^{21b} where the aromaticity of the aromatic ring is lost and a Wheland intermediate²⁴ is formed (Scheme 2).

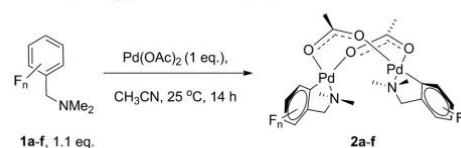
In this paper we present an investigation of the regioselectivity of directed intramolecular reactions¹² of fluorobenzylamines at palladium(II) to form palladacycles fluorinated at various positions. We report ¹H and ¹⁹F NMR spectroscopic and crystallographic studies of the products obtained from stoichiometric reactions of several mono- and difluorinated tertiary benzylamines and show that there is no regioselectivity in substrates that undergo cyclopalladation to form acetato-bridged palladacycles, while we observe *para* selectivity in formation of chloride-bridged palladacycles. MS studies employing LIFDI methods²⁵ confirm that dinuclear palladacycles are present in solution, as well as in the solid state. These results contrast with the reported regioselectivity of intermolecular C–H functionalization reactions of fluorinated benzenes with Pd(OAc)₂ that show preference for reaction

ortho to fluorine substituents²⁶ and with the cyclometalation reactions at Rh and Ir.¹⁶

RESULTS

Reactions of Fluorinated Tertiary Amines with Pd(OAc)₂. Our studies of chelate-assisted versions of C–H functionalization of fluoroaromatics began with the reaction of unsubstituted *N,N*-dimethylbenzylamine with Pd₃(OAc)₆ (>99.9% purity, hereafter referred to as “Pd(OAc)₂”) forming palladacycle **2a** (Scheme 3).^{21a} Following a previous study by

Scheme 3. Cyclopalladation Reactions of Tertiary Amines with Pd(OAc)₂ (see also Table 1)



Fairlamb et al.,²⁷ we synthesized the palladacycles **2a–f** from Pd(OAc)₂ and the relevant functionalized benzylamine (**1a–f**) in acetonitrile, instead of chloroform, at 25 °C, giving excellent yields (75–90% in Table 1). Five different substrates were chosen (**1a–f** in Table 1): **1b** and **1d** are monofluorinated and difluorinated tertiary benzylamines, respectively, presenting just one possibility (C-6) for C–H bond functionalization, while **1c** and **1e** are monofluorinated and difluorinated benzylamines, respectively, offering two possibilities for attack at C-2 or C-6, via path **2** or **6**, respectively. There is no choice for substrate **1f** since C-2 and C-6 positions are equivalent.

Reaction of Pd(OAc)₂ with *N,N*-dimethyl-2-fluorobenzylamine (**1b**, 1.1 equiv) in acetonitrile for 14 h at 25 °C yielded the palladacycle **2b** in 85% yield, which was crystallized by slow diffusion of hexane into a saturated solution in chloroform. The spectra of **2b** are consistent with a C₂-symmetric dinuclear

Table 1. Intramolecular C–H Functionalization of Fluorinated Tertiary Amines with Pd(OAc)₂^a

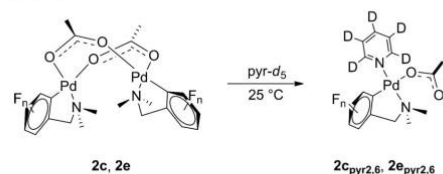
Substrate 1	Complex 2	Yield / %
		90
		85
		76
		78
		75
		82

^aThe nomenclature of the complex, e.g., **2c₆**, indicates complex **2** formed from substrate **1e** by C–H functionalization in position **6** (numbering from nitrogen). Arrows represent the available sites for C–H functionalization.

complex, as shown by the diastereotopic CH₂ group appearing as an AB quartet ($J_{H-H} = 14.2$ Hz) at δ 3.47 (chemical shift difference $\delta_{AB} = 11.2$ Hz = 0.028 ppm). The high-field component of the AB quartet shows an additional doublet ($J_{H-F} = 1.4$ Hz). The *N*-methyl carbons and proton signals are split into two sets, which are assigned to axial and equatorial positions of the five-membered ring. The protons resonate at δ 2.07 and 2.83, compared to δ 2.28 for the free substrate. The ¹³C resonances are shifted downfield from δ 45.3 to two

separate signals at 51.6 and 52.9. The ¹⁹F NMR spectrum shows a doublet of doublets at δ –115.01 ($J = 9.7, 5.5$ Hz). The chemical shift is slightly changed from the free substrate, but the value of J_{H-F} *ortho* is reduced substantially on reaction ($J_{H-F} = 15.9$ Hz in free substrate **1b**). Mass spectra were recorded by the LIFDI method,²⁵ resulting in the molecular ion as the only peak with characteristic isotope structure for a dinuclear Pd₂ species ($m/z = 636.02$). These data are consistent with those reported for the nonfluorinated acetate-bridged palladacycle^{21a,22} and confirm that the dinuclear Pd₂ species is present in solution.²⁷


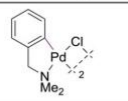

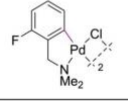

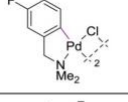

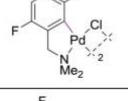

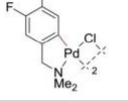
The methods of synthesis, characterization, and crystallization for **2c** and for difluorinated acetate-bridged palladacycles **2d–2f** were similar to those for **2b** (see Experimental Section). Reaction of Pd(OAc)₂ with *N,N*-dimethyl-3-fluorobenzylamine (**1c**) tested the effect of the fluorine on the regioselectivity of intramolecular C–H functionalization (arrows in Table 1). The reaction yielded a mixture of isomeric forms of palladacycle **2c** (**2c₂**, **2c₆**, and **2c_{2,6}** in Table 1) (76% overall yield), giving a disordered crystal structure due to the different positions of the fluorine atom. The ¹⁹F NMR spectrum of the mixture of isomers shows four different signals belonging to the four different environments: two doublets of doublets at δ –104.25 ($J = 8.8, 5.2$ Hz) and δ –104.47 ($J = 8.8, 5.1$ Hz) for the fluorines *ortho* to palladium in **2c₂** and **2c_{2,6}** and a multiplet at δ –119.45 corresponding to two overlapping signals (observed in a ¹⁹F-COSY NMR spectrum) for the fluorine *para* to palladium in **2c₆** and **2c_{2,6}**. In order to calculate the ratio between the three isomers, the mixture of palladacycles was reacted with pyridine-*d*₅, which coordinates to the palladium, splitting the palladacycles into two monomers (Scheme 4). The resulting

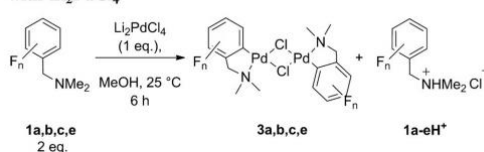
Scheme 4. Formation of Monomers **2c_{pyr2,6}** and **2e_{pyr2,6}** from **2c** and **2e**

products show just two different environments in the ¹⁹F NMR spectrum: a doublet of doublets at δ –100.98 ($J = 8.7, 5.4$ Hz) for monomer **2c_{pyr2}** with the fluorine *ortho* to palladium and a doublet of doublets at δ –119.88 ($J = 15.9, 9.6$ Hz) for monomer **2c_{pyr6}** with the fluorine *para* to palladium. The integration of these signals gives a ratio of 1:0.9, indicating that the C–H functionalization was nonselective. The mixture of palladacycles **2e₂**, **2e₆**, and **2e_{2,6}** was also obtained by a similar procedure to the synthesis of **2b** (overall yield 75%), giving a disordered crystal structure.

Reactions of Fluorinated Tertiary Amines with Li₂PdCl₄. Our syntheses of the chloride-bridged fluorinated palladacycles (Table 2) were based on the procedure reported by Cope and co-workers for di- μ -chlorobis(*N,N*-dimethylbenzylamine-2-*C,N*)dipalladium(II) (**3a**).^{21b} The reactions of Li₂PdCl₄ with substituted benzylamines (Scheme 5) were performed with the same substrates (**1a–e**) as those used in the syntheses of palladacycles **2a–f** (Table 2).

Table 2. Intramolecular C–H Functionalization of Fluorinated Tertiary Amines with Li_2PdCl_4 ^a

Substrate 1	Complex 3	Yield / %
		70
		86
		76
		67
		71

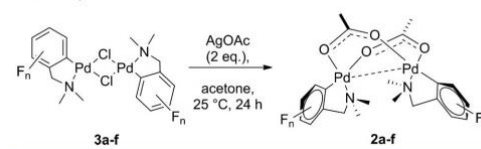
^aThe nomenclature follows Table 1.**Scheme 5.** Cyclopalladation Reactions of Tertiary Amines with Li_2PdCl_4 

Reaction of Li_2PdCl_4 with *N,N*-dimethyl-2-fluorobenzylamine (**1b**, 2 equiv), in methanol for 6 h at 25 °C, gave palladacycle **3b** in 86% yield along with the protonated substrate **1bH⁺**. Chloride-bridged palladacycles all exhibit two different geometrical isomers in solution, assigned as *syn* and *anti*, depending on the relative position of the Pd–C bonds,^{20d} with NMR data consistent with those reported for the nonfluorinated palladacycle **3a**.^{21b} Whereas the free substrate **1b** shows a single resonance in the ¹H NMR spectrum at δ 2.28 for the methyl groups, **3b** exhibits two resonances, δ 2.88 and 2.86, because of the *syn* and *anti* isomeric forms. The methylene protons resonate at δ 3.52 in the free substrate and at δ 4.01 for **3b**, and the ¹⁹F NMR spectrum shows a multiplet at δ –113.97 (overlap of the *syn* and *anti* signals) shifted downfield with respect to the free substrate **1b** (δ –118.10). The LIFDI mass spectrum shows the molecular ion for the dinuclear complex at 587.92 (100%).

Reaction of Li_2PdCl_4 with *N,N*-dimethyl-3-fluorobenzylamine (**1c**) allowed us to study the regioselectivity of the cyclopalladation reaction since the benzylamine **1c** offers a choice between the C-2 position (path 2 in Table 2) or C-6 position (path 6 in Table 2) for C–H functionalization. The

reaction gives exclusively the palladacycle **3c₆** in 76% yield and the protonated substrate **1cH⁺**, meaning that the cyclopalladation occurs only in position C-6, *para* with respect to the fluorine atom. The ¹⁹F NMR spectrum shows two doublets of doublets respectively at δ –119.01 (J = 15.4, 9.4 Hz) and δ –119.10 (J = 15.4, 9.2 Hz) in the ratio 1:1.2, corresponding to the *minor* and the *major* isomers. The ¹H NMR spectrum shows a multiplet at δ 7.10 and a doublet at δ 6.65 (J = 9.2 Hz) for the aromatic protons coupled to each other and to the fluorine, a broad singlet for the methylene protons at δ 3.90, and two singlets at δ 2.83 and 2.86 for the methyl groups bound to the nitrogen. The ¹³C NMR spectrum shows two sets of signals for the two geometrical isomers. Two doublets at δ 161.41 and 161.38, with coupling constants of 241.5 and 241.6 Hz, respectively, correspond to the carbons bonded to fluorine for the two isomers, where the former is more intense than the latter. Two other sets of doublets appear at δ 147.6 (with coupling constants of 6.3 and 6.5 Hz, respectively), corresponding to the aromatic carbon *ortho* to the C–F bond, and another set of doublets, again for the two geometrical isomers, appears at δ 112.0 and 111.9 (with coupling constants of 9.8 Hz), corresponding to the aromatic carbon *para* to the C–F bond. Two singlets at δ 109.0 and 108.8 are assigned to the two *ipso* carbons of the two geometrical isomers, and a ¹³C-DEPT-135 NMR spectrum confirms that the two doublets at δ 73.2 and 73.0 (with coupling constants of 2.6 and 2.9 Hz, respectively) derive from the methylene carbons of the *syn* and *anti* isomers. The two methyl groups bound to the nitrogen in each isomer (*syn* and *anti*) resonate as two singlets at δ 53.1 and 52.8 of different intensities. The same selectivity was obtained in the reaction of Li_2PdCl_4 with *N,N*-dimethyl-3,4-difluorobenzylamine (**1e**), giving the palladacycle **3e₆** in 71% yield, which was crystallized by slow evaporation of a saturated solution of the compound in chloroform at –20 °C.

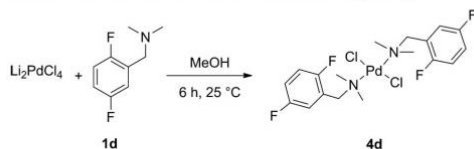
Chloride-bridged palladacycles **3c₆** and **3e₆** were reacted with silver acetate (1 equiv per palladium) in acetone at 25 °C (Scheme 6) to give exclusively the *para* isomer of palladacycles

Scheme 6. Bridge Conversion Reaction of Chloride-Bridged Palladacycles

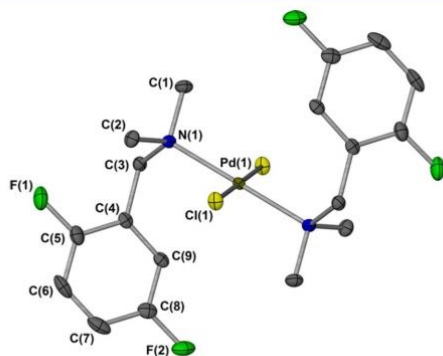
2c and **2e** (**2c₆** and **2e₆**). These products were crystallized by slow diffusion of hexane into a saturated solution of the compound in chloroform.

Reaction of Li_2PdCl_4 with *N,N*-dimethyl-2,4-difluorobenzylamine (**1d**) under the conditions used for the other substrates (**1a–c**) did not give a cyclometalated product, but gave dichloropalladiumbis-2,4-difluoro-*N,N*-dimethylbenzylamine (**4d** in Scheme 7) in 73% yield.

The ¹H NMR spectrum of **4d** shows two doublets of doublets at δ 8.77 (J = 8.8, 5.5, 3.2 Hz) and at δ 7.12 (J = 14.3, 7.3, 3.7 Hz) for the aromatic protons coupling to each other and to the two fluorine atoms and shows two singlets at δ 3.90 and 2.60 for the methylene and methyl protons, respectively. The ¹⁹F NMR spectrum shows two

Scheme 7. Reaction of Substrate 1d with Li₂PdCl₄

multiplets at δ -121.52 and -118.22 for the two inequivalent fluorine atoms. Complex **4d** was crystallized by slow diffusion of a saturated solution of the complex in dichloromethane at 2 °C (Figure 2).

Figure 2. X-ray crystal structure of palladium complex **4d**.

The cyclometalated product **3d** was obtained under the same reaction conditions used for the other substrates (**1a–c**) but with a reaction time of 1 week, along with the protonated substrate **1dH⁺**, suggesting that complex **4d** is one of the species at equilibrium in the electrophilic aromatic substitution mechanism. The NMR spectra of **3d** follow the same pattern as those described for **3c₆**.

The cyclopalladation reactions with Li₂PdCl₄ were also carried out in acetonitrile to evaluate the role of the solvent in the regioselectivity obtained for substrates **1c** and **1e**. The C–H functionalization also occurred *para* to fluorine, showing that the regioselectivity in these systems is solvent independent. A similar experiment was also performed, reacting the fluorinated substrate **1c** and **1e** with Pd(OAc)₂ in MeOH: no regioselectivity was obtained.

The observed selectivity raises questions of thermodynamic or kinetic control in the Pd–C bond-forming step. If there is to be thermodynamic control of the acetate system, the second and third steps of Figure 1 (with appropriate fluorine substituents) need to be reversible. For the reactions of lithium tetrachloropalladate, the last three steps of Scheme 2 need to be reversible. We therefore carried out a number of reactions to test (a) for changes in the isomer distribution at higher temperature than the standard reaction and (b) for exchange of the substrate between nonfluorinated palladacycles **2a** in the presence of fluorinated benzylamine **1c**. For the acetate complexes, we reacted **2c₆** with acetic acid in CD₃CN at 75 °C and monitored the reaction over 16 h, but observed no conversion to other isomers. Further, we reacted **2a** with **1c** (1 equiv per Pd) in refluxing toluene in the presence of acetic acid

(3 equiv) for 24 h. The ¹⁹F NMR spectra showed formation of palladacycle **2c** (conversion ca. 33%) with fluorine occupying both *ortho* and *para* positions in approximately equal proportions. For the chloride systems, **3c₆** was reacted with [1cH]Cl in CD₃CN as above, and no formation of the *ortho* isomer was observed. We also repeated the reaction of Scheme 5 with **1c** in refluxing methanol, resulting in formation of **3c₆** only. The lack of evidence for reversibility suggests that these reactions are under kinetic control.

Molecular Structures of Acetate-Bridged Palladacycles. All the acetate-bridged palladacycles (**2a–f**) were analyzed by single-crystal X-ray diffraction (crystallographic data are reported in the Supporting Information, and selected bond lengths and bond angles are in Table 4). Molecular structures of nonfluorinated palladacycle **2a**, monofluorinated palladacycle **2b**, and difluorinated palladacycle **2d** are shown in Figures 3, 4, and 5, respectively.

Table 3. Selected Distances (Å) and Angles (deg) in Acetate-Bridged Palladium Dimer Structures^a

entry	Pd–Pd	interplane angle	N–Pd–Pd'–N'
2a no F ^b	2.9324(6)	19.5(3)	-104.3(3)
	2.9279(7)	19.3(3)	104.4(3)
2b one F	2.9600(2)	9.45(16)	71.94(9)
2c₆ one F	3.0185(7)	37.22(13)	-98.18(12)
2d two F	3.0974(8)	85.66(15)	-84.03(11)
2e₆ two F	3.0369(7)	37.88(13)	-99.83(9)
2f two F	3.0285(5)	86.30(11)	-77.81(13)

^aSee Supporting Information for angles not reported here. ^bTwo independent molecules in the asymmetric unit.

All the crystal structures are nonplanar at palladium and, as reported by Bercaw et al.²⁸ for [(2-phenylpyridine)Pd(μ-OAc)]₂, have a “clamshell” structure where the coordination plane containing the Pd atom is almost perpendicular to the acetate bridges. They suggested that this geometry is a consequence of the d⁸–d⁸ interaction of the two Pd atoms and π-stacking interaction between the aromatic rings. All the ligands (*N,N*-dimethylbenzylamine and fluorinated *N,N*-dimethylbenzylamines) are bonded to the di-μ-acetate-bridged unit through the nitrogen atom, forming a five-membered ring with an aromatic carbon atom (Csp²). The biggest changes in the geometries of the clamshell structures are found in the following parameters listed in Table 3. More minor changes in planes and torsions are given in the Supporting Information (Table S1).

- Pd··Pd distance;
- interplane angle: angle between plane Pd(1)–C(ipso)–C(aromatic metalocycle) and the corresponding plane of Pd(2);
- torsion angle N–Pd–Pd'–N';

Analysis of the data in Table 3 reveals a correlation between Pd··Pd distance and the number of fluorine atoms in the aromatic ring, potentially due to a decrease in the d⁸–d⁸ interaction resulting from the withdrawal of the electron density by the fluorine atoms. The interplane angles (see Table 3), for the series of acetate-bridged palladacycles, increase from 9.45(16)° for the monofluorinated palladacycle **2b** and 19.5(3)° for the nonfluorinated **2a** to 37.22(13)° and 37.88(13)° for palladacycles **2c₆** and **2e₆** (mono- and difluorinated, respectively) and to 86.30(11)° for the

Table 4. Selected Distances (Å) and Angles (deg) in Acetate-Bridged Palladium Dimer Structures

bond length	2a	2b	2c _e	2d	2e _e	2f
C(1)–Pd(1)	1.963(7)	1.952(3)	1.958(2)	1.966(2)	1.9525(19)	1.974(2)
O(1)–Pd(1)	2.145(5)	2.135(2)	2.1426(16)	2.0996(17)	2.1383(14)	2.0363(17)
O(n)–Pd(1)	O(3) 2.040(5)	O(3) 2.0510(19)	O(2) 2.0358(16)	O(2) 2.0276(17)	O(2) 2.0328(13)	O(2) 2.1192(17)
N(1)–Pd(1)	2.064(6)	2.070(2)	2.0608(18)	2.0500(19)	2.0639(16)	2.057(2)
C(n)–F(n)		C(5)–F(1) 1.368(3)	C(4)–F(1) 1.363(3)	C(2)–F(1) 1.371(3)	C(3)–F(1) 1.363(2)	C(2)–F(1) 1.366(3)
				C(5)–F(2) 1.357(3)	C(4)–F(2) 1.348(2)	C(4)–F(2) 1.363(3)
bond angle	2a	2b	2c _e	2d	2e _e	2f
C(1)–Pd(1)–O(n)	O(3) 92.5(3)	O(3) 92.36(10)	O(1) 91.51(8)	O(2) 95.10(8)	O(2) 91.42(7)	
C(1)–Pd(1)–N(1)	82.2(3)	82.06(10)	82.58(8)	81.72(8)	82.26(7)	81.25(9)
O(n)–Pd(1)–O(1)	O(3) 91.8(2)	O(3) 90.04(8)	O(2) 91.36(7)	O(2) 87.48(8)	O(2) 91.41(5)	
N(1)–Pd(1)–O(n)	O(1) 93.3(2)	O(1) 95.60(8)	O(1) 93.70(7)	O(1) 94.30(7)	O(1) 94.15(6)	O(2) 93.70(7)

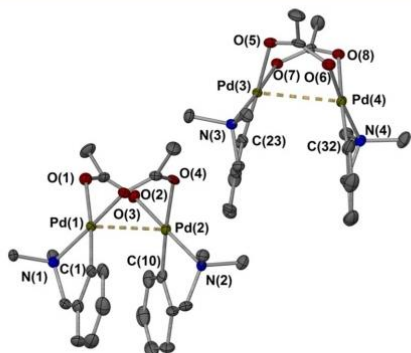


Figure 3. X-ray crystal structure of palladacycle 2a.

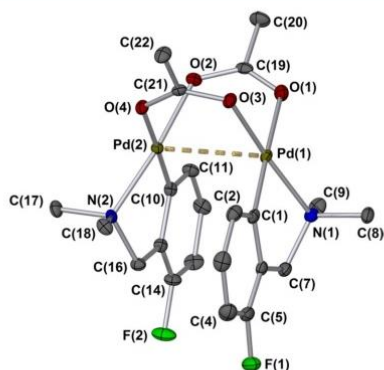


Figure 4. X-ray crystal structure of palladacycle 2b.

difluorinated palladacycle **2d**. There are corresponding increases in γ , the angle between the two benzene ring planes (Table S1). Not only the number but also the position of the fluorine atoms have an effect on these values; the highest value is for the palladacycle **2d**, where one of the fluorine atoms lies *ortho* to the Pd–C bond. We propose that the twisting of the benzene ring with respect to the coordination plane is due to the electronic repulsion between the fluorine atom and the

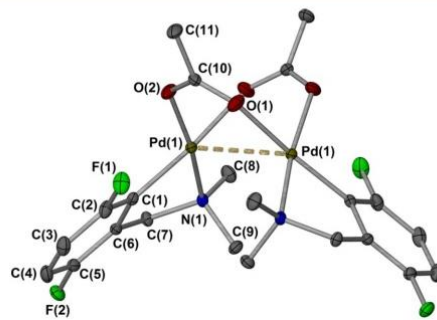


Figure 5. X-ray crystal structure of palladacycle 2d.

oxygen atom of the acetate bridge (distance (F(1)⋯O(2) is 2.886(2) Å in **2d**, compared to the sum of the van der Waals radii of 2.99 Å, a reduction of only 3%).²⁹ Additionally, we note wide variations in the torsion N–Pd–Pd–N' from 71.94(9)° in **2b** to 104.4(3)° in **2a**.

Molecular Structures of Chlorine-Bridged Palladacycles. All the chloride-bridged palladacycles (**3b–e**) were analyzed by single-crystal X-ray diffraction (see Table 5 for selected bond angles and bond structures and Supporting Information for the crystallographic data). The X-ray crystal structure of palladacycle **3d** is shown in Figure 6.

As reported by Mentés et al.³⁰ for the nonfluorinated palladacycle **3a**, the palladium atoms in **3d** exhibit a square planar geometry with two ligands, which are bound through a M–C(sp²) bond and a M–N bond, forming two equivalent five-membered rings. Unlike in the acetate palladium complexes, there is almost no folding at the bridging atom. Indeed, a survey of the Cambridge Structural Database shows that the vast majority of closely related complexes also have Pd₂Cl₂ units that are planar or very close to planar. The lengths of the Pd–Cl bonds (Table 5) are slightly different from each other due to the different *trans* influence of the C(sp²) and the nitrogen and are similar to the values reported by Mentés for **3a** (Pd–Cl *trans* to N: 2.3287(1) Å and Pd–Cl *trans* to C 2.4658(1) Å).³⁰ Complex **3d** has the potential for repulsion between Cl and F(1): the Cl⋯F(1) distance is 2.9264(1) Å, 9% smaller than the sum of the van der Waals radii (3.22 Å).²⁹ A twist of the five-membered ring is observed with respect to the

Table 5. Selected Distances (Å) and Angles (deg) in Chloride-Bridged Palladium Dimer Structures

bond length	3b	3c ₆	3d	3e ₆
C(1)–Pd(1)	1.967(4)	1.975(2)	1.997(3)	1.972(4)
C(n)–F(n)	C(5)–F(5) 1.363(5)	C(4)–F(1) 1.365(2)	C(2)–F(1) 1.366(3) C(5)–F(2) 1.369(3)	C(3)–F(1) 1.361(5) C(4)–F(2) 1.353(5)
Cl(1)–Pd(1)	2.4565(11)	2.4658(6)	2.4379(7)	2.3415(10)
N(1)–Pd(1)	2.073(3)	2.0820(19)	2.079(2)	2.080(3)
Pd(1)–Cl(1')	2.3264(10)	2.3352(6)	2.3277(7)	2.4336(11)
bond angle	3b	3c ₆	3d	3e ₆
C(1)–Pd(1)–Cl(1')	94.51(12)	95.16(7)	98.22(8)	94.89(11)
C(1)–Pd(1)–N(1)	82.69(14)	81.96(8)	82.18(10)	81.99(15)
Cl(1')–Pd(1)–Cl(1)	85.92(4)	85.42(2)	84.36(3)	85.38(4)
N(1)–Pd(1)–Cl(1)	96.85(9)	97.49(5)	95.25(7)	97.73(10)

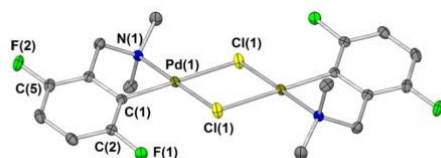


Figure 6. X-ray crystal structure of palladacycle 3d.

plane containing both palladium atoms and both chlorine atoms especially for palladacycle 3d. A similar observation was reported by Smith and co-workers for the three isomers of the methoxy-substituted di- μ -chlorobis(dialkylbenzylamine-2-*C,N*)-dipalladium(II).³¹ In the solid state the structure adopts the *anti* form, while in solution both *syn* and *anti* isomers were observed. Thus, these complexes are expected to have effective C_{2h} symmetry for the *anti* isomer and C_{2v} symmetry for the *syn* isomer in NMR spectra in solution, where the five-membered ring inverts rapidly. The geometries of the planar structure are also defined by the corresponding angles to those mentioned above for the acetate-bridged complexes, and all the data are reported in Table S2 in the Supporting Information.

DISCUSSION

The cyclopalladation reaction of *N,N*-dimethylbenzylamine with Pd(OAc)₂ was initially thought to proceed via a Wheland intermediate in an electrophilic aromatic substitution mechanism (S_EAr), where the intramolecular attack on the C–H bond by the electrophilic palladium followed the N-coordination of the amine to the metal center.³² DFT calculations performed in 2005 by Macgregor and co-workers showed that the reaction proceeds via a concerted metalation deprotonation (CMD or AMLA(6)) mechanism (Figure 1), where the Pd–C bond is formed at the same time as the acetate group coordinated to the metal deprotonates the C–H site on the benzene ring.¹² Our study shows that a fluorinated substrate, with the possibility of undergoing C–H functionalization with Pd *ortho* to F (position C-2, path 2 in Table 1) or *para* to F (position C-6, path 6 in Table 1), does not show any regioselectivity in its cyclometalation reaction. For substrates 1c and 1e we observe the formation of three different isomers where the C–H functionalization occurs in position C-2 (isomers 2c₂ and 2e₂), in position C-6 (isomers 2c₆ and 2e₆), and in both positions C-2 and C-6 in the same molecule at two sides of the palladacycle (isomers 2c_{2,6} and 2e_{2,6}). The ratio of *para*- and *ortho*-functionalized product is close to 1:1.

It is plausible that the lack of any regioselectivity is the result of two opposing effects: the *ortho* position is favored due to the *ortho* fluorine effect (M–C bond strength and C–H kinetic acidity), but also disfavored because of electronic repulsion between the lone pair of the fluorine atom and the oxygen of the acetate ring pointing toward the aromatic ring. To test this theory we decided to investigate a different cyclopalladation reaction that is suggested to proceed via an electrophilic aromatic substitution (S_EAr) instead of CMD mechanism, using the same substrates. When substrates 1c and 1e, where positions C-2 and C-6 are available, were reacted with Li₂PdCl₄, we obtained a single regioisomer with C–H functionalization *para* to the fluorine. We suggest that formation of the isomers 3c₂ and 3e₂ is prevented by electronic repulsion between the lone pair of the chlorine atom and the lone pair of the fluorine pointing toward the chloride bridge in the dinuclear Pd₂ complex. In the chloride-bridged system, the fluorinated ring cannot twist away as we observed in the X-ray crystal structure of compound 3d, because the palladacycle is planar and not a clamshell structure. Since the reactions appear to be under kinetic control, corresponding repulsive interactions would need to be significant in the transition states. In this context, we note that Pd–C bond formation may be formed in dinuclear complexes rather than in mononuclear complexes, as illustrated in Figure 1 and Scheme 2.

The regioselectivity of these cyclometalation reactions at palladium seems to be associated with electronic factors in addition to the particular mechanism involved in the reaction. However, Jones et al. have found regioselectivity *ortho* to fluorine for similar cyclometalation reactions of fluorinated phenylamines at iridium and rhodium, proceeding via an S_EAr mechanism.¹⁶ The difference in regioselectivity between Jones' system and ours may be associated with a change in the rate-determining step of the reactions rather than with a change in the mechanism itself, although differences in ligand identity and associated conformations may also play a role.

CONCLUSIONS

We have shown that when fluorinated benzylamines (1c and 1e) react with Li₂PdCl₄, cyclopalladated products are formed with complete selectivity for the C–H functionalization *para* to fluorine. In contrast, the same substrates do not exhibit any regioselectivity when reacting with Pd(OAc)₂ to form acetate-bridged complexes. The chloride-bridged complexes can readily be converted to acetate-bridged products if required, maintaining the regiochemistry. Thus, the Li₂PdCl₄ reactions should be used in preference to the acetate reactions when regioselectivity is required. The lack of selectivity of the

intramolecular CMD reactions of the acetate contrasts with the *ortho* selectivity observed for intermolecular CMD reactions of fluoroaromatics at palladium.^{11a} In common with the intramolecular reactions of fluorinated imines at iridium and rhodium,¹⁶ the reactions of Li₂PdCl₄ proceed via an S₂Ar mechanism; however, the imines show *ortho*-selectivity, whereas the fluorinated benzylamines show *para*-selectivity.

The introduction of fluorine substituents has a marked effect on the clamshell structures of the acetate-bridged complexes. The difluorinated palladacycles adopt a more open clamshell structure than the nonfluorinated palladacycle, consistent with weaker d⁸–d⁸ interaction between the palladium atoms. Moreover, not just the number of fluorines but also their position on the aromatic ring affect the shape of the dinuclear structure. The structure of **2d** shows that the twisting relieves the repulsion between the oxygen and the *ortho* fluorine. By contrast, the chloride-bridged palladacycles do not show great structural variation between the mono- and difluorinated palladacycles and show similar bond lengths to the known nonfluorinated palladacycles. The rigid planar structure of these compounds means that the formation of the *ortho* isomer is disfavored due to the repulsion between the lone pairs of the chlorine and the fluorine atoms, resulting in the formation of the *para* isomer exclusively when there is a choice. In the case of **3d**, in which the fluorine has to occupy the *ortho* position, a close approach of the *ortho* fluorine to the bridging chlorine cannot be avoided (Figure 6).

EXPERIMENTAL SECTION

General Details. ¹H, ¹³C{¹H}, and ¹⁹F NMR, spectra were recorded on Jeol ECS400 (400, 100, 376, MHz, respectively) or with Bruker AV500 (500, 126, 471 MHz, respectively) where specified. ¹³C and ¹⁹F NMR spectra were obtained with ¹H decoupling. ¹⁹F NMR spectra were externally referenced to CFCl₃. ¹H and ¹³C were referenced using the chemical shifts of residual proton resonance. Chemical shifts are reported in parts per million. Coupling constants have been quoted to ±0.2 Hz. Spectra were typically recorded at 298 K unless otherwise stated. Spectra were processed using MestReNova software (and chemical structures were drawn with ChemDraw). IR spectroscopy was performed using a Unicam Research Series FTIR using an ATR attachment on solid compounds. Far-IR spectroscopy was performed using a Bruker Tensor 37. The relative intensities of the peaks are denoted as (s) strong, (m) medium, (w) weak, and (br) broad. Mass spectrometry was performed using a Bruker Daltonics microTOF spectrometer, an Agilent series 1200 LC using electrospray ionization (ESI) with less than 5 ppm error for HRMS. Liquid injection field desorption ionization (LIFDI) mass spectrometry was performed using a Waters GCT Premier mass spectrometer. Mass spectral data are quoted as the *m/z* ratio along with the relative peak height in parentheses (base peak: 100). Elemental analysis was carried out on an Exeter Analytical CE-440 elemental analyzer. X-ray crystallographic data were collected on an Agilent SuperNova diffractometer with Mo K α radiation ($\lambda = 0.71073$ Å) at 110.00(10) K. The structures were solved and refined using Olex2³³ implementing SHELX algorithms and the Superflip³⁴ structure solution program. Structures were solved by charge flipping, Patterson, or direct methods and refined with the ShelXL³⁵ package using full matrix least-squares minimization. All non-hydrogen atoms were refined anisotropically. Hydrogen atoms were placed at calculated positions and refined using a "riding model". Crystallographic parameters are given in the Supporting Information.

General Synthetic Procedures. Reagents were purchased from Fluorochem, Alfa Aesar, or Sigma-Aldrich and used without any further purification unless otherwise specified. Solvents were HPLC grade and used without further purification. Reactions were carried out in air. Pd(OAc)₂ (>99.9%) was obtained from Precious Metals Online.

The synthesis of fluorinated *N,N*-dimethylbenzylamines is described in the Supporting Information.

Procedure A: Synthesis of Fluorinated Acetate-Bridged Palladacycle. To a solution of Pd(OAc)₂ (1 equiv) in acetonitrile (20 mL mmol⁻¹) was added the relevant fluorinated *N,N*-dimethylbenzylamine (1.2 equiv), and the reaction mixture was stirred for 14 h at 25 °C. The resulting green-to-yellow solution was filtered through cotton wool and reduced *in vacuo*. The residue was triturated with diethyl ether and dried to obtain the desired product. The product was crystallized by slow diffusion of hexane into a saturated solution in chloroform.

Procedure B: Synthesis of Fluorinated Chloride-Bridged Palladacycle. The fluorinated chloride-bridged amino-derived palladacycles were synthesized using a modified literature procedure reported by Cope and co-workers.^{21b} To a solution of lithium tetrachloropalladate(II) (1 equiv) in methanol (25 mL mmol⁻¹) was added the relevant fluorinated *N,N*-dimethylbenzylamine (2 equiv). The initially clear red reaction mixture very quickly became slightly orange, and after about 10 min at room temperature a yellow solid began to precipitate. After stirring for 6 h, the yellow product was filtered and washed with MeOH and dried on the Schlenk line. These products were crystallized in air by slow diffusion of hexane into a saturated solution of the compound in chloroform.

Procedure C: Synthesis of Fluorinated Acetate-Bridged Palladacycle from Chloride-Bridged Palladacycle. The fluorinated acetate-bridged palladacycles were synthesized from chloride-bridged palladacycles modifying the known procedure reported by Cotton and co-workers.³⁶ To a solution of chloride-bridged amino-derived palladacycle (1 equiv) in acetone (100 mL mol⁻¹) was added silver acetate (2 equiv). The reaction mixture was stirred for 24 h at 25 °C. The resulting greenish solution was filtered through Celite to remove the silver acetate in excess and reduced to dryness *in vacuo* to obtain the product as a yellow powder. The product was crystallized as above.

Procedure D: Synthesis of Fluorinated Chloride-Bridged Palladacycle from Acetate-Bridged Palladacycle. The fluorinated chloride-bridged amino-derived palladacycles from acetate-bridged amino-derived palladacycles were synthesized as reported by Hiraki and co-workers.³⁷ To a solution of acetate-bridged amino-derived palladacycle (1 equiv) in a mixture of H₂O/acetone (1:20, 0.34 mL mol⁻¹) was added lithium chloride (8 equiv). The reaction mixture was stirred for 24 h at 25 °C. The resulting yellow solution was filtered through Celite and reduced to dryness *in vacuo* to obtain the product as yellow powder. The powder was washed with H₂O to remove the excess lithium chloride and dried on the Schlenk line.

Synthesis and NMR Experiments. For compound numbering see Supporting Information.

Di- μ -acetatobis[*o*-dimethylaminomethylphenyl-*C,N*]-dipalladium(II) (2a**).** Complex **2a** was prepared according to general procedure A, on a 0.26 mmol scale, to afford the product as a green powder (78 mg, 91%). Mp: 197–199 °C (dec) (lit. 210–211 °C).^{21a} ¹H NMR (500 MHz, CDCl₃): δ 7.02 (d, *J* = 7.1 Hz, 2H), 6.97 (t, *J* = 7.3 Hz, 2H), 6.89 (t, *J* = 7.2 Hz, 2H), 6.84 (d, *J* = 7.2 Hz, 2H), 3.58 (d, *J* = 13.7 Hz, 2H, RCH₂N), 3.09 (d, *J* = 13.7 Hz, 2H, CH₂), 2.80 (s, 6H, NCH₃), 2.06 (s, 6H, NCH₃), 2.05 (s, 6H, CH₃CO). ¹³C{¹H} NMR (126 MHz, CDCl₃): δ 180.9 (CO), 147.2 (aromatic), 144.1 (aromatic), 132.3 (aromatic), 124.8 (aromatic), 124.4 (aromatic), 121.2 (aromatic), 72.3 (CH₂), 52.7 (NCH₃), 51.3 (NCH₃), 24.7 (CH₃CO). IR (ATR, ν cm⁻¹): 1727 (w), 1588 (m), 1569 (m), 1412 (s), 1345 (w), 1260 (s), 1072 (m, br), 1020 (s, br), 799 (s), 737 (s), 680 (m). LRMS (LIFDI): *m/z* 599.94 (100%, [M]⁺). All data are in accordance with the literature.²²

Di- μ -acetatobis[*o*-dimethylaminomethyl-2-fluorophenyl-*C,N*]-dipalladium(II) (2b**).** Complex **2b** was prepared according to general procedure A, on a 0.27 mmol scale, to afford the product as a yellow powder (72.8 mg, 85%). Mp: 190–193 °C (dec). ¹H NMR (400 MHz, CDCl₃): δ 6.91 (td, *J* = 7.8, 5.6 Hz, 2H, H-4), 6.79 (d, *J* = 7.4 Hz, 2H, H-5), 6.71 (ddd, *J* = 9.5, 8.1, 0.9 Hz, 2H, H-3), 3.50 (d, *J* = 14.1 Hz, 2H, CHH'), 3.45 (dd, *J* = 14.3, 1.4 Hz, 2H, CHH'), 2.83 (s, 6H, NCH₃), 2.07 (s, 6H, NCH₃), 2.06 (s, 6H, CH₃CO). ¹³C{¹H} NMR (126 MHz, CDCl₃): δ 181.2 (CO), 156.4 (d, *J* = 250.2 Hz, C-2), 132.6 (d, *J* = 10.1 Hz, C-1), 127.8 (d, *J* = 2.9 Hz, C-5), 126.3 (d, *J*

= 6.4 Hz, C-4), 111.1 (d, $J = 20.2$ Hz, C-3), 67.7 (CH₂), 52.9 (NCH₃), 51.6 (NCH₃), 24.6 (CH₃CO). ¹⁹F NMR (471 MHz, CDCl₃): δ -115.01 (dd, $J = 9.7, 5.5$ Hz). IR (ATR, ν cm⁻¹): 1601 (m), 1576 (s), 1558 (s), 1455 (m), 1410 (s), 1345 (m), 1232 (s), 1127 (w), 986 (w), 874 (m), 844 (m), 769 (s), 678 (s). LRMS (LIFDI): m/z 636.02 (100%, [M]⁺). Anal. Calcd for C₂₂H₂₈F₂N₂O₄Pd₂: C, 41.58; H, 4.39; N, 4.22. Found: C, 41.59; H, 4.44; N, 4.51.

Acetato- κ O-[o-dimethylaminomethyl-3-fluorophenyl-C,N]-(pyridine-*d*₅)palladium(II) (2c_{pyr2,d}). A portion of the mixture of isomers of di- μ -acetatobis[o-dimethylaminomethyl-3-fluorophenyl-C,N]dipalladium(II) (2c) was dissolved in pyridine-*d*₅ to obtain the two isomers of 2c. ¹H NMR (400 MHz, CDCl₃): δ 7.07 (td, $J = 5.5, 7.7$ Hz, 1H), 6.90 (m, 2H), 6.77 (m, 1H), 6.65 (t, $J = 8.4$ Hz, 1H), 6.28 (dd, $J = 8.4, 6.2$ Hz, 1H), 3.93 (s, 2H), 3.86 (s, 2H), 2.84 (s, 6H), 2.76 (s, 6H), 2.19 (s, 6H). ¹⁹F NMR (376 MHz, CDCl₃): δ -100.98 (dd, $J = 8.7, 5.4$ Hz), -119.88 (dd, $J = 15.9, 9.6$ Hz).

Di- μ -acetatobis[o-dimethylaminomethyl-3-*p*-fluorophenyl-C,N]-dipalladium(II) (2c_d). Complex 2c_d was prepared according to general procedure C, on a 0.17 mmol scale, to afford the product as a yellow powder (105.4 mg, 98%). Mp: 191–195 °C (dec). ¹H NMR (500 MHz, CDCl₃): δ 6.95 (dd, $J = 8.3, 6.2$ Hz, 2H, H-1), 6.71–6.61 (m, 4H, H-2, H-4), 3.52 (d, $J = 13.9$ Hz, 2H, CHH'), 3.09 (d, $J = 13.9$ Hz, 2H, CHH'), 2.79 (s, 6H, NCH₃), 2.06 (s, 6H, NCH₃), 2.05 (s, 6H, CH₃CO). ¹³C{¹H} NMR (126 MHz, CDCl₃): δ 181.1 (CO), 161.3 (d, $J = 240.6$ Hz, C-3), 147.7 (d, $J = 6.2$ Hz, C-1), 137.2 (d, $J = 2.5$ Hz, C-6), 133.0 (d, $J = 6.8$ Hz, C-5), 111.5 (d, $J = 19.7$ Hz, C-4), 108.6 (d, $J = 21.4$ Hz, C-2), 72.0 (CH₂), 52.7 (NCH₃), 51.3 (NCH₃), 24.6 (CH₃CO). ¹⁹F NMR (471 MHz, CDCl₃): δ -119.31 (td, $J = 9.6, 6.2$ Hz). LRMS (LIFDI): m/z 636.00 (100%, [M]⁺). Anal. Calcd for C₂₂H₂₈F₂N₂O₄Pd₂·0.2AgCl: C, 39.8; H, 4.25; N, 4.22. Found: C, 39.87; H, 4.26; N, 3.97.

Di- μ -acetatobis[o-dimethylaminomethyl-2,5-*o*,*m*-difluorophenyl-C,N]dipalladium(II) (2d). Complex 2d was prepared according to general procedure A, on a 0.26 mmol scale, to afford the product as a yellow-green powder (70.2 mg, 78%). Mp: 187–190 °C (dec). ¹H NMR (400 MHz, CDCl₃): δ 6.67 (td, $J = 8.7, 3.7$ Hz, 2H, H-3), 6.51 (td, $J = 7.7, 4$ Hz, 2H, H-4), 3.76 (dd, $J = 14.4, 1.8$ Hz, 2H, CHH'), 3.54 (d, $J = 14.4$ Hz, 2H, CHH'), 2.83 (s, 6H, NCH₃), 2.23 (s, 6H, NCH₃), 2.00 (s, 6H, CH₃CO). ¹³C{¹H} NMR (126 MHz, CDCl₃): δ 182.2 (CO), 163.6 (dd, $J = 235.5, 1.8$ Hz, C-5), 153.1 (dd, $J = 244.9, 2.2$ Hz, C-2), 134.7 (dd, $J = 15.1, 12.4$ Hz, C-1), 127.9 (d, $J = 36.9$ Hz, C-6), 114.5 (dd, $J = 31.5, 7.6$ Hz, C-4), 112.1 (dd, $J = 23.4, 8.6$ Hz, C-3), 69.0 (CH₂), 52.8 (NCH₃), 51.9 (NCH₃), 23.6 (d, $J = 2.1$ Hz, CH₃CO). ¹⁹F NMR (376 MHz, CDCl₃): δ -111.12 (ddd, $J = 20.9, 7.6, 3.6$ Hz, 2F), -120.86 to -121.28 (m, 2F). IR (ATR, ν cm⁻¹): 1590 (s), 1571 (s), 1458 (s), 1418 (s, br), 1349 (m), 1213 (s), 1023 (m), 972 (m), 838 (s), 805 (s), 727 (s), 683 (m). LRMS (LIFDI): m/z 672.02 (100%, [M]⁺). Anal. Calcd for C₂₂H₂₆F₄N₂O₄Pd₂: C, 39.36; H, 3.90; N, 4.17. Found: C, 38.99; H, 3.91; N, 4.31.

Di- μ -acetatobis[o-dimethylaminomethyl-3,4-*p*,*m*-difluorophenyl-C,N]dipalladium(II) (2e_d). Complex 2e_d was prepared according to general procedure C, on a 0.16 mmol scale, to afford the product as a yellow powder (102 mg, 95%). Mp: 188–190 °C (dec). ¹H NMR (500 MHz, CDCl₃): δ 6.78–6.72 (m, 4H, H-2, H-5), 3.58 (d, $J = 13.8$ Hz, 2H, CHH'), 3.13 (d, $J = 13.8$ Hz, 2H, CHH'), 2.79 (s, 6H, NCH₃), 2.11 (s, 6H, NCH₃), 2.06 (s, 6H, CH₃CO). ¹³C{¹H} NMR (126 MHz, CDCl₃): δ 181.6 (CO), 148.3 (dd, $J = 243.2, 13.7$ Hz, C-3), 146.7 (dd, $J = 250.6, 12.1$ Hz, C-4), 142.0 (dd, $J = 4.8, 3.7$ Hz, C-6), 138.9 (dd, $J = 3.7, 2.9$ Hz, C-1), 120.0 (d, $J = 14.7$ Hz, C-5), 110.3 (d, $J = 17.5$ Hz, C-2), 72.0 (CH₂), 52.6 (NCH₃), 51.5 (NCH₃), 24.6 (CH₃CO). ¹⁹F NMR (471 MHz, CDCl₃): δ -140.86 to -141.00 (m, 2F), -143.94 (ddd, $J = 19.7, 10.7, 8.8$ Hz, 2F). LRMS (LIFDI): m/z 672.00 (100%, [M]⁺). Anal. Calcd for C₂₂H₂₆F₄N₂O₄Pd₂·0.1AgCl: C, 38.54; H, 3.82; N, 4.09. Found: C, 38.56; H, 3.85; N, 3.92.

Di- μ -acetatobis[o-dimethylaminomethyl-3,5-*o*,*m*-difluorophenyl-C,N]dipalladium(II) (2f). Complex 2f was prepared according to general procedure A, on a 0.26 mmol scale, to afford the product as a yellow powder (71 mg, 82%). Mp: 205–208 °C (dec). ¹H NMR (400 MHz, CDCl₃): δ 6.54 (dd, $J = 8.4$ Hz, 2, 4, 2H, H-2), 6.37–6.31 (m, 2H, H-4), 3.56–3.46 (m, 4H, CHH', CHH'), 2.80 (s, 6H, NCH₃),

2.18 (s, 6H, NCH₃), 2.00 (s, 6H, CH₃CO). ¹³C{¹H} NMR (126 MHz, CDCl₃): δ 182.1 (CO), 167.7 (dd, $J = 242.6, 11.2$ Hz, C-5), 161.4 (dd, $J = 243.2, 11.9$ Hz, C-3), 150.1 (dd, $J = 17.2, 8.2$ Hz, C-6), 119.1 (dd, $J = 34.3, 3.2$ Hz, C-1), 105.1 (dd, $J = 21.1, 3.3$ Hz, C-2), 101.6 (dd, $J = 32.2, 23.7$ Hz, C-4), 73.5 (d, $J = 3.1$ Hz, CH₂), 52.6 (NCH₃), 51.6 (NCH₃), 23.7 (d, $J = 1.7$ Hz, CH₃CO). ¹⁹F NMR (376 MHz, CDCl₃): δ -100.78 to -100.85 (m, 2F), -116.37 (dd, $J = 17.6, 8.2$ Hz, 2F). LRMS (LIFDI): m/z 671.99 (100%, [M]⁺). Anal. Calcd for C₂₂H₂₆F₄N₂O₄Pd₂: C, 39.36; H, 3.90; N, 4.17. Found: C, 39.28; H, 3.89; N, 3.90.

Di- μ -chlorobis[o-dimethylaminomethyl-phenyl-C,N]dipalladium(II) (3a). Complex 3a was prepared according to general procedure D, on a 1.69 mmol scale, to afford the product as a yellow powder (462 mg, 46%). Mp: 173–175 °C (dec) (lit. 183–185 °C). ¹H NMR (500 MHz, CDCl₃): δ 7.17 (dd, $J = 19.3, 7.6$ Hz, 2H), 6.99–6.94 (m, 2H), 6.87 (t, $J = 6.8$ Hz, 4H), 3.93 (s, 4H), 2.87 (s, 6H), 2.84 (s, 6H). IR (ATR, ν cm⁻¹): 1738 (w), 1578 (w), 1447 (m), 1259 (s). 1095 (s, br), 1043 (s), 1017 (s, br), 982 (m), 861 (m), 799 (s), 733 (s), 698 (m). Far-IR (ATR, ν cm⁻¹): 516.04 (m), 498.64 (w), 477.33 (w), 422.85 (m), 398.60 (w), 368.37 (w), 329.15 (m), 280.00 (m), 265.76 (m), 247.08 (s), 244.39 (m), 232.86 (w), 217.42 (s). LRMS (LIFDI): m/z 551.96 (100%, [M]⁺). All data are in accordance with the literature.^{21b}

Di- μ -chlorobis[o-dimethylaminomethyl-2-*m*-fluorophenyl-C,N]dipalladium(II) (3b). Complex 3b was prepared according to general procedure B, on a 0.26 mmol scale, to afford the product in a mixture of geometrical isomers (*syn* and *anti*) as a yellow powder (74 mg, 86%). Mp: 180–182 °C (dec). ¹H NMR (500 MHz, CDCl₃): δ 6.94 (dd, $J = 20.1, 7.7$ Hz, 2H), 6.70 (dd, $J = 13.6, 4.9$ Hz, 2H), 6.87 (td, $J = 7.9, 5.6$ Hz, 2H), 4.01 (d, $J = 2.3$ Hz, 4H), 2.88 (s, 6H), 2.86 (s, 6H). ¹³C{¹H} NMR (126 MHz, CDCl₃): δ 156.1 ($J = 249.6, 2.4$ Hz), 144.9 (d, $J = 13.12$ Hz), 132.8 (t, $J = 11.1$ Hz), 128.8 (dd, $J = 67.6, 2.9$ Hz), 126.5 (dd, $J = 13.4, 6.6$ Hz), 111.6 (d, $J = 20.2$ Hz), 68.6 (d, $J = 22.3$ Hz), 53.3, 53.0. ¹⁹F NMR (376 MHz, CDCl₃): δ -113.91 to -114.05 (m). LRMS (LIFDI): m/z 587.92 (100%, [M]⁺). Anal. Calcd for C₁₈H₂₂F₂N₂Cl₂Pd₂: C, 36.76; H, 3.77; N, 4.76. Found: C, 36.63; H, 3.64; N, 4.40.

Di- μ -chlorobis[o-dimethylaminomethyl-3-*p*-fluorophenyl-C,N]dipalladium(II) (3c_d). Complex 3c_d was prepared according to general procedure B, on a 0.77 mmol scale, to afford the product in a mixture of geometrical isomers (*syn* and *anti*) as a yellow powder (171 mg, 76%). Mp: 174.4–176.2 °C (dec). ¹H NMR (500 MHz, CDCl₃): δ 7.17–6.98 (m, 2H), 6.65 (d, $J = 9.2$ Hz, 4H), 3.90 (br s, 4H), 2.86 (s, 6H), 2.83 (s, 6H). ¹³C{¹H} NMR (126 MHz, CDCl₃): δ 161.4 (d, $J = 241.5$ Hz, *major*), 161.4 (d, $J = 241.6$ Hz, *minor* isomer), 147.6 (d, $J = 6.3$ Hz, *major* isomer), 147.6 (d, $J = 6.5$ Hz, *minor* isomer), 136.1 (d, $J = 2.2$ Hz, *major* isomer), 136.0 (d, $J = 2.2$ Hz, *minor* isomer), 133.8 (d, $J = 6.9$ Hz, *major* isomer), 134.3 (d, $J = 7.0$ Hz, *minor* isomer), 112.0 (d, $J = 9.8$ Hz, *major* isomer), 111.9 (d, $J = 9.8$ Hz, *minor* isomer), 109.0 (s, *major* isomer), 108.8 (s, *minor* isomer), 73.2 (d, $J = 2.6$ Hz, *major* isomer), 73.0 (d, $J = 2.9$ Hz, *major* isomer), 53.1 (s, *major* isomer), 52.8 (s, *minor* isomer). ¹⁹F NMR (471 MHz, CDCl₃): δ -119.01 (dd, $J = 15.4, 9.4$ Hz, *syn* isomer), -119.10 (dd, $J = 15.4, 9.2$ Hz, *anti* isomer). Far-IR (ATR, ν cm⁻¹): 576.72 (m), 553.97 (w), 518.76 (w), 441.67 (m), 427.53 (m), 337.55 (m), 316.09 (s), 274.60 (m), 255.36 (w), 252.25 (w), 239.54 (s), 215.26 (s), 196.34 (m). LRMS (LIFDI): m/z 587.89 (100%, [M]⁺). Anal. Calcd for C₁₈H₂₂F₂N₂Cl₂Pd₂: C, 36.76; H, 3.77; N, 4.76. Found: C, 36.61; H, 3.77; N, 4.53.

Chloro- κ O-[o-dimethylaminomethyl-3-*p*-fluorophenyl-C,N]-(pyridine-*d*₅)palladium(II) (3c_{pyr}). A portion of di- μ -chlorobis[o-dimethylaminomethyl-3-*p*-fluorophenyl-C,N]dipalladium(II) (3c_d) was dissolved in pyridine-*d*₅ to obtain the *title compound*. ¹H NMR (500 MHz, CDCl₃): δ 6.93 (dd, $J = 9.6, 2.5$ Hz, 1H), 6.78 (t, $J = 7.8$ Hz, 1H), 6.27–6.17 (m, 1H), 3.91 (s, 2H), 2.94 (s, 6H). ¹⁹F NMR (471 MHz, CDCl₃): δ -119.35 to -119.46 (dd, $J = 16.4, 10.3$ Hz).

Di- μ -chlorobis[o-dimethylaminomethyl-2,4-*o*,*m*-difluorophenyl-C,N]dipalladium(II) (3d). Complex 3d was obtained according to general procedure B, with a reaction time of 1 week, on a 0.1 mmol scale, to afford the product in a mixture of geometrical isomers (*syn* and *anti*) as a yellow product (21 mg, 67%). Mp: 172.9–174.0 °C

(dec). ^1H NMR (500 MHz, CDCl_3): δ 6.66 (qd, $J = 8.5, 3.6$ Hz, 2H), 6.52 (m, 2H), 4.05 (d, $J = 4.1$ Hz, 4H), 2.77 (s, 6H), 2.75 (s, 6H). $^{13}\text{C}\{^1\text{H}\}$ NMR (126 MHz, CDCl_3 , major isomer): δ 162.3 (dd, $J = 239.3, 19.6$ Hz), 152.7 (d, $J = 244.6$ Hz), 134.2 (m), 126.8 (m), 114.7 (m), 112.4 (m), 69.4 (d, $J = 9.3$ Hz), 53.1, 52.7. ^{19}F NMR (376 MHz, CDCl_3 , minor and major isomer): δ -102.94 (ddd, $J = 20.0, 7.7, 3.6$ Hz), -105.75 (ddd, $J = 20.1, 7.9, 3.6$ Hz), -120.43 to -120.56 (m), -120.83 to -120.96 (m). LRMS (LIFDI): m/z 623.94 (100%, $[\text{M}]^+$). Anal. Calcd for $\text{C}_{18}\text{H}_{20}\text{F}_4\text{N}_2\text{Cl}_2\text{Pd}_2$: C, 34.64; H, 3.23; N, 4.49. Found: C, 34.49; H, 3.16; N, 4.25.

*Di- μ -chlorobis[*o*-dimethylaminomethyl-3,4-*p,m*-difluorophenyl-*C,N*]dipalladium(II) (**3e_o**)*. Complex **3e_o** was prepared according to general procedure B, on a 0.77 mmol scale, to afford the product in a mixture of geometrical isomers (*syn* and *anti*) as a yellow powder (171 mg, 71%). Mp: 178.6–180.2 °C (dec). ^1H NMR (400 MHz, CDCl_3): δ 6.92 (ddd, $J = 19.1, 10.6, 8.6$ Hz, 2H), 6.74 (dd, $J = 10.6, 7.6$ Hz, 2H), 3.88 (s, 4H), 2.85 (s, 6H), 2.82 (s, 6H). ^{19}F NMR (376 MHz, CDCl_3): δ -140.16 to -140.28 (m, major isomer), -140.48 to -140.62 (m, minor isomer), -143.44 to -143.56 (m, major isomer), -143.61 to -143.73 (m, minor isomer). HSQC NMR (500, 126 MHz): δ (6.92, 121.1), (6.74, 109.9), (3.88, 72.5), (2.85, 52.6). Far-IR (ATR, ν cm^{-1}): 520.26 (w), 466.51 (w), 439.59 (m), 374.08 (m), 319.81 (s), 278.79 (m), 263.58 (m), 236.05 (m), 211.74 (w), 180.23 (w). LRMS (LIFDI): m/z 623.89 (100%, $[\text{M}]^+$). Anal. Calcd for $\text{C}_{18}\text{H}_{20}\text{F}_4\text{N}_2\text{Cl}_2\text{Pd}_2$: C, 34.64; H, 3.23; N, 4.49. Found: C, 34.64; H, 3.19; N, 4.28.

*Chloro- κ -[*o*-dimethylaminomethyl-3,4-*p,m*-difluorophenyl-*C,N*]-(pyridine-*d*₅)palladium(II) (**3e_{pyr}**)*. A portion of di- μ -chlorobis[*o*-dimethylaminomethyl-3,4-*p,m*-difluorophenyl-*C,N*]dipalladium(II) (**3e_o**) was dissolved in pyridine-*d*₅ to obtain the title compound. ^1H NMR (500 MHz, CDCl_3): δ 7.03–6.96 (m, 1H), 6.04 (t, $J = 9.5$ Hz, 1H), 3.88 (s, 2H), 2.94 (s, 6H). ^{19}F NMR (471 MHz, CDCl_3): δ -142.28 to -142.52 (m), -144.96 to -145.08 (m).

*Dichlorobis(2,4-difluoro-*N,N*-dimethylbenzylamine) (**4d**)*. Complex **4d** was prepared according to general procedure B, on a 0.29 mmol scale, to afford the product as an orange powder (111 mg, 73%). The product was crystallized in air by slow diffusion of hexane into a saturated solution of the compound in chloroform. Mp: 132.0–135.4 °C (dec). ^1H NMR (500 MHz, CDCl_3): δ 8.77 (ddd, $J = 8.8, 5.5, 3.2$ Hz, 2H), 7.12 (ddd, $J = 14.3, 7.3, 3.7$ Hz, 4H), 3.90 (s, 4H), 2.60 (s, 12H). $^{13}\text{C}\{^1\text{H}\}$ NMR (126 MHz, CDCl_3): δ 158.4 (dd, $J = 242.4, 2.2$ Hz), 157.9 (dd, $J = 243.70, 2.5$ Hz), 123.1 (dd, $J = 16.62, 8.12$ Hz), 120.5 (dd, $J = 24.9, 3.7$ Hz), 117.62 (dd, $J = 24.1, 8.9$ Hz), 116.78 (dd, $J = 26.1, 8.6$ Hz), 60.09, 54.01 (d, $J = 0.6$ Hz). ^{19}F NMR (376 MHz, CDCl_3): -118.27 to -118.28 (m), -121.45 to -121.59 (m). HRMS (ESI): m/z 483.0453 (100%, $[\text{M} + \text{H} - \text{Cl}]^+$) (calculated for $\text{C}_{18}\text{H}_{22}\text{F}_4\text{N}_2\text{PdCl}$ 483.0441, difference $\Delta = -1.2$ mDa). Anal. Calcd for $\text{C}_{18}\text{H}_{22}\text{F}_4\text{N}_2\text{Cl}_2\text{Pd}$: C, 41.60; H, 4.27; N, 5.39. Found: C, 41.28; H, 4.14; N, 5.13.

■ ASSOCIATED CONTENT

Supporting Information

The Supporting Information is available free of charge on the ACS Publications website at DOI: 10.1021/acs.organomet.5b00608.

The synthetic procedure for the synthesis of fluorinated benzylamines, figures of the X-ray diffraction structures of compounds **2b**, **2c_o**, **2e_o**, **2f**, **3b**, **3c_o**, and **3e_o**, further X-ray diffraction analysis, X-ray data summary tables, and representative NMR spectra for all compounds (PDF) Crystallographic data (CIF)

■ AUTHOR INFORMATION

Corresponding Authors

*E-mail: ian.fairlamb@york.ac.uk.

*E-mail: robin.perutz@york.ac.uk.

Notes

The authors declare no competing financial interest.

■ ACKNOWLEDGMENTS

We acknowledge helpful discussions with Professor Odile Eisenstein. We are grateful to the University of York and Wild Fund for funding the Ph.D. studentship of J.M. EPSRC supported the purchase of some equipment used in this study (ENERGY grant, ref no. EP/K031589/1). We also acknowledge a Strategic Equipment Award from the University of York.

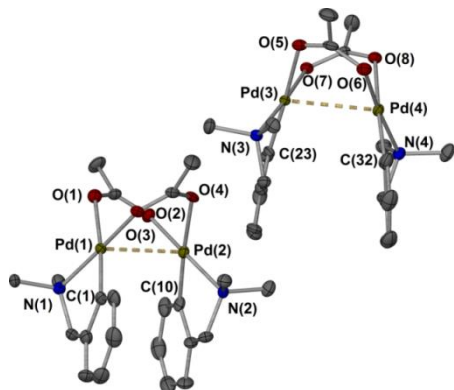
■ REFERENCES

- (1) Yamaguchi, J.; Yamaguchi, A. D.; Itami, K. *Angew. Chem., Int. Ed.* **2012**, *51*, 8960–9009.
- (2) (a) Stuart, D. R.; Fagnou, K. *Science* **2007**, *316*, 1172–1175. (b) Ackermann, L. *J. Org. Chem.* **2014**, *79*, 8948–8954. (c) Alberico, D.; Scott, M. E.; Lautens, M. *Chem. Rev.* **2007**, *107*, 174–238. (d) McNally, A.; Haffmeyer, B.; Collins, B. S. L.; Gaunt, M. J. *Nature* **2014**, *510*, 129–133.
- (3) (a) Anctil, E. J. G.; Snieckus, V. In *Metal-Catalyzed Cross-Coupling Reactions*; de Meijere, A., Diederich, F., Eds.; Wiley-VCH Verlag GmbH: Weinheim, 2008; pp 761–813. (b) Denmark, S. E.; Sweis, R. F. In *Metal-Catalyzed Cross-Coupling Reactions*; de Meijere, A., Diederich, F., Eds.; Wiley-VCH Verlag GmbH: Weinheim, 2008; pp 163–216. (c) Knochel, P.; Calaza, M. I.; Hupe, E. In *Metal-Catalyzed Cross-Coupling Reactions*; de Meijere, A., Diederich, F., Eds.; Wiley-VCH Verlag GmbH: Weinheim, 2008; pp 619–670.
- (4) (a) Källäne, S. I.; Braun, T. *Angew. Chem., Int. Ed.* **2014**, *53*, 9311–9315. (b) Carr, K. J. T.; Davies, D. L.; Macgregor, S. A.; Singh, K.; Villa-Marcos, B. *Chem. Sci.* **2014**, *5*, 2340–2346. (c) Ciana, C.-L.; Phipps, R. J.; Brandt, J. R.; Meyer, F.-M.; Gaunt, M. J. *Angew. Chem., Int. Ed.* **2011**, *50*, 458–462.
- (5) (a) Tang, R.-Y.; Li, G.; Yu, J.-Q. *Nature* **2014**, *507*, 215–220. (b) Kuhl, N.; Hopkinson, M. N.; Wencel-Delord, J.; Glorius, F. *Angew. Chem., Int. Ed.* **2012**, *51*, 10236–10254.
- (6) Luo, J.; Preciado, S.; Larrosa, I. *J. Am. Chem. Soc.* **2014**, *136*, 4109–4112.
- (7) (a) Clot, E.; Mégret, C.; Eisenstein, O.; Perutz, R. N. *J. Am. Chem. Soc.* **2009**, *131*, 7817–7827. (b) Burling, S.; Elliott, P. I. P.; Jasim, N. A.; Lindup, R. J.; McKenna, J.; Perutz, R. N.; Archibald, S. J.; Whitwood, A. C. *Dalton Trans.* **2005**, 3686–3695. (c) Clot, E.; Besora, M.; Maseras, F.; Megret, C.; Eisenstein, O.; Oelckers, B.; Perutz, R. N. *Chem. Commun.* **2003**, 490–491. (d) Weaver, J.; Senaweera, S. *Tetrahedron* **2014**, *70*, 7413–7428. (e) Amii, H.; Uneyama, K. *Chem. Rev.* **2009**, *109*, 2119–2183. (f) Ahrens, T.; Köhlmann, J.; Ahrens, M.; Braun, T. *Chem. Rev.* **2015**, *115*, 931–972. (g) Selmeczy, A. D.; Jones, W. D.; Partridge, M. G.; Perutz, R. N. *Organometallics* **1994**, *13*, 522–532. (h) Evans, M. E.; Burke, C. L.; Yaibuathes, S.; Clot, E.; Eisenstein, O.; Jones, W. D. *J. Am. Chem. Soc.* **2009**, *131*, 13464–13473.
- (8) Campeau, L.-C.; Parisien, M.; Leblanc, M.; Fagnou, K. *J. Am. Chem. Soc.* **2004**, *126*, 9186–9187.
- (9) Ackermann, L. *Chem. Rev.* **2011**, *111*, 1315–1345.
- (10) Grushin, V. V.; Thorn, D. L.; Marshall, W. J.; Petrov, V. A. In *Activation and Functionalization of C-H Bonds*; American Chemical Society: Washington, DC, 2004; Vol. 885, pp 393–406.
- (11) (a) Lafrance, M.; Rowley, C. N.; Woo, T. K.; Fagnou, K. *J. Am. Chem. Soc.* **2006**, *128*, 8754–8756. (b) Garcia-Cuadrado, D.; de Mendoza, P.; Braga, A. A. C.; Maseras, F.; Echavarren, A. M. *J. Am. Chem. Soc.* **2007**, *129*, 6880–6886.
- (12) Davies, D. L.; Donald, S. M. A.; Macgregor, S. A. *J. Am. Chem. Soc.* **2005**, *127*, 13754–13755.
- (13) Boutadla, Y.; Davies, D. L.; Macgregor, S. A.; Poblador-Bahamonde, A. I. *Dalton Trans.* **2009**, 5820–5831.
- (14) Gorelsky, S. I. *Coord. Chem. Rev.* **2013**, *257*, 153–164.
- (15) Guilhaumé, J.; Clot, E.; Eisenstein, O.; Perutz, R. N. *Dalton Trans.* **2010**, 39, 10510–10519.
- (16) Li, L.; Brennessel, W. W.; Jones, W. D. *Organometallics* **2009**, *28*, 3492–3500.

- (17) Fairlamb, I. J. S.; Grant, S.; McCormack, P.; Whittall, J. *Dalton Trans.* **2007**, 859–865.
- (18) Fairlamb, I. J. S.; Kapdi, A. R.; Lee, A. F.; Sanchez, G.; Lopez, G.; Serrano, J. L.; Garcia, L.; Perez, J.; Perez, E. *Dalton Trans.* **2004**, 3970–3981.
- (19) (a) Serrano, J. L.; Garcia, L.; Pérez, J.; Pérez, E.; Garcia, J.; Sánchez, G.; Sehnal, P.; De Ornellas, S.; Williams, T. J.; Fairlamb, I. J. S. *Organometallics* **2011**, *30*, 5095–5109. (b) Kapdi, A. R.; Dhangar, G.; Serrano, J. L.; Perez, J.; Garcia, L.; Fairlamb, I. J. S. *Chem. Commun.* **2014**, *50*, 9859–9861.
- (20) (a) Bedford, R. B. *Chem. Commun.* **2003**, 1787–1796. (b) Herrmann, W. A.; Öfele, K.; Preysing, D. v.; Schneider, S. K. *J. Organomet. Chem.* **2003**, *687*, 229–248. (c) Beletskaya, I. P.; Cheprakov, A. V. *J. Organomet. Chem.* **2004**, *689*, 4055–4082. (d) Dupont, J.; Pfeffer, M. *Palladacycles: Synthesis, Characterization and Applications*; Wiley: Weinheim, 2008. (e) Dupont, J.; Consorti, C. S.; Spencer, J. *Chem. Rev.* **2005**, *105*, 2527–2572. (f) Crawforth, C. M.; Fairlamb, I. J. S.; Kapdi, A. R.; Serrano, J. L.; Taylor, R. J. K.; Sanchez, G. *Adv. Synth. Catal.* **2006**, *348*, 405–412.
- (21) (a) Thompson, J. M.; Heck, R. F. *J. Org. Chem.* **1975**, *40*, 2667–2674. (b) Cope, A. C.; Friedrich, E. C. *J. Am. Chem. Soc.* **1968**, *90*, 909–913.
- (22) Ryabov, A. D.; Sakodinskaya, I. K.; Yatsimirsky, A. K. *J. Chem. Soc., Dalton Trans.* **1985**, 2629–2638.
- (23) (a) Feng, R.; Yao, J.; Liang, Z.; Liu, Z.; Zhang, Y. *J. Org. Chem.* **2013**, *78*, 3688–3696. (b) Tan, P. W.; Haughey, M.; Dixon, D. J. *Chem. Commun.* **2015**, *51*, 4406–4409.
- (24) Lenoir, D. *Angew. Chem., Int. Ed.* **2003**, *42*, 854–857.
- (25) Gross, J.; Nieth, N.; Linden, H. B.; Blumbach, U.; Richter, F.; Tauchert, M.; Tompers, R.; Hofmann, P. *Anal. Bioanal. Chem.* **2006**, *386*, 52–58.
- (26) Lafrance, M.; Fagnou, K. *J. Am. Chem. Soc.* **2006**, *128*, 16496–16497.
- (27) Bajwa, S. E.; Storr, T. E.; Hatcher, L. E.; Williams, T. J.; Baumann, C. G.; Whitwood, A. C.; Allan, D. R.; Teat, S. J.; Raithby, P. R.; Fairlamb, I. J. S. *Chem. Sci.* **2012**, *3*, 1656–1661.
- (28) Bercaw, J. E.; Durrell, A. C.; Gray, H. B.; Green, J. C.; Hazari, N.; Labinger, J. A.; Winkler, J. R. *Inorg. Chem.* **2010**, *49*, 1801–1810.
- (29) Bondi, A. *J. Phys. Chem.* **1964**, *68*, 441–451.
- (30) Mentès, A.; Kemmitt, R. D. W.; Fawcett, J.; Russell, D. R. *J. Mol. Struct.* **2004**, *693*, 241–246.
- (31) Barr, N.; Dyke, S. F.; Smith, G.; Kennard, C. H. L.; McKee, V. *J. Organomet. Chem.* **1985**, *288*, 109–117.
- (32) Ryabov, A. D. *Inorg. Chem.* **1987**, *26*, 1252–1260.
- (33) Dolomanov, O. V.; Bourhis, L. J.; Gildea, R. J.; Howard, J. A. K.; Puschmann, H. *J. Appl. Crystallogr.* **2009**, *42*, 339–341.
- (34) (a) Palatinus, L.; Prathapa, S. J.; van Smaalen, S. *J. Appl. Crystallogr.* **2012**, *45*, 575–580. (b) Palatinus, L.; Chapuis, G. *J. Appl. Crystallogr.* **2007**, *40*, 786–790. (c) Palatinus, L.; van der Lee, A. *J. Appl. Crystallogr.* **2008**, *41*, 975–984.
- (35) Sheldrick, G. *Acta Crystallogr., Sect. A: Found. Crystallogr.* **2008**, *64*, 112–122.
- (36) Cotton, H. K.; Verboom, R. C.; Johansson, L.; Plietker, B. J.; Bäckvall, J.-E. *Organometallics* **2002**, *21*, 3367–3375.
- (37) Hiraki, K.; Fuchita, Y.; Uchiyama, T. *Inorg. Chim. Acta* **1983**, *69*, 187–190.

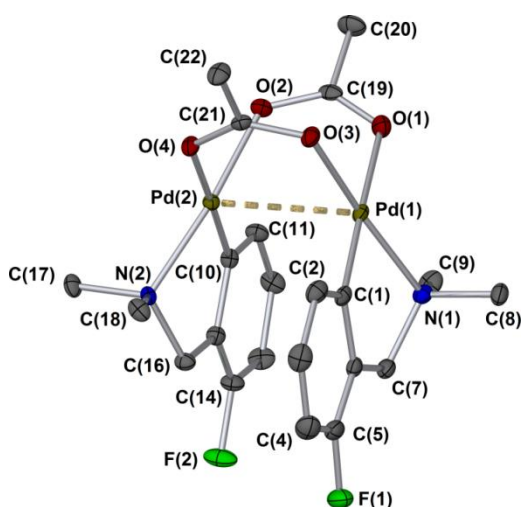
Appendix II: X-Ray diffraction data

Crystallographic data for compound 2.8a



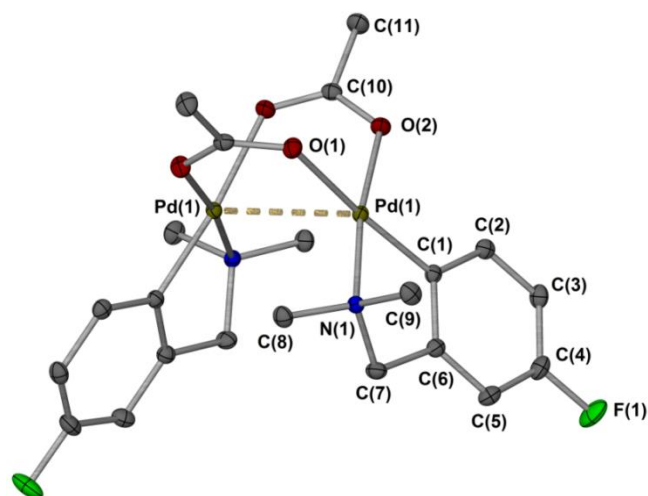
Identification code	ijsf1206c
Empirical formula	C ₂₂ H ₃₀ N ₂ O ₄ Pd ₂
Formula weight	599.28
Temperature/K	109.95(10)
Crystal system	monoclinic
Space group	P2 ₁
a/Å	9.31342(13)
b/Å	20.6214(2)
c/Å	13.02840(18)
α/°	90
β/°	110.8594(16)
γ/°	90
Volume/Å ³	2338.18(6)
Z	4
ρ _{calc} /cm ³	1.702
μ/mm ⁻¹	1.567
F(000)	1200.0
Crystal size/mm ³	0.2346 × 0.1923 × 0.1448
Radiation	MoKα (λ = 0.71073)
2θ range for data collection/°	6.126 to 64.542
Index ranges	-13 ≤ h ≤ 10, -30 ≤ k ≤ 30, -18 ≤ l ≤ 19
Reflections collected	26130
Independent reflections	14096 [R _{int} = 0.0255, R _{sigma} = 0.0427]
Data/restraints/parameters	14096/1/553
Goodness-of-fit on F ²	1.228
Final R indexes [I ≥ 2σ(I)]	R ₁ = 0.0442, wR ₂ = 0.0868
Final R indexes [all data]	R ₁ = 0.0499, wR ₂ = 0.0891
Largest diff. peak/hole / e Å ⁻³	1.68/-1.58
Flack parameter	-0.005(16)

Crystallographic data for compound 2.8b



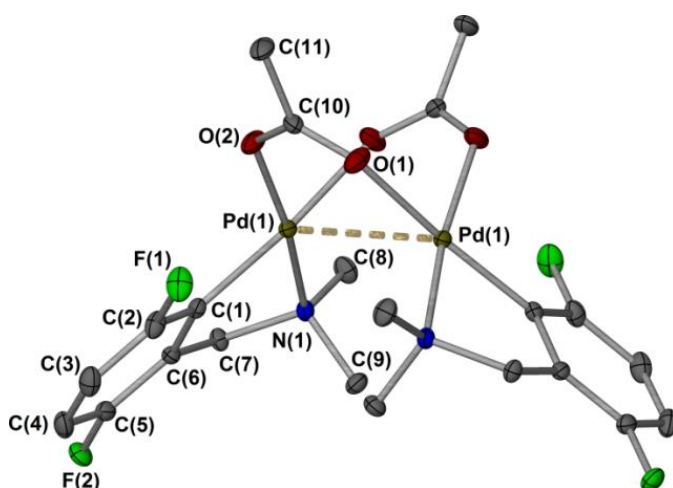
Identification code	ijsf1301
Empirical formula	C ₂₂ H ₂₈ F ₂ N ₂ O ₄ Pd ₂
Formula weight	635.26
Temperature/K	110.00(10)
Crystal system	monoclinic
Space group	P2 ₁
a/Å	8.34276(13)
b/Å	14.9448(2)
c/Å	9.77429(16)
α/°	90.00
β/°	106.0050(17)
γ/°	90.00
Volume/Å ³	1171.43(3)
Z	2
ρ _{calc} /mg/mm ³	1.801
m/mm ⁻¹	1.581
F(000)	632.0
Crystal size/mm ³	0.2526 × 0.1866 × 0.1103
2θ range for data collection	5.7 to 64.32°
Index ranges	-11 ≤ h ≤ 12, -22 ≤ k ≤ 22, -14 ≤ l ≤ 14
Reflections collected	14799
Independent reflections	7245[R(int) = 0.0300]
Data/restraints/parameters	7245/1/295
Goodness-of-fit on F ²	1.037
Final R indexes [I ≥ 2σ(I)]	R ₁ = 0.0267, wR ₂ = 0.0501
Final R indexes [all data]	R ₁ = 0.0293, wR ₂ = 0.0520
Largest diff. peak/hole / e Å ⁻³	0.41/-0.58
Flack parameter	-0.031(17)

Crystallographic data for compound 2.8c₆



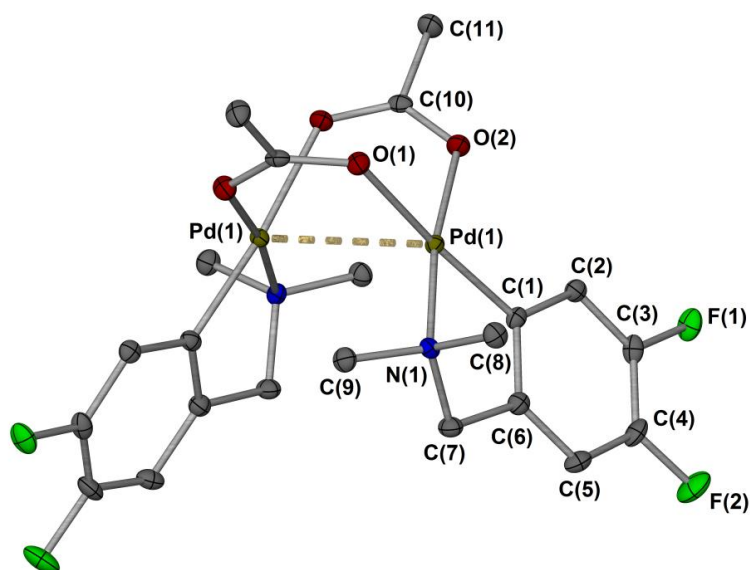
Identification code	rnp1401
Empirical formula	C ₂₂ H ₂₈ F ₂ N ₂ O ₄ Pd ₂
Formula weight	635.26
Temperature/K	110.05(10)
Crystal system	monoclinic
Space group	C2/c
a/Å	17.4700(4)
b/Å	7.50467(16)
c/Å	17.5432(3)
α/°	90
β/°	92.9917(19)
γ/°	90
Volume/Å ³	2296.90(8)
Z	4
ρ _{calc} /cm ³	1.837
μ/mm ⁻¹	1.613
F(000)	1264.0
Crystal size/mm ³	0.1975 × 0.139 × 0.1055
Radiation	MoKα (λ = 0.71073)
2θ range for data collection/°	5.91 to 64.19
Index ranges	-26 ≤ h ≤ 23, -10 ≤ k ≤ 11, -21 ≤ l ≤ 25
Reflections collected	6007
Independent reflections	3621 [R _{int} = 0.0239, R _{sigma} = 0.0428]
Data/restraints/parameters	3621/0/148
Goodness-of-fit on F ²	1.055
Final R indexes [I ≥ 2σ (I)]	R ₁ = 0.0283, wR ₂ = 0.0577
Final R indexes [all data]	R ₁ = 0.0346, wR ₂ = 0.0625
Largest diff. peak/hole / e Å ⁻³	0.50/-0.73

Crystallographic data for compound 2.8d



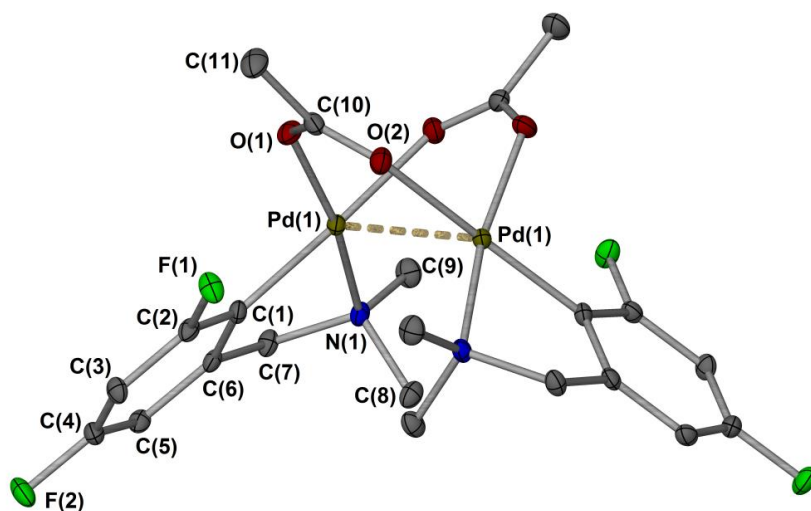
Identification code	ijsf1230a
Empirical formula	C ₂₂ H ₂₆ F ₄ N ₂ O ₄ Pd ₂
Formula weight	671.25
Temperature/K	110.00(10)
Crystal system	monoclinic
Space group	C2/c
a/Å	20.2373(7)
b/Å	9.09573(16)
c/Å	15.6668(5)
α/°	90
β/°	127.316(5)
γ/°	90
Volume/Å ³	2293.53(19)
Z	4
ρ _{calc} /cm ³	1.944
μ/mm ⁻¹	1.633
F(000)	1328.0
Crystal size/mm ³	0.3141 × 0.1863 × 0.1693
Radiation	MoKα (λ = 0.71073)
2θ range for data collection/°	6.54 to 63.96
Index ranges	-29 ≤ h ≤ 28, -12 ≤ k ≤ 13, -23 ≤ l ≤ 22
Reflections collected	6669
Independent reflections	3642 [R _{int} = 0.0228, R _{sigma} = 0.0422]
Data/restraints/parameters	3642/0/157
Goodness-of-fit on F ²	1.087
Final R indexes [I ≥ 2σ (I)]	R ₁ = 0.0274, wR ₂ = 0.0551
Final R indexes [all data]	R ₁ = 0.0386, wR ₂ = 0.0658
Largest diff. peak/hole / e Å ⁻³	0.52/-0.63

Crystallographic data for compound 2.8e₆



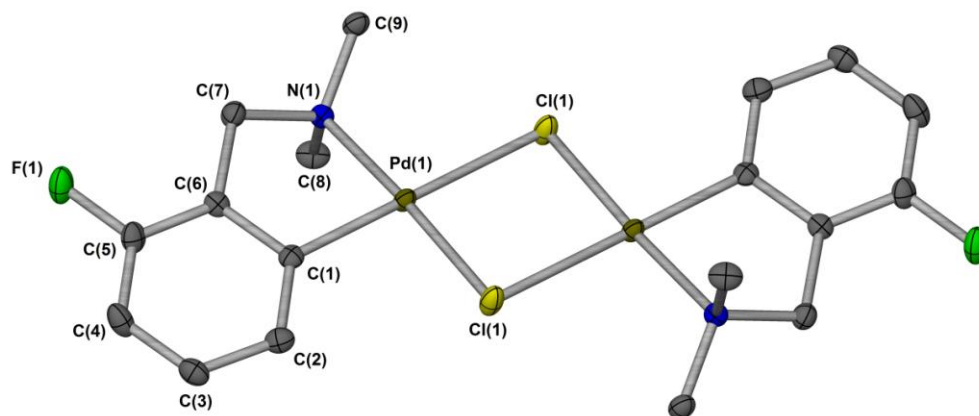
Identification code	rnp1402
Empirical formula	C ₂₂ H ₂₆ F ₄ N ₂ O ₄ Pd ₂
Formula weight	671.25
Temperature/K	110.05(10)
Crystal system	monoclinic
Space group	C2/c
a/Å	17.6919(3)
b/Å	7.43257(15)
c/Å	17.7733(3)
α/°	90
β/°	92.3531(17)
γ/°	90
Volume/Å ³	2335.14(7)
Z	4
ρ _{calc} /cm ³	1.909
μ/mm ⁻¹	1.604
F(000)	1328.0
Crystal size/mm ³	0.2194 × 0.1447 × 0.1195
Radiation	MoKα (λ = 0.71073)
2θ range for data collection/°	5.946 to 60.046
Index ranges	-24 ≤ h ≤ 22, -10 ≤ k ≤ 4, -24 ≤ l ≤ 25
Reflections collected	5735
Independent reflections	3399 [R _{int} = 0.0191, R _{sigma} = 0.0359]
Data/restraints/parameters	3399/0/157
Goodness-of-fit on F ²	1.053
Final R indexes [I ≥ 2σ (I)]	R ₁ = 0.0240, wR ₂ = 0.0536
Final R indexes [all data]	R ₁ = 0.0289, wR ₂ = 0.0566
Largest diff. peak/hole / e Å ⁻³	0.50/-0.75

Crystallographic data for compound 2.8f



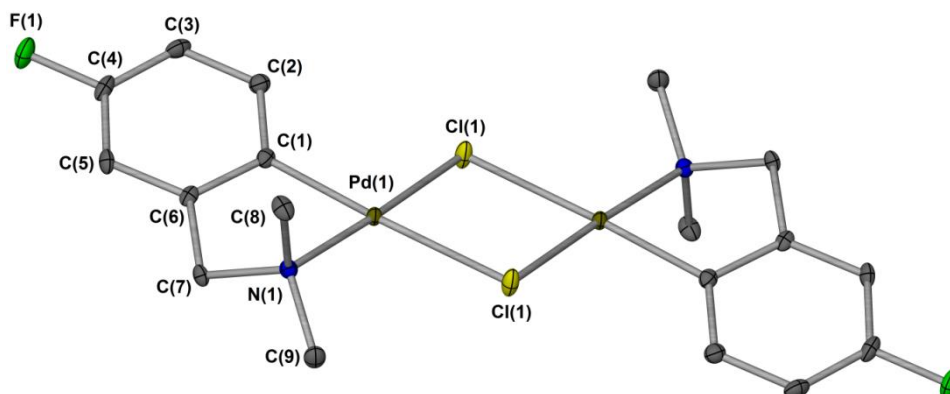
Identification code	rnp1335_twin1_hklf4
Empirical formula	C ₂₂ H ₂₆ F ₄ N ₂ O ₄ Pd ₂
Formula weight	671.25
Temperature/K	110.05(10)
Crystal system	monoclinic
Space group	P2/n
a/Å	10.9551(4)
b/Å	8.3786(6)
c/Å	12.6805(4)
α/°	90
β/°	95.351(3)
γ/°	90
Volume/Å ³	1158.85(10)
Z	2
ρ _{calc} /cm ³	1.924
μ/mm ⁻¹	1.616
F(000)	664.0
Crystal size/mm ³	0.3204 × 0.0568 × 0.055
Radiation	MoKα (λ = 0.71073)
2θ range for data collection/°	5.836 to 60.428
Index ranges	-15 ≤ h ≤ 15, -11 ≤ k ≤ 11, -17 ≤ l ≤ 17
Reflections collected	3553
Independent reflections	3553 [R _{int} = ?, R _{sigma} = 0.0296]
Data/restraints/parameters	3553/0/158
Goodness-of-fit on F ²	0.997
Final R indexes [I ≥ 2σ (I)]	R ₁ = 0.0277, wR ₂ = 0.0727
Final R indexes [all data]	R ₁ = 0.0336, wR ₂ = 0.0746
Largest diff. peak/hole / e Å ⁻³	1.42/-1.17

Crystallographic data for compound 2.9b



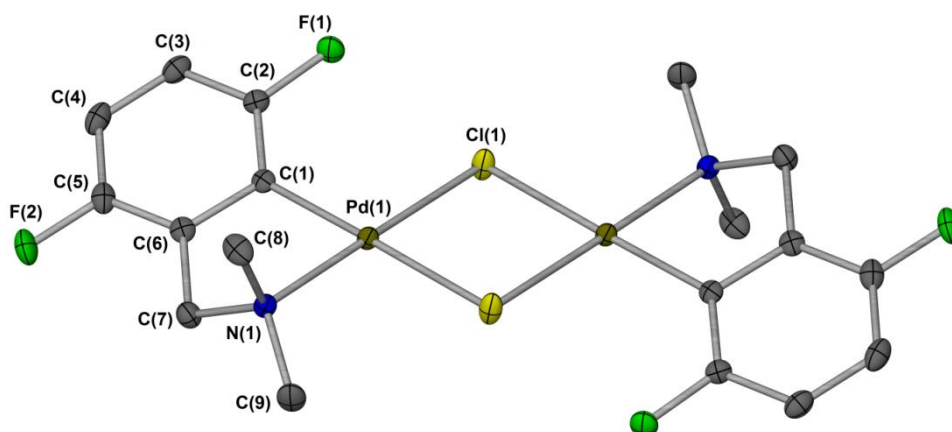
Identification code	rnp1502
Empirical formula	C ₁₈ H ₂₂ Cl ₂ F ₂ N ₂ Pd ₂
Formula weight	588.07
Temperature/K	110.05(10)
Crystal system	monoclinic
Space group	P2 ₁ /c
a/Å	7.5434(4)
b/Å	16.2089(5)
c/Å	8.2984(3)
α/°	90
β/°	106.421(4)
γ/°	90
Volume/Å ³	973.26(7)
Z	2
ρ _{calc} /cm ³	2.007
μ/mm ⁻¹	2.145
F(000)	576.0
Crystal size/mm ³	0.1846 × 0.1174 × 0.1041
Radiation	MoKα (λ = 0.71073)
2θ range for data collection/°	6.924 to 64.354
Index ranges	-8 ≤ h ≤ 11, -23 ≤ k ≤ 20, -11 ≤ l ≤ 12
Reflections collected	5624
Independent reflections	3060 [R _{int} = 0.0299, R _{sigma} = 0.0508]
Data/restraints/parameters	3060/0/120
Goodness-of-fit on F ²	1.140
Final R indexes [I ≥ 2σ (I)]	R ₁ = 0.0389, wR ₂ = 0.0812
Final R indexes [all data]	R ₁ = 0.0505, wR ₂ = 0.0865
Largest diff. peak/hole / e Å ⁻³	1.73/-1.08

Crystallographic data for compound 2.9c₆



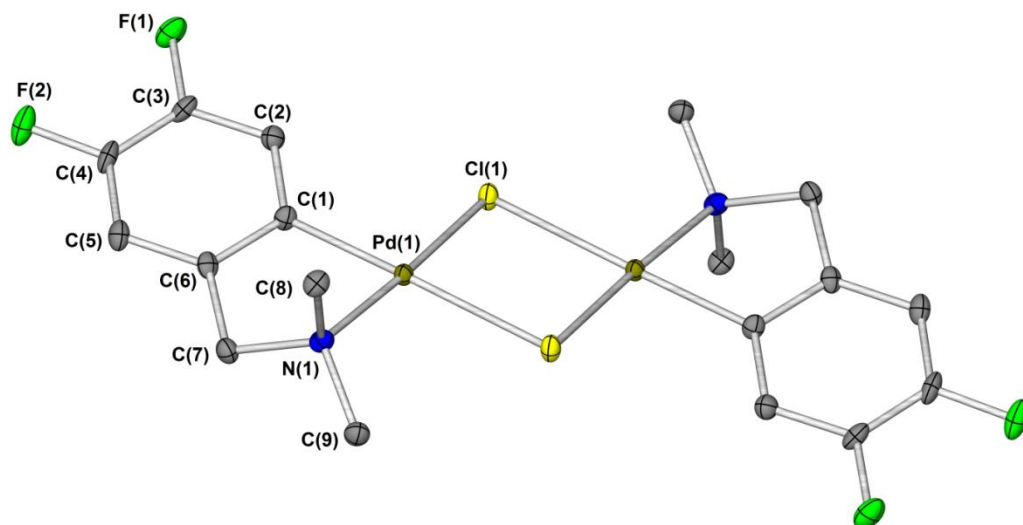
Identification code	rnp1501
Empirical formula	C ₁₈ H ₂₂ Cl ₂ F ₂ N ₂ Pd ₂
Formula weight	588.07
Temperature/K	110.05(10)
Crystal system	triclinic
Space group	P-1
a/Å	7.1636(7)
b/Å	8.0381(8)
c/Å	9.4603(9)
α/°	70.599(9)
β/°	72.092(9)
γ/°	80.881(8)
Volume/Å ³	487.95(9)
Z	1
ρ _{calc} /cm ³	2.001
μ/mm ⁻¹	2.139
F(000)	288.0
Crystal size/mm ³	0.23 × 0.1067 × 0.0992
Radiation	MoKα (λ = 0.71073)
2θ range for data collection/°	6.546 to 64.28
Index ranges	-5 ≤ h ≤ 10, -11 ≤ k ≤ 12, -13 ≤ l ≤ 14
Reflections collected	5092
Independent reflections	3033 [R _{int} = 0.0234, R _{sigma} = 0.0455]
Data/restraints/parameters	3033/0/120
Goodness-of-fit on F ²	1.051
Final R indexes [I ≥ 2σ (I)]	R ₁ = 0.0257, wR ₂ = 0.0522
Final R indexes [all data]	R ₁ = 0.0296, wR ₂ = 0.0557
Largest diff. peak/hole / e Å ⁻³	0.64/-0.92

Crystallographic data for compound 2.9d



Identification code	ijsf1452
Empirical formula	C ₁₈ H ₂₀ Cl ₂ F ₄ N ₂ Pd ₂
Formula weight	624.06
Temperature/K	110.05(10)
Crystal system	monoclinic
Space group	P2 ₁ /c
a/Å	5.67526(12)
b/Å	26.5650(6)
c/Å	6.85327(14)
α/°	90
β/°	94.9534(19)
γ/°	90
Volume/Å ³	1029.36(4)
Z	2
ρ _{calc} /cm ³	2.013
μ/mm ⁻¹	2.048
F(000)	608.0
Crystal size/mm ³	0.4419 × 0.0621 × 0.0294
Radiation	MoKα (λ = 0.71073)
2θ range for data collection/°	6.134 to 64.306
Index ranges	-7 ≤ h ≤ 8, -39 ≤ k ≤ 39, -10 ≤ l ≤ 9
Reflections collected	18211
Independent reflections	3380 [R _{int} = 0.0405, R _{sigma} = 0.0305]
Data/restraints/parameters	3380/0/129
Goodness-of-fit on F ²	1.352
Final R indexes [I ≥ 2σ (I)]	R ₁ = 0.0390, wR ₂ = 0.0650
Final R indexes [all data]	R ₁ = 0.0428, wR ₂ = 0.0662
Largest diff. peak/hole / e Å ⁻³	1.03/-0.95
<i>Structure solved by Jessica Milani / Natalie Pridmore</i>	

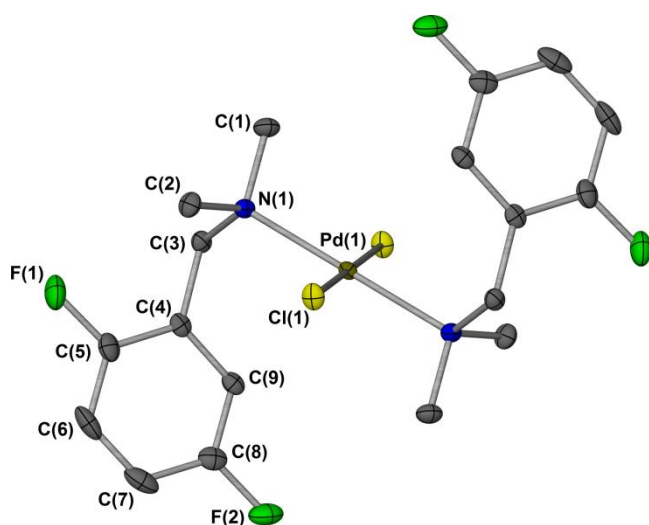
Crystallographic data for compound 2.9e₆



Identification code	ijsf1412
Empirical formula	C ₁₈ H ₂₀ Cl ₂ F ₄ N ₂ Pd ₂
Formula weight	624.06
Temperature/K	110.00(14)
Crystal system	triclinic
Space group	P-1
a/Å	7.3719(12)
b/Å	8.4847(12)
c/Å	9.1417(13)
α/°	81.053(12)
β/°	66.775(15)
γ/°	73.087(13)
Volume/Å ³	502.19(14)
Z	1
ρ _{calc} /mg/mm ³	2.064
m/mm ⁻¹	2.099
F(000)	304.0
Crystal size/mm ³	0.1223 × 0.0586 × 0.0309
Radiation	MoKα (λ = 0.71073)
2θ range for data collection	6.21 to 63.694°
Index ranges	-10 ≤ h ≤ 10, -12 ≤ k ≤ 10, -12 ≤ l ≤ 13
Reflections collected	4767
Independent reflections	3097 [R _{int} = 0.0269, R _{sigma} = 0.0515]
Data/restraints/parameters	3097/0/129
Goodness-of-fit on F ²	1.162
Final R indexes [I ≥ 2σ (I)]	R ₁ = 0.0384, wR ₂ = 0.0891
Final R indexes [all data]	R ₁ = 0.0422, wR ₂ = 0.0914
Largest diff. peak/hole / e Å ⁻³	1.31/-0.85

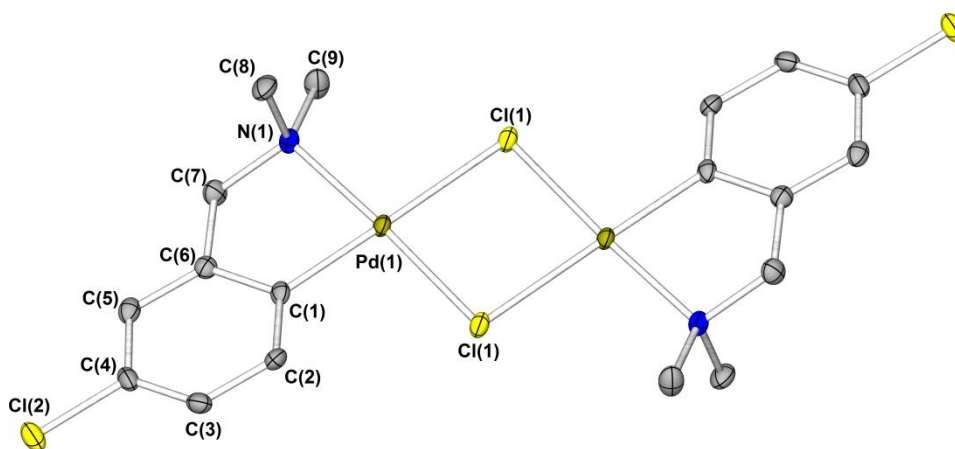
Structure solved by Natalie Pridmore

Crystallographic data for compound 2.28d



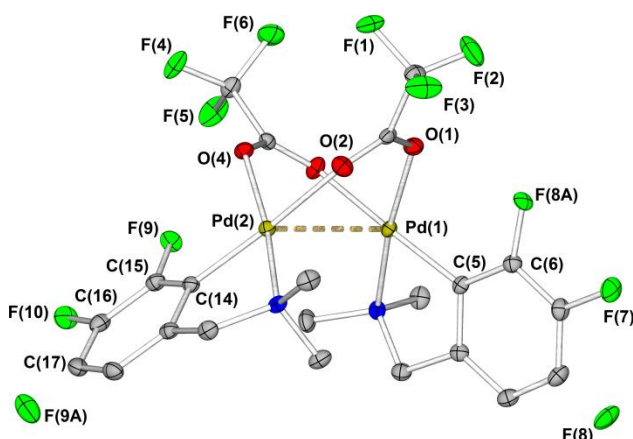
Identification code	rnp1516
Empirical formula	$C_{18}H_{22}Cl_2F_4N_2Pd$
Formula weight	519.67
Temperature/K	110.05(10)
Crystal system	monoclinic
Space group	$P2_1/c$
$a/\text{\AA}$	8.8260(2)
$b/\text{\AA}$	11.8134(2)
$c/\text{\AA}$	10.0300(2)
$\alpha/^\circ$	90
$\beta/^\circ$	108.378(3)
$\gamma/^\circ$	90
Volume/ \AA^3	992.44(4)
Z	2
$\rho_{\text{calc}}/\text{g/cm}^3$	1.739
μ/mm^{-1}	1.246
F(000)	520.0
Crystal size/ mm^3	$0.2084 \times 0.1004 \times 0.0873$
Radiation	MoK α ($\lambda = 0.71073$)
2 θ range for data collection/ $^\circ$	6.898 to 60.052
Index ranges	$-11 \leq h \leq 12, -15 \leq k \leq 16, -13 \leq l \leq 14$
Reflections collected	5221
Independent reflections	2573 [$R_{\text{int}} = 0.0215, R_{\text{sigma}} = 0.0334$]
Data/restraints/parameters	2573/0/126
Goodness-of-fit on F^2	1.076
Final R indexes [$I \geq 2\sigma(I)$]	$R_1 = 0.0242, wR_2 = 0.0508$
Final R indexes [all data]	$R_1 = 0.0294, wR_2 = 0.0550$
Largest diff. peak/hole / $e \text{\AA}^{-3}$	0.55/-0.64

Crystallographic data for compound 2.9g



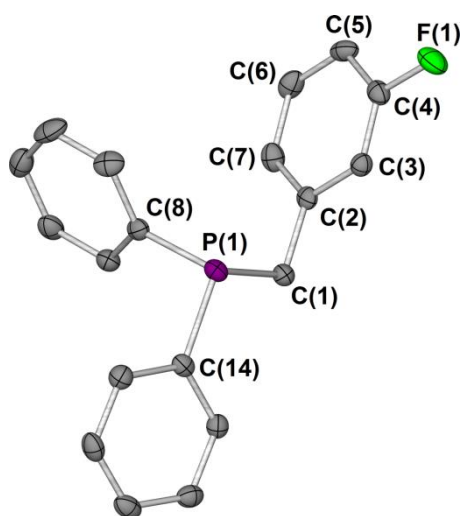
Identification code	ijsf1474
Empirical formula	C ₁₈ H ₂₂ Cl ₄ N ₂ Pd ₂
Formula weight	620.97
Temperature/K	110.05(10)
Crystal system	monoclinic
Space group	I2/c
a/Å	14.1764(4)
b/Å	5.54107(16)
c/Å	26.6827(7)
α/°	90
β/°	98.324(3)
γ/°	90
Volume/Å ³	2073.91(11)
Z	4
ρ _{calc} /cm ³	1.989
μ/mm ⁻¹	2.255
F(000)	1216.0
Crystal size/mm ³	0.2683 × 0.1982 × 0.0378
Radiation	MoKα (λ = 0.71073)
2θ range for data collection/°	6.962 to 64.422
Index ranges	-20 ≤ h ≤ 17, -7 ≤ k ≤ 6, -39 ≤ l ≤ 29
Reflections collected	5671
Independent reflections	3276 [R _{int} = 0.0260, R _{sigma} = 0.0433]
Data/restraints/parameters	3276/0/120
Goodness-of-fit on F ²	1.063
Final R indexes [I ≥ 2σ (I)]	R ₁ = 0.0281, wR ₂ = 0.0535
Final R indexes [all data]	R ₁ = 0.0363, wR ₂ = 0.0587
Largest diff. peak/hole / e Å ⁻³	0.57/-0.46

Crystallographic data for compound 2.30



Identification code	ijsf1454
Empirical formula	$C_{22}H_{24}F_6N_2O_4Pd_2$
Formula weight	707.23
Temperature/K	110.05(10)
Crystal system	orthorhombic
Space group	$Pna2_1$
$a/\text{\AA}$	13.9642(5)
$b/\text{\AA}$	16.9116(6)
$c/\text{\AA}$	10.4352(5)
$\alpha/^\circ$	90
$\beta/^\circ$	90
$\gamma/^\circ$	90
Volume/ \AA^3	2464.33(16)
Z	4
$\rho_{\text{calc}}/\text{g cm}^{-3}$	1.906
μ/mm^{-1}	1.537
F(000)	1392.0
Crystal size/ mm^3	$0.3626 \times 0.1099 \times 0.0941$
Radiation	$\text{MoK}\alpha$ ($\lambda = 0.7107$)
2θ range for data collection/ $^\circ$	5.828 to 64.474
Index ranges	$-9 \leq h \leq 20, -25 \leq k \leq 11, -8 \leq l \leq 15$
Reflections collected	10081
Independent reflections	5264 [$R_{\text{int}} = 0.0307, R_{\text{sigma}} = 0.0417$]
Data/restraints/parameters	5264/37/339
Goodness-of-fit on F^2	1.178
Final R indexes [$I \geq 2\sigma(I)$]	$R_1 = 0.0334, wR_2 = 0.0787$
Final R indexes [all data]	$R_1 = 0.0368, wR_2 = 0.0809$
Largest diff. peak/hole / $e \text{\AA}^{-3}$	0.95/-0.80
Flack parameter	-0.04(3)

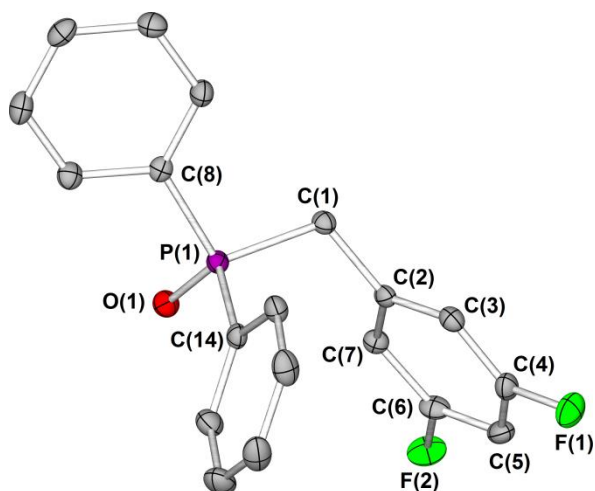
Crystallographic data for compound 3.3



Identification code	rnp1343
Empirical formula	C ₁₉ H ₁₆ FP
Formula weight	294.29
Temperature/K	110.05(10)
Crystal system	monoclinic
Space group	P2 ₁ /c
a/Å	12.2509(3)
b/Å	18.1309(5)
c/Å	7.0183(2)
α/°	90
β/°	101.841(3)
γ/°	90
Volume/Å ³	1525.73(7)
Z	4
ρ _{calc} /mg/mm ³	1.281
m/mm ⁻¹	0.181
F(000)	616.0
Crystal size/mm ³	0.1592 × 0.0947 × 0.0197
Radiation	MoKα (λ = 0.7107)
2θ range for data collection	5.628 to 55.98°
Index ranges	-16 ≤ h ≤ 10, -22 ≤ k ≤ 10, -9 ≤ l ≤ 8
Reflections collected	5326
Independent reflections	3075 [R _{int} = 0.0262, R _{sigma} = 0.0482]
Data/restraints/parameters	3075/0/190
Goodness-of-fit on F ²	1.084
Final R indexes [I ≥ 2σ (I)]	R ₁ = 0.0425, wR ₂ = 0.0943
Final R indexes [all data]	R ₁ = 0.0584, wR ₂ = 0.1035
Largest diff. peak/hole / e Å ⁻³	0.45/-0.27

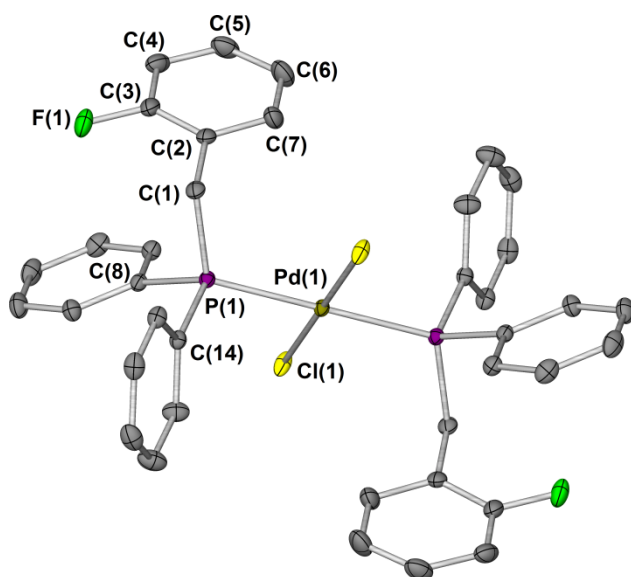
Structure solved by Natalie Pridmore

Crystallographic data for compound 3.5 oxide



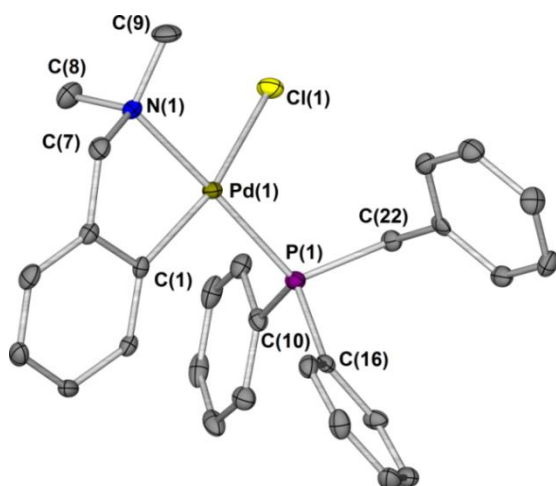
Identification code	ijsf1475
Empirical formula	C ₁₉ H ₁₅ F ₂ OP
Formula weight	328.28
Temperature/K	110.05(10)
Crystal system	triclinic
Space group	P-1
a/Å	5.7921(4)
b/Å	10.8895(9)
c/Å	13.5552(9)
α/°	68.131(7)
β/°	80.824(6)
γ/°	80.864(7)
Volume/Å ³	778.66(11)
Z	2
ρ _{calc} /cm ³	1.400
μ/mm ⁻¹	1.772
F(000)	340.0
Crystal size/mm ³	0.4485 × 0.0756 × 0.0286
Radiation	CuKα (λ = 1.54184)
2θ range for data collection/°	7.07 to 142.568
Index ranges	-6 ≤ h ≤ 7, -13 ≤ k ≤ 11, -15 ≤ l ≤ 16
Reflections collected	8403
Independent reflections	2944 [R _{int} = 0.0461, R _{sigma} = 0.0480]
Data/restraints/parameters	2944/0/208
Goodness-of-fit on F ²	1.060
Final R indexes [I ≥ 2σ (I)]	R ₁ = 0.0438, wR ₂ = 0.1156
Final R indexes [all data]	R ₁ = 0.0558, wR ₂ = 0.1275
Largest diff. peak/hole / e Å ⁻³	0.59/-0.56

Crystallographic data for compound 3.24



Identification code	ijsf1483
Empirical formula	C ₃₈ H ₃₂ Cl ₂ F ₂ P ₂ Pd
Formula weight	765.87
Temperature/K	110.05(10)
Crystal system	monoclinic
Space group	P2 ₁ /c
a/Å	10.30231(13)
b/Å	12.86918(12)
c/Å	12.84340(13)
α/°	90
β/°	99.1419(11)
γ/°	90
Volume/Å ³	1681.18(3)
Z	2
ρ _{calc} /cm ³	1.513
μ/mm ⁻¹	0.844
F(000)	776.0
Crystal size/mm ³	0.2301 × 0.1582 × 0.132
Radiation	MoKα (λ = 0.71073)
2θ range for data collection/°	7.006 to 64.314
Index ranges	-15 ≤ h ≤ 15, -18 ≤ k ≤ 19, -18 ≤ l ≤ 18
Reflections collected	18463
Independent reflections	5447 [R _{int} = 0.0254, R _{sigma} = 0.0268]
Data/restraints/parameters	5447/0/205
Goodness-of-fit on F ²	1.079
Final R indexes [I >= 2σ (I)]	R ₁ = 0.0272, wR ₂ = 0.0710
Final R indexes [all data]	R ₁ = 0.0317, wR ₂ = 0.0740
Largest diff. peak/hole / e Å ⁻³	1.03/-0.90

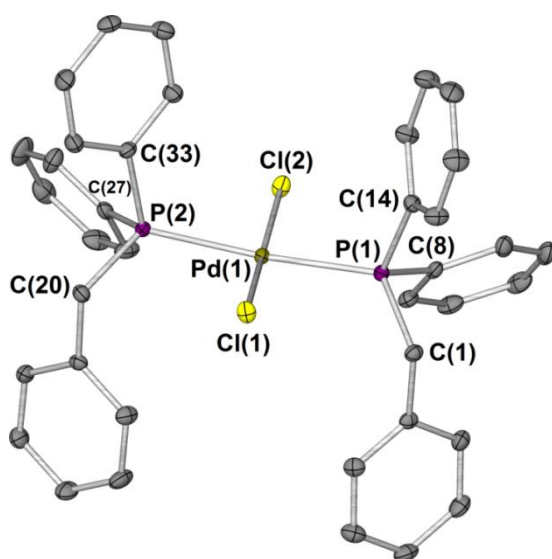
Crystallographic data for compound 3.26



Identification code	rnp1327
Empirical formula	C ₂₈ H ₂₉ ClNPPd
Formula weight	552.34
Temperature/K	110.05(10)
Crystal system	monoclinic
Space group	P2 ₁ /c
a/Å	10.3589(4)
b/Å	9.2275(4)
c/Å	25.5444(10)
α/°	90.00
β/°	92.686(4)
γ/°	90.00
Volume/Å ³	2439.03(16)
Z	4
ρ _{calc} /mg/mm ³	1.504
m/mm ⁻¹	0.952
F(000)	1128.0
Crystal size/mm ³	0.102 × 0.0773 × 0.0437
2θ range for data collection	5.92 to 56°
Index ranges	-8 ≤ h ≤ 13, -5 ≤ k ≤ 11, -31 ≤ l ≤ 32
Reflections collected	9223
Independent reflections	4939[R(int) = 0.0298]
Data/restraints/parameters	4939/0/291
Goodness-of-fit on F ²	1.049
Final R indexes [I ≥ 2σ(I)]	R ₁ = 0.0319, wR ₂ = 0.0603
Final R indexes [all data]	R ₁ = 0.0432, wR ₂ = 0.0648
Largest diff. peak/hole / e Å ⁻³	0.56/-0.43

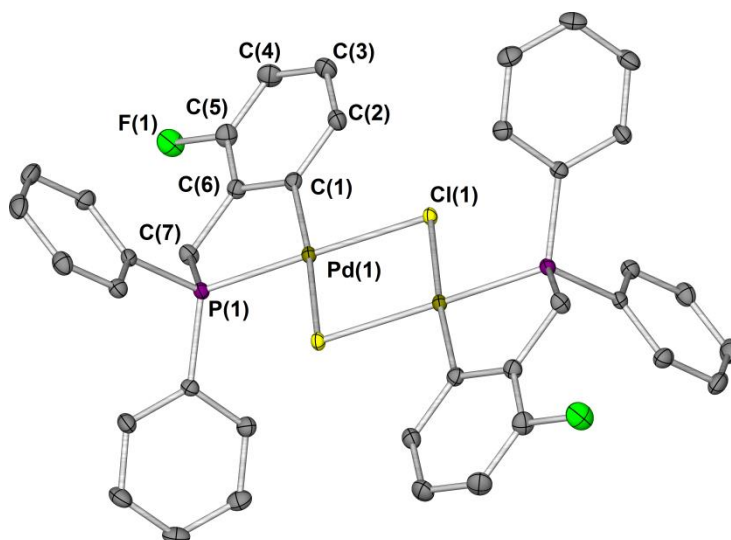
Structure solved by Natalie Pridmore

Crystallographic data for compound 3.27



Identification code	ijsf1316
Empirical formula	$C_{38}H_{34}Cl_2P_2Pd$
Formula weight	729.89
Temperature/K	110.3(4)
Crystal system	triclinic
Space group	P-1
$a/\text{\AA}$	9.5620(4)
$b/\text{\AA}$	13.3839(6)
$c/\text{\AA}$	14.7428(7)
$\alpha/^\circ$	66.077(4)
$\beta/^\circ$	73.025(4)
$\gamma/^\circ$	88.110(3)
Volume/ \AA^3	1641.63(14)
Z	2
$\rho_{\text{calc}}/\text{mg/mm}^3$	1.477
m/mm^{-1}	0.852
F(000)	744.0
Crystal size/ mm^3	$0.2309 \times 0.1586 \times 0.1109$
2θ range for data collection	5.82 to 60.06°
Index ranges	$-12 \leq h \leq 13$, $-18 \leq k \leq 18$, $-20 \leq l \leq 19$
Reflections collected	15464
Independent reflections	9526[R(int) = 0.0215]
Data/restraints/parameters	9526/0/388
Goodness-of-fit on F^2	1.022
Final R indexes [$I \geq 2\sigma(I)$]	$R_1 = 0.0273$, $wR_2 = 0.0609$
Final R indexes [all data]	$R_1 = 0.0321$, $wR_2 = 0.0640$
Largest diff. peak/hole / $e \text{\AA}^{-3}$	0.52/-0.57

Crystallographic data for compound 3.23

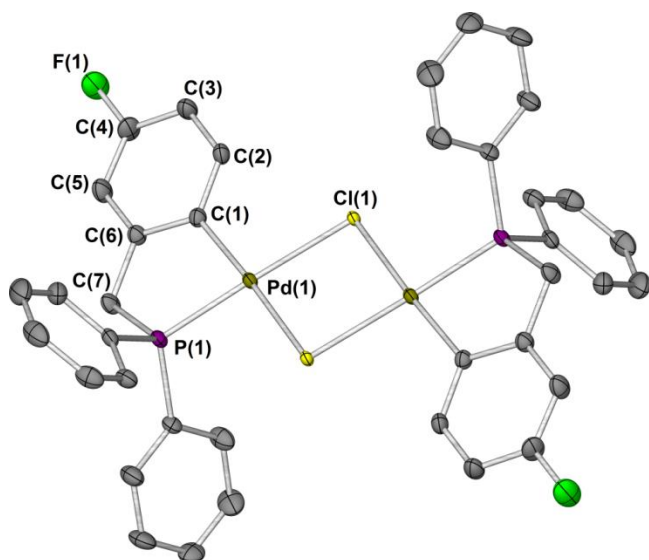


Identification code	ijsf1449
Empirical formula	C ₄₀ H ₃₄ Cl ₆ F ₂ P ₂ Pd ₂
Formula weight	1040.11
Temperature/K	110.00(14)
Crystal system	monoclinic
Space group	C2/c
a/Å	29.7555(4)
b/Å	9.10694(10)
c/Å	14.89351(19)
α/°	90
β/°	102.3937(12)
γ/°	90
Volume/Å ³	3941.82(8)
Z	4
ρ _{calc} /cm ³	1.753
μ/mm ⁻¹	1.440
F(000)	2064.0
Crystal size/mm ³	0.2747 × 0.1422 × 0.1057
Radiation	MoKα (λ = 0.71073)
2θ range for data collection/°	5.596 to 64.362
Index ranges	-43 ≤ h ≤ 44, -13 ≤ k ≤ 13, -21 ≤ l ≤ 22
Reflections collected	35361
Independent reflections	6563 [R _{int} = 0.0290, R _{sigma} = 0.0214]
Data/restraints/parameters	6563/1/239
Goodness-of-fit on F ²	1.038
Final R indexes [I ≥ 2σ (I)]	R ₁ = 0.0257, wR ₂ = 0.0607
Final R indexes [all data]	R ₁ = 0.0297, wR ₂ = 0.0632
Largest diff. peak/hole / e Å ⁻³	1.00/-0.97

Structure solved by Jessica Milani and Natalie Pridmore

Molecule of toluene in the unit cell not shown in the image above

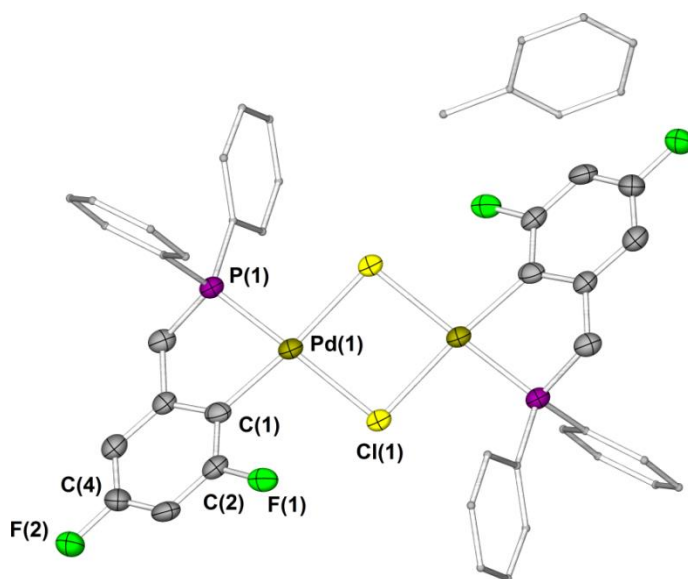
Crystallographic data for compound 3.28p



Identification code	ijsf1451
Empirical formula	C ₄₅ H ₃₈ Cl ₂ F ₂ P ₂ Pd ₂
Formula weight	962.39
Temperature/K	110.05(10)
Crystal system	triclinic
Space group	P-1
a/Å	8.3240(7)
b/Å	9.1137(5)
c/Å	14.4204(6)
α/°	82.369(4)
β/°	88.656(5)
γ/°	64.142(7)
Volume/Å ³	974.98(13)
Z	1
ρ _{calc} /cm ³	1.639
μ/mm ⁻¹	1.184
F(000)	482.0
Crystal size/mm ³	0.3105 × 0.1274 × 0.0431
Radiation	MoKα (λ = 0.71073)
2θ range for data collection/°	5.7 to 64.302
Index ranges	-11 ≤ h ≤ 10, -12 ≤ k ≤ 13, -20 ≤ l ≤ 21
Reflections collected	10050
Independent reflections	6094 [R _{int} = 0.0266, R _{sigma} = 0.0484]
Data/restraints/parameters	6094/3/266
Goodness-of-fit on F ²	1.054
Final R indexes [I ≥ 2σ (I)]	R ₁ = 0.0363, wR ₂ = 0.0823
Final R indexes [all data]	R ₁ = 0.0435, wR ₂ = 0.0886
Largest diff. peak/hole / e Å ⁻³	1.48/-0.96
<i>Structure solved by Natalie Pridmore and Jess Milani</i>	

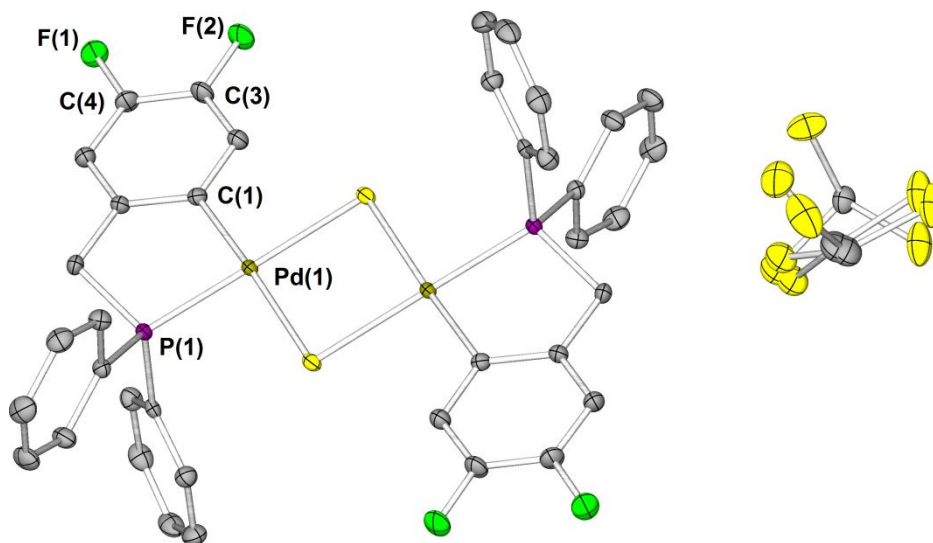
Molecule of toluene in the unit cell not shown in the image above

Crystallographic data for compound 3.29



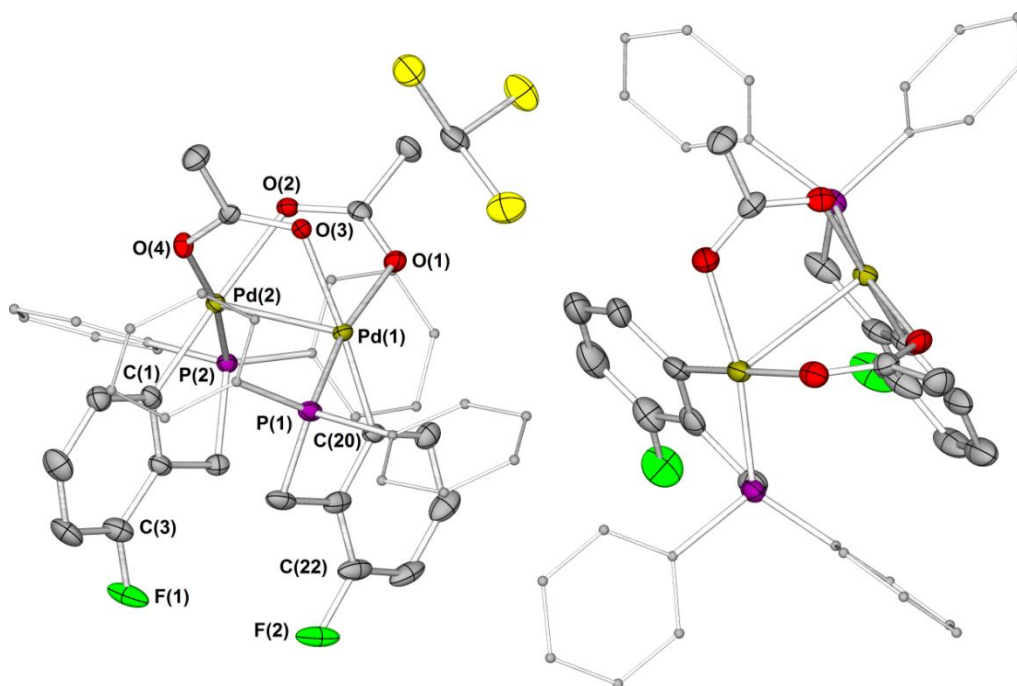
Identification code	rnp1421
Empirical formula	$C_{42.62}H_{33.28}Cl_2F_4P_2Pd_2$
Formula weight	967.05
Temperature/K	110.05(10)
Crystal system	trigonal
Space group	R-3
a/Å	26.323(3)
b/Å	26.323(3)
c/Å	15.0669(11)
$\alpha/^\circ$	90
$\beta/^\circ$	90
$\gamma/^\circ$	120
Volume/Å ³	9041.0(19)
Z	9
$\rho_{\text{calc}}/\text{cm}^3$	1.599
μ/mm^{-1}	9.605
F(000)	4329.0
Crystal size/mm ³	0.0831 × 0.0468 × 0.0264
Radiation	CuK α ($\lambda = 1.54184$)
2 θ range for data collection/ $^\circ$	7.032 to 142.198
Index ranges	-23 ≤ h ≤ 31, -31 ≤ k ≤ 23, -17 ≤ l ≤ 18
Reflections collected	10890
Independent reflections	3821 [$R_{\text{int}} = 0.0588$, $R_{\text{sigma}} = 0.0561$]
Data/restraints/parameters	3821/3/264
Goodness-of-fit on F ²	1.062
Final R indexes [$I \geq 2\sigma(I)$]	$R_1 = 0.0585$, $wR_2 = 0.1374$
Final R indexes [all data]	$R_1 = 0.0765$, $wR_2 = 0.1527$
Largest diff. peak/hole / e Å ⁻³	1.94/-2.07
<i>Structure solved by Natalie Pridmore</i>	

Crystallographic data for compound 3.30



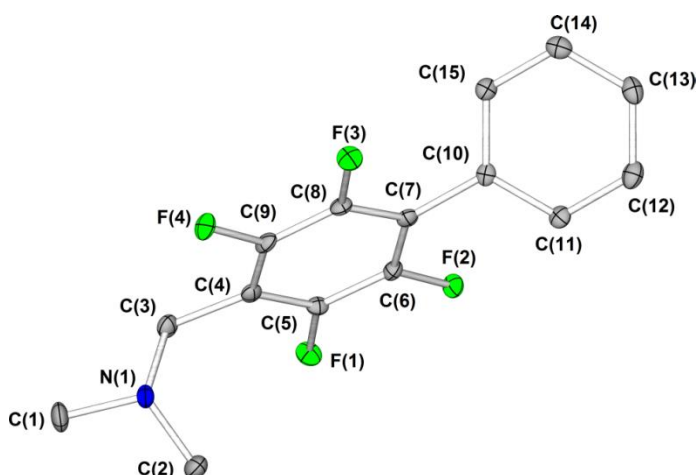
Identification code	rnpl519
Empirical formula	$C_{39.99}H_{29.99}Cl_{7.97}F_4P_2Pd_2$
Formula weight	1143.78
Temperature/K	110.05(10)
Crystal system	monoclinic
Space group	$P2_1/c$
$a/\text{\AA}$	15.0141(5)
$b/\text{\AA}$	9.1642(2)
$c/\text{\AA}$	15.2815(4)
$\alpha/^\circ$	90
$\beta/^\circ$	103.856(3)
$\gamma/^\circ$	90
Volume/ \AA^3	2041.43(10)
Z	2
$\rho_{\text{calc}}/\text{g cm}^{-3}$	1.861
μ/mm^{-1}	1.531
F(000)	1126.8
Crystal size/ mm^3	$0.364 \times 0.1613 \times 0.0501$
Radiation	MoK α ($\lambda = 0.71073$)
2θ range for data collection/ $^\circ$	6.732 to 64.43
Index ranges	$-22 \leq h \leq 15, -13 \leq k \leq 13, -21 \leq l \leq 22$
Reflections collected	14204
Independent reflections	6505 [$R_{\text{int}} = 0.0266, R_{\text{sigma}} = 0.0389$]
Data/restraints/parameters	6505/19/292
Goodness-of-fit on F^2	1.031
Final R indexes [$I \geq 2\sigma(I)$]	$R_1 = 0.0327, wR_2 = 0.0725$
Final R indexes [all data]	$R_1 = 0.0420, wR_2 = 0.0786$
Largest diff. peak/hole / $e \text{\AA}^{-3}$	1.06/-1.01

Crystallographic data for compound 3.31



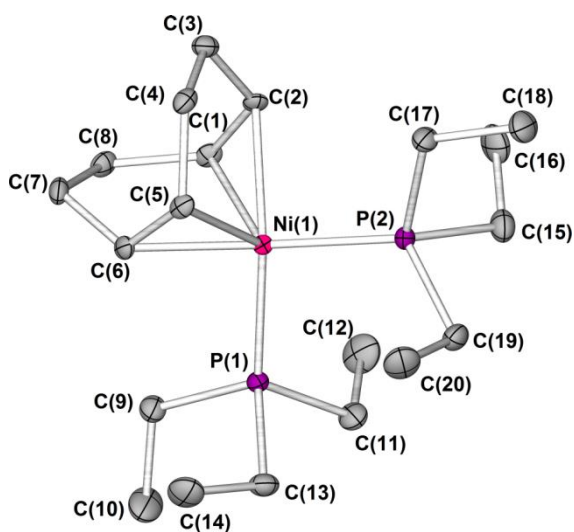
Identification code	ijsf1476
Empirical formula	$C_{85}H_{73}Cl_3F_4O_8P_4Pd_4$
Formula weight	1954.26
Temperature/K	110.00(14)
Crystal system	monoclinic
Space group	$P2_1/n$
$a/\text{\AA}$	21.5641(3)
$b/\text{\AA}$	12.31614(12)
$c/\text{\AA}$	30.4374(4)
$\alpha/^\circ$	90
$\beta/^\circ$	101.2766(12)
$\gamma/^\circ$	90
Volume/ \AA^3	7927.70(16)
Z	4
$\rho_{\text{calc}}/\text{g cm}^{-3}$	1.637
μ/mm^{-1}	9.443
F(000)	3912.0
Crystal size/ mm^3	$0.118 \times 0.1043 \times 0.0262$
Radiation	$\text{CuK}\alpha$ ($\lambda = 1.54184$)
2θ range for data collection/ $^\circ$	7.766 to 142.714
Index ranges	$-26 \leq h \leq 26, -13 \leq k \leq 14, -32 \leq l \leq 37$
Reflections collected	31513
Independent reflections	15014 [$R_{\text{int}} = 0.0338, R_{\text{sigma}} = 0.0457$]
Data/restraints/parameters	15014/0/977
Goodness-of-fit on F^2	1.073
Final R indexes [$I \geq 2\sigma(I)$]	$R_1 = 0.0382, wR_2 = 0.0861$
Final R indexes [all data]	$R_1 = 0.0502, wR_2 = 0.0919$
Largest diff. peak/hole / $e \text{\AA}^{-3}$	0.90/-0.85

Crystallographic data for compound 5.30



Identification code	rnp1520
Empirical formula	C ₁₅ H ₁₃ F ₄ N
Formula weight	283.26
Temperature/K	110.05(10)
Crystal system	monoclinic
Space group	C2
a/Å	17.9962(10)
b/Å	5.8727(3)
c/Å	12.0479(8)
α/°	90
β/°	101.698(6)
γ/°	90
Volume/Å ³	1246.85(13)
Z	4
ρ _{calc} /cm ³	1.509
μ/mm ⁻¹	1.130
F(000)	584.0
Crystal size/mm ³	0.4733 × 0.0884 × 0.0355
Radiation	CuKα (λ = 1.54184)
2θ range for data collection/°	7.494 to 141.752
Index ranges	-22 ≤ h ≤ 22, -5 ≤ k ≤ 7, -14 ≤ l ≤ 14
Reflections collected	3699
Independent reflections	1845 [R _{int} = 0.0292, R _{sigma} = 0.0397]
Data/restraints/parameters	1845/1/183
Goodness-of-fit on F ²	1.075
Final R indexes [I ≥ 2σ (I)]	R ₁ = 0.0345, wR ₂ = 0.0836
Final R indexes [all data]	R ₁ = 0.0378, wR ₂ = 0.0876
Largest diff. peak/hole / e Å ⁻³	0.15/-0.28
Flack parameter	-0.08(14)

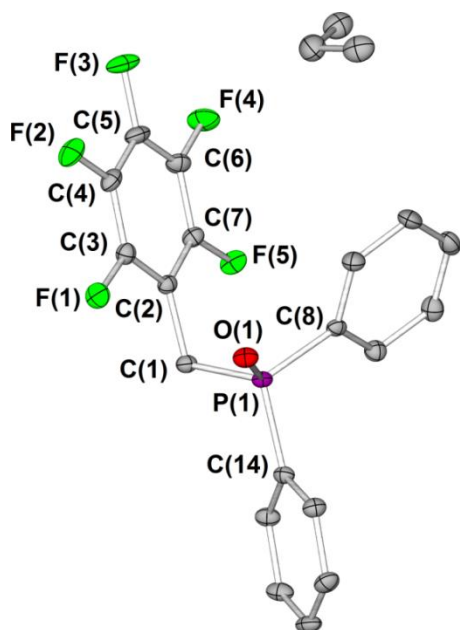
Crystallographic data for compound 5.44



Identification code	rnp1427
Empirical formula	C ₂₀ H ₄₂ NiP ₂
Formula weight	403.18
Temperature/K	110.05(10)
Crystal system	orthorhombic
Space group	P2 ₁ 2 ₁ 2 ₁
a/Å	9.79470(18)
b/Å	12.5653(2)
c/Å	18.1315(4)
α/°	90
β/°	90
γ/°	90
Volume/Å ³	2231.51(7)
Z	4
ρ _{calc} /cm ³	1.200
μ/mm ⁻¹	2.571
F(000)	880.0
Crystal size/mm ³	0.1112 × 0.1105 × 0.0191
Radiation	CuKα (λ = 1.54184)
2θ range for data collection/°	8.562 to 142.662
Index ranges	-11 ≤ h ≤ 11, -15 ≤ k ≤ 11, -20 ≤ l ≤ 22
Reflections collected	15032
Independent reflections	4270 [R _{int} = 0.0316, R _{sigma} = 0.0306]
Data/restraints/parameters	4270/0/214
Goodness-of-fit on F ²	1.035
Final R indexes [I ≥ 2σ (I)]	R ₁ = 0.0223, wR ₂ = 0.0510
Final R indexes [all data]	R ₁ = 0.0253, wR ₂ = 0.0525
Largest diff. peak/hole / e Å ⁻³	0.24/-0.27

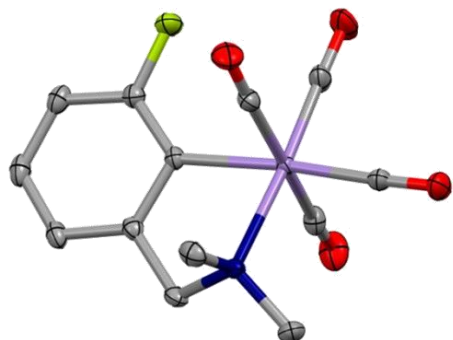
Structure solved by Natalie Pridmore

Crystallographic data for compound 5.48 oxide



Identification code	rnp1509
Empirical formula	C ₂₂ H ₁₅ F ₅ OP
Formula weight	421.31
Temperature/K	110.05(10)
Crystal system	monoclinic
Space group	P2 ₁ /n
a/Å	5.71790(18)
b/Å	12.5516(5)
c/Å	25.6946(8)
α/°	90
β/°	94.884(3)
γ/°	90
Volume/Å ³	1837.37(11)
Z	4
ρ _{calc} /cm ³	1.523
μ/mm ⁻¹	0.210
F(000)	860.0
Crystal size/mm ³	0.2064 × 0.1378 × 0.1017
Radiation	MoKα (λ = 0.71073)
2θ range for data collection/°	6.684 to 64.466
Index ranges	-8 ≤ h ≤ 8, -18 ≤ k ≤ 18, -38 ≤ l ≤ 37
Reflections collected	23024
Independent reflections	6045 [R _{int} = 0.0325, R _{sigma} = 0.0296]
Data/restraints/parameters	6045/0/262
Goodness-of-fit on F ²	1.070
Final R indexes [I ≥ 2σ (I)]	R ₁ = 0.0403, wR ₂ = 0.0957
Final R indexes [all data]	R ₁ = 0.0529, wR ₂ = 0.1025
Largest diff. peak/hole / e Å ⁻³	0.39/-0.34

Crystallographic data for compound 6.6



Identification code	ijsf1517
Empirical formula	C ₁₃ H ₁₁ FMnNO ₄
Formula weight	319.17
Temperature/K	110.05(10)
Crystal system	monoclinic
Space group	C2/c
a/Å	27.0737(8)
b/Å	6.5891(2)
c/Å	15.3507(5)
α/°	90.00
β/°	93.243(3)
γ/°	90.00
Volume/Å ³	2734.04(14)
Z	8
ρ _{calc} /cm ³	1.551
μ/mm ⁻¹	0.988
F(000)	1296.0
Crystal size/mm ³	0.2923 × 0.1824 × 0.1058
Radiation	MoKα (λ = 0.71073)
2θ range for data collection/°	6.86 to 63.92
Index ranges	-39 ≤ h ≤ 39, -9 ≤ k ≤ 9, -22 ≤ l ≤ 22
Reflections collected	23045
Independent reflections	4465 [R _{int} = 0.0259, R _{sigma} = 0.0150]
Data/restraints/parameters	4465/0/183
Goodness-of-fit on F ²	1.088
Final R indexes [I ≥ 2σ (I)]	R ₁ = 0.0238, wR ₂ = 0.0656
Final R indexes [all data]	R ₁ = 0.0254, wR ₂ = 0.0667
Largest diff. peak/hole / e Å ⁻³	0.44/-0.33

Abbreviations

aq.	aqueous
Ac	acetyl
acac	acetylacetonone
AMLA	ambiphilic metal ligand activation
ATR	attenuated total reflectance
Bn	benzyl
σ -CAM	sigma-complex-assisted metathesis
CMD	concerted metalation deprotonation
COD	1,5-cyclooctadiene
Cp*	pentamethylcyclopentadienyl
Cy	cyclohexyl
DCE	dichloroethane
DCM	dichloromethane
dec.	decomposition
dmba	dimethylbenzylamine
DMF	dimethylformamide
DMSO	dimethylsulfoxide
eq.	equivalent
ESI	electrospray ionisation
Et	ethyl
Het	heteroatom
HFIP	hexafluoroisopropanol
HSQC	heteronuclear single quantum coherence spectroscopy
IC ₅₀	half maximal inhibitory concentration
IR	infrared
KIE	kinetic isotopic effect

L	ligand
LIFDI	Liquid Injection Field Desorption/Ionization
lit.	literature
<i>m-</i>	<i>meta</i>
[M]	metal
M.P.	melting point
Me	methyl
MTT	3-(4,5-dimethylthiazol-2-yl)-2,5-diphenyltetrazolium bromide
Mw	molecular weight
NBE	norbornene
ⁿ BuLi	<i>n</i> -butyllithium
NMR	nuclear magnetic resonance
<i>o-</i>	<i>ortho-</i>
<i>p-</i>	<i>para-</i>
PBS	phosphate-buffered saline
Ph	phenyl
ppm	parts per million
Pr	propyl
PTFE	polytetrafluoroethylene
pyr	pyridine
Rf	retention factor
RT	room temperature
<i>s-</i>	<i>secondary</i>
S _E Ar	electrophilic aromatic substitution
TFE	2,2,2-trifluoroethanol
THF	tetrahydrofuran
TLC	Thin Layer Chromatography

TMEDA	N,N,N',N'-tetramethylethylenediamine
TMS	trimethylsilane
tol	toluene
w.r.t	with respect to

References

1. Schlosser, M. *Angew. Chem., Int. Ed.* **1998**, *37*, 1496–1513.
2. Goldman Alan, S.; Goldberg Karen, I. In *Activation and Functionalization of C–H Bonds*; American Chemical Society: 2004; Vol. 885, p 1–43.
3. Arndtsen, B. A.; Bergman, R. G.; Mobley, T. A.; Peterson, T. H. *Acc. Chem. Res.* **1995**, *28*, 154–162.
4. Shilov, A. E.; Shul'pin, G. B. *Chem. Rev.* **1997**, *97*, 2879–2932.
5. Yamaguchi, J.; Yamaguchi, A. D.; Itami, K. *Angew. Chem., Int. Ed.* **2012**, *51*, 8960–9009.
6. Stuart, D. R.; Fagnou, K. *Science* **2007**, *316*, 1172–1175.
7. Alberico, D.; Scott, M. E.; Lautens, M. *Chem. Rev.* **2007**, *107*, 174–238.
8. Ackermann, L. *Chem. Rev.* **2011**, *111*, 1315–1345.
9. McNally, A.; Haffemayer, B.; Collins, B. S. L.; Gaunt, M. J. *Nature* **2014**, *510*, 129–133.
10. Anctil, E. J. G.; Snieckus, V. In *Metal-Catalyzed Cross-Coupling Reactions*; Wiley-VCH Verlag GmbH: 2008, p 761–813.
11. Bräse, S.; Meijere, A. D. In *Metal-Catalyzed Cross-Coupling Reactions*; Wiley-VCH Verlag GmbH: 2008, p 217–315.
12. Denmark, S. E.; Sweis, R. F. In *Metal-Catalyzed Cross-Coupling Reactions*; Wiley-VCH Verlag GmbH: 2008, p 163–216.
13. Knochel, P.; Calaza, M. I.; Hupe, E. In *Metal-Catalyzed Cross-Coupling Reactions*; Wiley-VCH Verlag GmbH: 2008, p 619–670.
14. Gorelsky, S. I. *Coord. Chem. Rev.* **2013**, *257*, 153–164.
15. Bugaut, X.; Glorius, F. *Angew. Chem., Int. Ed.* **2011**, *50*, 7479–7481.
16. Ciana, C.-L.; Phipps, R. J.; Brandt, J. R.; Meyer, F.-M.; Gaunt, M. J. *Angew. Chem., Int. Ed.* **2011**, *50*, 458–462.
17. Kuhl, N.; Hopkinson, M. N.; Glorius, F. *Angew. Chem., Int. Ed.* **2012**, *51*, 8230–8234.
18. Lebrasseur, N.; Larrosa, I. *J. Am. Chem. Soc.* **2008**, *130*, 2926–2927.
19. Ricci, P.; Krämer, K.; Cambeiro, X. C.; Larrosa, I. *J. Am. Chem. Soc.* **2013**, *135*, 13258–13261.
20. Lafrance, M.; Rowley, C. N.; Woo, T. K.; Fagnou, K. *J. Am. Chem. Soc.* **2006**, *128*, 8754–8756.
21. Tredwell, M. J.; Gullias, M.; Gaunt Bremeyer, N.; Johansson, C. C. C.; Collins, B. S. L.; Gaunt, M. J. *Angew. Chem., Int. Ed.* **2011**, *50*, 1076–1079.
22. Kuhl, N.; Hopkinson, M. N.; Wencel-Delord, J.; Glorius, F. *Angew. Chem., Int. Ed.* **2012**, *51*, 10236–10254.

23. Arroniz, C.; Ironmonger, A.; Rassias, G.; Larrosa, I. *Org. Lett.* **2013**, *15*, 910–913.
24. Lyons, T. W.; Sanford, M. S. *Chem. Rev.* **2010**, *110*, 1147–1169.
25. Wang, X.; Yu, D.-G.; Glorius, F. *Angew. Chem., Int. Ed.* **2015**, *54*, 10280–10283.
26. Gensch, T.; Vásquez-Céspedes, S.; Yu, D.-G.; Glorius, F. *Org. Lett.* **2015**, *17*, 3714–3717.
27. Dastbaravardeh, N.; Toba, T.; Farmer, M. E.; Yu, J.-Q. *J. Am. Chem. Soc.* **2015**, *137*, 9877–9884.
28. Sharma, R.; Thakur, K.; Kumar, R.; Kumar, I.; Sharma, U. *Catal. Rev.* **2015**, *57*, 345–405.
29. Zhang, F.-L.; Hong, K.; Li, T.-J.; Park, H.; Yu, J.-Q. *Science* **2016**, *351*, 252–256.
30. Phipps, R. J.; Gaunt, M. J. *Science* **2009**, *323*, 1593–1597.
31. Catellani, M.; Chiusoli, G. P.; Costa, M. *J. Organomet. Chem.* **1995**, *500*, 69–80.
32. Dong, Z.; Wang, J.; Dong, G. *J. Am. Chem. Soc.* **2015**, *137*, 5887–5890.
33. Tang, R.-Y.; Li, G.; Yu, J.-Q. *Nature* **2014**, *507*, 215–220.
34. Clot, E.; Eisenstein, O.; Jasim, N.; Macgregor, S. A.; McGrady, J. E.; Perutz, R. N. *Acc. Chem. Res.* **2011**, *44*, 333–348.
35. Selmecky, A. D.; Jones, W. D.; Partridge, M. G.; Perutz, R. N. *Organometallics* **1994**, *13*, 522–532.
36. Clot, E.; Oelckers, B.; Klahn, A. H.; Eisenstein, O.; Perutz, R. N. *Dalton Trans.* **2003**, 4065–4074.
37. Clot, E.; Mégret, C.; Eisenstein, O.; Perutz, R. N. *J. Am. Chem. Soc.* **2009**, *131*, 7817–7827.
38. Tsang, J. Y. K.; Buschhaus, M. S. A.; Legzdins, P.; Patrick, B. O. *Organometallics* **2006**, *25*, 4215–4225.
39. Lafrance, M.; Shore, D.; Fagnou, K. *Org. Lett.* **2006**, *8*, 5097–5100.
40. René, O.; Fagnou, K. *Org. Lett.* **2010**, *12*, 2116–2119.
41. Lapointe, D.; Fagnou, K. *Chem. Lett.* **2010**, *39*, 1118–1126.
42. Fang, X.; Huang, Y.; Chen, X.; Lin, X.; Bai, Z.; Huang, K.-W.; Yuan, Y.; Weng, Z. *J. Fluorine Chem.* **2013**, *151*, 50–57.
43. Ackermann, L.; Fenner, S. *Chem. Commun.* **2011**, *47*, 430–432.
44. Guo, F.; Han, J.; Mao, S.; Li, J.; Geng, X.; Yu, J.; Wang, L. *RSC Advances* **2013**, *3*, 6267–6270.
45. Li, H.; Liu, J.; Sun, C.-L.; Li, B.-J.; Shi, Z.-J. *Org. Lett.* **2011**, *13*, 276–279.
46. Do, H.-Q.; Daugulis, O. *J. Am. Chem. Soc.* **2008**, *130*, 1128–1129.
47. Yan, T.; Zhao, L.; He, M.; Soulé, J.-F.; Bruneau, C.; Doucet, H. *Adv. Synth. Catal.* **2014**, *356*, 1586–1596.

48. He, M.; Soulé, J.-F.; Doucet, H. *ChemCatChem* **2015**, *7*, 2130–2140.
49. Müller, K.; Faeh, C.; Diederich, F. *Science* **2007**, *317*, 1881–1886.
50. Smart, B. E. *J. Fluorine Chem.* **2001**, *109*, 3–11.
51. Wilkinson, J. A. *Chem. Rev.* **1992**, *92*, 505–519.
52. Hollingworth, C.; Gouverneur, V. *Chem. Commun.* **2012**, *48*, 2929–2942.
53. Furuya, T.; Kamlet, A. S.; Ritter, T. *Nature* **2011**, *473*, 470–477.
54. Campbell, M. G.; Ritter, T. *Chem. Rev.* **2015**, *115*, 612–633.
55. McMurtrey, K. B.; Racowski, J. M.; Sanford, M. S. *Org. Lett.* **2012**, *14*, 4094–4097.
56. Hull, K. L.; Anani, W. Q.; Sanford, M. S. *J. Am. Chem. Soc.* **2006**, *128*, 7134–7135.
57. Boutadla, Y.; Davies, D. L.; Macgregor, S. A.; Poblador-Bahamonde, A. I. *Dalton Trans.* **2009**, 5820–5831.
58. Khan, M. S.; Haque, A.; Al-Suti, M. K.; Raithby, P. R. *J. Organomet. Chem.* **2015**, *793*, 114–133.
59. Labinger, J. A.; Bercaw, J. E. *Nature* **2002**, *417*, 507–514.
60. Albrecht, M. *Chem. Rev.* **2010**, *110*, 576–623.
61. Bénéaud, O.; Berthet, J.-C.; Thuéry, P.; Ephritikhine, M. *Inorg. Chem.* **2010**, *49*, 8117–8130.
62. Perutz, R. N.; Sabo-Etienne, S. *Angew. Chem., Int. Ed.* **2007**, *46*, 2578–2592.
63. Conejero, S.; Paneque, M.; Poveda, M. L.; Santos, L. L.; Carmona, E. *Acc. Chem. Res.* **2010**, *43*, 572–580.
64. Ryabov, A. D. *Inorg. Chem.* **1987**, *26*, 1252–1260.
65. Mayer, I. *Chem. Phys. Lett.* **1983**, *97*, 270–274.
66. García-Cuadrado, D.; de Mendoza, P.; Braga, A. A. C.; Maseras, F.; Echavarren, A. M. *J. Am. Chem. Soc.* **2007**, *129*, 6880–6886.
67. Boutadla, Y.; Davies, D. L.; Macgregor, S. A.; Poblador-Bahamonde, A. I. *Dalton Trans.* **2009**, 5887–5893.
68. Guihaume, J.; Clot, E.; Eisenstein, O.; Perutz, R. N. *Dalton Trans.* **2010**, *39*, 10510–10519.
69. Cope, A. C.; Siekman, R. W. *J. Am. Chem. Soc.* **1965**, *87*, 3272–3273.
70. Kleiman, J. P.; Dubeck, M. *J. Am. Chem. Soc.* **1963**, *85*, 1544–1545.
71. Trofimenko, S. *Inorg. Chem.* **1973**, *12*, 1215–1221.
72. Dupont, J.; Pfeffer, M. *Palladacycles: Synthesis, Characterization and Applications*; Wiley, 2008.
73. Crespo, M.; Martinez, M.; Sales, J. *Organometallics* **1993**, *12*, 4297–4304.

74. Wang, T.; Alfonso, B. J.; Love, J. A. *Org. Lett.* **2007**, *9*, 5629–5631.
75. Wang, T.; Keyes, L.; Patrick, B. O.; Love, J. A. *Organometallics* **2012**, *31*, 1397–1407.
76. Lu, F.; Sun, H.; Li, X. *Chin. J. Chem.* **2013**, *31*, 927–932.
77. Procacci, B.; Blagg, R. J.; Perutz, R. N.; Rendón, N.; Whitwood, A. C. *Organometallics* **2014**, *33*, 45–52.
78. Crespo, M. *Organometallics* **2012**, *31*, 1216–1234.
79. Dehand, J.; Pfeffer, M. *Coord. Chem. Rev.* **1976**, *18*, 327–352.
80. Ryabov, A. D. *Synthesis* **1985**, *1985*, 233–252.
81. Pfeffer, M. *Pure Appl. Chem.* **1992**, *64*, 335–342.
82. Dupont, J.; Pfeffer, M.; Spencer, J. *Eur. J. Inorg. Chem.* **2001**, *2001*, 1917–1927.
83. Selander, N.; Szabo, K. J. *Dalton Trans.* **2009**, 6267–6279.
84. Bedford, R. B. *Chem. Commun.* **2003**, 1787–1796.
85. Omae, I. *Coord. Chem. Rev.* **2004**, *248*, 995–1023.
86. Omae, I. *J. Organomet. Chem.* **2007**, *692*, 2608–2632.
87. Lewis, L. N. *J. Am. Chem. Soc.* **1986**, *108*, 743–749.
88. Kapdi, A. R.; Fairlamb, I. J. S. *Chem. Soc. Rev.* **2014**, *43*, 4751–4777.
89. Dyson, P. J.; Sava, G. *Dalton Trans.* **2006**, 1929–1933.
90. Dupont, J.; Consorti, C. S.; Spencer, J. *Chem. Rev.* **2005**, *105*, 2527–2572.
91. Beweries, T.; Rosenthal, U. *Nat Chem* **2013**, *5*, 649–650.
92. Canty, A. J.; van Koten, G. *Acc. Chem. Res.* **1995**, *28*, 406–413.
93. Ryabov, A. D. *Chem. Rev.* **1990**, *90*, 403–424.
94. Davies, D. L.; Donald, S. M. A.; Macgregor, S. A. *J. Am. Chem. Soc.* **2005**, *127*, 13754–13755.
95. Dehand, J.; Pfeffer, M.; Zinsius, M. *Inorg. Chim. Acta* **1975**, *13*, 229–232.
96. Dehand, J.; Jordanov, J.; Pfeffer, M.; Zinsius, M. *Comptes Rendus Hebdomadaires Des Seances De L Academie Des Sciences Serie C* **1975**, *281*, 651–654.
97. Cope, A. C.; Friedric. *J. Am. Chem. Soc.* **1968**, *90*, 909–&.
98. Braunstein, P.; Dehand, J.; Pfeffer, M. *Inorganic & Nuclear Chemistry Letters* **1974**, *10*, 581–585.
99. Dupont, J.; Beydoun, N.; Pfeffer, M. *J. Chem. Soc., Dalton Trans.* **1989**, 1715–1720.
100. Hiraki, K.; Fuchita, Y.; Uchiyama, T. *Inorg. Chim. Acta* **1983**, *69*, 187–190.
101. Dunina, V. V.; Zalevskaya, O. A.; Potapov, V. M. *Usp. Khim.* **1988**, *57*, 434–473.
102. Shaw, B. L.; Truelock, M. M. *J. Organomet. Chem.* **1975**, *102*, 517–525.

103. Duff, J. M.; Mann, B. E.; Shaw, B. L.; Turtle, B. *J. Chem. Soc., Dalton Trans.* **1974**, 139–145.
104. Thompson, J. M.; Heck, R. F. *J. Org. Chem.* **1975**, *40*, 2667–2674.
105. Cheney, A. J.; Shaw, B. L. *J. Chem. Soc., Dalton Trans.* **1972**, 860–865.
106. Fuchita, Y.; Hiraki, K.; Uchiyama, T. *J. Chem. Soc., Dalton Trans.* **1983**, 897–899.
107. Brown, K. J.; Berry, M. S.; Waterman, K. C.; Lingenfelter, D.; Murdoch, J. R. *J. Am. Chem. Soc.* **1984**, *106*, 4717–4723.
108. Valeria, V. D.; Olga, N. G. *Russ. Chem. Rev.* **2005**, *74*, 871.
109. Bajwa, S. E.; Storr, T. E.; Hatcher, L. E.; Williams, T. J.; Baumann, C. G.; Whitwood, A. C.; Allan, D. R.; Teat, S. J.; Raithby, P. R.; Fairlamb, I. J. S. *Chem. Sci.* **2012**, *3*, 1656–1661.
110. Bakhmutov, V. I.; Berry, J. F.; Cotton, F. A.; Ibragimov, S.; Murillo, C. A. *Dalton Trans.* **2005**, 1989–1992.
111. Granell, J.; Sales, J.; Vilarrasa, J.; Declercq, J. P.; Germain, G.; Miravittles, C.; Solans, X. *J. Chem. Soc., Dalton Trans.* **1983**, 2441–2446.
112. Ceder, R. M.; Sales, J. *J. Organomet. Chem.* **1984**, *276*, c31–c32.
113. Albrecht, M.; Dani, P.; Lutz, M.; Spek, A. L.; van Koten, G. *J. Am. Chem. Soc.* **2000**, *122*, 11822–11833.
114. Ryabov, A. D.; Yatsimirskii, A. K. *Inorg. Chem.* **1984**, *23*, 789–790.
115. Lohner, P.; Pfeffer, M.; de Clan, A.; Fischer, J. *C. R. Acad. Sci. - Series IIC - Chemistry* **1998**, *1*, 615–620.
116. Li, L.; Brennessel, W. W.; Jones, W. D. *Organometallics* **2009**, *28*, 3492–3500.
117. Davies, D. L.; Al-Duaij, O.; Fawcett, J.; Giardiello, M.; Hilton, S. T.; Russell, D. R. *Dalton Trans.* **2003**, 4132–4138.
118. Davies, D. L.; Donald, S. M. A.; Al-Duaij, O.; Macgregor, S. A.; Pölleth, M. *J. Am. Chem. Soc.* **2006**, *128*, 4210–4211.
119. Fernandez, S.; Pfeffer, M.; Ritleng, V.; Sirlin, C. *Organometallics* **1999**, *18*, 2390–2394.
120. Sortais, J.-B.; Pannetier, N.; Holuigue, A.; Barloy, L.; Sirlin, C.; Pfeffer, M.; Kyritsakas, N. *Organometallics* **2007**, *26*, 1856–1867.
121. Djukic, J.-P.; Sortais, J.-B.; Barloy, L.; Pfeffer, M. *Eur. J. Inorg. Chem.* **2009**, *2009*, 817–853.
122. Milani, J.; Pridmore, N. E.; Whitwood, A. C.; Fairlamb, I. J. S.; Perutz, R. N. *Organometallics* **2015**, *34*, 4376–4386.
123. Alsters, P. L.; Engel, P. F.; Hogerheide, M. P.; Copijn, M.; Spek, A. L.; van Koten, G. *Organometallics* **1993**, *12*, 1831–1844.
124. Ryabov, A. D.; Sakodinskaya, I. K.; Yatsimirsky, A. K. *J. Chem. Soc., Dalton Trans.* **1985**, *0*, 2629–2638.

125. Vladimir, V. G.; David, L. T.; William, J. M.; Viacheslav, A. P. In *Activation and Functionalization of C-H Bonds*; American Chemical Society: 2004; Vol. 885, p 393–406.
126. Liu, Z.; Sayre, L. M. *Tetrahedron* **2004**, *60*, 1601–1610.
127. Bercaw, J. E.; Durrell, A. C.; Gray, H. B.; Green, J. C.; Hazari, N.; Labinger, J. A.; Winkler, J. R. *Inorg. Chem.* **2010**, *49*, 1801–1810.
128. Luo, J.; Khusnutdinova, J. R.; Rath, N. P.; Mirica, L. M. *Chem. Commun.* **2012**, *48*, 1532–1534.
129. Mentos, A.; Kemmitt, R. D. W.; Fawcett, J.; Russell, D. R. *J. Mol. Struct.* **2004**, *693*, 241–246.
130. Serrano, J. L.; García, L.; Pérez, J.; Pérez, E.; García, J.; Sánchez, G.; Sehnal, P.; De Ornellas, S.; Williams, T. J.; Fairlamb, I. J. S. *Organometallics* **2011**, *30*, 5095–5109.
131. Kapdi, A. R.; Dhangar, G.; Serrano, J. L.; Perez, J.; Garcia, L.; Fairlamb, I. J. S. *Chem. Commun.* **2014**, *50*, 9859–9861.
132. Fairlamb, I. J. S.; Lee, A. F.; Loe-Mie, F. E. M.; Niemelä, E. H.; O'Brien, C. T.; Whitwood, A. C. *Tetrahedron* **2005**, *61*, 9827–9838.
133. Herrmann, W. A.; Öfele, K.; v. Preysing, D.; Schneider, S. K. *J. Organomet. Chem.* **2003**, *687*, 229–248.
134. Beletskaya, I. P.; Cheprakov, A. V. *J. Organomet. Chem.* **2004**, *689*, 4055–4082.
135. Fairlamb, I. J. S.; Grant, S.; McCormack, P.; Whittall, J. *Dalton Trans.* **2007**, 859–865.
136. Gross, J.; Nieth, N.; Linden, H. B.; Blumbach, U.; Richter, F.; Tauchert, M.; Tompers, R.; Hofmann, P. *Anal. Bioanal. Chem.* **2006**, *386*, 52–58.
137. Deeming, A. J.; Rothwell, I. P.; Hursthouse, M. B.; New, L. *J. Chem. Soc., Dalton Trans.* **1978**, *0*, 1490–1496.
138. Bondi, A. *J. Phys. Chem.* **1964**, *68*, 441–451.
139. Barr, N.; Dyke, S. F.; Smith, G.; Kennard, C. H. L.; McKee, V. *J. Organomet. Chem.* **1985**, *288*, 109–117.
140. Karami, K.; Kharat, M. H.; Rizzoli, C.; Lipkowski, J. *J. Organomet. Chem.* **2013**, *728*, 16–22.
141. Karami, K.; kharat, M. H.; Sadeghi-Aliabadi, H.; Lipkowski, J.; Mirian, M. *Polyhedron* **2013**, *50*, 187–192.
142. Patani, G. A.; LaVoie, E. J. *Chem. Rev.* **1996**, *96*, 3147–3176.
143. Hagmann, W. K. *J. Med. Chem.* **2008**, *51*, 4359–4369.
144. Herrmann, W. A.; Böhm, V. P. W.; Reisinger, C.-P. *J. Organomet. Chem.* **1999**, *576*, 23–41.
145. Herrmann, W. A.; Reisinger, C.-P.; Öfele, K.; Broßmer, C.; Beller, M.; Fischer, H. *J. Mol. Catal. A: Chem.* **1996**, *108*, 51–56.
146. Herrmann, W. A.; Brossmer, C.; Öfele, K.; Reisinger, C.-P.; Priermeier, T.; Beller, M.; Fischer, H. *Angew. Chem., Int. Ed. Engl.* **1995**, *34*, 1844–1848.

147. Dunina, V. V.; Gorunova, O. N. *Russ. Chem. Rev.* **2004**, *73*, 309–350.
148. Orpen, A. G.; Connelly, N. G. *Organometallics* **1990**, *9*, 1206–1210.
149. Marynick, D. S. *J. Am. Chem. Soc.* **1984**, *106*, 4064–4065.
150. Pacchioni, G.; Bagus, P. S. *Inorg. Chem.* **1992**, *31*, 4391–4398.
151. Cheney, A. J.; Mann, B. E.; Shaw, B. L.; Slade, R. M. *Journal of the Chemical Society D: Chemical Communications* **1970**, 1176–1177.
152. Cheney, A. J.; Mann, B. E.; Shaw, B. L.; Slade, R. M. *J. Chem. Soc. A* **1971**, 3833–3842.
153. Hietkamp, S.; Stufkens, D. J.; Vrieze, K. *J. Organomet. Chem.* **1979**, *168*, 351–361.
154. Parshall, G. W. *Acc. Chem. Res.* **1970**, *3*, 139–144.
155. Chatt, J.; Davidson, J. M. *Journal of the Chemical Society (Resumed)* **1965**, 843–855.
156. Shaw, B. L. *J. Am. Chem. Soc.* **1975**, *97*, 3856–3857.
157. Allinger, N. L.; Zalkow, V. *J. Org. Chem.* **1960**, *25*, 701–704.
158. Hyde, E. M.; Shaw, B. L.; Shepherd, I. *J. Chem. Soc., Dalton Trans.* **1978**, 1696–1705.
159. Duff, J. M.; Shaw, B. L. *J. Chem. Soc., Dalton Trans.* **1972**, 2219–2225.
160. Ng, J. K.-P.; Li, Y.; Tan, G.-K.; Koh, L.-L.; Vittal, J. J.; Leung, P.-H. *Inorg. Chem.* **2005**, *44*, 9874–9886.
161. Ryabov, A. D.; Usatov, A. V.; Kalinin, V. N.; Zakharkin, L. I. *Bulletin of the Academy of Sciences of the USSR, Division of chemical science* **1986**, *35*, 2559–2562.
162. Stepanova, V. A.; Egan, L. M.; Stahl, L.; Smoliakova, I. P. *J. Organomet. Chem.* **2011**, *696*, 3162–3168.
163. Kosolapoff, G. M.; Maier, L. *Organic Phosphorus Compounds*; R. E. Krieger Publishing Company, 1981.
164. Kyba, E. P.; Kerby, M. C.; Rines, S. P. *Organometallics* **1986**, *5*, 1189–1194.
165. Gilbertson, S. R.; Starkey, G. W. *J. Org. Chem.* **1996**, *61*, 2922–2923.
166. Coote, S. J.; Dawson, G. J.; Frost, C. G.; Williams, J. M. J. *Synlett* **1993**, *1993*, 509–510.
167. Ahn, S. Y.; Ha, Y. *Mol. Cryst. Liq. Cryst.* **2010**, *520*, 68/[344]–374/[350].
168. Freitag, S.; Henning, J.; Schubert, H.; Wesemann, L. *Angew. Chem., Int. Ed.* **2013**, *52*, 5640–5643.
169. Gorunova, O. N.; Keuseman, K. J.; Goebel, B. M.; Kataeva, N. A.; Churakov, A. V.; Kuz'mina, L. G.; Dunina, V. V.; Smoliakova, I. P. *J. Organomet. Chem.* **2004**, *689*, 2382–2394.
170. Meyer, N. H.; Zangger, K. *Angew. Chem., Int. Ed.* **2013**, *52*, 7143–7146.
171. Zangger, K.; Sterk, H. *J. Magn. Reson.* **1997**, *124*, 486–489.

172. Suntioinen, S.; Laatikainen, R. *Magn. Reson. Chem.* **1992**, *30*, 415–419.
173. Hutton, H. M.; Richardson, B.; Schaefer, T. *Can. J. Chem.* **1967**, *45*, 1795–1800.
174. Barfield, M.; Johnston, M. D. *Chem. Rev.* **1973**, *73*, 53–73.
175. Wasylishen, R.; Schaefer, T. *Can. J. Chem.* **1971**, *49*, 94–101.
176. Omae, I. *Coord. Chem. Rev.* **1980**, *32*, 235–271.
177. Takahashi, H.; Tsuji, J. *J. Organomet. Chem.* **1967**, *10*, 511–517.
178. Wang, C.-C.; Lin, P.-S.; Cheng, C.-H. *J. Am. Chem. Soc.* **2002**, *124*, 9696–9697.
179. Chen, Q.-A.; Kim, D. K.; Dong, V. M. *J. Am. Chem. Soc.* **2014**, *136*, 3772–3775.
180. Ackermann, L. *Org. Lett.* **2005**, *7*, 3123–3125.
181. Gunanathan, C.; Milstein, D. *Chem. Rev.* **2014**, *114*, 12024–12087.
182. Davenport, A. J.; Davies, D. L.; Fawcett, J.; Russell, D. R. *J. Organomet. Chem.* **2006**, *691*, 2221–2227.
183. Vaughan, B. A.; Webster-Gardiner, M. S.; Cundari, T. R.; Gunnoe, T. B. *Science* **2015**, *348*, 421–424.
184. Abbenhuis, H. C. L.; Pfeffer, M.; Sutter, J. P.; de Cian, A.; Fischer, J.; Ji, H. L.; Nelson, J. H. *Organometallics* **1993**, *12*, 4464–4472.
185. Attar, S.; Nelson, J. H.; Fischer, J.; de Cian, A.; Sutter, J.-P.; Pfeffer, M. *Organometallics* **1995**, *14*, 4559–4569.
186. Ritleng, V.; Bertani, P.; Pfeffer, M.; Sirlin, C.; Hirschinger, J. *Inorg. Chem.* **2001**, *40*, 5117–5122.
187. Kisenyi, J. M.; Sunley, G. J.; Cabeza, J. A.; Smith, A. J.; Adams, H.; Salt, N. J.; Maitlis, P. M. *J. Chem. Soc., Dalton Trans.* **1987**, 2459–2466.
188. Ahrens, T.; Kohlmann, J.; Ahrens, M.; Braun, T. *Chem. Rev.* **2015**, *115*, 931–972.
189. Chen, Z.; He, C.-Y.; Yin, Z.; Chen, L.; He, Y.; Zhang, X. *Angew. Chem., Int. Ed.* **2013**, *52*, 5813–5817.
190. Keyes, L.; Love, J. A. In *C-H and C-X Bond Functionalization: Transition Metal Mediation*; The Royal Society of Chemistry: 2013, p 159–192.
191. Kiso, Y.; Tamao, K.; Kumada, M. *J. Organomet. Chem.* **1973**, *50*, C12–C14.
192. Edelbach, B. L.; Kraft, B. M.; Jones, W. D. *J. Am. Chem. Soc.* **1999**, *121*, 10327–10331.
193. Böhm, V. P. W.; Gstöttmayr, C. W. K.; Weskamp, T.; Herrmann, W. A. *Angew. Chem., Int. Ed.* **2001**, *40*, 3387–3389.
194. Ackermann, L.; Born, R.; Spatz, J. H.; Meyer, D. *Angew. Chem., Int. Ed.* **2005**, *44*, 7216–7219.
195. Cronin, L.; Higgitt, C. L.; Karch, R.; Perutz, R. N. *Organometallics* **1997**, *16*, 4920–4928.

196. Braun, T.; Foxon, S. P.; Perutz, R. N.; Walton, P. H. *Angew. Chem., Int. Ed.* **1999**, *38*, 3326–3329.
197. Braun, T.; Perutz, R. N.; Sladek, M. I. *Chem. Commun.* **2001**, 2254–2255.
198. Steffen, A.; Sladek, M. I.; Braun, T.; Neumann, B.; Stammler, H.-G. *Organometallics* **2005**, *24*, 4057–4064.
199. Schaub, T.; Backes, M.; Radius, U. *J. Am. Chem. Soc.* **2006**, *128*, 15964–15965.
200. Ohashi, M.; Doi, R.; Ogoshi, S. *Chem. Eur. J* **2014**, *20*, 2040–2048.
201. Banks, R. E.; Burgess, J. E.; Cheng, W. M.; Haszeldine, R. N. *Journal of the Chemical Society (Resumed)* **1965**, 575–581.
202. Perutz, R. N.; Braun, T. In *Comprehensive Organometallic Chemistry III*; Crabtree, D. M. P. M. H., Ed.; Elsevier: Oxford, 2007, p 725–758.
203. Weaver, J.; Senaweera, S. *Tetrahedron* **2014**, *70*, 7413–7428.
204. Fahey, D. R.; Mahan, J. E. *J. Am. Chem. Soc.* **1977**, *99*, 2501–2508.
205. Braun, T.; Perutz, R. N. *Chem. Commun.* **2002**, 2749–2757.
206. Archibald, S. J.; Braun, T.; Gaunt, J. A.; Hobson, J. E.; Perutz, R. N. *J. Chem. Soc., Dalton Trans.* **2000**, 2013–2018.
207. Jasim, N. A.; Perutz, R. N.; Whitwood, A. C.; Braun, T.; Izundu, J.; Neumann, B.; Rothfeld, S.; Stammler, H.-G. *Organometallics* **2004**, *23*, 6140–6149.
208. Jones, W. D.; Partridge, M. G.; Perutz, R. N. *J. Chem. Soc., Chem. Commun.* **1991**, 264–266.
209. Burling, S.; Elliott, P. I. P.; Jasim, N. A.; Lindup, R. J.; McKenna, J.; Perutz, R. N.; Archibald, S. J.; Whitwood, A. C. *Dalton Trans.* **2005**, 3686–3695.
210. Honaker, M. T.; Sandefur, B. J.; Hargett, J. L.; McDaniel, A. L.; Salvatore, R. N. *Tetrahedron Lett.* **2003**, *44*, 8373–8377.
211. J. Ager, D.; A. Laneman, S. *Chem. Commun.* **1997**, 2359–2360.
212. Dornhaus, F.; Bolte, M.; Lerner, H.-W.; Wagner, M. *Eur. J. Inorg. Chem.* **2006**, *2006*, 1777–1785.
213. Drury, W. J.; Zimmermann, N.; Keenan, M.; Hayashi, M.; Kaiser, S.; Goddard, R.; Pfaltz, A. *Angew. Chem.* **2004**, *116*, 72–76.
214. Dean, R. R.; McFarlane, W. *Journal of the Chemical Society B: Physical Organic* **1969**, 509–512.
215. Nova, A.; Erhardt, S.; Jasim, N. A.; Perutz, R. N.; Macgregor, S. A.; McGrady, J. E.; Whitwood, A. C. *J. Am. Chem. Soc.* **2008**, *130*, 15499–15511.
216. Fornies, J.; Green, M.; Spencer, J. L.; Stone, F. G. A. *J. Chem. Soc., Dalton Trans.* **1977**, 1006–1009.
217. Chan, D.; Duckett, S. B.; Heath, S. L.; Khazal, I. G.; Perutz, R. N.; Sabo-Etienne, S.; Timmins, P. L. *Organometallics* **2004**, *23*, 5744–5756.

218. Braunschweig, H.; Damme, A.; Dewhurst, R. D.; Vargas, A. *Nat Chem* **2013**, *5*, 115–121.
219. Giese, C.; Lepthien, S.; Metzner, L.; Brandsch, M.; Budisa, N.; Lilie, H. *ChemMedChem* **2008**, *3*, 1449–1456.
220. Smith, D. A.; Beweries, T.; Blasius, C.; Jasim, N.; Nazir, R.; Nazir, S.; Robertson, C. C.; Whitwood, A. C.; Hunter, C. A.; Brammer, L.; Perutz, R. N. *J. Am. Chem. Soc.* **2015**, *137*, 11820–11831.
221. Jasim, N. A.; Perutz, R. N. *J. Am. Chem. Soc.* **2000**, *122*, 8685–8693.
222. Barbarich, T. J.; Rithner, C. D.; Miller, S. M.; Anderson, O. P.; Strauss, S. H. *J. Am. Chem. Soc.* **1999**, *121*, 4280–4281.
223. Giuffredi, G. T.; Gouverneur, V.; Bernet, B. *Angew. Chem.* **2013**, *125*, 10718–10722.
224. López, G.; Ruiz, J.; García, G.; Martí, J. M.; Sánchez, G.; García, J. *J. Organomet. Chem.* **1991**, *412*, 435–443.
225. Unpublished results; synthesis performed by Stefan Blackburn (IJSF summer student) and Amy Bishop (IJSF MChem student)
226. Dolomanov, O. V.; Bourhis, L. J.; Gildea, R. J.; Howard, J. A. K.; Puschmann, H. *J. Appl. Crystallogr.* **2009**, *42*, 339–341.
227. Palatinus, L.; Prathapa, S. J.; van Smaalen, S. *J. Appl. Crystallogr.* **2012**, *45*, 575–580.
228. Palatinus, L.; Chapuis, G. *J. Appl. Crystallogr.* **2007**, *40*, 786–790.
229. Palatinus, L.; van der Lee, A. *J. Appl. Crystallogr.* **2008**, *41*, 975–984.
230. Sheldrick, G. *Acta Crystallogr., Sect. A: Found. Crystallogr.* **2008**, *64*, 112–122.
231. Cotton, H. K.; Verboom, R. C.; Johansson, L.; Plietker, B. J.; Bäckvall, J.-E. *Organometallics* **2002**, *21*, 3367–3375.
232. White, C.; Yates, A.; Maitlis, P. M.; Heinekey, D. M. In *Inorg. Synth.*; John Wiley & Sons, Inc.: 2007, p 228–234.
233. Bennett, M. A.; Smith, A. K. *J. Chem. Soc., Dalton Trans.* **1974**, 233–241.
234. Tanabe, M.; Ishikawa, N.; Osakada, K. *Organometallics* **2006**, *25*, 796–798.
235. Roering, A. J.; Hale, L. V. A.; Squier, P. A.; Ringgold, M. A.; Wiederspan, E. R.; Clark, T. B. *Org. Lett.* **2012**, *14*, 3558–3561.